# Development of Acellular Porcine Peripheral Nerves


The University Of Sheffield.

**Thesis submitted to the University of Sheffield for the degree of Doctor of Philosophy**

**Department of Materials Science and Engineering**

**Leyla Žilić**

**October 2016**

## Acknowledgments

I would like to firstly thank my supervisors, Professor John Haycock and Dr Stacy-Paul Wilshaw for their guidance and support throughout my years at the University of Sheffield and University of Leeds. I would also like to acknowledge Dr James Phillips for his guidance and contribution in the TEM and *in vivo* studies carried out in this study.

I would like to say a thank you to all the staff members with a special mention to Mark Wagner, Dr Adam Glen and Dr Sabiniano Roman who have helped me on numerous occasions in the labs. I would also like to give thanks to all the people in the Ingham and Kroto labs who have helped me and given me support throughout the years with a special mention to Ruth Craven, Lindsey Dew, Giulia Gigliobianco Ahtasham Raza, Dharaminder Singh and Assad Fiaz.

Lastly I would like to give a special mention to my family especially my mother Dudiya. She has provided me with endless support and is my role model, for which I will be eternally grateful.

# Abstract

Peripheral nerve injuries can lead to a major loss of function and affect quality of life. Current autologous treatments and commercially available products such as nerve guide conduits all have limitations. The aim of this study was to develop biocompatible, non-immunogenic nerve grafts using low concentration SDS to decellularise porcine peripheral nerves. Initially the porcine nerve anatomy was defined. Acellular nerves were then used as the basis for an *in vitro* study of perfused flow within the tissue for the introduction of Schwann cells - as the delivery of these cells is reported to stimulate axon regeneration. Furthermore, an *in vivo* study using a rat sciatic nerve injury model was conducted to evaluate the regenerative capacity of acellular porcine grafts.

Histology confirmed an absence of cells and retention of the native nerve histioarchitecture. DNA levels were reduced by >95 % throughout the decellularised tissue. Immunohistochemistry showed retention of important extracellular matrix proteins such as collagen, laminin and fibronectin. *In vitro* biocompatibility studies indicated the acellular nerves were not cytotoxic to human dermal fibroblasts and primary rat Schwann cells. Uniaxial tensile testing showed a significant increase in ultimate tensile strength (UTS) and strain between native and acellular nerve tissues. In addition, mechanical testing of the nerves revealed porcine peroneal nerves to have a higher UTS value in comparison to the porcine tibial nerves. Analysis of the nerves using transmission electron microscopy concluded that the mechanical properties of nerves could not be determined exclusively by their ultrastructure or collagen fibril diameter.

Porcine acellular nerve grafts were used as an *in vitro* and *in vivo* model for the introduction of primary rat Schwann cells. The *in vitro* nerve model confirmed that reseeded Schwann cells under perfusion maintained their phenotype and had a lower rate of cell death when compared to static conditions. A rat sciatic nerve *in vivo* gap injury model demonstrated that porcine grafts were able to promote axonal regeneration; however, they were not as effective as the autologous graft. In summary, acellular peripheral nerve tissue was found to have excellent potential for development of a tissue engineered graft to aid peripheral nerve regeneration.

## Contents Page

# Presentations and Publications

## Oral presentation

The 2014 Annual Tissue & Cell Engineering Society Meeting

Development of an Acellular Xenogeneic Nerve Graft

**L.Zilic, J.W Haycock and S-P Wilshaw**

## Poster presentations

TERMIS EU, Genova, Italy (June 2014)

Development of an Acellular Xenogeneic Nerve Graft

The 2015 Annual Tissue & Cell Engineering Society Meeting

Development of an *in vitro* peripheral nerve model using xenogeneic nerve tissue

**L.Zilic, J.W Haycock and S-P Wilshaw**

## Publications

Zilic, L., P. E. Garner, et al. (2015). "An anatomical study of porcine peripheral nerve and its potential use in nerve tissue engineering." Journal of anatomy 227(3): 302-314.

Zilic, L., S.-P. Wilshaw, et al. (2016). "Decellularisation and histological characterisation of porcine peripheral nerves." Biotechnology and Bioengineering.

## Publication under review

Zilic, L., S.-P. Wilshaw, et al. (2016). The mechanical properties of porcine tibial and peroneal nerves in relation to their structure. Journal of anatomy

# List of Tables

# List of Figures

# Abbreviations

**%** percentage
**α** alpha
**β** beta
**$\lambda_{ex}$** excitation wavelength
**$\lambda_{em}$** emission wavelength
**µg** microgram
**µl** microlitre
**µM** micromolar
**µm** micrometer
**2D** two dimensional
**3D** three dimensional
**Ab** antibody
**ADSCs** adipose-derived stem cells
**ANOVA** Analysis of variance
**BSA** Bovine serum albumin
**$CaCl_2$** Calcium chloride
**CHAPS** 3-[(3-cholamidopropyl) dimethylammonio]-1-propanesulfonate
**C.I.** Confidence intervals
**DAPI** 4',6-diamidino-2-phenylindole
**DMEM** Dulbecco's modified Eagles Medium
**DMSO** Dimethylsulphoxide
**DNA** Deoxyribonucleic acid
**DNAse** Deoxyribonuclease
**ECM** Extracellular matrix
**EDTA** Ethylenediaminetetraacetic acid
**FCS** Foetal calf serum
**GAG** Glycosaminoglycan
**H&E** Haematoxylin & Eosin
**$H_2O_2$** Hydrogen peroxide
**HCl** Hydrochloric acid
**IMS** industrial methylated spirit
**$MgCl_2$** Magnesium chloride
**MTT** 3-(4,5-Dimethylthiazol-2-yl)-2,5-diphenyltetrazolium bromide
**N** Newton
**NaOH** Sodium hydroxide
**NBF** Neutral buffered formalin
**OCT** optimal cutting temperature compound
**PAA** Peracetic acid
**PBS** Phosphate buffered saline
**PLC** Polycaprolactone
**PLGA** Poly (lactic-co-glycolic acid)
**PLLA** Poly-L-lactic acid
**RNA** Ribonucleic Acid
**RNAse** Ribonuclease
**rpm** Revolutions per minute
**SDS** Sodium dodecyl sulfate
**SE** Standard error
**s** Second (SI unit)

**StDev** Standard deviation
**TBS** Tris buffered saline
**TE** Tris-EDTA
**UTS** ultimate tensile strength
**v** Volume
**w/v** weight/volume
**YM** Young's modulus
**V** Voltage

# 1. Introduction

Injuries to the peripheral nerves are common and debilitating, affecting 2.8 % of trauma patients (Noble, Munro et al. 1998). Whilst the capacity of regeneration is a possibility, any defect size greater than 5-10 mm often results in poor functional recovery (Pfister, Gordon et al. 2011).

For treatment of larger gap injuries autologous nerve grafts are considered the "gold standard", however limitations of this technique include donor site morbidity and the need for multiple surgeries. Research into peripheral nerve regeneration has therefore focused on the use of alternative treatments in the form of nerve guide conduits (NGC) and acellular grafts, with the Food and Drug Administration (FDA) and Conformit Europe (CE) approving a relatively small number of NGCs (manufactured from naturally derived or synthetic material) and acellular grafts for clinical peripheral nerve repair (Kehoe, Zhang et al. 2011, Kehoe, Zhang et al. 2012).

Clinical data demonstrates that NGC have the ability to promote nerve repair up to 25 mm however drawbacks include toxic degradation products, lack of mechanical properties and overall limited efficacy in nerve regeneration compared to autologous nerve grafts (Weber, Breidenbach et al. 2000). It is postulated that a reason for the NGCs limited efficacy in nerve regeneration is its lack of surface topography such as the extracellular matrix (ECM) and basal lamina. It is hypothesised that substrate topography plays a significant role on cell morphology, behaviour, and cell-substrate interaction, as well as cell-cell interactions (Spivey, Khaing et al. 2012).

Use of cadaveric or donor nerve tissues can provide an ECM that mimics the native nerve tissue as well as offering the potential for size/length and motor/sensory specificity (Moore, MacEwan et al. 2011). These grafts contain an endoneurial microstructure and ECM components which can provide the same level of guidance and regenerative support as nerve autografts. The immunogenic components from the donor nerve graft can be removed through a processing condition called decellularisation to produce a non-immunogenic acellular nerve graft.

AxoGen Inc is the only medical device company which offers comercially available acellular allografts for peripheral nerve regeneration, the Avance® Nerve Graft. Avance® utilises the decellularised ECM from donated human peripheral

nerve tissue which has been processed using a combination of treatments including chemical decellularisation (detergent processing) to selectively remove cellular components and debris.

Clinical studies have shown the Avance ® graft surpassing the NGCs in terms of nerve regeneration and myelination (Whitlock, Tuffaha et al. 2009). Nonetheless the acellular graft does have its limitations. The use of human nerve donor tissue is fraught with complications in terms of gaining approval and cost. Furthermore clinical studies have shown that the Avance® graft only supports nerve regeneration over limited distances (up to 60 mm) (Saheb-Al-Zamani, Yan et al. 2013). Moreover, when compared to native nerve autografts the Avance® graft still only possessed reduced regenerative capacities (Whitlock, Tuffaha et al. 2009).

In recent years' focus has shifted in the use of xenogeneic ECM as scaffolds or grafts due to ease of harvesting and availability. The use of xenogeneic material has been used in a variety of biomedical applications such as heart valves (Booth, Korossis et al. 2002) and Matristem® for ulcer repairs (Badylak and Gilbert 2008). In addition, acellular xenogeneic nerve tissue from rat, rabbit and pigs have been widely used for peripheral nerve studies (Gutmann and Sanders 1943, Osawa, Tohyama et al. 1990, Hudson, Liu et al. 2004, Whitlock, Tuffaha et al. 2009, Zhang, Luo et al. 2010).

The limited regeneration reported in the Avance ® graft is most likely due to the grafts dependency on *in situ* Schwan cells to support axonal regeneration (Moore, MacEwan et al. 2011). Schwann cells play a crucial role in supporting axonal growth and migration. Following injury, these cells become activated, undergoing a phenotypic change from myelinating to growth supportive to help lead regenerating axons towards the distal nerve stump. It has therefore been hypothesised that the repopulation of the grafts with Schwann cells can help improve axon regeneration as well as extending the workable length of acellular grafts (Hadlock, Sundback et al. 2001, Zhang, Blain et al. 2002, Chang, Hsu et al. 2005).

This study describes the development of an acellular xenogeneic nerve graft through the combination of physical, chemical and enzymatic processess. Furthemore the study details the introduction of primary Schwann cells within the

graft for the study of cell-graft behaviour *in vitro* and peripheral nerve regeneration *in vivo*.

## 1.1 Physiology of the nervous system

The nervous system is one of the most highly organised systems within the human body, integrating various bodily processes and reactions of the organism to its environment. It is subdivided into the central nervous system (CNS) and peripheral nervous system (PNS), both differing in their physiology and function. The CNS is the larger system, comprising of the brain and spinal cord. The CNS conducts and interprets signals as well as providing stimuli to the PNS (Schmidt and Leach 2003). The PNS comprises a vast network of spinal and cranial nerves that are linked to the brain and the spinal cord receptors. The function of the PNS is to help process changes in the internal and external environment through sensory receptors that informs the CNS of the stimuli and motor neurons running from the CNS to the muscles and glands (Noback 2005) .

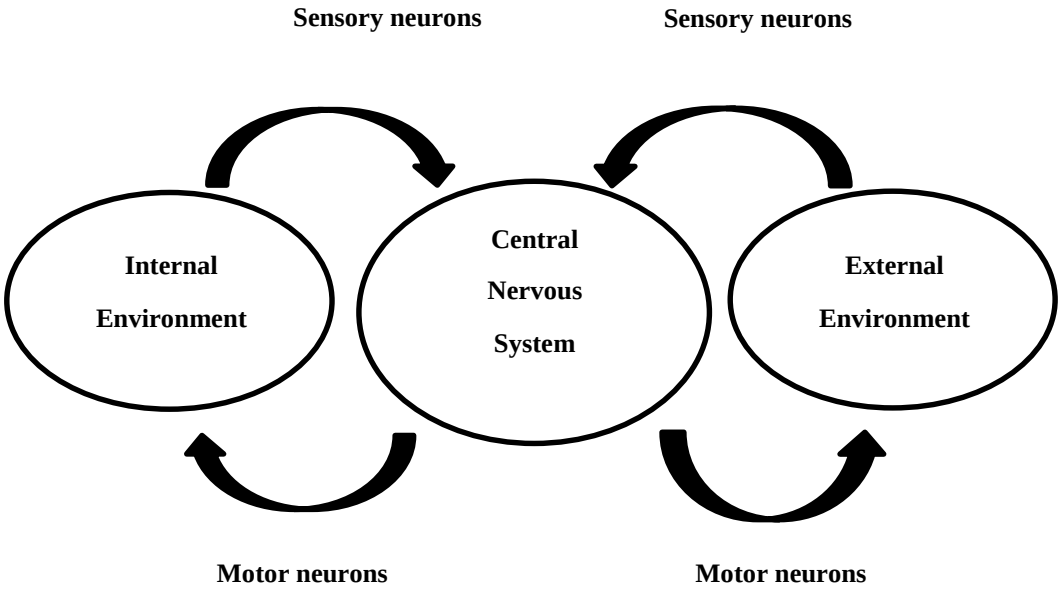


**Figure 1.1 Schematic depiction of how the CNS and PNS work together to process changes in the environment through sensory and motor neurons. Adapted from Huang and Huang (2006)**

## 1.2 Cellular components of the nervous system

Cells of the nervous system can be divided into two broad categories; nerve cells (or neurons) and supporting cells, neuroglia or glia. Neurons are specialised for electrical signalling over long distances. Glial cells aid the function of neurons and include astrocytes, microglial and oligodendrocytes in the CNS and Schwann cells in the PNS (Purves 2004).

Neurons are the basic structural and functional elements of the nervous system, consisting of a cell body (soma) and its extensions (axons and dendrites). The cell body contains the nucleus and organelles of the cells, dendrites transmit electrical signals to the neuron cell body and the axon conducts impulses away. The axon usually ends in several small branches known as the axon terminals. Neurons are often connected in networks; however, they never come in contact with one another. The axon terminals of one neuron are separated from the dendrites of an adjacent neuron by a small gap known as a synapse.

The electrical impulse moving through a neuron begins in the dendrites. From there, it passes through the cell body and travels along the axon. When the electrical impulse reaches the synapse at the end of the axon, it causes the release of specialised chemicals known as neurotransmitters. These neurotransmitters carry the signal across the synapse to the dendrites of the next neuron, starting the process again in the next cell. Neurons cannot divide by mitosis; however, they can regenerate a severed portion or sprout new processes under certain conditions.

Neuroglia or glial cells are the most abundant cell types, outnumbering neurons by a ratio of 3 to 1 in the brain. They are in direct contact with neurons, often surrounding them, unlike neurons, glial cells have some capacity for cell division (Huang and Huang 2006). Roles of glial cells include maintaining the ionic gradient of nerve cells, modulating the rate of nerve cell propagation, modulating synaptic action by controlling the uptake of neurotransmitters, providing a scaffold for neural development and aiding (or impeding in some cases) recovery from neural injury.

### 1.2.1 Cellular components of the CNS

In the CNS there are three types of glial cells; astrocytes, oligodendrocytes and microglial cells. Astrocytes, which are restricted to the brain and spinal cord, maintain an appropriate chemical environment for neuronal signalling. Microglial (immune) cells are primarily scavenger cells that remove cellular debris from sites of injury or normal cell turnover. In addition, these cells secrete cytokines that modulate local inflammation and influence cell survival or apoptosis. Oligodendrocytes lay down a lipid-rich sheath called myelin around specific axons. The myelin sheath acts as an electrical insulator, preventing short-circuiting between axons as well as increasing the propagation velocity of the nerve impulse, which is vital for those axons that extend long distances (up to 1 mm) (Schmidt and Leach 2003). The nodes of Ranvier are the only points where the axon is uncovered by myelin and ions of $Na^+$ and $K^+$ can be exchanged between it and the extracellular fluid. Depolarization of the axonal membrane at the nodes of Ranvier boosts the action potential that is transmitted along the axon and is the basis of jumping conduction.

### 1.2.2 Cellular components of the PNS

In the PNS, sheaths of Schwann cells surround all axons. Schwann cells enclose and separate unmyelinated nerve fibres from each other as well as producing myelin sheaths which wrap around large diameter axons of all motor neurons and some sensory neurons (Figure 1.2).

Myelinated axons are enclosed by many layers of compacted Schwann cell membranes, which form the myelin sheath, whereas unmyelinated axons retract into grooves in the Schwann cell cytoplasm (Maravilla and Bowen 1998). Each myelinating Schwann cell associates with a single axon and creates the myelin sheath necessary for salutatory nerve conduction. Non-myelinating Schwann cells are associated with small-diameter axons of C-fibres emanating from many sensory and all postganglionic sympathetic neurons. Each non-myelinating Schwann cell wraps around several sensory axons to form a Remak bundle, keeping individual axons separated by thin extensions of the Schwann cell body (Corfas, Velardez et al. 2004) .

In the CNS, oligodendrocytes make multiple segments of myelin that wrap around many axons. In contrast, in the PNS each Schwann cell makes only one segment of myelin. This is a reason why peripheral myelin regenerates more

efficiently. On the outer surface of the Schwann cell layer is a continuous basement membrane, neurilemma. Unlike CNS glial cells, Schwann cells secrete collagen, laminin and fibronectin (extracellular adhesive proteins). These proteins are the main constituent of the basal and basement lamina that surrounds the cell membrane of axons.

Schwann cells have many important functions in the peripheral nerve including aiding the conduction of nervous impulses along axons, nerve development and regeneration, trophic support for neurons, production of the nerve extracellular matrix (ECM), modulation of neuromuscular synaptic activity, and presentation of antigens to T-lymphocytes.

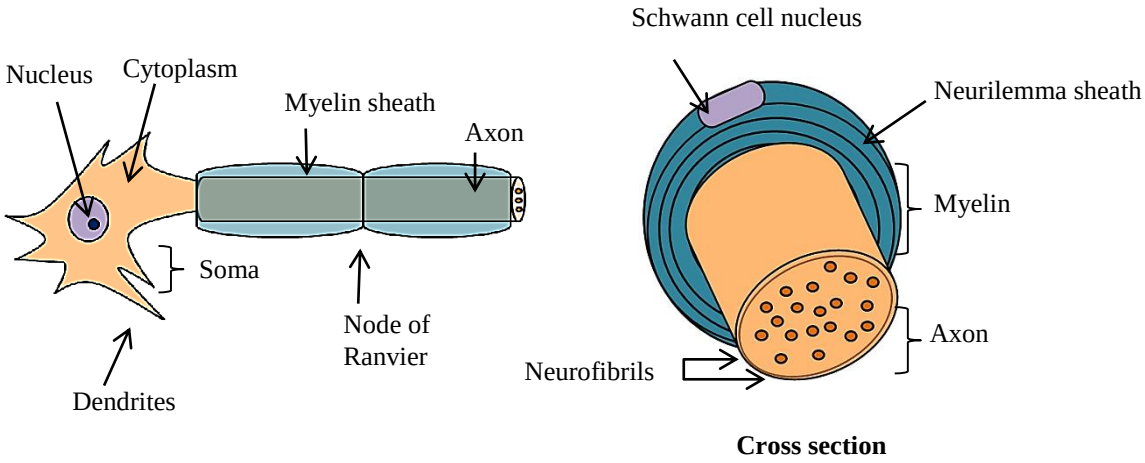


**Figure 1.2. Schematic representation of a Schwann cell. Peripheral motor neuron cell body and a cross section of the neuron.**

## 1.3 Anatomy of the nervous system: spinal cord and peripheral nerve

### 1.3.1 Anatomy of the spinal cord

The spinal cord is composed of dendrites, axons and cell bodies. The centre of the spinal cord is referred to as the grey matter containing neurons, glial cells and blood vessels. The grey matter is surrounded by white matter which helps protect and insulate the spinal cord. White matter consists of axons, oligodendrocytes, astrocytes and microglia. Axons project from the white matter in fascicles which exit the encasing bone of the spinal column, travel through the PNS-CNS transition zone and enter the PNS. The transition zone is a region where the glial cells in the CNS are separated from those in the PNS.

### 1.3.2 Anatomy of the peripheral nerve

Peripheral nerves consist of motor and sensory axons bundled together by support tissue into an atomically defined trunk. Each peripheral nerve consists of axons, Schwann cells, myelin sheath and connective tissue (endoneurium, perineurium and epineurium). Connective tissue encases the nerves to ensure flexibility as well as protecting the nerves from stretch and compression forces during body movement (Figure 1.3).

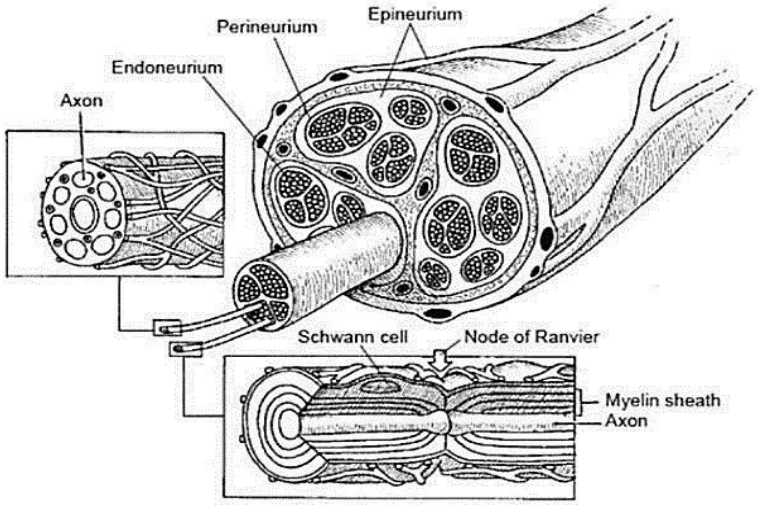


**Figure 1.3. Anatomical overview of the PNS. Figure reproduced from "Nerve Anatomy." A.D.A.M. Anatomy (Maki 2009)**

The endoneurium is the innermost component of the peripheral nerve sheath with Schwann cells being the most predominant cell type. The endoneurium also contains to a lesser extent fibroblasts, endothelial cells, macrophages and mast cells in addition to the collagen fibres and capillaries (Causey and Barton 1959). The perineurium consists of alternating concentrically arranged layers of flattened perineurial cells and collagen (Bunge, Wood et al. 1989); these layers are each enclosed by basal lamina and separated by spaces housing capillaries, collagen fibrils and elastic fibres (Thomas and Jones 1967).

The perineurium enclose individual fascicles of nerve fibres and function as a diffusion barrier to the movement of ionic compounds and macromolecules between non-neural tissues and the endoneurium (Alovskaya, Alekseeva et al. 2007). The epineurium, an outer sheath of loose connective tissue containing fibroblasts, collagen and fat, binds individual nerve fascicles into a nerve trunk. Peripheral nerves are vascularised by capillaries within the connective tissue of the

nerve trunk or by vessels that penetrate the nerve from surrounding arteries and veins (Schmidt and Leach 2003).

### 1.3.3 Peripheral nerve extracellular matrix (ECM)

The basal lamina and ECM are the non-cellular components of the nerve tissue that along with Schwann cells and axons comprise the endoneurium and form nerve fascicles. The basal lamina is a Schwann cell product consisting of continuous laminin tubes (~10μm diameter) embedded within the ECM (Figure 1.4). The basal lamina also contains fibronectin, collagen type IV and V, heparin sulphate proteoglycan, tenascin and entactin, all of which help promote axonal outgrowth (Weinstein 1999).

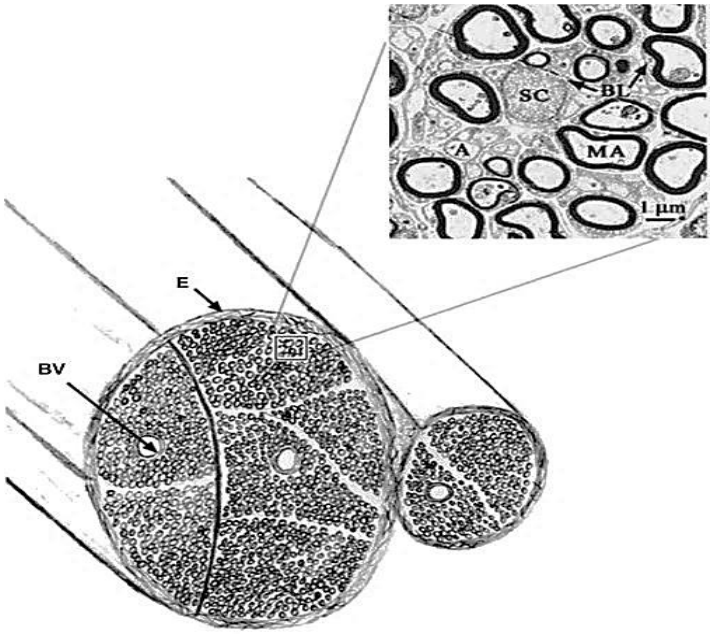


**Figure 1.4. Illustration and transmission electron microscopy (TEM) image of a cross-section of a peripheral nerve. The TEM image is of a rat sciatic nerve; Axons (A), Schwann cells (SC), blood vessels (BV) and an extracellular matrix (ECM) are held within the nerve by the epineurium (E). Schwann cells wrap around individual axons to form myelinated axons (MA). The ECM includes the epineurium, basal laminae (BL), and the interstitial endoneurium. Basal laminae surround myelinated axons, and the interstitial endoneurium provides structural support between the basal laminae. Reproduced from Hudson, Liu et al. (2004)**

The ECM is a highly dynamic three dimensional network represented by the secreted products of resident cells (i.e. Schwann cells) such as proteins, glycoproteins and proteoglycans. The ECM provides structural support for tissues, cell layers and individual cells as well as fundamental cell processes such as cell growth, adhesion, migration, proliferation, differentiation and gene expression (Gao, Wang et al. 2013) by sensing different environmental stimuli and providing specific inputs to the surrounding cells. In addition, the ECM captures a wide range of cellular growth factors so changes in the physiological conditions and specific stimuli can trigger the local release and activation of those factors. In the PNS the three dimensional ultrastructure, surface topology and composition of the ECM provide precise guidance for axonal regeneration. In peripheral nerve tissue, the important ECM components include collagen types I, III, IV and V, laminin, fibronectin and chondroitin sulphate proteoglycans (CSPGs) (Gao, Wang et al. 2013).

Collagen is a structural protein and is the main ECM constituent found in all three connective tissue layers within the PNS. Collagen type I and III together constitute approximately 49% of total protein in the nerves (Bunge, Bunge et al. 1989). The collagenous matrix surrounds and protects individual axons and their Schwann cell sheaths from trauma (Lundborg 2004). In the PNS, two classes of collagen molecules are expressed; fibril forming collagens (type I, III, and V) and basement membrane collagens (type IV) (Koopmans, Hasse et al. 2009). Collagen I, the most predominant collagen in the human body, is localised primarily in the epineurium whilst collagen III is located within the endoneurium and perineurium. Collagen V co-localises with both collagen I and III, however it is also present in the basal lamina, enveloping myelinating Schwann cells (Chernousov, Rothblum et al. 2006).

Whilst the bulk of fibril forming collagen is synthesized by fibroblasts, Schwann cells and perineurial cells secrete the non-fibrillar type IV collagen of the basal lamina. Collagen IV is an important structural component of basement membranes, integrating ECM proteins such as laminin and perlican into a stable supramolecular aggregate (Hudson, Reeders et al. 1993), lining the outer aspect of endoneurial capillaries as well as surrounding the processes of Schwann cells and perineurial cells (Alovskaya, Alekseeva et al. 2007).

Laminins are glycoproteins, existing within the endoneurium and perineurium of the peripheral nerve (Palm and Furcht 1983), forming a major structural element of the basement membrane, the basal lamina (Timpl 1996). They are produced by Schwann cells and are distributed along the cell surface in a continuous band. Evidence suggests that Schwann cells require the formation of an organised basal lamina to properly ensheath and myelinate axons (Obremski, Johnson et al. 1993). Laminin plays many roles within the PNS including promoting neurite outgrowth and survival (Edgar, Timpl et al. 1984) such as laminin-2 (α2β1γ1) and laminin-8 (α2β1γ1), which are important for postnatal nerve development and are upregulated for axonal regeneration after injury (Wallquist, Patarroyo et al. 2002). Laminin also act as a ligand for cell surface receptors (e.g. integrins, heparin and α-dystroglycan), thereby initiating signals that influence cell behaviour and survival (Schwartz 2001) such as cell adhesion (Nomizu, Kuratomi et al. 1998), proliferation (Kubota, Tashiro et al. 1992), migration (Colucci, Giannelli et al. 1996) and differentiation (Rozzo, Ratti et al. 1993). In addition laminin also provides attachment points for axons to extend and exert forces on the ECM (Laura, Leipzig et al. 2008).

Fibronectin is a cell surface associated glycoprotein produced by Schwann cells, predominantly located in the perineurium. They contain different functional domains that directly bind onto various molecules such as fibrin, collagen and heparin (White and Muro 2011), as well as two domains that support cell adhesion. In the PNS neurons can extend neurites on the two domains (Humphries, Akiyama et al. 1988). Fibronectin also plays a role in peripheral nerve repair as they promote Schwann cell growth (Baron-Van Evercooren, Kleinman et al. 1982).

GAGs such as CSPGs are proteoglycans consisting of a protein core and a chondroitin sulphate side chain, which are produced by Schwann cells. In the PNS they exist mainly in the basal lamina and ECM surrounding collagen fibrils (Aquino, Margolis et al. 1984). These proteoglycans have been implicated in the regulation of axonal growth, however it has been found that CSPGs bind to and inhibit the neurite-promoting activity of laminin. It has been observed that after a nerve injury there are markedly upregulated levels of inhibitory CSPGs levels which accumulate in the endoneurial tissue surrounding the Schwann cell basal laminae (Zuo, Hernandez et al. 1998); consequently CSPGs play a negative role in nerve regeneration.

## 1.4 Nerve injury and regeneration

When the CNS is injured the physiological response from the body is the slow infiltration of macrophages to the site of injury. A blood-spine barrier delays the removal of the inhibitory myelin by limiting macrophage entry to only the site of injury (Avellino, Hart et al. 1995). In addition, cell adhesion molecules in the distal end of the injured spinal cord are not readily upregulated, thereby limiting macrophage recruitment. Astrocytes also respond to the injury by proliferating and producing glial scars that inhibit regeneration (McKeon, Schreiber et al. 1991).

The PNS is typically damaged by traumatic injury (i.e. stretch, crush, lacerations and ischemia), surgery or repetitive compression (e.g. carpel tunnel syndrome). A recent study revealed that 87% of PNS injuries were from trauma and 12% due to surgery. Over 81% of nerve injuries occurred in the upper extremities and 11% in the lower extremities with the balance in other locations (Pfister, Gordon et al. 2011). Injury to the PNS can range from severe, leading to major loss of function or intractable neuropathic pain, to mild, with some sensory and/or motor deficits affecting quality of life (Pfister, Gordon et al. 2011). In contrast to the CNS, the microenvironment surrounding an injury site in the PNS is often more permissive to axonal regeneration. Over relatively short distances (less than 5 mm), axons can spontaneously regenerate (Rangappa, Romero et al. 2000).

### 1.4.1 Peripheral nerve regeneration

When a nerve is injured or transected, the transected fibres distal to the lesion are disconnected from the neuronal body. Immediately after, the proximal and distal nerve stumps retract, axoplasma (cytoplasm within the axon of a neuron) leaks out and breakdown of the cytoskeleton and dissolution of the cell membrane occurs. The proximal end of the nerve stump however experiences minimal damage. This process is known as chromatolysis and reflects the change from the production of neurotransmitters needed for synaptic activity to the production of materials needed for axonal growth and repair (Seckel 1990). At the distal end Schwann cells shed their myelin lipids and surround the axons. Macrophages are recruited to the site of lesion and contribute to the lysis and phagocytosis of myelin and axon debris and subsequent Schwann cell proliferation. Both cell types play a role in enhancing axonal regeneration and myelination by secreting cytokines and growth factors.

In the first few days' post injury Wallerian degeneration takes place in the distal axonal stump. This is a process which serves to create a microenvironment distal to the injury site that favours axonal growth. This involves the degeneration of axons, myelin sheath detachment and degradation of the distal portion of the nerve by protease activity and the separation from the metabolic resources of the nerve cell bodies. During the degeneration the basal lamina which had formerly covered the myelinating Schwann cell-axon unit is spared. This leaves intact "endotubes" formed by the residual basal lamina and Schwann cells which still remain viable. These endotubes form channels into which the regenerated axons will grow (Weinstein 1999)

Following debris clearance by activated macrophages, and a local inflammatory environment, Schwann cells within the distal stump are stimulated to proliferate within their basal lamina tubes forming the bands of Büngner. This proliferation carries on for approximately 2 weeks with the Schwann cells forming "rail tracks" which guide the regenerating axons to their target (Terenghi 1999). Regeneration begins at the proximal end and continues towards the distal stump with new axonal sprouts emanating from the nodes of Ranvier to restore function (Figure 1.5). In humans, axon regeneration occurs at a rate of 1 mm/day (Allodi, Udina et al. 2012).

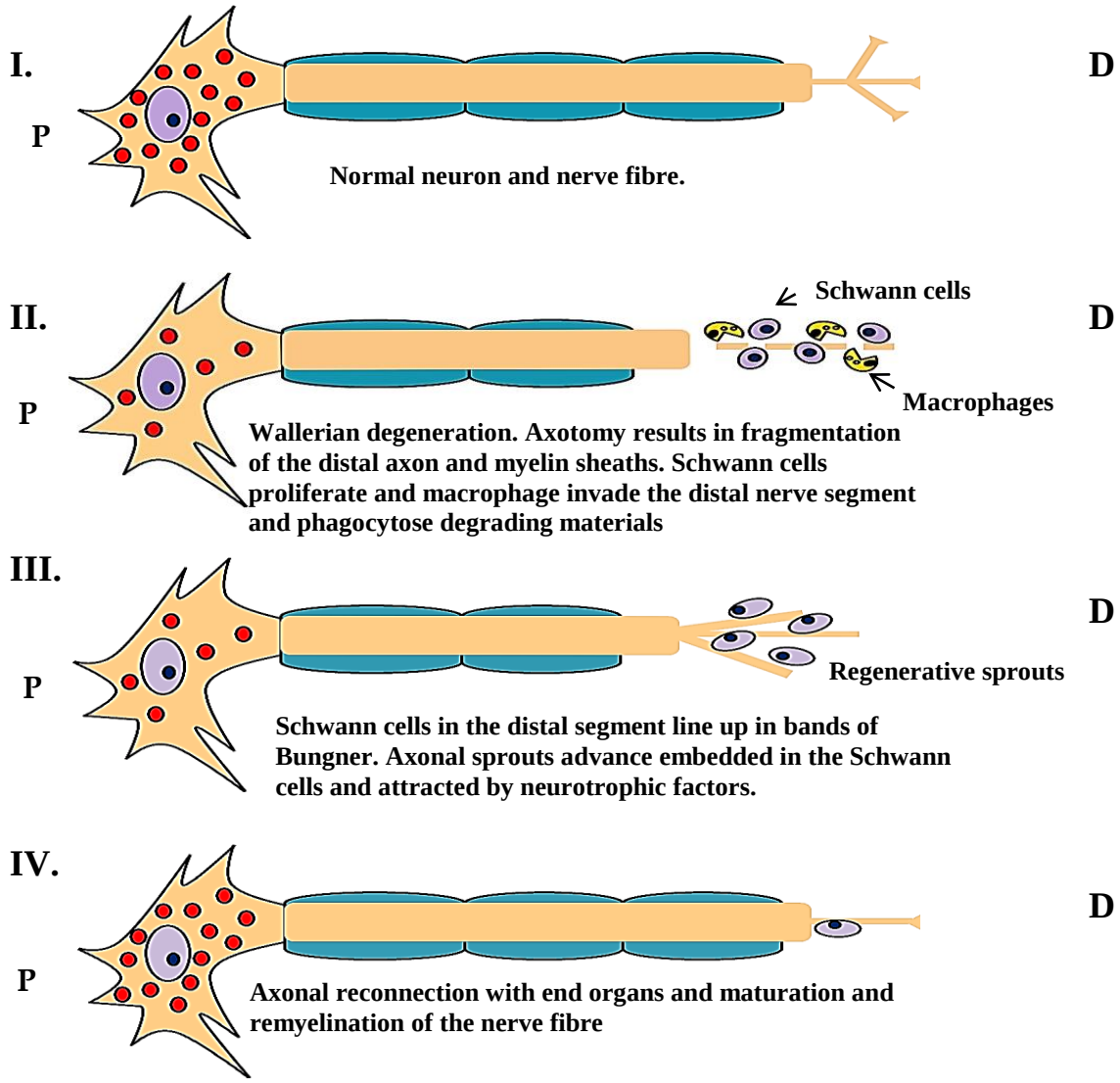


**Figure 1. 5. Degeneration and regeneration after peripheral nerve injury. P = proximal and D = distal. Adapted from Allodi, Udna et al. (2012) and Chaudhry, Glass et al. (1992).**

The regenerative sprouting of the proximal axon requires elongation of the axon. This is mediated by the growth cone (Seckel 1990). A growth cone is a motile extension of the regenerating nerve fibre seeking its synaptic target. It advances through the tissue by releasing a protease which dissolves the matrix (Krystosek and Seeds 1981).

Growth cones consist of mobile filopodia extruding from a flattened sheet of lamellipodia. This enables them to move and to explore the microenvironment of the regenerating axons. Actin influences this motility. The growth cone plays an essential role in axon guidance and responds to contact guidance clues afforded by adhesive molecules that are presented on a neighbouring cell surface such as

transmembrane cell adhesion molecules (CAMs) or those that are assembled into the ECM such as laminin and fibronectin (Figure 1.6).

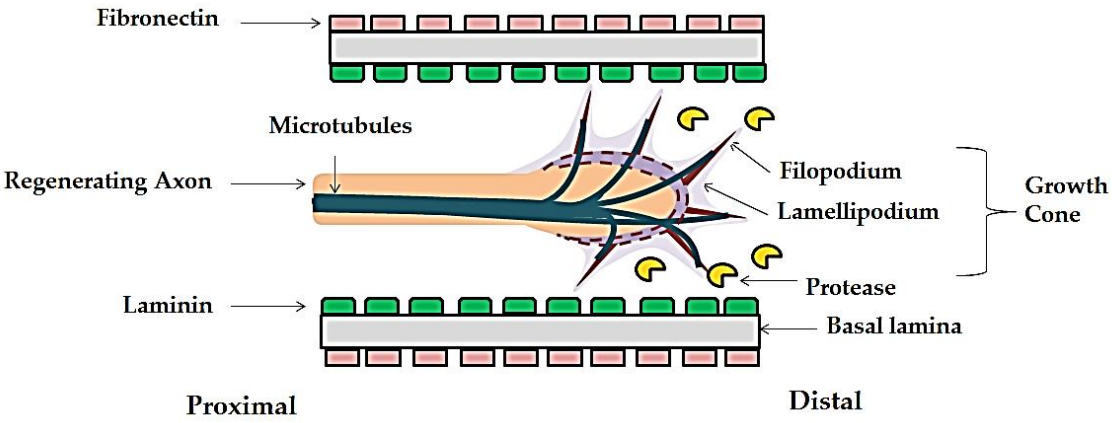


**Figure 1.6. Growth cone of a regenerating axon. Adapted from Lowery and Van Vactor (2009)**

### 1.4.2 Classifications of nerve injury

There are different classifications of nerve injury; neurapraxia, axonotmesis and neurotemesis are the three discrete types first described by Sir Herbert Seddon in 1943 with the addition of two intermediate steps in 1954. Dellon and Mackinnon described a 6$^{th}$ degree nerve injury, one which combines several of these degrees of injuries per fascicle (Table 1.1) (Evans 2001). The classification of the 6$^{th}$ degree of nerve injury allows possible replacements of individual fascicles as opposed to the entire injured nerve. When surgical repair of the nerve is required, the goal is to guide regenerating sensory, motor, and autonomic axons to the distal, degenerating nerve segment to maximize the chance of target reinnervation.

| Degree of Injury | Pathology | Treatment | TEC | Prognosis |
|---|---|---|---|---|
| **I. Neurapraxia** | Axons not disrupted. Possible segmented demyelination | None | No | Full recovery<br>Days up to 3 months |
| **II. Axonotmesis** | Axon lost. Endoneurium, perineurium and epineurium intact | None. Slow regeneration<br>2–3 cm per month | No | Good, rate is slow |
| **III.** | Axon lost. Endoneurium disrupted. Perineurium and epineurium intact | None. Surgery only if no recovery in 2–3 months.<br>Slow regeneration<br>2–3 cm per<br>month | ? | Incomplete<br>axonal loss and misdirection |
| **IV.** | Axon lost. Endoneurium and perineurium disrupted.<br>Epineurium intact | Surgery required to remove scar tissue. Autograft or<br>conduit for gaps | Yes | Regeneration only after repair. Availability of graft material |
| **V. Neurotmesis** | Complete disruption of nerve | Surgical repair to proximate the two ends. Direct repair, autograft or<br>conduit for gaps | Yes | Regeneration only after repair. Availability of graft<br>material |
| **VI. Mixed injury** | | Surgical repair | Yes | |

**Table 1.1. Classification of peripheral nerve injuries; TEC = tissue engineered constructs. Adapted from Pfister, Gordon et al. 2011**

Each category has its own complications and clinical symptoms; however, evidence is in support that an increase in the degree of injury indicates an increase in severity and decrease in recovery. After axonotmesis the connective sheaths of the nerve are preserved and only the axons are injured so functional recovery is good. In contrast after neurotmesis (nerve transection) the endoneurial tubes lose their continuity, axons are misdirected and reinnervate incorrect target organs leading to poor functional outcomes. Witzel et al. (2005) estimated that only 10% of axons after a nerve transection and ‘‘best’’ surgical apposition reach target organs (Witzel, Rohde et al. 2005).

Inappropriate targets can be reinnervated by axtomised nerves i.e. efferent motor axons may be misdirected to sensory end organs resulting in degradation or loss of function depending on the severity of the mismatch (Allodi, Udina et al. 2012). As surgical repair techniques cannot be further refined there is a need for new and improved strategies to enhance specific axonal regeneration.

## 1.4 Clinical need for peripheral nerve repair

Several hundred thousand nerve injuries occur worldwide each year, with over 300,000 cases reported annually in Europe (Mohanna, Young et al. 2003) and over 360,000 (of the upper extremity) in the USA (Belkas, Shoichet et al. 2004); this has associated annual costs of $7 billion (American Paralysis Association, 1997). Currently, there is no effective treatment for damage to the CNS, and acute spinal cord injury has been resistant to treatment (Evans 2001). Compared to spinal cord injury, injuries of the peripheral nerves are more common and debilitating, affecting 2.8% of trauma patients. Nevertheless despite recent advancements peripheral nerve injury remains a critical clinical issue with over 50,000 procedures performed annually in the United States alone (Noble, Munro et al. 1998).

The assumption has been that peripheral nerve injuries recover, given the observation of spontaneous axonal regeneration following injury. Whilst this capacity of regeneration is higher than that of the CNS, complete recovery is infrequent, misdirected or associated with debilitating neuropathic pain. Axon regeneration progresses at a slow rate. The rate of axon regeneration varies from 1-2 mm/day in small nerves and 5 mm/day in large nerves (Recknor and Mallapragada 2006) and any defect size greater than 5-10 mm often results in poor functional recovery (Pfister, Gordon et al. 2011). Nerve transection is usually

associated with poor outgrowth, particularly when the distance between injury and target is long.

Despite best efforts and modern surgical techniques functional restoration is often incomplete, with approximately 50% of surgical cases achieving normal to good restoration of function.The incidence of PNS injury is grossly underestimated due to the span of causes and the intervention from many clinical disciplines, including orthopaedic surgery, plastic surgery and neurosurgery however it presents a critical clinical issue (Pfister, Gordon et al. 2011). Therefore, there is need for biomedical research to develop novel strategies to improve outcomes following nerve damage

## 1.5 Current clinical approaches for treating peripheral nerve injuries

Current treatment for peripheral nerve injury consists of either direct end-to-end surgical suturing of the damaged nerve ends or the use of an autologous nerve graft. Suturing is limited to the repair of small defects or gaps in the nerve, for longer nerve gaps this approach is not desirable because any tension introduced into the nerve cable would inhibit nerve regeneration.

For longer nerve gaps the current “gold standard” treatment is autologous grafting; using donor sensory nerve tissue (usually the sural nerve) which is harvested from another site in the body to replace the injured tissue. Limitations using this method include donor site morbidity and chronic pain. Sural nerves in general possess a typically small diameter so multiple sural nerve segments are placed side by side to match the width of the nerve being replaced (Dahlin 2008). This means that there is also the risk of lack of donor nerve tissue if the nerve injury is substantial. In addition, sural nerves also possess smaller fascicular patterns (i.e. the number and size of fascicles) which do not match the fascicular patterns of the nerve being grafted (Meek and Coert 2002) which can cause misdirection and misalignment, and is why the autologous clinical functional recovery rates is only 80% (Schmidt and Leach 2003).

## 1.6 Nerve guides conduits (NGCs) and grafts to aid peripheral nerve regeneration

It is commonly accepted that physical guidance of axons is a vital component of nerve repair and regeneration. In the 1960's Millesi determined that nerve grafts reduced the tension on damaged nerves as well as enhancing functional recovery. Current research focuses on "entubulating" opposing nerve stumps of the severed nerve in an autograft tube known as a Nerve Guidance Conduit (NGC) (Kehoe, Zhang et al. 2011). These conduits can be used for defects of 20 mm - 25 mm and eliminates the need to graft. Advantages of NGCs over autografts is their unlimited supply, no donor-site morbidity, no restriction by fascicular sizes and they can provide the regenerating nerve fibres with the ability to seek their own path to their targets with a high degree of specificity through neurotropism (Shin, Friedrich et al. 2009).

Once nerves are sutured into the ends of the conduit, protein-rich (axoplasmic) fluid, containing growth factors exudates from the stumps and are released into the NGC. Within days a fibrin matrix forms, providing support for the migration of Schwann cells, fibroblasts and macrophages (Figure 1.7).

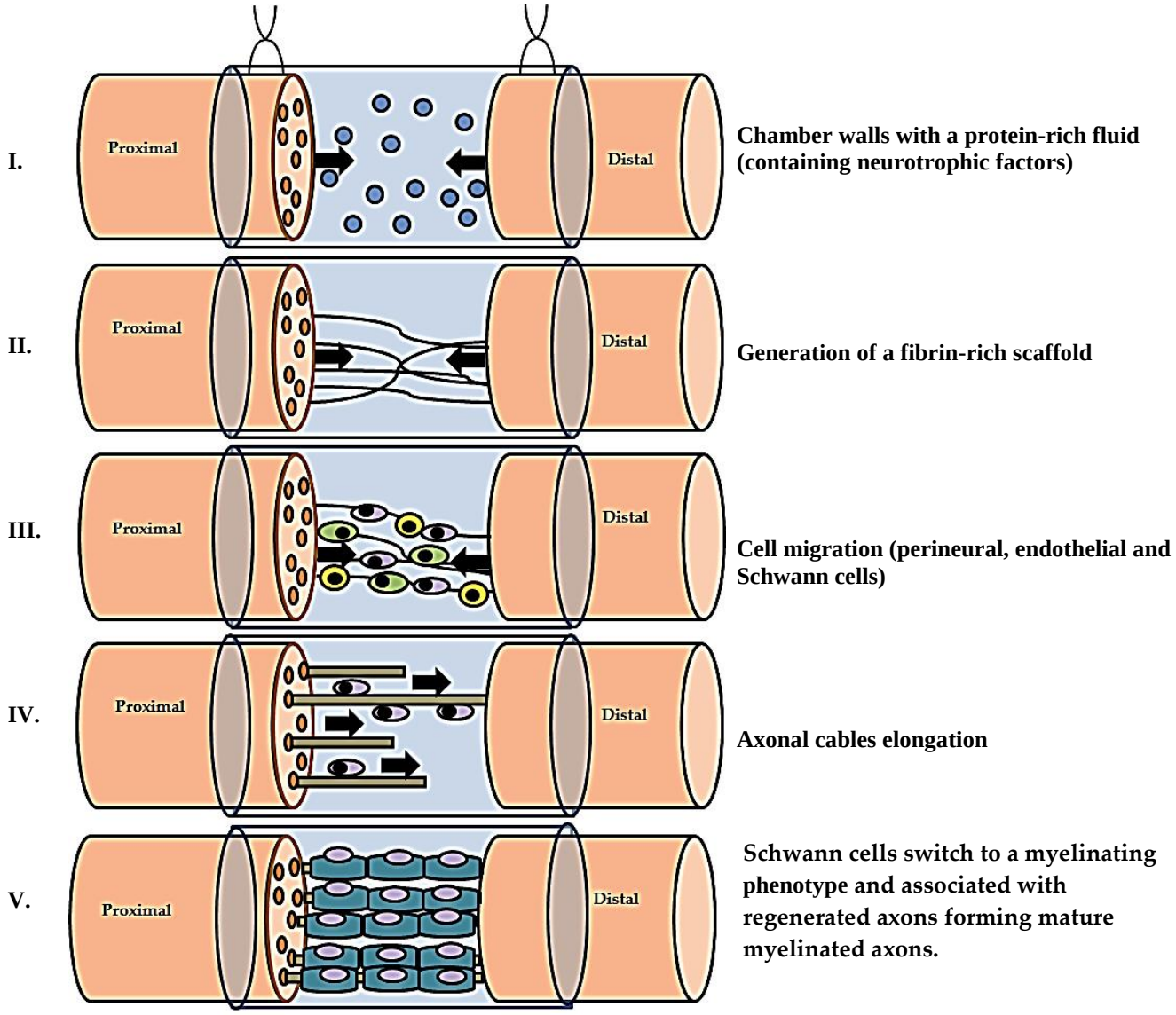


**Figure 1.7; Principle of nerve entubulisation and the sequence of events leading to the growth of a new nerve cable: Adapted from Heath and Rutkowski (1998); Belkas, Shoichett et al. (2004); Daly, Yao et al. (2012)**

The role of an NGC is to mechanically support and direct axonal sprouting between the injured nerve stumps by providing a guidance cue (via a tubular 3D structure). The NGC also needs to prevent fibrous tissue ingrowth into the injury site and retain the neurotrophic factors secreted by damaged nerve ends. The design criteria of an NGC should include:

I. Biocompatibility so to not evoke an inflammatory response
II. Biodegradability, however the NGC must retain a mechanically stable architecture during the regeneration process
III. Flexibility, to prevent compression of regenerating axons and limit tissue inflammation
IV. Semi-permeability to allow diffusion of oxygen and nutrients through pores. Ideal pore size range between 5-30µm. Pore sizes less than 5µm inhibits cell and tissue proliferation whilst pore sizes exceeding 30µm increases infiltration of inflammatory cells into the conduit
V. Meeting clinical requirements for further production, sterilization, long-term storage and surgical handling such as suturing.

The Food and Drug Administration (FDA) and Conformit Europe (CE) have approved a relatively small number of guidance conduits for clinical repair of peripheral nerves. These NGC devices can be grouped into naturally derived or synthetic as well as resorbable and non-resorbable material (Table 1.2).

| Commercial Name | Company | Material |
|---|---|---|
| **Neuragen ®/NeuraWrap ™** | Integra | Type I collagen |
| **Neurolac ®** | Polyganics | PDDL/CL |
| **Neurotube ®** | Synovis | PGA |
| **Neuromatrix/Neuro*flex*™ Conduits and NeuroMend ™ wrap** | Collagen matrix Inc | Type I collagen |
| **Salubridge ™/SaluTunnel ™** | Salumedica | Polyvinyl alcohol hydrogel |
| **Surgisis ®/Axoguard ™** | AxoGen Inc | Porcine small intestinal submucosa |

**Table 1.2 Summary of commercially available nerve guides and wraps. Adapted from Waldram (2003); Bell and Haycock (2011)**

### 1.6.1 Naturally derived nerve guides

There has been great focus on using purified natural ECM proteins and GAGs as natural scaffolds for nerve regeneration. ECM molecules such as collagen, laminin and fibronectin have shown to play a significant role in axonal development and repair *in vivo.* Furthermore proteoglycans and GAGs are known to modulate neural activity and neurite extension as well as providing stimulatory and inhibitory cues (Bovolenta and Fernaud-Espinosa 2000).

Investigation using silicone tubes filled with ECM molecules have shown improved regeneration over a 10 mm rat sciatic nerve gap compared to controls (Chen, Hsieh et al. 2000). Other studies have shown that orientated fibres of collagen within gels can provide an ideal template for neurite extension as well as an ideal matrix for Schwann and neurite migration (Ceballos, Navarro et al. 1999).

Additional naturally derived molecules currently under investigation include hyaluronic acid, fibrinogen, agarose, alginate, chitosan and self-assembling peptides. Tissue engineering techniques are being applied to modify these materials to make them applicable for nerve repair applications by applying chemical cross-linking, magnetic fields or the addition of biomolecules (Schmidt and Leach 2003).

### 1.6.1.1 Clinically available naturally derived resorbable devices

Neuragen® and Neuromatrix/Neuro*flex*™ conduits are derived from collagen I. Collagen I, a major component of the ECM is a commonly used biomaterial as it can be easily isolated and purified and made to offer varying degrees of resorbability. Collagen has an established record of biocompatibility and has been shown to support and guide tissue regeneration *in vivo.* However, despite its abundance there is still an issue of batch-to-batch variations that can compromise reproducible performances. Furthermore undesirable immune responses may occur in some devices, therefore there is a requirement to use immunosuppressive drugs (Kehoe, Zhang et al. 2011).

Neuragen® conduits degrade after 48 months and have been reported to have comparable efficacy to autologous grafts in defects up to 20 mm in clinical studies. In addition, pre-clinical studies showing efficacy in defects up to 40 mm. To this date no other FDA device has reported levels of efficacy up to this gap length in literature. However, the limitation is the time required for complete biodegradation to occur may lead to nerve compression. In contrast Neuromatrix/Neuro*flex*™ conduit resorbs *in vivo* over a period of 4-8 months. However these conduits have been designed to bridge nerve gap defects that do not exceed 2.5 cm (Kehoe, Zhang et al. 2011).

| **Available FDA/CE-approved naturally derived resorbable nerve conduits** | | |
|---|---|---|
| | NeuraGen ® | NeuroMatrix/NeuroFlex™ |
| **Composition** | Type I collagen | Type I collagen |
| **Company** | Integra NeuroSciences Plainsboru, NJ, USA | Collagen Matrix Inc Franklin Lakes, NJ, USA |
| **Maximum Length** | 3 cm | 2.5 cm |
| **Diameter** | 1.5-7 mm | 2-6 mm |
| **Clinical data (PubMed)** | Yes | No |
| **Degradation Time** | 4 years | 4-8 months |
| **Price (The Netherlands)** | €1200 | €600 |

**Table 1.3. Summary of clinically approved naturally derived resorbable nerve conduits. Reproduced from Meek and Coert (2008)**

### 1.6.2 Synthetic nerve guides

Synthetic materials are ideal as their chemical and physical properties (degradation rate, porosity, mechanical strength) can be optimised for particular applications. Their limitation however lies in their biocompatibility *in vivo* as the body's response can vary from one material to another. In some cases, the material may cause an inflammatory response or may be incompatible with cell adhesion or tissue repair, hindering the regeneration process. However, through tissue engineering there are various ways to modify the material to make it more biocompatible.

A number of different synthetic materials have been explored for use in aiding nerve regeneration including non-degradable polymers like silicone, biodegradable polymers such as poly(lactic-*co*-glycolic acid) (PLGA), poly (ε-caprolactone (PCL), poly L-lactic acid (PLLA) (Subramanian, Krishnan et al. 2009). Researchers have also shown that electrical charges play a significant role in stimulating cellular different for various tissue types. Piezoelectric material such as poly (vinylidene fluoride) (PVDF) and electrically conducting polymers (polypyrrole, polyaniline) are known to significantly enhance neurite extension. Further modification of these materials with biological stimuli i.e. hyaluronic acid may create interactive biomaterials for use as nerve guidance channels (Schmidt and Leach 2003).

#### 1.6.2.1 Clinically available synthetic resorbable devices

Synthetic resorbable devices are deemed desirable as surface erosion permits the device to retain its structural stability for a longer time after implantation. A surface eroding polymeric device is also expected to provide better contact guidance cues for nerve regeneration.

Neurotube®, a highly porous bioresorbable device made from polyglycolide acid (PGA), is a woven tubular device with a grooved surface. The grooved surface helps the resistance of occlusive forces of surrounding soft tissue. Neurotube® shows excellent degradability, good initial mechanical properties and is associated with high levels of cell viability. Amongst surgeons it is considered the preferential synthetic device due to its length (2 cm), price and wide availability of clinical data.

In randomised clinical trials the device has been reported to have comparable efficacy to autologous treatment in defects up to 20mm. Moreover, pre-clinical data exists for this device showing efficacy in gap defects up to 30 mm.

However, limitations include its high rate of degradation and the device losing its initial strength (1-2 months *in vivo*). Other disadvantages include the production of acidic degradation products (glycolate and pyruvate) as well as its low solubility.

Neurolac® is the only approved transparent device, a feature which helps aid the clinician during surgical insertion across the nerve gap defect. It is composed of the co-polymer poly (D, L-lactide-co-ε-caprolactone) (PCL) and is highly soluble in a wide range of organic solvents and its crystalline nature enables it to form at relatively low temperatures. The device is able to degrade at a steady rate without producing toxic degradation products.

In clinical trials Neurolac® has been reported to have comparable efficacy to the autologous standard in defects up to 20 mm. Limitations of this device however include its high rigidity, with Meek et al 2008 noting frequent breakages of needles when suturing the device in place (Meek and Coert 2008). Rigidity can also lead to nerve stumps being torn out of the NGC lumen during the regeneration period due to the inflexibility over the joints during immobilisation. Other limitations associated with the device include severe foreign body reactions and swelling, fragmentation due to incomplete degradation as well as early collapse of the device leading to neuroma formation.

| **Available FDA/CE-approved synthetic resorbable nerve conduits** | | |
|---|---|---|
| | Neurotube ® | Neurolac ® |
| Composition | Polyglycolic acid | Poly ($^{65}/_{35}$($^{85}/_{15}$$^{L}/_{D}$) lactide-ε-caprolactone) |
| Company | Synovis | Polyganics BV |
| Maximum Length | 4 cm | 3 cm |
| Diameter | 2.3-8 mm | 1.5-10 mm |
| Clinical data (PubMed) | Yes | Yes |
| Degradation Time | 6-12 months | 2-3 years |
| Price (The Netherlands) | ±Euro 340 | ±Euro 700 up to 1800 |

**Table 1.4. Summary of clinically approved synthetic resorbable nerve conduits. Reproduced from Meek and Coert (2008)**

### 1.6.2.2 Clinically available synthetic non-resorbable device

Salubridge ™ / SaluTunnel ™ are non-resorbable nerve cuff hydrogels composed of a hydrophilic and non-degradable biomaterial called Salubria™. The Salubria™ hydrogel mimics human tissue in terms of its softness and compliancy. SaluTunnel™ is identical in structure and composition to the Salubridge™ apart from a longitudinal slit to facilitate ease of surgical placement; thereby this device is used in the management of peripheral nerve injuries in which there has been no substantial loss of nerve tissue. However, the non-resorbable nature of these devices can lead to issues relating to higher risks of infection and chronic inflammation as well as nerve compression and tension at the suture lines after nerve regeneration.

| **Available FDA/CE-approved synthetic non-resorbable nerve conduits** | |
|---|---|
| **Salubridge ™ /SaluTunnel ™** | |
| **Composition** | Salubria-polyvinyl alcohol (PVA) hydrogel |
| **Company** | Salumedica LLC, Atlanta, GA, USA |
| **Maximum Length** | 6.35 cm |
| **Degradation Time** | Non-biodegradable |

**Table 1.5. Summary of clinically approved synthetic non-resorbable nerve conduits. Reproduced from Meek and Coert (2008)**

## 1.6.3 Motor outcomes after reconstruction of nerve defect using NGCs

The majority of data reporting the clinical success of NGCs in promoting nerve regeneration has been with respect to sensory nerve recovery (Weber, Breidenbach et al. 2000, Taras and Jacoby 2008).

There have been few case reports on motor nerve recovery (Ashley, Weatherly et al. 2006, Donoghoe, Rosson et al. 2007, Inada, Hosoi et al. 2007), however the focus was primarily on animals and the evaluation carried out using either compound muscle action potentials or walking track analysis to quantify motor recovery are known to have high variability and are indirect (Shin, Friedrich et al. 2009).

Clinically motor recovery is inferior to sensory recovery following repair (Gattuso, Glasby et al. 1989, Duteille, Petry et al. 2001). Motor nerve reconstruction differs from the sensory reconstruction as there are time dependant

degradation and ultrastructural changes of the muscle as well as irreversible changes that occur at the motor end plate (Bain, Veltri et al. 2001, Shin, Friedrich et al. 2009).

A study conducted by Shin et al 2009 used a rat sciatic nerve model to compare the efficacy of the three clinically synthetic bioabsorbable NGCs (Neurolac®, Neurotube® and NeuraGen®) in terms of motor nerve recovery. Maximum isometric tetanic force with optimisation of variables was used as the primary measure of motor outcomes. Results showed no significant difference between the Neurolac® conduit and autograft in all the assessments. Neurolac® did however outperform the other commercially available NGCs and Neurotube® repairs were significantly worse than other repairs in all assessments (Table 1.6). Nonetheless other studies with Neurotube® show a more positive outcome in human studies (Bain, Veltri et al. 2001, Navissano, Malan et al. 2005, Inada, Hosoi et al. 2007). This disparity may be attributed to a number of factors such high degradation rate and nerve lumen size mismatch.

| | Autograft | Neurolac ® | NeuraGen ® | Neurotube ® |
|---|---|---|---|---|
| **Isometric tetanic force** | | | | |
| **Anterior isometric tetanic force recovery of tibialis anterior (%)** | 37 ± 17 | 34 ± 13 | 23 ± 11 | 3 ± 5 |
| **Recovery rate of tibialis anterior (%)** | 100 (20/20) | 94 (17/18) | 100 (19/19) | 29 (4/17) |
| **Compound muscle action potentials** | | | | |
| **Recovery of tibialis anterior† (%)** | 51 ± 51 | 32 ± 16 | 25 ± 14 | 3 ± 7 |
| **Recovery rate of tibialis anterior (%)** | 100(15/15) | 93 (14/15) | 100 (15/15) | 15 (2/13) |
| **Recovery of flexor digiti quinti brevis† (%)** | 10 ± 12 | 10 ± 11 | 3 ±4 | 0 |
| **Recovery rate of flexor digiti quinti brevis (%)** | 53 (8/15) | 73 (11/15) | 33 (5/15) | 0 (0/15) |
| **Weight (normalised to contralateral side)** | | | | |
| **Muscle weight of tibialis anterior† (%)** | 58 ±7 | 54 ± 10 | 49 ±9 | 19 ± 8 |
| **No. tested** | 20 | 20 | 20 | 19 |
| **Histomorphometry (%)** | | | | |
| **Peroneal axon count** | 118 ± 24 | 112 ± 23 | 86 ± 15 | 47 ± 16 |
| **Peroneal nerve area (µm)** | 89 ± 17 | 88 ± 20 | 74 ± 13 | 58 ± 11 |
| **Peroneal nerve fibre area (µm)** | 39 ±4 | 34 ±5 | 41 ± 19 | 35 ± 2 |
| **Peroneal myelin thickness (µm)** | 87 ±9 | 84 ±8 | 90 ±5 | 76 ± 7 |

**Table 1.6 Summary of the effectiveness of commercially available NGCs in repairing motor nerve regeneration. Overall the autograft is the most effective in promoting motor nerve recovery followed by Neurolac®. Neurotube® is deemed the least effective for promoting motor nerve regeneration. Reproduced from Shin, Freidrich et al. 2009)**

The study conducted by Shin et al. (2009) demonstrated the functional regenerative potential of NGCs in motor nerve repair and their limitations. In addition, it also highlights the necessity to consider both sensory and motor functions when creating NGCs or grafts for nerve repair.

### 1.6.4 Clinical efficacy of autografts and NGCS in treating peripheral nerve repair

Due to the lack of multicentres and prospective, randomised, controlled studies based around peripheral nerve repair research, surgeons have come to rely on experimental data from expert and institutional publications when determining expected outcomes or forming an evidenced based approach for treatment of peripheral nerve injuries. For the "gold standard" autograft there is a wealth of single centre experimental data available. In a review by Frykman and Gramyk (1991), meaningful functional recovery was reported in 80% of nerve autograft repairs in digital nerve gaps less than 50 mm, 63-81% meaningful motor funtion in mixed nerves of the forearm and 75-78% meaningful levels of sensory function (Frykman 1991).

For autograft alternatives (NGCs) the largest published randomised controlled study was by Weber et al (2000). The study was a direct comparison of conduits with direct suture and autograft for sensory only digital nerve repairs. The NGC's performed well in a gap of 4 mm or less with 100% meaningful recovery, however with gap lengths between 5-25 mm only 34% reported meaningful recovery (Weber, Breidenbach et al. 2000). Table 1.7 summerises published studies which have been carried out on autograft and NGCs for peripheral nerve repair.

| Study | Number of Repairs | Nerve injury type | Test article | Positive Outcomes |
|---|---|---|---|---|
| **Wangensteen and Kallianien (2009)** | 64 | Sensory, mixed and motor nerves | Neuragen® | 43% |
| **Kim and Kline (2001-2006)** | 52 | Sensory and mixed nerves | Direct Suture and autograft | 67-86% |
| **Frykman and Gramyk (1991)** | 91 | Mixed nerves | Direct Suture and autograft | 75-78% |
| **Frykman and Gramyk (1991)** | 384 | Sensory nerves | Autograft for digital nerve injury under 5cm | 80% |
| **Weber et al. (2000)** | 62 | Sensory nerves | Neurotube® | 74% |
| **Weber et al. (2000)** | 74 | Sensory nerves | Direct repair and autograft | 86% |
| **Kallio et al. (1993)** | 254 | Sensory nerves | Autograft and direct repair | 70% |
| **Lohmeyer et al. (2009)** | 12 | Sensory nerves | NeuraGen® Type I Bovine Collagen Tube | 75% |

**Table 1.7. Comparison of different types of nerve repair in reference to historical literature based on individual study parameters for acceptable recovery: M3-M5, S3-S4. Reproduced by Brooks, Weber et al. (2012)**

### 1.6.5 Limitations of NGCs in promoting regeneration across critical gap length

A study comparing autograft to conduit repair of digital nerve injuries concluded that conduits were limited to defects of up to 25 mm. It was also noted that the quality of recovery decreased as the gap size increased and that a third of repairs for gaps between 5 and 25 mm had poor outcomes (Weber, Breidenbach et al. 2000).

Fibrin clot instability seems to a leading factor leading to the failure of NGCs to provide sufficient regeneration across larger gaps. A study by Lundborg et al. (1982) demonstrated loss of fibrin stability with an increasing distance between nerve ends within a silicone nerve tube (Lundborg, Dahlin et al. 1982). The failure to form a fibrin clot means that Schwann cells and axons would not have a scaffold to guide and support their migration across the conduit. Other factors which may also limit the NGCs are neurotrophic factors, Schwann cell invasion (Daly, Yao et al. 2012) and absence of physical guidance such as the Schwann cell basal lamina and ECM (Spivey, Khaing et al. 2012).

## 1.7 Importance of ECM and Schwann cell basal lamina in nerve regeneration

During the last decade many trials have been undertaken with nerve tubes of different materials, growth factors as well as cells, all with the aim of increasing the speed of nerve regeneration and directing nerve fibres for target specificity. These grafts avoid the problem of availability, donor site morbidity and immune-rejection however they have limited efficacy in nerve regeneration. A plausible explanation for this is the absence of physical guidance for the cells at a relevant scale (~50μm) such as the Schwann cell basal lamina and ECM (Spivey, Khaing et al. 2012).

The nanostructure of basal laminae is primarily composed of collagen and laminin so it can be inferred that they present aligned, linear nano-scale features to cells. Laminin is known to promote neurite extension both *in vitro* and *in vivo* (Corey, Lin et al. 2007; Nguyen, Sanes et al. 2002; Smeal et al. 2005)

An *in vitro* studies of dorsal root ganglia exposed to aligned, nanofibrous surfaces show that axon extension is strongly influenced by the alignment of nanotopography to support this hypothesis (Corey, Lin et al. 2007).

An *in vivo* study using a murine model where the structure of the nerve tissue (including the basal laminae) was preserved during a crush-type axotomy showed the motor axons retracing their original pathways to re-establish neuromuscular junctions at the original sites with little variation (Nguyen, Sanes et al. 2002). A study by Smeal et al. (2005) demonstrated that axon regeneration was more effective when presented with smaller diameter tube structures and that axons are sensitive to substrate curvature, demonstrating more directional extension when exposed to a smaller radius of curvature (Smeal, Rabbitt et al. 2005).

It is therefore hypothesised that as a prerequisite for efficient axon extension, next generation NGC's and grafts should incorporate cell-scale topography consisting of continuous, tube-like micron scale structure that are both linear and aligned over macroscopic distances.

## 1.8 Tissue decellularisation

Use of cadaveric or donor nerve tissues can provide an ECM that mimics the native nerve tissue as well as offering the potential for clinically relevant size/length and motor/sensory specificity (Moore, MacEwan et al. 2011). Such grafts contain an endoneurial microstructure which provides the same level of guidance and regenerative support as nerve autografts.

Nevertheless, when used clinically these grafts possess risks from the immune response from the body due to the presence of foreign cells. Taking immunosuppressant's will allow the host axons and Schwann cells to regenerate across the allograft scaffold; however side effects may result in opportunistic infections, neoplasia or tumour formation (Mackinnon, Doolabh et al. 2001).

Alternatively, the immunogenic components from the graft can be removed through a process called decellularisation, producing a non-immunogenic acellular tissue graft. Decellularisation can remove DNA, remove/mask antigenic epitopes, (Gilbert, Sellaro et al. 2006, Badylak and Gilbert 2008) and damage associated molecular pattern (DAMP) molecules (Rubartelli and Lotze 2007). Theoretically acellular grafts still retain the 3D structure and ECM components of the native tissue; however, such a graft may be used clinically without eliciting an adverse immune response. ECM components are generally conserved amongst species and are tolerated well by recipients in the absence of immunogenic cellular components.

### 1.8.1 Clinical relevance for the use of acellular scaffolds

There is an increasing use of ECM derived from acellular tissue in tissue engineering and regenerative applications. Acellular scaffolds have been commonly used for the surgical reconstruction of a variety of tissues including tendons (Coons and Barber 2006), dermal (Brigido 2006) and gastrointestinal (Ueno, Pickett et al. 2004). Recent strategies have also included whole organ decellularisation such as the heart, liver and lung (Ott, Matthiesen et al. 2008, Petersen, Calle et al. 2010, Uygun, Soto-Gutierrez et al. 2010). Table 1.8 summarises the current clinical acellular products, which are obtained from a variety of allogeneic or xenogeneic tissue sources.

| Product | Tissue source | Application |
|---|---|---|
| **AlloDerm® (Lifecell Corp.)** | Human dermis | Soft tissue |
| **AlloPatch HD™, FlexHD® (Musculoskeletal Transplant Foundation)** | Human dermis | Tendon, breast |
| **NeoForm™ (Mentor Worldwide LLC)** | Human dermis | Breast |
| **GraftJacket® (Wright Medical Technology Inc.)** | Human dermis | Soft tissue, chronic wounds |
| **Strattice™ (Lifecell Corp.)** | Porcine dermis | Soft tissue |
| **Zimmer Collagen Repair Patch™ (Zimmer Inc.)** | Porcine dermis | Soft tissue |
| **TissueMend® (Stryker Corp.)** | Bovine dermis | Soft tissue |
| **MatriStem®, Acell Vet (Acell Inc.)** | Porcine urinary bladder | Soft tissue |
| **Oasis®, Surgisis® (Cook Biotech Inc.)** | Porcine small intestine | Soft tissue |
| **Restore™ (DePuy Orthopaedics)** | Porcine small intestine | Soft tissue |
| **FortaFlex® (Organogenesis Inc.)** | Porcine small intestine | Soft tissue |
| **CorMatrix ECM™ (CorMatrix® Cardiovascular Inc.)** | Porcine small intestine | Pericardium, cardiac tissue |
| **Meso BioMatrix™ (Kensey Nash Corp.)** | Porcine mesothelium | Soft tissue |
| **IOPatch™ (IOP Inc.)** | Human pericardium | Ophthalmology |
| **OrthAdapt®, Unite® (Synovis Orthopedic and Woundcare Inc.)** | Equine pericardium | Soft tissue, chronic wounds |
| **CopiOs® (Zimmer Inc.)** | Bovine pericardium | Dentistry |
| **Lyoplant® (B. Braun Melsungen AG)** | Bovine pericardium | Dura mater |
| **Perimount® (Edwards Lifesciences LLC)** | Bovine pericardium | Valve replacement |
| **Hancock® II, Mosaic®, Freestyle® (Medtronic Inc.)** | Porcine heart valve | Valve replacement |
| **Prima™ Plus (Edwards Lifesciences LLC)** | Porcine heart valve | Valve replacement |
| **Epic™, SJM Biocor® (St. Jude Medical Inc.)** | Porcine heart valve | Valve replacement |

**Table 1.8 Clinical products composed of acellular tissue. Reproduced from Crapo, Gilbert et al. (2011)**

### 1.8.2 Decellularisation methods

The aim of any decellularisation process is to efficiently remove all cellular and nuclear material whilst minimising any adverse effect on the composition, biological activity and mechanical integrity of the remaining ECM. Nonetheless any process that requires the removal of cells is likely to alter the native three dimensional architecture of the ECM.

Numerous methods exist for preparing acellular scaffolds (Table 1.9). Despite inherent differences all processing techniques aim to reduce the tissue immunogenicity and enhance the regenerative capacity through preservation of the native ECM.

| Method | Mode of action | Effect on ECM |
|---|---|---|
| **Physical:**<br>▪ **Snap freezing**<br>▪ **Mechanical force**<br>▪ **Mechanical agitation**<br>▪ **Electroporation** | Disrupt cell membrane, burst cells and tissue, cell lysis | Disrupts and damage ECM |
| **Chemical:** | | |
| ▪ **Acids and alkalines** | Solubilises cytoplasmic and nuclear cellular membranes. | Damages collagen and removes GAG's, growth factors and cytoplasmic proteins. |
| ▪ **Ionic, non-ionic and zwitterionic detergents** | Disrupts lipid-lipid, lipid-protein and protein-protein interactions | Disrupts tissue ultrastructure, removes GAG's and cytoplasmic proteins and damages collagen. Effective cell removal<br>Does not effectively remove the cellular remnants |
| ▪ **Hypo and hypertonic solutions** | Cell lysis by osmotic shock, disrupts DNA-protein interactions | |
| **Enzymatic:** | | |
| ▪ **Trypsin** | Cleaves peptide bonds on the carboxyl-side (COOH) of Arg and Lys | Prolonged exposure can disrupt ECM structure; remove laminin, fibronectin collagen IV, elastin and GAGs. |
| ▪ **Dipases** | Cleaves specific peptides, mainly fibronectin and collagen IV | Difficult to remove from tissue and can invoke an immune response. |
| ▪ **Endo and exonucleases** | Catalyse the hydrolysis of the interior and terminal bonds of ribonucleotide and deoxyribonucleotide chains | |
| **Chelating agents:**<br>▪ **EDTA, EGTA** | Bind divalent metallic ions, thereby disrupting cell adhesion to ECM | No isolated exposure, typically used with enzymatic methods (e.g. trypsin) |

**Table 1.9 Summary of the decellularisation methods used and their effect on the ECM. Reproduced from Gilbert, Sellaro et al. (2006)**

### 1.8.3 Decellularisation solutions and agents

#### 1.8.3.1 Detergents

##### 1.8.3.1.1 Ionic detergents

Ionic detergents solubilise both cytoplasmic and nuclear cellular membranes; however they also denature proteins by disrupting protein-protein interactions (Seddon, Curnow et al. 2004). Common ionic detergents include sodium dodecyl sulphate (SDS) (Wilshaw, Rooney et al. 2011, Wakimura, Wang et al. 2015), sodium deoxycholate (Wang, Itoh et al. 2015) and Triton X-200 (Hudson, Liu et al. 2004).

SDS is efficient in removing cellular components from tissue as well as nuclear remnants and cytoplasmic proteins (Woods and Gratzer 2005). Drawbacks of SDS include potential disruption to the native tissue structure, decrease GAG content and disruption of collagen integrity (Gilbert, Sellaro et al. 2006). However, SDS does not appear to solubilise or remove collagen from the tissue. Sodium deoxycholate is also effective in removing cell remnants; however it tends to cause greater disruption to the tissue and has to be used in conjunction with other zwitterionic detergents or Triton X 200 (Hudson, Liu et al. 2004). Residual chemicals from the ECM must be flushed away after decellularisation especially if using detergents that penetrate into dense tissue such as SDS. Residual detergent within the tissue may cause cytotoxicity, inhibiting the beneficial properties of an acellular scaffold

##### 1.8.3.1.2 Non-ionic detergents

Non-ionic detergents have been extensively used due to their mild effects upon tissue structure. These detergents disrupt the lipid-lipid and lipid-protein interactions whilst leaving protein-protein interactions intact so that the proteins within the tissue can be left in a functional confirmation (Seddon, Curnow et al. 2004).

Triton X-100 is the most commonly studied non-ionic detergent for the decellularisation protocol. The use of this detergent on different tissue types however has shown mixed results in terms of the removal of nuclear material (Dahl, Koh et al. 2003, Grauss, Hazekamp et al. 2005). In regards to the ECM components there has been a complete loss of GAGs as well as a decrease in laminin and

fibronectin content (Grauss, Hazekamp et al. 2005). The efficacy of Triton X-100 is dependent upon the tissue being decellularised as well as the other methods with which it is combined in a given decellularisation protocol.

#### 1.8.3.1.3 Zwitterionic detergents

These detergents exhibit the properties of both non-ionic and ionic detergents and include 3-[(3-cholamidopropyl) dimethylammonio]-1-propanesulfonate (CHAPS), sulfobetaine-10 (SB-10) and -16 (SB-16). CHAPs treated artery tissue showed retention of collagen and elastin but decreased the mechanical integrity of the tissue (Dahl, Koh et al. 2003). SB-10 and SB-16 in conjunction with Triton X-200 have shown to have a less detrimental effect on the ECM of peripheral nerve tissue (Hudson, Liu et al. 2004).

### 1.8.3.2 Hypotonic and hypertonic treatments

Hypertonic solutions dissociate DNA from proteins whilst hypotonic solutions are used to lyse the cells within tissues through osmotic shock with minimal changes in matrix molecules and architecture. For a maximum osmotic effect, it is common for the tissue to be immersed alternatively in hyper and hypotonic solutions. This treatment however does not remove the cellular remnants from the tissue therefore additional enzymatic or chemical treatments are necessary for the removal of the cellular debris (Crapo, Gilbert et al. 2011).

### 1.8.3.3 Chelating agents

Chelating agents such as EDTA and EGTA form a ring-shaped molecular complex that binds and isolates a central metal ion. Divalent cations such as $Ca^{2+}$ and $Mg^{2+}$ are needed for cell attachment to collagen and fibronectin at the Arg-Gly-Asp receptor(Klebe 1974, Gailit and Ruoslahti 1988). By binding the divalent cations present at the cell adhesions to the ECM the chelating agents facilitate in the removal of the cellular material from the tissue.

### 1.8.3.4 Enzymatic methods

These methods include the use of protein digestion, calcium chelating agents and nucleases (Bader, Schilling et al. 1998, Gamba, Conconi et al. 2002, McFetridge, Daniel et al. 2004). Trypsin is a commonly used proteolytic enzyme in decellularisation. This enzyme cleaves the peptide bonds on the carbon side of arginine and lysine if the next residue is not proline (Voet, Voet et al. 1999).

Nucleases such as endonucleases catalyse the hydrolysis of the interior bonds of deoxyribonucleotide or ribonucleotide chains whereas exonucleases catalyse the hydrolysis of the terminal bonds which ultimately leads to the degradation of RNA and DNA (Freyman 2008).

The effectiveness of enzymatic treatment for the removal of cellular material from the ECM has been studied in a variety of tissues with varied results (Schenke-Layland, Vasilevski et al. 2003, Grauss, Hazekamp et al. 2005). Prolonged treatment with trypsin/EDTA can cause disruption of the ECM structure but does not affect the overall amount of collagen in the tissue. Trypsin/EDTA has however been shown to substantially reduce the laminin and fibronectin content of the ECM (Schenke-Layland, Vasilevski et al. 2003). Prolonged exposure with trypsin/EDTA can also decrease the elastin and GAG content (chondroitin sulphates, keratin sulphates and dermatan sulphates) over time. A loss of these components can result in the decrease in tensile strength of up to 50% (Schenke-Layland, Vasilevski et al. 2003, Grauss, Hazekamp et al. 2005).

#### 1.8.3.5 Protease inhibitors

During the decellularisation process, proteases can be released from the disrupted cells, which in turn can damage the native ECM ultrastructure. Protease inhibitors such as aprotinin are therefore added to solutions. Buffered solutions of pH 7-8 as well as temperature control and time of exposure to the lysis solutions can also limit protease activity (Gilbert, Sellaro et al. 2006).

#### 1.8.3.6 Antibiotics

The presence of bacteria can contaminate tissues which have been subjected to prolonged chemical decellularisation methods. Antibiotics such as penicillin, streptomycin or amphotericin have been included in many decellularisation protocols (Costa, Dohmen et al. 2004, Hilbert, Yanagida et al. 2004, Woods and Gratzer 2005). However antibiotic residues may remain in the tissue material after the decellularisation protocol which may increase the complexity of regulatory approval.

## 1.9 Sterilisation of acellular tissue

Following the completion of the decellularisation process the tissues must be sterilised prior to *in vitro* cell seeding or *in vivo* studies. Sterilisation of biological scaffolds is vital to eliminate endotoxins and viral and bacterial DNA that may be present. Sterilisation methods have included incubation in acids or solvents, ethylene oxide exposure, gamma irradiation and electron beam irradiation (Hodde and Hiles 2002).

Ethylene oxide, gamma irradiation and electron beam irradiation are known to alter ECM ultrastructure and mechanical properties of the tissue (Freytes, Stoner et al. 2008, Gouk, Lim et al. 2008, Sun and Leung 2008). Irradiation has been shown to causes ECM degradation due to the denaturation of structural proteins such as collagen (Sun and Leung 2008). Gamma irradiation causes lipids to become cytotoxic as well as accelerating enzymatic degradation of ECM (Moreau, Gallois et al. 2000, Gouk, Lim et al. 2008). Supercritical carbon dioxide has been recently investigated and demonstrated effective reduction of bacterial and viral loads within porcine dermal ECM with minimal effect on the mechanical properties (Qiu, Leamy et al. 2009).

Acid and alkaline treatments solubilise the cytoplasmic component of the cells as well as removing nucleic acids such as RNA and DNA through hydrolytic degradation. Bases such as calcium hydroxide, sodium sulphide and sodium hydroxide are harsh chemicals that can eliminate growth factors from the matrix and decrease ECM mechanical properties by cleaving collagen fibrils and disrupting collagen crosslinking (Gilbert, Sellaro et al. 2006).

Acids such as peracetic (PAA), sulphuric and hydrochloric can effectively disrupt cell membranes and intracellular organelles. PAA is an oxidising agent and an effective chemical sterilant (Pruss, Kao et al. 1999, Hodde and Hiles 2002). PAA also doubles up as a decellularisation agent with the removal of residual nucleic acid (Badylak, Tullius et al. 1995) as well as being an excellent agent for inhibiting viruses (Hodde and Hiles 2002).

## 1.10 Immune response to biological scaffolds

The immune response to acellular scaffolds involves both the innate and adaptive immune system. They determine the eventual clinical outcome of the scaffolds. The innate (non-specific) system consists of cells and proteins that are always present and ready to fight microbes at the site of infection. The main components of the innate immune system include the physical epithelial barriers, phagocytic leukocytes, dendritic cells, natural killer (NK) cell (granular lymphocyte), and circulating plasma proteins.

The adaptive (specific) system is activated against pathogens that have evaded the innate immune defence system. There are two types of adaptive immune responses; humoral immunity, mediated by antibodies produced by B lymphocytes, and cell-mediated immunity, mediated by T lymphocytes (Chaplin 2010).

### 1.10.1 Constructive remodelling versus pro-inflammatory response to biological scaffolds

The host cellular response and remodelling outcomes differ amongst the tissue engineered scaffold and is affected by variables such as the processing steps involved in creating the scaffold, intended clinical application, tissue source from which the ECM is harvested and the tissues *in vivo* degradability (Badylak, Freytes et al. 2009).

#### 1.10.1.1 Th1 versus Th2 lymphocyte response

The T helper (Th) cells have distinct phenotypic polarisation profiles known as Th1 and Th2. Polarisation is a process when cells express different functional programs in response to signals from the microenvironment (Mantovani, Sozzani et al. 2002). Th1 lymphocytes produce cytokines such as interleukin (IL)-2, interferon (IFN)-γ, and tumour necrosis factor (TNF)-β. This leads to macrophage activation, stimulation of complement fixing Ab isotypes and differentiation of $CD8^+$ cells to a cytotoxic phenotype (Abbas, Murphy et al. 1996). Activation of this pathway is associated with transplant rejection (Strom, Roy-Chaudhury et al. 1996).

Th2 lymphocytes produce IL-4, IL-5, IL-6, and IL-10, cytokines that do not activate macrophages and that lead to production of non-complement fixing Ab isotypes. Activation of the Th2 pathway is associated with transplant acceptance (Chen and Field 1995, Piccotti, Chan et al. 1997).

#### 1.10.1.2 M1 versus M2 macrophage response

Similarly, to the Th1/Th2 lymphocytes there is also a distinct phenotypic polarisation profile for the mononuclear macrophages. M1 are macrophages which possess a pro-inflammatory, cytotoxic phenotype. They are characterised as cells that promote pathogen killing and are associated with classic signs of inflammation. M2 are anti-inflammatory macrophages. These cells promote immunoregulation, tissue repair and tissue remodelling (Mosser 2003, Mantovani, Sica et al. 2005).

These mononuclear macrophages are morphologically similar however they can be distinguished by their cell surface markers and their cytokine and gene expression profiles (Mantovani, Sica et al. 2004, Stout, Jiang et al. 2005). In rats M1 macrophages are characterized by $CD68^+$ and $CD80^+$ cell surface markers. These cells also produce large amounts of nitric oxide and other reactive oxygen intermediates as well and copious amounts of pro-inflammatory cytokines such as IL-12 and TNFα. Conversely, M2 macrophages express CD163 surface markers in rats. These cells produce high levels of IL-10 and TGF-β expression, produce large amounts of arginase, inhibit release of proinflammatory cytokines, scavenge debris, promote angiogenesis, and recruit cells involved in constructive tissue remodelling.

### 1.10.2 Degradation of biological scaffolds

ECM derived scaffolds which have not been cross-linked rapidly degrade after implantation. Studies using small intestinal submucosa for tendon repair (Gilbert, Stewart-Akers et al. 2007) and urinary bladder repair (Record, Hillegonds et al. 2001) reported approximately 60% of the mass was degraded and resorbed within 4 weeks of implantation and completely degraded by 3 months.

The duration of the ECM scaffold *in vivo* in relation to the host immune response is unknown however recent studies suggest that degradation of the scaffold is shown to induce constructive host remodelling response. During degradation low molecular weight peptides are formed. *In vitro* analysis have shown that these peptides have a chemoattractant potential for several cell types, including multipotential progenitor cells (Li, Li et al. 2004) . In addition *in vivo* studies have shown the recruitment of bone-marrow derived cells to the degradation site where they participate in the long term remodelling of the ECM

(Badylak, Park et al. 2001). Therefore, degradation may actually be a requisite needed to pave the way for the remodelling events that follow.

## 1.11 Acellular nerve grafts

A number of methods have been documented for the preparation of acellular nerve grafts from donor nerve tissue. The most commonly utilised method for decellularisation of nerve tissue involves physical (Hiles 1972, Gulati 1988, Evans, Mackinnon et al. 1998, Ide, Tohyama et al. 1998), chemical (Sondell, Lundborg et al. 1998, Hudson, Liu et al. 2004) or enzymatic treatments (Wang, Itoh et al. 2015).

### 1.11.1 Avance® Nerve Graft

AxoGen Inc is the only medical device company that offers comercially available acellular allografts for peripheral nerve regeneration. Avance® Nerve Graft, an allograft with lengths ranging between 15-70 mm utilises the decellularised ECM from donated human peripheral nerve tissue. The tissue undergoes a combination of treatments including chemical decellularisation (detergent processing) to selectively remove cellular components and debris, and gamma-irradiation for sterilization. In addition these allografts also undergo pre-Wallerian degeneration, an enzymatic digestion of chondroitin sulfate proteoglycan (CSPG). CSPG is a known inhibitor of axonal growth, through acute enzymatic treatment using chondroitinase the quantity of CSPG can be effectively reduced and therby increases axonal regeneration (Muir 2010). The whole processing technique renders the tissue non-immunogenic whilst preserving the inherent and relevant structural characteristics of the tissue.

### 1.11.2 Clinical studies on Avance® Nerve Graft

A comparison study between Avance® Grafts and NeuraGen® was carried out in a rat sciatic model. The study saw regeneration of 20 times more myelinated axons in the Avance® Graft. In addition in both 14 and 28 mm defects, the Avance® Graft contained significantly more nerve fibres at all-time points (Whitlock, Tuffaha et al. 2009). In a subsequent study examining nerve fibre density Avance® graft was found to have more evenly distributed nerve fibres across the cross section of the nerve when compared to NeuraGen® (Johnson, Newton et al. 2011) .

Early clinical studies carried about at the Mayo Clinic have demonstrated that the Avance® Graft (mean length of 2.23 cm) has the ability to repair segmental nerve defects ranging from 0.5 - 3cm within the hand and fingers (Figure 1.8).

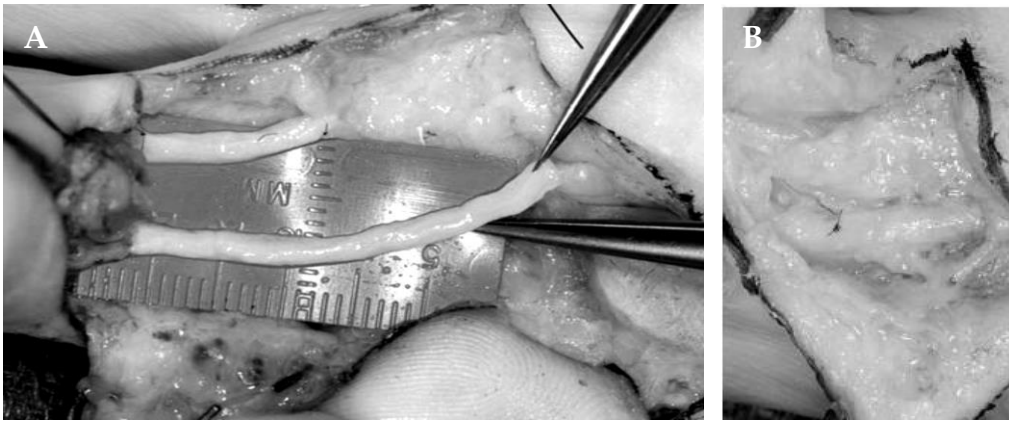


**Figure 1.8 AxoGen® Nerve Graft being used to repair segmental nerve defects.** A bilateral digital nerve injury being repaired (A); nerve graft at 8 weeks following implantation (B). Reproduced from Karabekmez, Duymaz et al. (2009).

Eight digital and two dorsal sensory nerves were repaired with a follow-up time of 9 months (Table 1.10). There were no reported cases of infection or rejection and the grafts may provide an option for segmental nerve gaps beyond 2 cm (Karabekmez, Duymaz et al. 2009).

| No. | Injured nerve | Etiology | Length (mm) | Diameter (mm) | Follow-up (mm) |
|---|---|---|---|---|---|
| 1 | Digital nerve | Laceration | 0.5 | 2 | 5.5 |
| 2 | Dorsal sensory branch of the ulna | Neuroma excision | 3 | 1 | 8.5 |
| 3 | Dorsal sensory branch of the ulna | Neuroma excision | 3 | 2 | 8.5 |
| 4 | Ring finger radial digital nerve | Laceration | 1 | 2 | 12 |
| 5 | Ring finger ulnar digital nerve | Laceration | 3 | 2 | 12 |
| 6 | Long finger radial digital nerve | Laceration | 3 | 2 | 9 |
| 7 | Digital nerve | Laceration | 3 | 2 | 5 |
| 8 | Digital nerve | Laceration | 3 | 2 | 5 |
| 9 | Thumb radial digital nerve | Laceration | 1 | 2 | 12 |
| 10 | Thumb ulnar digital nerve | Laceration | 1 | 2 | 12 |
| AVG | | | 2.15 | 1.90 | 8.95 |

**Table 1.10. Summary of ten nerve reconstructions with defect length and follow up values. Reproduced by Karabekmez, Duymaz et al. (2009)**

Between 2007-2012 a comprehensive clinical study was carried out from a multicentre, evaluating the efficacy outcomes for Avance® Grafts in sensory, mixed and motor nerve injuries with a mean graft length of 27±14 (5-50) mm. A total of 108 subjects were involved in the study with 132 nerve repairs, termed the Utilisation Population (UP). Subjects that provided sufficient follow up assessments to evaluate functional outcomes were placed into the Outcome Population (OP). With both the UP and OP studies there were no reported implant complications, tissue rejections or any adverse events related to the use of the graft.

The majority of repairs were digital nerves in the hand (60%) followed by upper extremity nerves (32%), head/neck region (5%) and lower extremities (3%) (Table 1.11). Although not all the repairs in the UP reported sufficient follow up for outcomes analysis the demographic between the subject, injury and repair found the OP to be comparable to the UP. Table 1.12 shows on average 89.5% of all subjects with different nerve injuries reported a positve response to the treatment using the Avance® Graft whilst 87.3% achieved meaningful recovery.

No obvious conclusion could be drawn in regards to the relationship between the nerve type, gap length patient age and outcomes. This may have been attributed to the number of subjects in each group, distribution of variables across the group, or the surgeon's approach. This study has certain limitations such as increased risk of heterogeniety in the datasets; variability between subjects and injuries and multiple sources of data. Observational studies were also limited in the fact that they couldn't be conducted in a prospective, randomised fashion.

| Nerve | Utilisation population | Outcomes population |
|---|---|---|
| **Digital** | 73 | 48 |
| **Median** | 22 | 11 |
| **Ulnar** | 15 | 6 |
| **Radial** | 4 | 2 |
| **Peroneal** | 5 | 2 |
| **Musculocutaneous** | 1 | 1 |
| **Anterior interosseous** | 1 | 0 |
| **Facial** | 3 | 3 |
| **Tibial** | 2 | 0 |
| **Sciatic** | 1 | 0 |
| **Spinal Accessory** | 2 | 1 |
| **Posterior Interosseous** | 1 | 0 |
| **Axillary nerve** | 1 | 1 |
| **Ulnar nerve motor branch** | 1 | 1 |
| **Total Repairs** | 132 | 76 |

**Table 1.11. Summary of the nerves treated in the Utilisation Population and Outcome Population. Reproduced by Brooks, Weber et al. (2012)**

| Nerve Type | Number | Gap (mm) | Response Rate | Meaningful Recovery |
|---|---|---|---|---|
| **Sensory** | 49 | 19±8 | 91.8% | 88.6% |
| **Mixed** | 18 | 29±12 | 83.3% | 77.0% |
| **Motor** | 9 | 29±13 | 88.8% | 85.7% |

**Table 1.12. Summary of the demographic characteristics of subjects in the Outcome Population. Reproduced by Brooks, Weber et al. (2012)**

A direct comparison of the clinical results obtained with acellular graft repairs versus those achieved with NGCs is not possible based on the current literature. Currently only positive results on the clinical use of Avance ® Grafts have been published whilst there have been mixed results for the commercially available NGCs. This may skewer the impressions as to which treatment is best for promoting nerve regeneration. It is important to note that the experimental studies to date have only investigated small-diameter, small gap defects and future studies still need to be undertaken to compare acellular grafts to autograft and NGCs. A major factor that limits such studies is the identification of a low-cost acellular nerve graft that is both comparable to commercially available acellular nerve grafts, and beneficial for laboratory use.

### 1.11.3 Use of xenogeneic acellular nerve grafts

In recent years' focus has shifted in the use of xenogeneic ECM as scaffolds or grafts due to ease of harvesting and availability. The use of xenogeneic material has been used in a variety of biomedical applications such as heart valves (Booth, Korossis et al. 2002) and tissue patches such as and Matristem® for ulcer repairs (Badylak and Gilbert 2008).

When used clinically, xenografts do possess some risks due to α-Gal epitopes found in some unmodified xenogeneic tissue, which can trigger an immune response. To remove the potential threat of α-Gal epitopes, tissues can be crosslinked i.e. with glutaraldehyde or enzymatically treated with α-galactosidase (Badylak and Gilbert 2008). This enzymatic treatment has been shown to effectively remove the α-Gal epitope from both porcine cartilage and ACL tissues (Stone, Ayala et al. 1998, Stone, Abdel-Motal et al. 2007, Stone, Walgenbach et al. 2007). Table 1.13 shows the clinically available xenogeneic products, some of which have been crosslinked to remove the α-Gal epitope.

| | Species/Tissue origin | Crosslinking |
|---|---|---|
| **Oasis™, Surgisis™ Cook Biotech, Inc.)** | Porcine small intestinal submucosa | n/a |
| **Restore™ (DePuy Orthopaedics)** | Porcine small intestinal submucosa | n/a |
| **CuffPatch™ (Organogenesis, Inc)** | Porcine small intestinal submucosa | Carbodiimide |
| **Acell Vet (Acell, Inc.)** | Porcine urinary bladder basement membrane and mucosa | n/a |
| **Zimmer Collagen Repair Patch™ (Zimmer, Inc.)** | Porcine dermis | Isocyanate |
| **TissueMend® (Stryker)** | Bovine dermis | Proprietary |
| **Mosaic®, Freestyle® (Medtronic, Inc.)** | Porcine heart valve | Glutaraldehyde |
| **OrthAdapt™ (Pegasus, Inc.)** | Equine Pericardium | Proprietary |

**Table 1.13. Source tissue and processing methods for commercially available devices produced from extracellular matrix scaffold material. Reproduced from Badylak and Gilbert (2008)**

Acellular xenogeneic nerve tissue from rat, rabbit and pigs has been widely used for peripheral nerve studies. Several studies have demonstrated that xenogeneic nerve tissue possess an ECM and basement membrane that serve as physical guidance cues for axonal growth (Gutmann and Sanders 1943, Osawa, Tohyama et al. 1990, Hudson, Liu et al. 2004, Whitlock, Tuffaha et al. 2009, Zhang, Luo et al. 2010).

### 1.11.4 Limitations of acellular nerve grafts

The Avance® nerve graft has shown to be superior over the comercially available NGCs in promoting nerve regeneration. Nonetheless, like with the autografts and comercially available NGCs, the acellular graft does have limitations. The Avance® Nerve Graft uses human nerve donor tissue, which is fraught with complications in terms of gaining approval and cost as they need to be kept frozen until implantation, which can create additional overhead costs.

Clinical studies have shown Avance® to be an effective nerve substitute, however the graft only supports nerve regeneration over limited distances (up to 60 mm) (Saheb-Al-Zamani, Yan et al. 2013). In addition, when compared to native nerve autografts the Avance® graft still only possessed reduced regenerative capacities. It was demonstrated that the number of fibres supported by the Avance® graft was only 30% of that supported by autografts (Whitlock, Tuffaha et al. 2009).

The limited regeneration in acellular grafts is due to the grafts dependency on in situ Schwan cells to support axonal regeneration (Moore, MacEwan et al. 2011). It has been proposed that populating longer acellular nerve grafts places a greater proliferative demand on in situ Schwan cells, which may cause them to senesce (Saheb-Al-Zamani, Yan et al. 2013). Although the acellular graft length seems to be limited by the Schwann cell migration problem, the critical gap size is not yet known. There are reports of acellular grafts up to 70 mm in length currently being utilised for clinical nerve reconstruction but in the absence of supporting data (Moore, MacEwan et al. 2011).

To improve axon regeneration and extend the workable length of the acellular graft focus has shifted to repopulating the graft with support cells. With this come many new challenges such as identifying the cell type, isolating and proliferating this cell, and seeding the cells into the acellular material.

## 1.12 Importance of cellular therapies for nerve regeneration

The similarities between the developing and regenerating nerve such as axon outgrowth and myelination may seem that regeneration recapitulates development. During development axons serve as a template to guide Schwann cell migration, establishing a Schwann cell-axon unit, a characteristic of a mature myelinated nerve. Conversely in the regenerating nerve, axons migrate into an environment where Schwann cells are already *in situ*. Furthermore the molecular events in the Schwann cell vary in the developing verses the regenerating nerve (Weinstein 1999). Schwann cells therefore play a crucial role in supporting axonal growth and migration following PNS injury.

Several investigations have highlighted the close relationship between Schwann cells and axon as a "regenerating unit" (Morris, Hudson et al. 1972, Brushart 2011). A study conducted by Enver and Hall (1994) used mitomycin C to block Schwann cell proliferation in the proximal and distal stumps in rats with inserted muscle basal lamina grafts. It was discovered that in the absence of cell migration axonal outgrowth was delayed until the Schwann cell population recovered from the anti-mitotic drug (Enver and Hall 1994). In another study by it was revealed that axons enter acellular grafts only when associated with co-migratory Schwann cells (Feneley, Fawcett et al. 1991).

### 1.12.1 Role of Schwann cells in nerve regeneration

The exact underlying mechanism through which Schwann cells and damaged axons communicate is poorly understood. It has been suggested that interactions between neurotransmitters and their upregulated receptors may be involved. Inhibition of the neurotransmitter acetylcholine to its receptor saw a decrease in axonal regeneration (Vrbova, Mehra et al. 2009). Another study states that the Toll-like receptors, expressed by Schwann cells act as mediators between the Schwann cells and degenerating axons to stimulate Schwann and immune cells to clear myelin and start the repair process (Goethals, Ydens et al. 2010).

Following PNS injury Schwann cells become activated, undergoing a phenotypic change from myelinating to growth supportive to help lead regenerating axons towards the distal nerve stump. This phenotype switch is associated with the up-regulation of several growth associated genes including neurotrophic factors (P75 NTR, GFAP, GAP-43 and netrin-1), cell adhesion molecules and receptors

including IL-1, N-cadherin, gamma integrins and neural cell adhesion molecule (N-CAM) (Rodrigues, Rodrigues et al. 2012). These molecules help support axonal migration and recruit further cells such as macrophages, mast cells and activated endothelial cells into the injury site (Hall 2005, Walsh and Midha 2009). Activated Schwann cells also provide a supportive environment by producing collagen and laminin which yields Schwann cell proliferation (4-17 times the original number seen in normal nerve) (Daly, Yao et al. 2012) and form longitudinally orientated strands (bands of Büngner) that guide regrowing axons (Bunge 1994).

If the axonal contact is not re-established or the gap length increases Schwann cell migration, proliferation and alignment decreases and the growth supportive environment cannot be maintained due to the cells losing their ability to express regeneration-assisting genes. As the capacity of the denervated distal nerve to support axonal regeneration is dependent on proliferating Schwann cells this translates to poor reinnervation outcomes (Walsh and Midha 2009). In an attempt to aid the regenerative cellular response to injury and to help stimulate nerve regeneration across long peripheral nerve defects cellular based therapies are considered essential for nerve repair.

### 1.12.2 Use of cellular therapy in nerve tissue engineering applications

Schwann cells have been used in synthetic and natural based NGC's as well as in acellular nerve tissue to improve functional recovery, regeneration and remyelination of injured peripheral nerves.

#### 1.12.2.1 Current cellular therapy for NGCs

Several different methods have been implemented to introduce cells into the conduit. These include injection, suspension within an intraluminal hydrogel, distributed along intraluminal guidance structures or released from the luminal wall. Hydrogels (alginate/fibronectin, gelatin, collagen and Matrigel) are commonly used as supporting substrates to deliver Schwan cells into the lumen of NGCs. Schwann cells have been successfully implanted in a number of studies with varying effects on nerve regeneration and functional recovery (Table 1.14).

| Cellular Components | Conduit Material | Animal model | Gap length | Major findings | Reference |
|---|---|---|---|---|---|
| Schwann cells (syngeneic) | PLGA coated with biomembranes | Rat sciatic nerve | 2 cm | Increased nerve regeneration | (Cheng and Chen 2002) |
| Schwann cells (syngeneic, heterologous) | PAN/PVC copolymer | Rat sciatic nerve | 8 mm | Successful nerve regeneration conditional to number of cells implanted | (Guenard, Kleitman et al. 1992) |
| Schwann cells (syngeneic) | Collagen (type I/III) | Rat sciatic nerve | 20 mm | Axonal regeneration | (Stang, Fansa et al. 2005) |
| Transduced Schwann cells (syngeneic) | PHB | Rat sciatic nerve | 10 mm | Increased regeneration process and enhanced axonal regeneration rate | (Mosahebi, Woodward et al. 2001) |
| Schwann cells (autologous) | Silicone | Rat sciatic nerve | 10 mm | Regeneration of nerve fibres | (Nilsson, Dahlin et al. 2005) |
| Schwann cells (allogeneic) plus FK-506 | Collagen | Mouse sciatic nerve | 0.6 cm | Successful regeneration and functional recovery | (Udina, Rodriguez et al. 2004) |
| Schwann cells (allogeneic) | Bioactive poly (L-lactic acid) | Rat sciatic nerve | 1.2 cm | Increased nerve regeneration | (Evans, Brandt et al. 2002) |
| Schwann cells | L-lactide /d ε-caprolactone | Rat sciatic nerve | 1.2 cm | Axonal regeneration | (Koshimune, Takamatsu et al. 2003) |
| Schwann cells (syngeneic) | Reinforced collagen | Rat sciatic nerve | 1.8 cm | Successful nerve regeneration conditional to number of cells implanted | (Ansselin, Fink et al. 1997) |
| Schwann cells and ultrasound | Hollow PLGA/silicone NGC | Rat sciatic nerve | 10 mm | Significant increase in nerve regeneration | (Chang, Hsu et al. 2005) |

**Table 1.14 Use of Schwann cells to help stimulate nerve regeneration in nerve guide conduits. Reproduced from Jiang, Lim et al. (2010); Daly, Yao et al. (2012) and Rodrigues, Rodrigues et al. (2012)**

#### 1.12.2.2 Current cellular therapy for acellular nerve grafts

The current studies which use acellular grafts in conjunction with cellular therapy to promote regeneration are summarised in Table 1.15. Several studies reported significant regeneration as well as structurally and functional repair with the inclusion of cells (Nishiura, Brandt et al. 2004, Hess, Brenner et al. 2007, Hu, Zhu et al. 2007, Zhang, Luo et al. 2010).

However other studies reported little effect of adding Schwann cells to acellular graft material (Frerichs, Fansa et al. 2002, Fansa and Keilhoff 2004, Fox, Schwetye et al. 2005). A reason for this could be that in situ Schwann cells migrating from the host stumps are able to cross short distances and provide sufficient regeneration despite the addition of exogenous cells. When Schwann cells migrate over long distances, such as in the case of large gap models (>20 mm – 'critical gap'), nerve regeneration fails. This suggests that cell supplementation of acellular grafts may be of greatest clinical use for large gaps, rather than those with adequate host Schwann cell migration (Nadim, Anderson et al. 1990).

| Cellular component | Acellular graft | Model | Gap length | Findings | Reference |
|---|---|---|---|---|---|
| **Autologous Schwann cells** | *Macaca fascicularis* ulnar nerve | *Macaca fascicularis* primate ulnar nerve | 60 mm | Significant regeneration across injury gap | (Hess, Brenner et al. 2007) |
| **Autologous non-hematopoietic MSCs** | Rhesus monkey sciatic nerve branches | Rhesus monkey ulnar nerve | 40 mm | Structural and functionally repair after 6 months. | (Hu, Zhu et al. 2007) |
| **ADSCs** | Porcine nerve graft | Rat sciatic nerve | 10 mm | Basal lamina of graft interacted with cells to form longitudinal cell alignment that resemble bands of Bünger | (Zhang, Luo et al. 2010) |
| **Skin-derived precursor cells pre-differentiated towards a Schwann cell phenotype (SKP-SCs)** | Rat sciatic nerve graft | Rat sciatic nerve | 12 mm | Nerve graft supported axonal elongation to the same extent as autograft, as well as providing axon regeneration, myelination and electrophysiological recovery. | (Walsh, Biernaskie et al. 2009) |
| **Schwann cells** | Rat tendon nerve graft | Rat sciatic nerve | 10 and 15 mm | Myelination was significantly increased in 10mm defects. No difference was seen in the 15 mm defect | (Arino, Brandt et al. 2008) |
| **Isogenic Schwann cells** | Rat muscle graft | Rat sciatic nerve | 20 mm | Systematic and organized regeneration including proper orientation of regenerated fibers. | (Fansa and Keilhoff 2004) |
| **Autologous Schwann cells** | Rat tibial nerve grafts | Rat sciatic nerve | 15 mm | Regeneration without evidence of rejection but the addition of cultured Schwann cells showed no additional benefit for nerve regeneration | (Fox, Schwetye et al. 2005) |
| **Isogenic Schwann cells** | Predegenerated acellular and acellular rat sciatic nerve grafts | Rat sciatic nerve | 20 mm | Predegenerated acellular nerve grafts showed superior results in axon density and histological appearance compared to acellular graft. Inclusion of cells did not show any significant improvement | (Frerichs, Fansa et al. 2002) |
| **Adult Schwann cells from predegenerated rat sciatic nerves** | Tendon autografts excised from rat tail. Freeze–thawed muscle graft | Rat sciatic nerve | 10 mm | Addition of cells to the two graft models improved regeneration by increasing the rate of axonal outgrowth when compared with grafts without added cells. | (Nishiura, Brandt et al. 2004) |

**Table 1.15. Studies conducted using cellular therapy in acellular grafts to help stimulate nerve regeneration**

### 1.12.3 Introduction of cells into acellular grafts

The current approaches in repopulating acellular nerve grafts involve injection of cells using a syringe into the ends of the graft *in vitro*. The reseeded grafts are then transplanted into an *in vivo* animal mode and harvested at a later time point for histological analysis (Brenner et al 2005; Fox et al 2005; Hess et al 2007). These animal models are useful in revealing aspects of PNS development as well as nerve regeneration after injury.

When working with acellular tissue it is important to establish a suitable approach to seeding cells into the graft. Previous methods using Schwann cells in acellular grafts have found mixed results. These inconsistencies may be attributed to the different cell seeding methods that have been implemented (Brenner et al 2005; Fox et al 2005; Hess et al 2007). A study by Jesuraj, Santosa et al. (2011) established a systematic approach to seeding Schwann cells in cold preserved acellular grafts (Figure 1.9). It was discovered that a sub-epineurial injection with a 27-gauge needle at a cell concentration of $1x10^6$/ 5µL resulted in the highest viability of cells with the least damage to the epineurium (Jesuraj, Santosa et al. 2011)

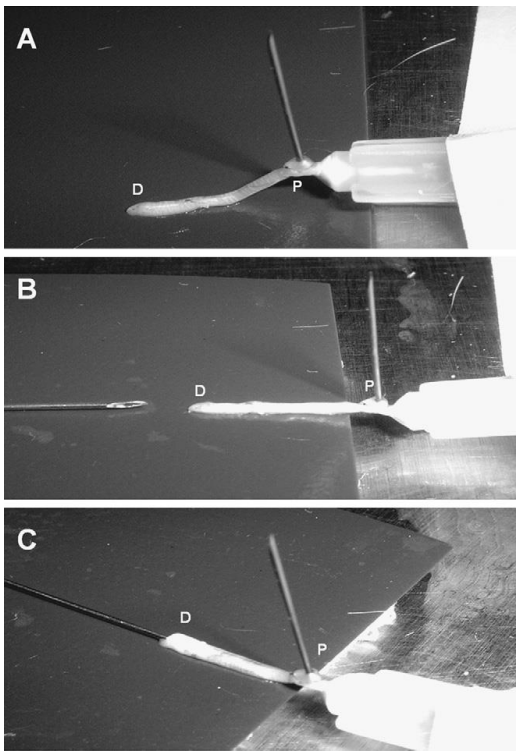


**Figure 1.9. *In vitro* set up model for Schwann cell injection into acellular graft.** The proximal (P) end of the graft was sutured to a sterile syringe bent to form a hook and secured under the microscope (A). Using a Hamilton™ syringe, Schwann cells were injected longitudinally under the epineurium of the distal stump (B and C). Figure reproduced from Jesuraj, Santosa et al. (2011)

To determine whether the injection was successful Jesuraj et al. (2011) also developed a method to track seeded Schwann cells prior to graft implantation to decrease the probability of experimental error such as low Schwann cell numbers due to injection error. The use of Qtracker® dye allowed the qualitative assessment of Schwann cell injection into the graft by fluorescence microscopy (Figure 1.10).

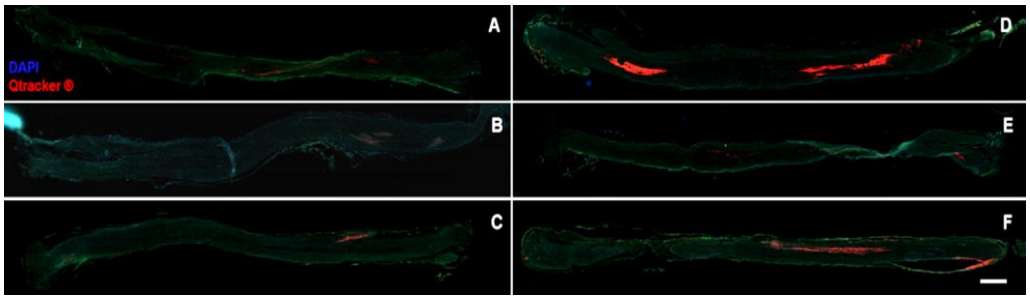


**Figure 1.10. Sagittal sections of acellular grafts post injection.** Grafts injected with $1x10^5$ (day 0 (A), day 1 (B), day 3 (C)) and $1x10^6$ (day 0 (D), day 1 (E), day 3 (F)) cells were frozen and sectioned for stereological counts. The presence of cells was confirmed with co-staining of DAPI (blue) and Qtracker® in the sections. Scale bar at 1.5mm. Figure reproduced from Jesuraj, Santosa et al. (2011)

## 1.13 *In vitro* acellular nerve model

Acellular grafts have been used *in vivo* and have shown to outperform the commercially available NGCs in terms of nerve regeneration. *In vivo* studies with reseeded acellular grafts have shown that they promote regeneration over longer distances. However, understanding the molecular, biochemical, and biological changes that occur *in vivo* during reinnervation is difficult, due to the inherent complexity of the regeneration process. These include the influence of Schwann cells, the impact of local inflammation, and the humoral response (Gingras, Bergeron et al. 2003).

*In vitro* models have value in a number of areas including developmental biology, disease studies and the design of devices and scaffolds for peripheral nerve repair (Daud, Pawar et al. 2012). Current studies involve the use of collagen gels and sponges which have shown to support axon ingrowth and Schwann cell proliferation (Allodi, Guzmán-Lenis et al. 2011) as well as myelination (Gingras, Beaulieu et al. 2008). A study by Daud, Pawar et al. (2012) developed a 3D *in vitro* peripheral nerve model using aligned electrospun polycaprolactone fibre scaffolds showed aligned neurite formation with dorsal root ganglion explants and co-localisation of Schwann cells with the neuritis (Daud, Pawar et al. 2012).

A 3D acellular nerve graft model can prove beneficial in understanding how cells interact, migrate and proliferate within the nerve matrix. The acellular nerve model can also be used as a basis for the study of perfused flow within the tissue for the introduction of Schwann cells. A study by Sun, Norton et al. (2007) for evaluating nerve guide conduits seeded with Schwannoma cells found that a continuous flow increased total cell number by 2.5-fold verses static culture (Sun, Norton et al. 2008).

## 1.14 Conclusion

In conclusion, the PNS plays a vital role in everyday life, helping process changes in the environment through sensory and motor receptors. When injured peripheral nerves have the capacity to spontaneously regenerate, however this is limited to relatively short distances of less than 5mm. For larger nerve gaps, autografts are considered the "gold standard" treatment; however, limitations include donor site morbidity and the need for multiple surgeries.

Scientists have taken advantage of the PNS's ability to spontaneously regenerate and developed a small number of clinically approved natural and synthetic nerve guides to treat larger nerve injuries. These devices help guide axons between the injured nerve stumps by providing a guidance cue; however, drawbacks include batch variation, degradation rates and breakdown products. The efficacy of these nerve guides are also not comparable to autograft and are limited to treating injuries up to 20 mm.

Current investigations into peripheral nerve repair have found a link between the role of cells and surface topography in the regeneration process. Peripheral nerve cells need an environment that can provide them with physical guidance such as the basal lamina and ECM. These non-cellular components provide precise guidance for axonal regeneration as well as cues that influence cell migration, proliferation and differentiation. Research has now turned to developing techniques in which cell scale topography can be incorporated into nerve guides. Decellularisation is a processing method in which native nerve tissue can be used to produce a non-immunogenic acellular nerve graft whilst retaining its non-cellular components. Despite their inherent native nerve architecture acellular nerve grafts are still not comparable to the autologous graft in terms of the

regenerative distance. This is thought to be due to the exclusion of support cells such as Schwann cells within the graft.

Schwann cells play a vital role in peripheral nerve regeneration and are important in synthesising several components of the ECM including laminin, collagen and proteoglycans. *In vivo* studies using acellular nerve grafts have shown that cell seeded scaffolds promoted better nerve regeneration compared to controls (unseeded scaffolds), however they are only effective when treating long nerve gap injuries (>20 mm).

Less is known however known on the migratory pattern and proliferation of cells when seeded into the acellular graft. It would therefore be of value to develop an *in vitro* 3D model using the acellular nerve as a scaffold for the introduction of primary Schwann cells. Primary cells are the best representation of cells found *in vivo*, maintaining many of the important markers and functions. Therefore, the data obtained from these *in vitro* models are more likely to predict the phenomena occurring *in vivo* during nerve regeneration than any other cell line-based models (Geuna, Raimondo et al. 2015).

The migration and survival of these cells within the scaffold are dependent on the maintenance of nutrient diffusion throughout the scaffold (Sun, Norton et al. 2005). *In situ* peripheral nerve cells receive constant nutrients from blood vessels which are located within the epineurium. Therefore, for primary Schwann cells growing on scaffolds it is likely that continuous perfusion with medium will better support metabolic activity and proliferation (Sun, Norton et al. 2008).

Based on the literature it is hypothesised that an acellular nerve graft can serve as a superior alternative to the current commercially available nerve guides due to its intact surface topography and natural ECM components. It is further postulated that acellular grafts could match the “gold standard” autograft with the addition of cell therapy to treat nerve gap injuries beyond 20 mm. Nonetheless further research is still required into creating a low cost, reproducible nerve graft which can also support the growth of Schwann cells for the study of nerve regeneration over long distances.

## 1.15 Aims and Objectives

**Aims:**

The aims of this study were to develop an acellular, biocompatible porcine peripheral nerve graft. The acellular graft would then be used as a basis for the study of perfused flow within the tissue for the introduction of primary Schwann cells, as the delivery of such cell types is reported to improve nerve cell development. Subsequently the acellular and recellularised grafts would be implanted in a rat sciatic nerve model to assess axonal regeneration across the grafts.

**Objectives:**

- To develop and optimise a process for the decellularisation of porcine peripheral nerves

- To assess the effects of the decellularisation process on the nerves histioarchitecture and the total amount of DNA left within the tissue

- To assess the biomechanical properties and the presence of specific matrix proteins within the graft

- To determine the *in vitro* biocompatibility of the acellular graft

- To define conditions for the introduction of primary Schwann cells into the acellular nerve graft

- To develop a bioreactor for the study of perfusion within the graft

- To analyse axonal regeneration within graft post implantation

# Chapter 2. Materials and Methods

## 2.1 Materials

### 2.1.1 Equipment

The equipment and suppliers used in this study are listed in Table 2.1

| Equipment | Model | Supplier |
|---|---|---|
| **Automatic pipettes** | Gilson P10-P1000 | Anachem Ltd. |
| **Balances** | GR200/GX2000 | Jencons PLC |
| **Bench top centrifuge** | 5415R | Eppendorf |
| **Bose tensile testing machine** | - | Electroforce test instruments |
| **Callipers** | - | Fisher Scientific |
| **Centrifuge machine** | Harrier 15/80 | SANYO Biomedical Europe BV |
| **Class II laminar flow cabinet** | Heraeus 85 | Kendro |
| **$CO_2$ Incubator** | MCO-20AIC SANYO | Biomedical Europe BV |
| **Confocal microscope** | LSM510 META | Carl Zeiss Ltd. |
| **Cryostat** | CM1850 | Leica |
| **Digital camera** | Image pro Plus v 5.1 | Media Cybernetics |
| **Freezer (-20°C)** | Electrolux 3000 | Jencons Plc |
| **Freezer (-80°C)** | R 404-A | VWR |
| **Freeze-dryer** | - | Cole-Parmer |
| **Fridge** | Electrolux ER8817C | Jencons Plc |
| **Fume cupboard/fume hood** | - | Whiteley |
| **Histology water bath** | MH8515 | Barnstead Electrothermal |
| **Hot plate** | E18.1 hotplate | Raymond A lamb |
| **Microliter syringes** | 10 µL cemented needles | Cole Parmer |
| **Micro plate spectrophotometer** | Multiskan spectrum | Thermo Scientific |
| **Microscope (upright)** | BX51 | Olympus, UK |
| **Microtome** | RM2125 RTR | Leica Microsystems |
| **Microwave (800 watt)** | KM19W, 800w | PROLINE |
| **Mounted needle** | | agar scientific |
| **Nanodrop spectrophotometer** | ND-100 | Labtech Int |
| **Orbital shaker** | Grant PSU-10i | Scientific Laboratory Supplies |
| **Oven** | OMT225 SANYO | Biomedical Europe BV |
| **pH meter** | Jenway 3010 | VWR International |
| **Phase contrast microscope** | CK40 | Olympus |

| | | |
|---|---|---|
| **Pipette boy** | Acu | Intergra Biosciences |
| **Plate reader** | Multiskan Spectrum 1500 | Thermo |
| **Plate shaker** | IKA KS130 basic | Jencons Plc |
| **Masterflex ® L/SPump** | | Cole Parmer |
| **Tissue embedder** | EG1150 | Leica Biosystems |
| **Tissue Processor** | TP11020 | Leica Microsystems |
| **Vortexer** | TopMix FB15024 | Fisher Scientific |
| **Water bath** | Grant | Jencons Plc |

**Table 2.1 Equipment used throughout the study**

### 2.1.2 General consumables

The general consumables and suppliers used in this study are listed in Table 2.2

| Item | Model/Size | Supplier |
|---|---|---|
| **Bijouxs** | 5 mL | Scientific Laboratory Supplies |
| **Surflo Straight I.V. Cannula (Yellow)** | 24 g x 0.75 x 50 | Terumo |
| **Centrifuge tubes** | 50 mL | Thermo Fisher Scientific Laboratory |
| **Falcon cell strainer** | 40 µm | Becton Dickenson |
| **Filter paper** | Whatman® Grades 1-5 | Whatman International Ltd |
| **Flat-bottomed 96 well plate** | - | Scientific Laboratory Supplies |
| **Forceps** | - | R.A. Lamb |
| **Glass coverslips** | - | Scientific Laboratory Supplies |
| **Haemocytometer** | - | Labtech |
| **Histology cassettes** | CMB-160-030R | Thermo Fisher Scientific Ltd |
| **ImmEdge Hydrophobic Barrier Pen** | H-000 | Vector Laboratories |
| **Magnetic stirrer** | Stuart SB161 | Scientific Laboratory Supplies |
| **Microtome blades** | SD3050835 | Fisher scientific |
| **Parafilm M** | - | Sigma-Aldrich |
| **Petri dishes** | 35 mm | IWAKI |
| **Pharmed tubes** | BPT NSF-51 | Cole Parmer |
| **Pipette tips (non-filtered)** | 10 µL, 20 µL, 200 µL, 1000 µL, 5000 µL | Star Labs |
| **Plastic syringes** | - | Scientific Laboratory Supplies |
| **Plates (24 wells)** | | Corning Incorporated |
| **Scalpel blade** | Size 22 | Fisher Scientific |
| **Sterile containers** | 60 mL, 150 mL, 250 mL | Scientific Laboratory Supplies |
| **Sterile syringe filter** | 0.2 µm | |

| | | |
|---|---|---|
| **Stripette ™ (disposable pipettes)** | 5 mL, 10 mL, 25 mL | Sigma-Aldrich |
| **Superfrost plus microscope slide** | - | Scientific Laboratory Supplies |
| **Sutures** | Ethicon3-0, 4-0 and 10-0 Prolene | Ethicon (Johnson&Johnson Ltd) |
| **Syringe needles** | | Thermo Fisher Scientific |
| **Tissue culture flasks** | 25 and 75 $cm^2$ | Thermo Fisher Scientific Ltd |
| **Universals** | 25 mL | Scientific Laboratory Supplies |

**Table 2.2 General consumables used throughout the study**

### 2.1.3 Chemicals and reagents

The chemicals/reagents and suppliers used in this study are listed in Table 2.3

| **Chemical/Reagent** | **Supplier** |
|---|---|
| **1,9 dimethylene blue** | Sigma-Aldrich |
| **Acetate** | Sigma-Aldrich |
| **Acetone** | European Bios |
| **Acetic acid** | Thermo Fisher Scientific Ltd |
| **Alcian blue** | Atom scientific |
| **Amphotericin B** | Sigma-Aldrich |
| **Aprotinin (10, 000 KIU.$mL^{-1}$)** | Nordic Pharma |
| **Aqueous periodic acid solution, 0.1%** | Sigma |
| **Benzonase Nuclease** | Novagen |
| **Bovine pituitary extract** | Sigma-Aldrich |
| **Bovine serum albumin** | Sigma-Aldrich |
| **Calcium chloride** | Sigma-Aldrich |
| **Chloramine T** | Sigma-Aldrich |
| **Chloroform** | Genta Medical |
| **Chondroitin sulphate B** | Sigma-Aldrich |
| **Citric acid (monohydrate)** | VWR International |
| **Collagenase I** | Sigma-Aldrich |
| **Collagen gel (rat tail)** | Sigma-Aldrich |
| **Cyanoacrylate contact adhesive** | Sigma-Aldrich |
| **DAPI stain (4',6-diamidino-2-phenylindole dihydrochloride)** | Sigma-Aldrich |
| **Diastase** | Sigma-Aldrich |
| **Di-sodium hydrogen orthophosphate** | VWR International |
| **DMSO** | Sigma-Aldrich |
| **DPX mountant** | Thermo Fisher Scientific Ltd |
| **Dulbecco's modified Eagle's media** | Biosera |
| **Dulbecco's PBS tablets** | Oxoid |
| **Eosin Y** | VWR International |
| **Ethanol** | Thermo Fisher Scientific Ltd |
| **Ethylenediaminetetraacetic acid (EDTA)** | Thermo Fisher Scientific Ltd |

| | |
|---|---|
| **Ferric ammonium sulphate (iron alum)** | BDH |
| **Fibronectin** | Sigma-Aldrich |
| **FITC conjugated secondary anti-rabbit antibody** | Sigma-Aldrich |
| **Foetal Calf Serum** | Biosera |
| **Formalin solution, neutral buffered, 10%** | Sigma-Aldrich |
| **Formic acid** | Sigma-Aldrich |
| **Forskolin** | Sigma-Aldrich |
| **Gentamycin sulphate** | Merck Millipore |
| **Giemsa Solution** | VWR International |
| **Gills no 3 Haematoxylin** | Sigma |
| **Glacial acetic acid** | VWR International |
| **Gold (III) chloride** | Sigma |
| **Harris Haematoxylin** | Thermo Fisher Scientific Ltd |
| **Hexane** | ProLab Scientific |
| **Hydrochloric acid** | VWR International |
| **Hydrogen peroxide (30% v/v)** | Sigma-Aldrich |
| **Industrial methylated spirit** | Biostain Ready Reagents |
| **Isopropyl Alcohol** | GPR |
| **Laminin solution (1mg $mL^{-1}$)** | Sigma-Aldrich |
| **Leica cryofact disinfectant** | Ecolab |
| **L-glutamine** | Invitrogen |
| **Liquid nitrogen** | BOC |
| **Magnesium chloride hexahydrate** | Thermo Fisher Scientific Ltd |
| **MEM- D-valine** | labtech |
| **Methanol** | Sigma-Aldrich |
| **Miller's stain** | Raymond A Lamb |
| **MTT reagent** | Sigma-Aldrich |
| **Neutral buffered formalin (10% w/v)** | Genta Medical |
| **N2 supplement** | Invitrogen |
| **OCT embedding matrix** | R.A. Lamb |
| **Oil Red O solution** | Sigma |
| **Oxalic acid** | VWR International |
| **Papain** | Sigma-Aldrich |
| **Paraffin wax** | Thermo Fisher Ltd |
| **Paraformaldehyde solution** | Sigma-Aldrich |
| **p-dimethylaminobenzaldehyde** | Sigma-Aldrich |
| **Phosphate buffered Saline (PBS) tablets** | Oxoid |
| **Penicillin- Streptomycin** | Sigma-Aldrich |
| **Peracetic acid** | Sigma-Aldrich |
| **Perchloric acid (60%)** | BDH |
| **Picric acid** | Sigma-Aldrich |
| **Potassium permanganate** | Thermo Fisher Ltd |

| | |
|---|---|
| **Poly-L-lysine (0.01% (wt/vol), mol.wt. 70,000-150,000)** | Sigma-Aldrich |
| **Polymyxin B** | Merck Millipore |
| **Porcine trypsin** | Sigma-Aldrich |
| **Propan-1-ol** | VWR International |
| **Rabbit anti-GFAP delta antibody (ab28926)** | abcam |
| **Rabbit anti-p75 NGF receptor antibody (ab38335)** | abcam |
| **Rabbit anti-S100 antibody-astrocyte marker (ab868)** | abcam |
| **Schiff's reagent** | Sigma-Aldrich |
| **Silver nitrate** | Sigma |
| **Sirius red** | VWR International |
| **Sodium acetate** | Thermo Fisher Ltd |
| **Sodium azide 1% solution** | G Biosciences |
| **Sodium chloride** | Thermo Fisher Ltd |
| **Sodium di-hydrogen orthophosphate** | VWR International |
| **Sodium dodecyl sulphate** | Invitrogen Life Technologies |
| **Sodium formate** | Sigma-Aldrich |
| **Sodium hydroxide** | Thermo Fisher Ltd |
| **Sodium phosphate dibasic ($Na_2HPO4$) (anhydrous)** | Sigma-Aldrich |
| **Sodium phosphate monobasic ($NaH_2PO4$) (anhydrous)** | Sigma-Aldrich |
| **Sodium thiosulphate pentahydrate** | VWR International |
| **Trans-4-hydroxy-L-proline** | Sigma-Aldrich |
| **Trypsin-EDTA solution** | Sigma-Aldrich |
| **Triton X-100** | BDH |
| **Trizma base** | Sigma-Aldrich |
| **Tween -20** | BDH |
| **Vancomycin hydrochloride** | VWR International |
| **Weigert's haematoxylin**<br>**Solution A**<br>**Solution B** | Atom Scientific |
| **Xylene** | Biostain Ready Reagents |

**Table 2.3 Chemicals and reagents used throughout the study**

### 2.1.4 Kits

The kits used in this study are listed in Table 2.4

| Kit | Catalogue Number | Supplier |
|---|---|---|
| **Cell Tracker ™ Red CMTPX Dye** | C34552 | Life Technologies |
| **DNeasy® Blood & Tissue Kit** | 69504 | QIAgen |

**Table 2.4. Kits used throughout the study**

### 2.1.5 Cells

The cells used in this study are listed in Table 2.5

| Cells | Species | Supplier |
|---|---|---|
| **Primary Schwann cell** | Rodent | Isolated using a selective D-valine protocol (Kaewkhaw, Scutt et al. 2012) |
| **Dermal Fibroblast** | Human; isolated from donor skin of abdominoplasty or breast reduction | Donated from patients of the Royal Hallamshire Hospital, Sheffield; in accordance with local ethically approved NHS guidelines and under HTA Research Tissue Bank license number 12179 regulations |
| **RN22 Schwann cell** | Rodent | European Collection of Cell Cultures (ECACC, batch number 93011414) |

**Table 2.5 Cells lines used throughout the study**

### 2.1.6 Animal tissue

There were no ethical issues in the procurement of the animal tissue throughout this study

#### 2.1.6.1 Porcine legs

Porcine legs, from large white Yorkshire pigs (24 - 26 weeks old) were obtained from a local abattoir (John Penny & Sons, Leeds, United Kingdom) within 24 hours of slaughter. The legs were stored at 4°C until required for dissection

#### 2.1.6.2 Rat sciatic nerve

Male Wistar rats (10-12 weeks old) were killed on the day by a Schedule 1 method (cervical dislocation) according to the regulation of the Animals (Scientific Procedures) Act 1986.

### 2.1.7 General chemical stock solutions

#### 2.1.7.1 Phosphate buffered saline (PBS)

Five PBS tablets were dissolved in 500 mL of distilled water and the pH adjusted to pH 7.4-7.6. The solution was sterilised by autoclaving and stored at room temperature until needed.

#### 2.1.7.2 Sodium hydroxide solution (6M)

Dissolve 120 g of sodium hydroxide into 500 mL of distilled water. Store at room temperature for up to three months

### 2.1.8 General cell work reagents/solutions

#### 2.1.8.1 Collagenase solution

Make a 0.05 % (w/v) collagenase solution by dissolving 5mg collagenase powder in 10 mL serum-free Dulbecco's Modified Eagles Medium (DMEM). Make fresh on the day of the experiment and filter-sterilize using a 0.2 µm syringe filter.

#### 2.1.8.2 Forskolin stock solution

Dissolve 10 mg of forskolin in 1 mL of DMSO to prepare a 25 mM stock solution. Store the aliquots at -20 °C for up to one month.

#### 2.1.8.3 Cell culture medium for fibroblasts and RN22

The standard cell culture medium used for fibroblast and RN22 cells was Dulbecco's modified Eagle's medium (DMEM) containing 10 % (v/v) FCS, 100 U/mL penicillin/ 100 µg. $mL^{-1}$ streptomycin, 0.25 µg. $mL^{-1}$ amphotericin and 2 mM L-glutamine. The culture medium was stored at 4 °C for up a month.

#### 2.1.8.4 Cell culture medium for purification and expansion of primary Schwann cells

The initial cell culture medium used for Schwann cell purification and expansion was Minimum Essential Medium (MEM) –d-valine containing 10 % (v/v) FCS, 2 mM glutamine, 1 % (v/v) N2 Supplement, 20 µg/mL (w/v) bovine pituitary extract, 5 µM forskolin, 100 U. $mL^{-1}$ penicillin 100 µg. $mL^{-1}$ streptomycin and 0.25 µg. $mL^{-1}$ amphotericin B. The culture medium was stored at 4 °C for up a month.

Once purity of Schwann cells was determined by immunolabelling cells with S100β marker, bovine pituitary extract and N2 supplemented could be omitted from the media, however for high Schwann cell purity and number forskolin needs to be present.

## 2.2 Methods

### 2.2.1 Histology techniques

#### 2.2.2.1 Cryo-embedding

Tissue samples (porcine) were dropped in liquid nitrogen to snap freeze. The frozen samples were then orientated in the correct position in plastic moulds and embedded with OCT embedding mix. Samples were then transferred to a -80 °C freezer to set.

#### 2.2.2.1.2 Tissue sectioning of cryo- embedded samples

The cryo-embedded tissue samples were sectioned using a Cryostat. The frozen tissues embedded in OCT were removed from the plastic mould and placed on the Peltier Chuck inside the cryostat in the required orientation. The tissue was sectioned at 10 µm. The tissue sections were collected onto Superfrost Plus® slides. These slides were electrostatically charged to prevent the sections from floating off the slides during staining. The slides were then put on a drying rack and left to dry

overnight at room temperature. The prepared slides were stored at -20 °C until further use.

#### 2.2.2.2 Paraffin embedding

Tissue samples were immersed in 3.7 % (v/v) formaldehyde for 24 hours. In the case of porcine tissue, 1 cm segments were cut from either end of the nerve whilst for rat sciatic nerve 30 mm segments were cut from either end of the nerve. The samples were them placed in plastic cassettes were then dehydrated in an automated tissue processor. The tissue processor sequentially immersed the tissue samples in: two consecutive one hour immersions in 70 % (v/v) industrial methylated spirit IMS followed by a 1.5 hours' immersion in 80, 85, 90, 95 % (v/v) IMS respectively. This was followed by two consecutive 1.5 hour immersions in 100 % (v/v) IMS, two 1.5 hour immersions in xylene and lastly two consecutive two hour immersions in paraffin wax. The cassettes were transferred to an embedding station containing hot wax at 60 °C. Samples were removed from the cassette and orientated in metal wax block moulds using forceps and then fully covered in wax. The wax blocks were then left to cool and solidify on ice (one - two hours), once set the blocks were removed from the metal moulds and the excess wax around the edges was trimmed.

##### 2.2.2.2.1 Tissue sectioning of paraffin embedded samples

Paraffin embedded tissue samples were sectioned using a microtome. For porcine tissue the thickness of the tissue sectioned ranged from 6-10 µm. For rat tissue the thickness of the tissue sectioned ranged from 4-6 µm. The tissue sections were transferred to a water bath set at 37 °C and collected onto Superfrost Plus® slides. These slides were electrostatically charged to prevent the sections from floating off the slides during staining. The slides were then put on a drying rack and left to dry overnight at room temperature. The prepared slides were stored at room temperature until further use.

##### 2.2.2.2.2 Dewaxing, rehydration and dehydration of paraffin embedded samples

Slides containing the tissue sections were dewaxed by two consecutive immersions in in xylene, ten minutes each time. The slides were then submerged three times in 100 % (v/v) IMS for three, two and one minutes respectively. The samples were

them placed in 70 % (v/v) IMS for one minute before being rinsed in slow running tap water for three minutes.

#### 2.2.2.2.3 Dehydration and clearing of paraffin embedded samples

Following staining the tissue sections the slides were then dehydrated and cleared by placing them back in 70 % (v/v) IMS for five seconds and then sequentially immersing them thrice in 100 % (v/v) IMS for one, two and three minutes respectively. Finally, the slides were submerged in xylene twice, for ten minutes each time. Each slide was then mounted using DPX mountant and a coverslip and left to dry overnight in a fume cupboard

### 2.2.3 Histological staining methods

#### 2.2.3.1 Haematoxylin and eosin (H & E) staining

H & E staining is used to visualise tissue histioarchitecture of tissue, evaluating the connective tissue and spatial distribution of cell nuclei.

**Reagents:**

1. **Harris haematoxylin**
2. **Eosin Y**
3. **IMS**
4. **Xylene**
5. **DPX mountant**

**Method:**

Prior to staining the tissue sections were dewaxed and rehydrated. Each section was immersed in Harris haematoxylin solution for one minute and rinsed under tap water for blueing for three minutes. Slides were then stained with eosin Y for three minutes before dehydrating and clearing. Each slide was then mounted using DPX mountant and a coverslip and left to dry overnight in a fume cupboard before being viewed under an upright microscope. Images were captured using a digital camera.

#### 2.2.3.2 Nuclei labelling using 4',6-diamidino-2-phenylindole (DAPI)

DAPI is a stain which binds A-T rich regions of the DNA double helix and can be therefore used to visualise cell nuclei.

**Reagents:**

1. **300 nM DAPI solution**

   To make DAPI working solution dissolve 10 µL aliquot of DAPI into 10 mL PBS and store away from light. Make on the day of the experiment

2. **PBS, pH 7.4**

   pH adjusted using 6 M hydrochloric acid or 6 M sodium hydroxide drop wise

**Method:**

Prior to staining tissue samples were dewaxed and rehydrated. Samples were incubated with 300 nM DAPI for twenty minutes in the dark, and then washed with PBS three times for five minutes each time in the dark. Nuclei were imaged using an upright fluorescent microscope and a DAPI filter ($\lambda_{ex}$ = 300 nm / $\lambda_{em}$ = 510 nm).

**2.2.3.3 Alcian Blue Periodic Acid Schiff's stain (ABPAS)**

ABPAS is used to localise GAGs in the tissue

**Reagents:**

1. **1 % (w/v) Alcian blue solution, pH 2.5**
2. **0.1 % (w/v) periodic acid solution**
3. **Schiff's reagent**
4. **Gills number 3 haematoxylin**
5. **IMS**
6. **Xylene**
7. **DPX mountant**

**Method:**

Prior to staining tissue samples were dewaxed and rehydrated. Samples were immersed in 1 % (w/v) Alcian blue solution (pH 2.5) for one minute and rinsed with tap water. The slides were then immersed in 0.1 % (w/v) periodic acid solution for five minutes and rinsed three times with distilled water. The slides were then immersed in Schiff's reagent for 15 minutes and rinsed with tap water for five minutes; cell nuclei were stained with Gills number 3 haematoxylin for 90 seconds. Samples were blued using tap water, dehydrated, cleared and mounted using DPX

mountant before being viewed using an upright microscope under Kohler illumination.

#### 2.2.3.4 Picro Sirius red and Millers elastic stain

Picro Sirius red and Millers elastic stain are used to visualise collagen and elastin in the tissue respectively.

**Reagents:**

1. **5 % (w/v) potassium permanganate solution**
   Add 15 g of potassium permanganate to 300 mL of distilled water and dissolve using a magnetic stirrer. Store the solution for up to six months at room temperature. Filter before use

2. **1 % (w/v) oxalic acid**
   Add 1 g oxalic acid to 100 mL of distilled water and dissolve using a magnetic stirrer. Use immediately.

3. **Weigert's iron haematoxylin**
   Mix equal volumes of solution A and solution B. Store mixed solutions at 4 ºC for one month.

4. **0.1 % (w/v) Picro-Sirius Red**
   Weigh out 0.1 g Sirius red powder in fume cupboard and dissolve into 100 mL of aqueous picric acid solution using a magnetic stirrer. Store at room temperature for up to six months and filter before use.
5. **Millers' stain**
6. **IMS**
7. **Xylene**
8. **DPX mountant**

**Method:**

Prior to staining tissue samples were dewaxed and rehydrated, the same slide was used to stain for both the collagen and elastin. Samples were immersed in 5 % (w/v) potassium permanganate for five minutes and then rinsed with distilled water, and

then submerged into 1 % (w/v) oxalic acid for two minutes, rinsed with water for a further four minutes and submerged in 95 % (v/v) IMS and 70 % (v/v) IMS for one minute respectively. Samples were then stained for one hour with Millers' stain and rinsed with 95 % (v/v) ethanol, 70 % (v/v) ethanol and distilled water respectively. Samples were subsequently stained with Weigert's iron haematoxylin for ten minutes and rinsed with distilled water for thirty seconds for blueing. Samples were then stained with 0.1 % (w/v) Picro-Sirius Red for one hour, rinsed with distilled water and blot dried. Sections were dehydrated, cleared and mounted using DPX mountant before being viewed under Kohler and polarised illumination.

#### 2.2.3.5 Reticulin stain

The reticulin stain is used to stain reticular fibres (collagen III) within formalin fixed, paraffin embedded tissue. Potassium permanganate sensitises the reticular fibres, allowing silver to be deposited. The silver solution readily precipitates, therefore formalin is used as a reducing agent to allow silver to be deposited in the form of a metal. Excess silver is subsequently removed using the hypo solution. Fibres stain neutral black with high intensity

**Reagents:**

1. **1 % (w/v) potassium permanganate**
   Add 1 g of potassium permanganate to 100 mL of deionised water and dissolve using a magnetic stirrer. Store the solution for up to six months at room temperature

2. **10 % (w/v) aqueous silver nitrate**
   Add 10 mg of silver nitrate to 10 mL deionised water and stir using a magnetic stirrer and bar.

3. **3 % (w/v) sodium hydroxide solution**
   Add 0.15 g sodium hydroxide to 5 mL deionised water and stir using a magnetic stirrer and bar

4. **Ammoniacal silver solution**
   Add ammonia drop by drop to 5 mL 10 % (w/v) aqueous silver nitrate solution until precipitate that forms has just dissolved. Add 5 mL of aqueous silver nitrate

solution to 5 mL of 3 % (w/v) sodium hydroxide. Add ammonia drop by drop until the resulting precipitate is completely dissolved and the solution retains a trace of opalescence and then make up to 50 mL with distilled water.

5. **1 % (w/v) oxalic acid**
   Add 1 g oxalic acid to 100 mL of distilled water and dissolve using a magnetic stirrer. Use immediately.

6. **2.5 % (w/v) aqueous iron alum**
   Add 2.5 g ferric ammonium sulphate (iron alum) to 100 mL distilled water and stir using a magnetic stirrer and bar

7. **0.2 % (w/v) gold chloride**
   Add 0.2 g gold chloride to 100 mL distilled water and mix thoroughly by inversion

8. **Hypo solution (5 % sodium thiosulphate)**
   Add 5 g sodium thiosulphate to 100 mL distilled water and stir using a magnetic stirrer and bar

9. **10 % (w/v) aqueous formalin**
10. **IMS**
11. **Xylene**
12. **DPX mountant**

**Method:**

Prior to staining tissue samples were dewaxed and rehydrated and then oxidised in 1 % acidified potassium permanganate for three minutes. Samples were then rinsed with tap water before bleaching them in 1 % oxalic acid for one minute. The samples were then rinsed with tap water before immersing them in 2.5 % iron alum for ten minutes. The slides were then rinsed twice in distilled water and then placed in ammoniacal silver solution for a further two minutes. Samples were rinsed twice in distilled water and then reduced in 10 % aqueous formalin for a further two minutes. Samples were then rinsed under running tap water before being immersed in 0.2 % gold chloride for two minutes. Samples were rinsed again with tap water

before being immersed in hypo solution for three minutes and then briefly rinsed again with tap water. Sections were dehydrated, cleared and mounted using DPX mountant before being viewed under Kohler illumination.

#### 2.2.3.6 Oil Red O staining

Cryosectioned native and decellularised nerve samples were stained for lipid and fat using Oil Red O solution. Presence of lipid within tissue was detected by presence of a bright reddish-orange colour.

**Reagents:**

1. **0.5 % (w/v) Oil Red O stock solution**
   Dissolve 0.5 g of Oil Red O into 100 mL isopropanol.

2. **Oil red O working solution**
   Dilute 30 mL of Oil Red O stock solution with 20 mL distilled water. Allow to stand for ten minutes and filter using a 0.2 μm syringe filter into a Coplin jar. Solution should be prepared on the day of use.

3. **Harris haematoxylin**
4. **IMS**
5. **DPX mountant**

**Method:**

Prior to staining tissue slides were fixed in 3.7 % formaldehyde for 5 minutes at room temperature. The tissue slides were immersed in Oil Red O working solution for ten minutes and rinsed in distilled water before being immersed in haematoxylin for ten seconds finally being rinsed again with distilled water. Each slide was then mounted using DPX mountant and a coverslip and left to dry overnight in a fume cupboard before being viewed under an upright microscope.

### 2.2.4 Immunolabelling using FITC-conjugated antibodies

#### 2.2.4.1 Tissue fixation

Tissues were fixed in 3.7 % (v/v) formaldehyde for 24 hours, placed into the automated tissue processor and wax embedded as described in Section 2.2.2.1.

| Antigen | Supplier | Isotype | Clone | Initial concentration | Working dilution |
|---|---|---|---|---|---|
| **Rabbit anti-laminin antibody L9393** | Sigma Aldrich | | Polyclonal | 0.5 mg. $mL^{-1}$ | 1°Ab 1:50<br>2°Ab 1:100 |
| **Rabbit anti-fibronectin antibody F3648** | Sigma Aldrich | | Polyclonal | | 1°Ab 1:400<br>2°Ab 1:100 |
| **Anti-S100 -astrocyte marker ab868** | abcam ® | IgG | Rabbit Polyclonal | | 1°Ab 1:200<br>2°Ab 1:400 |
| **Anti-GFAP delta primary antibody ab28926** | abcam ® | IgG | Rabbit Polyclonal | | 1°Ab 1:200<br>2°Ab 1:400 |
| **FITC-conjugated secondary anti-rabbit antibody** | Vector Labs | | | | |
| **Anti- PGP 9.5 antibody Z511601-2** | Dako | | Rabbit Polyclonal | | 1°Ab 1:200<br>2°Ab 1:100 |

**Table 2.5 Antibodies and working dilutions used for labelling tissue samples**

| Antigen | Supplier | Isotype | Clone | Initial concentration | Working dilution |
|---|---|---|---|---|---|
| **Anti-S100 - astrocyte marker ab868** | abcam ® | IgG | Rabbit Polyclonal | | 1°Ab 1:250<br>2°Ab 1:200 |
| **Anti-GFAP delta primary antibody ab28926** | abcam ® | IgG | Rabbit Polyclonal | | 1°Ab 1:250<br>2°Ab 1:200 |
| **Anti-p75 NGF receptor antibody** | abcam ® | IgG | Rabbit Polyclonal | 0.3 mg. $mL^{-1}$ | 1°Ab 1:50<br>2°Ab1:100 |
| **FITC-conjugated secondary anti-rabbit antibody** | Vector Labs | | | | |

**Table 2.6 Antibodies and working dilutions used for labelling cells**

**Reagents:**

1. **0.1 % (v/v) Triton X-100**
   Add 10 µL Triton x-100 to 9.99 mL PBS and mix using vortex

2. **1 % (w/v) BSA solution**
   Dissolve 0.1 g bovine serum albumin into 10 mL PBS and pass the solution through a 0.2 µm filter

3. **7.5 % (w/v) BSA solution**
   Dissolve 3.75 g bovine serum albumin into 5 mL PBS and pass the solution through a 0.2 µm filter

**Method:**

Prior to staining tissue samples were dewaxed and rehydrated. Tissue sections were circled with a hydrophobic marker and gently permeabilised with 0.1 % (v/v) Triton X-100 diluted in PBS for 20 minutes. Samples were then incubated with 7.5 % (w/v) bovine serum albumin diluted in PBS at room temperature for sixty minutes, followed by washing once with 1 % (w/v) BSA in PBS. Tissue samples were incubated with primary antibody (diluted to appropriate concentration with 1% BSA) at 4 °C overnight in a humidified chamber. The following day the samples are washed three times with PBS, five minutes each time and then incubated with secondary FITC conjugated antibody at room temperature in the dark for one hour. Each section is then washed three times with PBS for five minutes and counterstained with 300 nM DAPI in PBS and incubated for twenty minutes in the dark at room temperature. Sections are then washed three times with PBS for five minutes and then immersed in PBS. Images are captured using long focal distance (3.5 mm) 'water dipping' objective lenses (10 9/0.3 and 20 9/0.5; Zeiss Achroplan) and a Zeiss LSM510 META upright/inverted confocal microscope (xenon arc lamp to excite FITC ($\lambda_{ex}$ = 495 nm / $\lambda_{em}$ = 515 nm). Nuclei were visualised using $\lambda_{ex}$ = 300 nm / $\lambda_{em}$ = 510 nm.

## 2.2.5 Cell culture

### 2.2.5.1 Cell culture techniques

Human dermal fibroblast and RN22 cells used in this study were cultured in standard DMEM cell culture medium (Section 2.1.7.3). The primary rat Schwann cells were cultured in MEM-d-valine (Section 2.1.7.4). All medium changes were performed aseptically in a Class II cabinet. All medium and reagents added to the cells were warmed to 37 °C before use. Cells were cultured at 37 °C in 5 % $CO_2$ (v/v).

### 2.2.5.2 Resurrection and maintenance of cells

Cells were removed from liquid nitrogen storage, and thawed in a 37 °C water bath. A T75 cell culture flask with 10 mL cell culture medium was prepared. When the cells were defrosted, 1 mL of the defrosted cell stock was slowly added into the T75 flask. The flask was incubated at 37 °C in 5 % $CO_2$ (v/v) overnight to allow the cells to attach to the flask. The medium was changed every two days until the cells became confluent and ready to be passaged.

### 2.2.5.3 Cell viability using Trypan blue

Trypan blue dye is used to detect dead cells as the dye permeates into dead cells due to the loss of their membrane potential whilst live cells appear transparent. To perform the viability test, 20 µL of cell suspension was mixed with 20 µL of Trypan blue dye in a bijoux tube. 20 µL of this mixture was added to a haemocytometer. Viable cells were counted in *n* of the nine grids (*n* = the number of grids which allowed the viable cell count to fall between 100 and 300). The total number of viable cells per mL in the cell suspension was calculated as follows:

$$Number\ of\ cells/mL = \frac{Number\ of\ viable\ cells}{n} \times 10^4 \times Dilution\ factor$$

*n* was the number of grids used to count the cells

*Dilution factor* was the correction required due to the dilution of the cell suspension with Trypan blue dye (in this case, *Dilution factor* = 2)

#### 2.2.5.4 Cell passaging

The culture medium was aspirated from each cell culture flask, and the cell layer was washed in PBS for two minutes. Trypsin/EDTA (5 mL) was added to each T75 culture flask, and the flasks were incubated in 5 % CO2 (v/v) at 37 °C for 3 minutes. Following incubation, the cells were detached by gently tapping the flasks. The trypsin/EDTA was neutralised by adding 10 mL of culture medium to each flask. The cell suspension was transferred into a universal tube and centrifuged for five minutes at 1000 g. Following centrifugation, the supernatant was carefully removed and the cell pellet was resuspended in 5 mL of cell culture medium. A viable cell count (Section 2.2.5.3) was performed and cells were seeded into fresh flasks at the appropriate density. The cell culture medium was changed every other day until the cells became confluent and ready to be passaged again.

#### 2.2.5.5 Cell storage

Cells were isolated from the flasks (Section 2.2.6.4), and diluted to $1x10^6$/mL with cryopreservation medium (DMEM containing 20 % (v/v) FBS, 10 % (v/v) filter sterilised Dimethyl sulfoxide (DMSO). The addition of DMSO prevented the formation of ice crystals during freezing, but it is toxic to the cells. In order to avoid the toxic effects, the cells were frozen immediately after the addition of DMSO. The cell suspension was aliquoted into 1 mL cryovials, and placed into a cryo freezing pot which contained isopropanol and placed into a -80 °C freezer overnight. The following day all vials were transferred to liquid nitrogen for long-term storage.

### 2.2.6 Uniaxial tensile testing

The biomechanical properties of native and acellular porcine peripheral nerves (peroneal and tibial nerves) were compared using uniaxial tensile testing to failure in order to determine any significant effects of the decellularisation procedure on the mechanical properties of the tissue. The length of the nerve was kept to approximately 10 mm and the thickness of the tissue was measured using callipers. Three measurements were taken for each specimen at different positions along its length, and the average thickness was recorded.

Hydrated samples of freshly dissected porcine peripheral nerves and acellular nerves were clamped, using a standard clamping system into a BOSE

tensiometer, using a 450 N load cell. A single pull to failure test was carried out at a speed of 0.1 mm. $s^{-1}$ with a gauge length of 8 mm. The specimen was clamped in the holder with two grip blocks and the load cell recorded the strength produced by the sample (Figure 2.1). The first failure point or plateau was used to calculate the ultimate tensile strength (UTS) and the displacement at this point was recorded as strain at ultimate tensile strength. The initial linear gradient was used to calculate the Young's modulus (or elastic modulus). A typical stress-strain curve of peripheral nerve is illustrated in Figure 2.2.

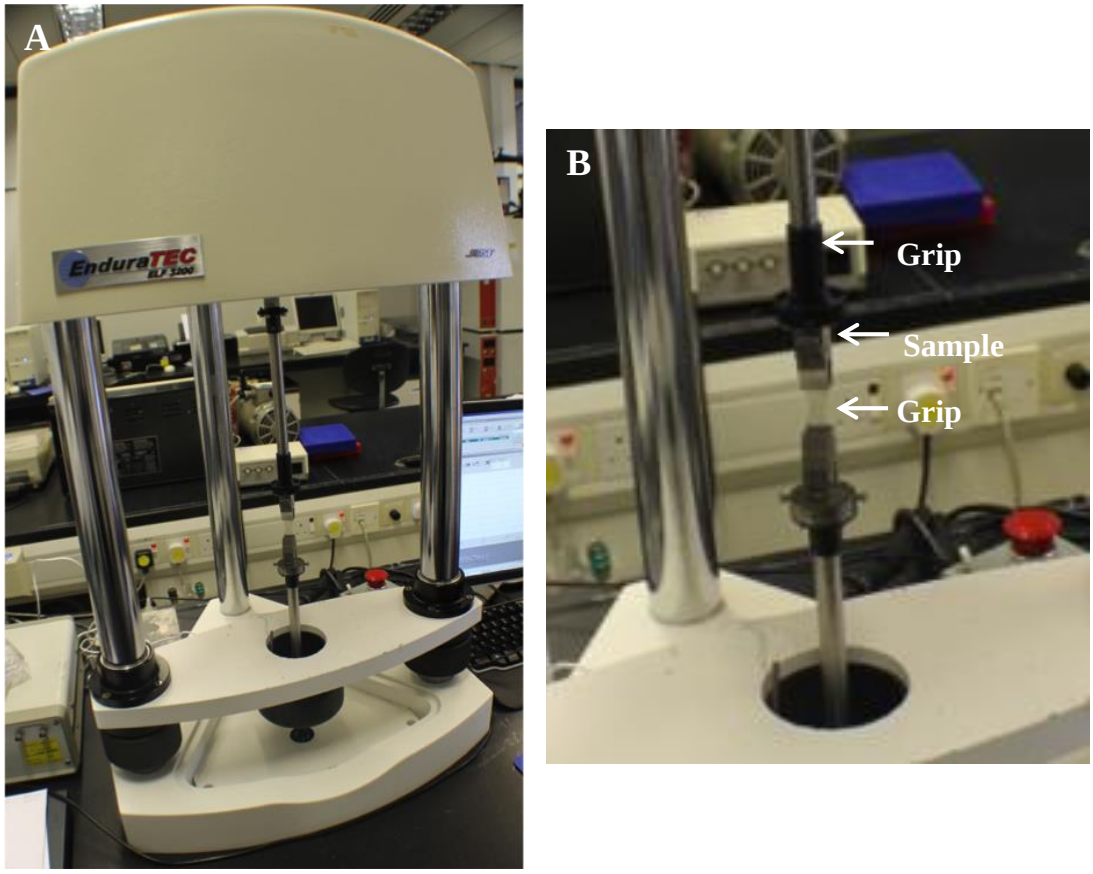


**Figure 2.1. Tensile testing of tissue sample.** The sample is placed between two grip fixtures which clamp the sample. Weight is then applied to the sample gripped at one end whilst the other is fixed. The weight or load keeps increasing at a controlled rate whilst at the same time measuring the change in length of the sample. (A) BOSE Electroforce test instrument. (B) Grips stretching sample.

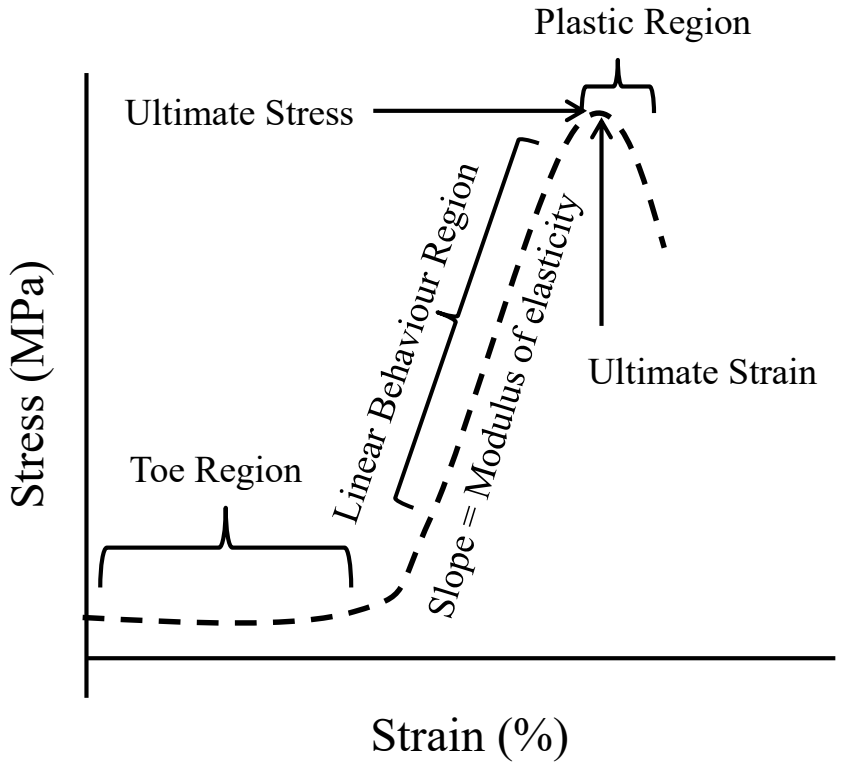


**Figure 2.2. Typical stress-strain curve for peripheral nerves.** The transition between the toe region and the linear region corresponds with the strain in situ. The slope of the stress-strain curve is called the modulus of elasticity and represents the stiffness of the nerve. If the slope is steep, then the nerve has more stiffness and is less compliant to elongation. If the slope is shallow, then the nerve has less stiffness and is more compliant to elongation. Once the nerve has reached the ultimate strain, the structural integrity of the nerve is overcome and the deformation is termed "plastic". Reproduced from Topp and Boyd (2006)

The tensile testing machine operating programme, WinTest® 2002 software (EnduraTEC) was used to analyse the data for each test run. Using the recorded load/displacement data, the stress was calculated for each data point according to:

$$\sigma = \frac{F}{A}$$

Where $\sigma$ represents the stress in MPa, $F$ the force in Newtons (N) and $A$ the cross sectional area of the nerve in $mm^2$. The cross sectional area was calculated as $A$ = nerve width × specimen thickness.

The strain was calculated according to:

$$\varepsilon = \frac{\Delta l}{l}$$

where $\varepsilon$ represents strain, $\Delta l$ the extension of the nerve in mm and $l$ the gauge length (8 mm)

The analysis of the results was carried out per treatment group (at least three replicates from three different porcine legs). The stress-strain curves for the specimens of each group were averaged over the number of samples in each test group using the Origin software program (Version 8.5, Microbal). In addition, the tensile strength, strain and YM for each nerve obtained from BOSE machine were averaged over the number of specimens in the group.

### 2.2.7 Statistical analysis

In this study, all numerical data was analysed using GraphPad Prism and are shown as mean values ± 95 % confidence limits. Statistical significance was assessed using a Student's *t*-test and one-way ANOVA was applied for the comparison of data from more than two groups using Tukey's procedure. *P*-values of <0.05 were considered significant.

# Chapter 3. Characterisation of Porcine Peripheral Nerves in the Lower Limb for Tissue Engineering Applications

## 3.1 Introduction

The peripheral nervous system (PNS) is comprised of nerves, enclosed bundles of long fibres or axons and neurons, which connect the central nervous system to the rest of the body (Saladin 2011). The primary function of the PNS is to allow for movement, sensation and changes in behaviour to be undertaken in response to external or internal stimuli. Peripheral nerves in the lower limb are composed of sensory, motor and sympathetic fibres. The sciatic nerve, situated in the posterior compartment of the leg, is the largest nerve beginning in the lower back and runs down towards the lower limb. Its function consists of providing motor innervation to the muscles of the posterior aspect of the thigh and those of the leg and foot, and sensory innervation to the skin of the lateral aspect of the leg and almost all of the foot (Williams PL 1995). The sciatic nerve divides into two terminal branches - the tibial and common peroneal nerve, with the tibial nerve being the larger of the branches. The tibial nerve provides motor innervation to the muscles of the posterior compartment of the leg and sensory innervation to the posterior aspect of the leg, via its contribution to the sural nerve and the sole of the foot. The peroneal nerve provides motor innervation to the muscles of the lateral compartment of the leg, which innervates the foot, and sensory innervation to the distal section and dorsum of the foot (McCrory, Bell et al. 2002). The sural nerve, formed by the junction of the medial sural cutaneous nerve with the peroneal branch, is a small superficial sensory nerve providing innervation to the posterior calf, lateral ankle, heel and foot (Riedl and Frey 2013).

When considering injuries to peripheral nerves it is reported that several hundred thousand such injuries occur each year in Europe (300,000 cases annually) (Mohanna, Young et al. 2003)]. Peripheral nerve injuries are more common than spinal cord injuries, and over 50,000 surgical procedures are performed annually in the United States to repair damaged peripheral nerves (Noble, Munro et al. 1998). Current treatment is comprised of either direct end-to-end surgical suturing of the damaged nerve ends or the use of an autologous nerve graft. Suturing is limited to a few millimetres for the repair of small defects or gaps. For longer nerve gaps (>20 mm), the current ‘gold standard’ treatment is autologous grafting; using

a sensory nerve such as the sural nerve to replace the injured tissue. There are limitations to using this method, most notably donor site morbidity, chronic pain, and a lack of suitable donor nerve tissue. Due to a relatively small diameter, multiple sural nerve segments may be placed side by side to match the width of the nerve being replaced (Dahlin 2008). In addition, sural nerves also possess smaller fascicular patterns (i.e. the number and size of fascicles), which may not match the fascicular patterns of the nerve being grafted (Meek and Coert 2002). Considering these limitations there are clinical requirements for better approaches to aid nerve regeneration (Schmidt and Leach 2003).

Tissue and organ decellularisation has been proposed as a method to create scaffolds for regenerative medicine applications. The process of decellularisation aims to remove all of the native cells from a given tissue without adversely affecting its biochemical and mechanical properties. A resulting decellularised graft should retain a native ECM, which does not elicit an immune response, and may provide a native microenvironment containing cell adhesive and growth supporting properties. It is hypothesised that such a graft will support axon regrowth for the repair of small gap nerve defects (Whitlock, Tuffaha et al. 2009)

Human donor nerves have been used in nerve repair. Avance® Nerve Graft, a commercial available decellularised human nerve allograft is reported to better support nerve regeneration compared with commercially available NGCs (Whitlock, Tuffaha et al. 2009). However, the supply of human nerve tissue for decellularisation and use as a graft material is extremely limited in the United Kingdom and therefore research has focused on use of xenogeneic tissue due to ease of harvesting and availability. For small gap repair, xenogeneic nerve tissue from rat, rabbit and pigs have been evaluated (Gutmann and Sanders 1943; Osawa, Tohyama et al. 1990; Hudson, Liu et al. 2004; Whitlock, Tuffaha et al. 2009; Zhang, Luo et al. 2010). Rat sciatic nerve has been extensively characterised and evaluated for use as a nerve graft due to its ease of harvest and availability (Osawa, Tohyama et al. 1990; Hudson, Liu et al. 2004; Whitlock, Tuffaha et al. 2009; Wang, Zhang et al. 2014). However, rat sciatic nerves have limitations on the size of nerve that can be obtained. In contrast, it is hypothesised that porcine nerves are anatomically similar to human nerves. Other pig tissues and organs closely approximate their human counterparts; cross-linked porcine heart valves for example have been widely used clinically. Moreover, porcine nerves have been

considered suitable for trauma studies of the facial nerve (Barrs, Trahan et al. 1991). In addition, porcine nerve tissue may have the potential to be used for longer and more specific nerve gap injuries due to their size, length, motor and sensory similarities to human nerves (Moore, MacEwan et al. 2011).

To the best of our knowledge there have been very few studies evaluating the potential of porcine peripheral nerves as grafts to repair short and long gap defects. However, in order to use porcine nerves clinically an understanding of the anatomy and physiology of porcine peripheral nerves is required, and this is currently absent from the literature.

## 3.2 Aims and objectives

**Aims:**

The aim of the study was to evaluate the anatomical organisation, structure and characteristics of the major peripheral nerves in the porcine hind leg.

**Objectives:**

- Dissect and identify the porcine nerves in the lower limb
- Evaluate the histioarchitecture (connective tissue and fascicular pattern) of each nerve by haematoxylin and eosin staining
- Assess the suitability of porcine peripheral nerves and rat sciatic nerves for tissue engineering applications

## 3.3 Methods

### 3.3.1 Dissection of porcine peripheral nerves in the lower limb

Large white Yorkshire pigs (24 - 26 weeks old) were obtained from a local abattoir (John Penny & Sons, Leeds, United Kingdom) within 24 hours of slaughter. The sciatic, tibial, common peroneal and sural nerves were isolated and dissected, with initial reference to the anatomy of human nervous system anatomy of the lower leg. The sciatic nerve was dissected from the posterior compartment of the leg. The sciatic nerve divided into two terminal branches; the tibial and common peroneal nerve. The tibial nerve was observed to travel in the posterior section of the leg and the peroneal nerve in the lateral section. The sural nerve was dissected by a longitudinal incision made from the popliteal fossa along the posterior midline and towards the posterior-inferior aspect of the lateral malleolus (Figure 3.1). Excess fat and connective tissue was removed from the nerve samples and tissues washed three times in PBS containing 0.1 % (w/v) EDTA to remove excess blood. Tissues were then stored at -80 °C on PBS moistened filter paper for future use. All nerves were 150 - 300 mm in length and varied in diameter, with the peroneal nerve ranging from 2 - 3 mm and the tibial nerve ranging from 2 - 4 mm.

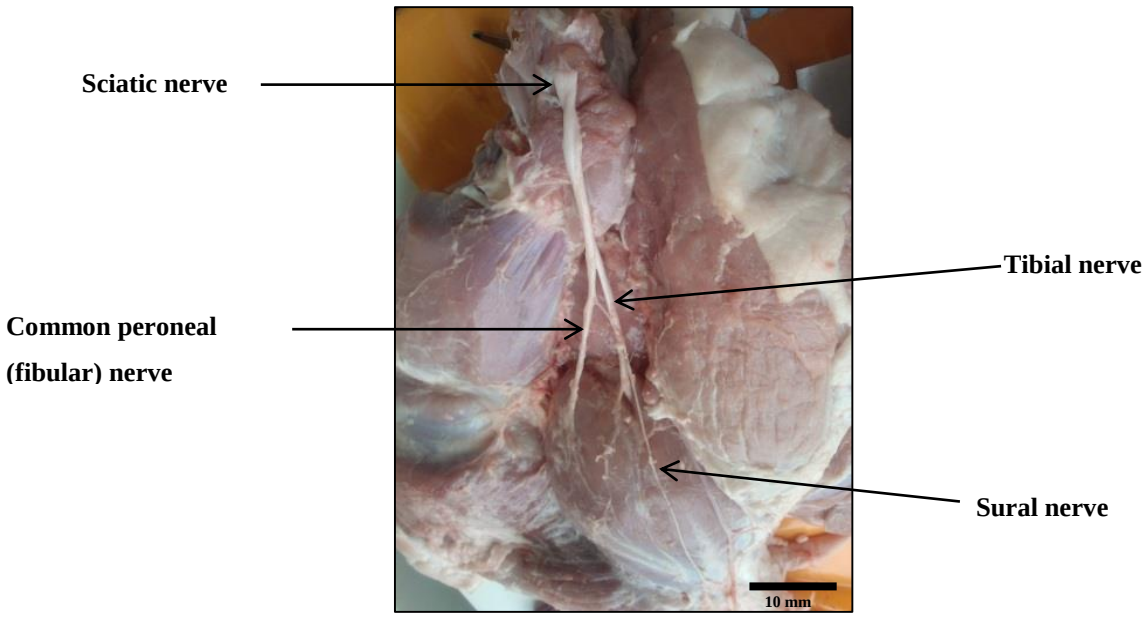


**Figure 3.1 Peripheral nerves dissected from the posterior section of the porcine hind limb.** The sciatic nerve divides into the tibial and common peroneal nerves. Both the tibial and peroneal nerves run caudal to the stifle joint with the tibial running into the muscle. Two cutaneous branches, the medial and lateral branch off from the tibial and peroneal nerve respectively to form the sural nerve. Scale bar at 10 mm.

### 3.3.2 Dissection of rat sciatic nerve

Male Wistar rats (10-12 weeks old) were killed by a Schedule 1 method (cervical dislocation). The rat skin was cut a around the abdominal region and skin above the gluteus maximus muscle was removed. The rat was then positioned ventral side down and a the sciatic nerve was bilaterally dissected by seperating the muscle tissue from the upper dorsal thigh, cutting the nerve just above this position at one end and immediatley above the knee at the other end to obtain a length of approxiamtley 1.5 cm The sciatic nerve was dissected

## 3.4 Results

### 3.4.1 Identification of porcine peripheral nerves

Porcine peripheral nerves were dissected from the posterior section of the porcine hind limb. The sciatic divided into two branches of the tibial and common peroneal nerve.

Both the tibial and peroneal nerve run caudal to the stifle joint with the tibial running into the muscle. Two cutaneous branches, the medial and lateral branch off from the tibial and peroneal nerve respectively to form the sural nerve (Figure 3.2).

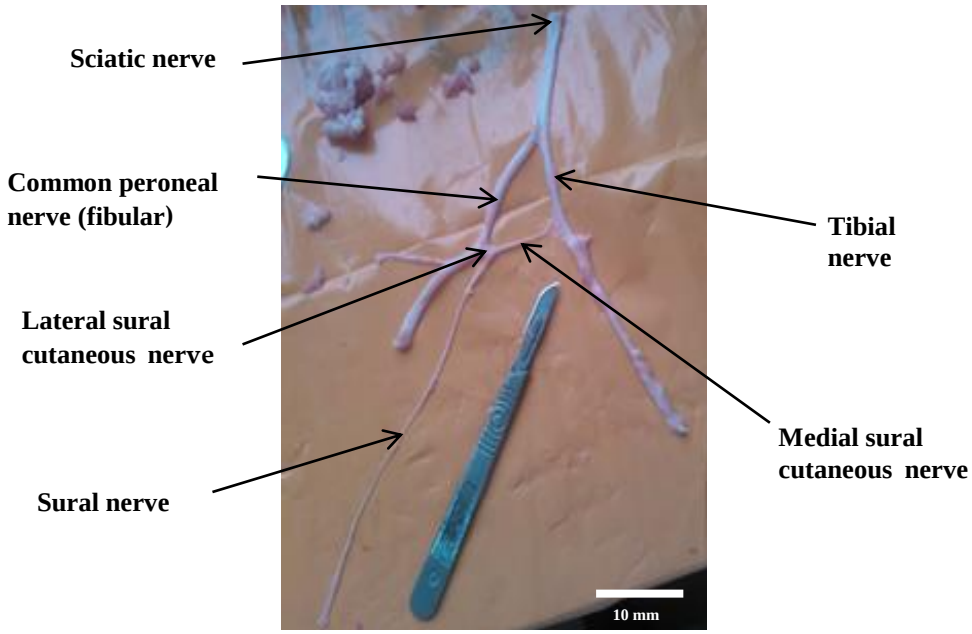


**Figure 3.2 Peripheral nerves dissected from the posterior section of the porcine hind limb.** The sciatic nerve divides into the tibial and common peroneal nerves. Two cutaneous branches, the medial and lateral nerves branch off from the tibial and peroneal nerves respectively to form the sural nerve. Scale bar at 10 mm.

### 3.4.2 Histological evaluation of native porcine peripheral and rat sciatic nerve

Peripheral nerves were embedded and sectioned transverly and longitudinally to reveal their histoarchitecture. Haematoxylin and eosin stained transverse and longitudinal sections revealed the nerve fasicles which contained a a large portion of cells embedded within the endoneurial connective tissue seen in blue. Each fasicle was surrounded by a perineurium layer, which also consisted of surrounding cells. The epineurium is the surrounding connective tissue (Figure 3.3).

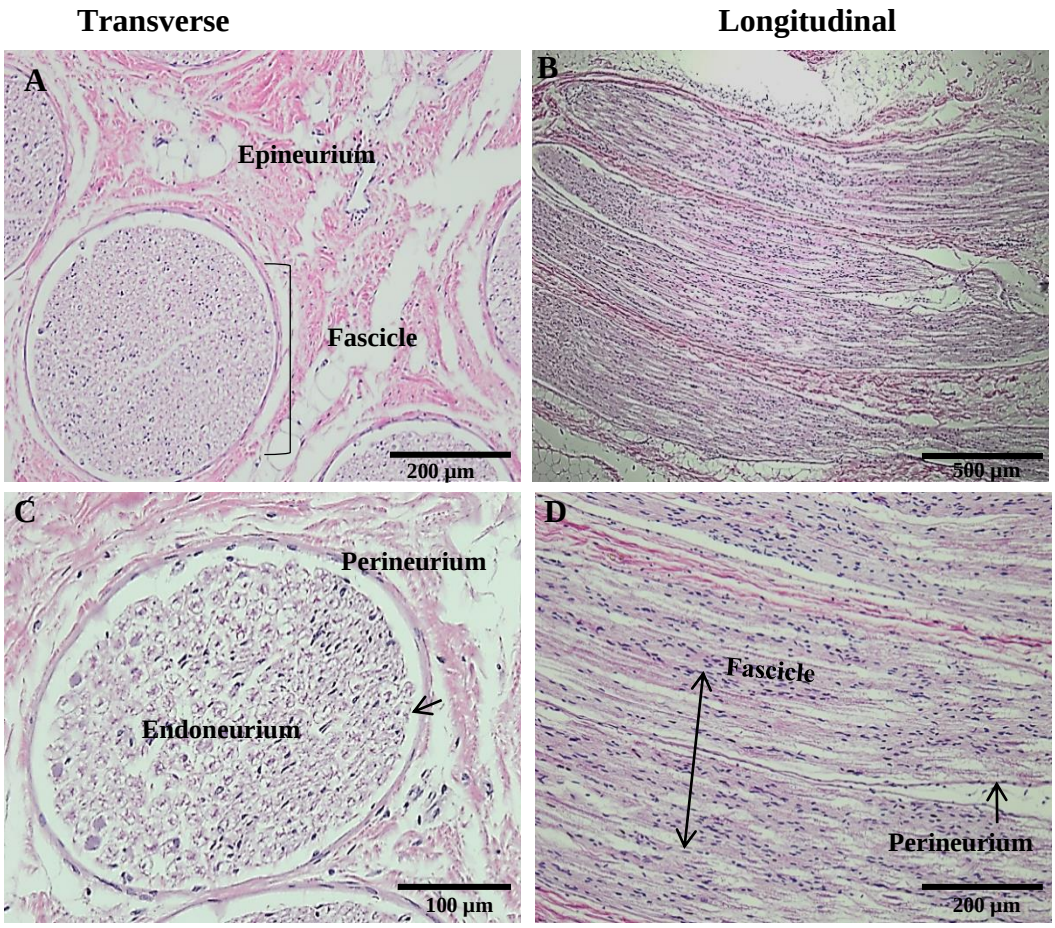


**Figure 3.3 Histoarchitecture of transverse and longitudinal porcine peripheral nerve sections stained with haemotoxylin and eosin.** Peripheral nerve in transverse orientation reveal circular fasicles (A&C). Peripheral nerve in longitudinal orientation reveal long fasicles (B&D). The surrounding connective tissue is stained pink and cell nuclei are stained blue. Scale bars at 500 µm, 200 µm and 100 µm.

By haemotoxylin and eosin, the porcine nerves showed variation in the funiculi pattern within each nerve segment as they branch. The sciatic nerve showed to possess slightly larger nerve fasicles than the rest of its branches, however it was found to possess a similar hstoarchitecture to its branches (pereoneal and tibial nerve) in displaying closely packed nerve fascicles within the epineneurium. In

contrast, the sural nerve and the cutaneous branches were found to contain a much smaller number of fasicles which are also smaller in size and sparsely distributed when compared to the sciatic nerve and its branches (Figures 3.4).

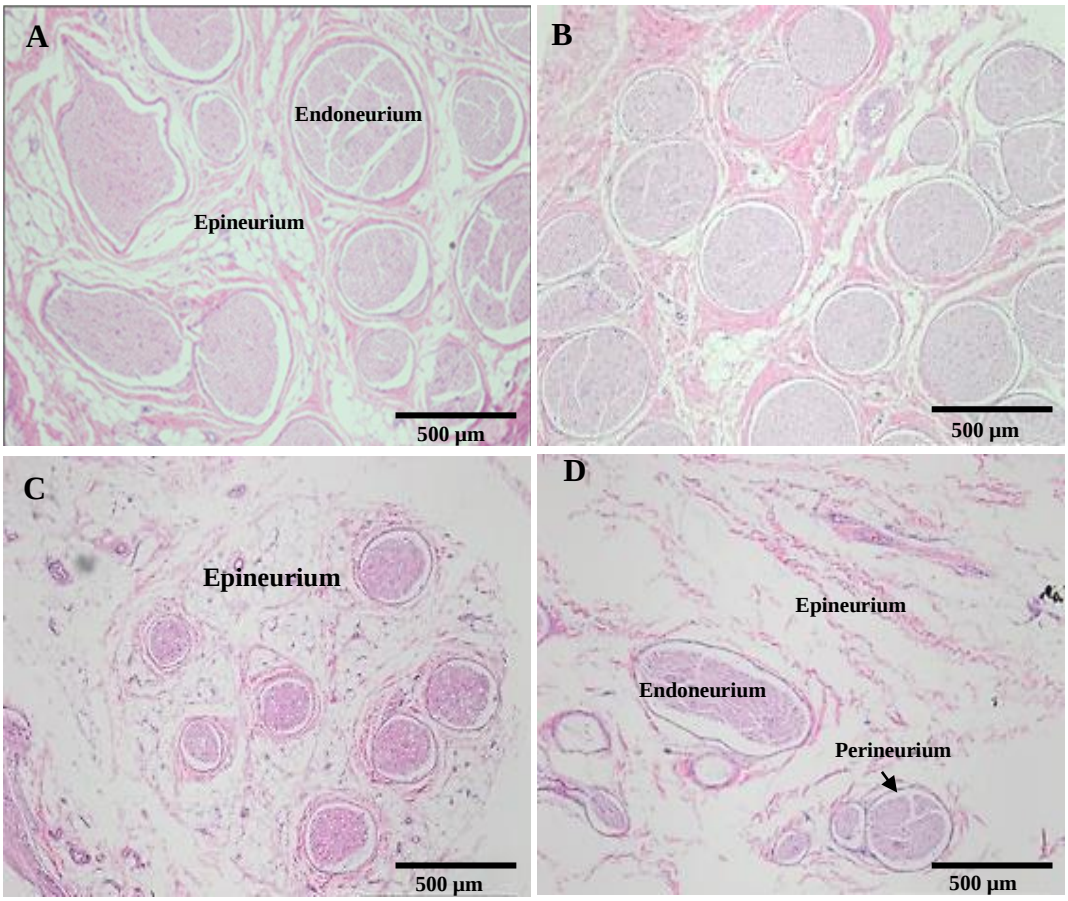


**Figure 3.4 Histoarchitecture of transverse porcine peripheral nerve sections using haemotoxylin and eosin stain.** The sciatic nerve (A) and its branches (pereoneal and tibial nerve) (B) have numerous nerve fascicles packed closely together within the epineneurium. The sural nerve (C) and the cutaneous branches (D) have much smaller and sparsely distributed nerve fascicles within the epineurium. Scale bar at 500 µm.

The rat sciatic nerve had larger but a fewer number of fasicles in comparison to the porcine nerves. Nevertheless, similar to the porcine sciatic nerve and its branches (peroneal and tibial), the fasicles found in the rat scaitic nerve were closely packed together with little epineurium space (Figure 3.5).

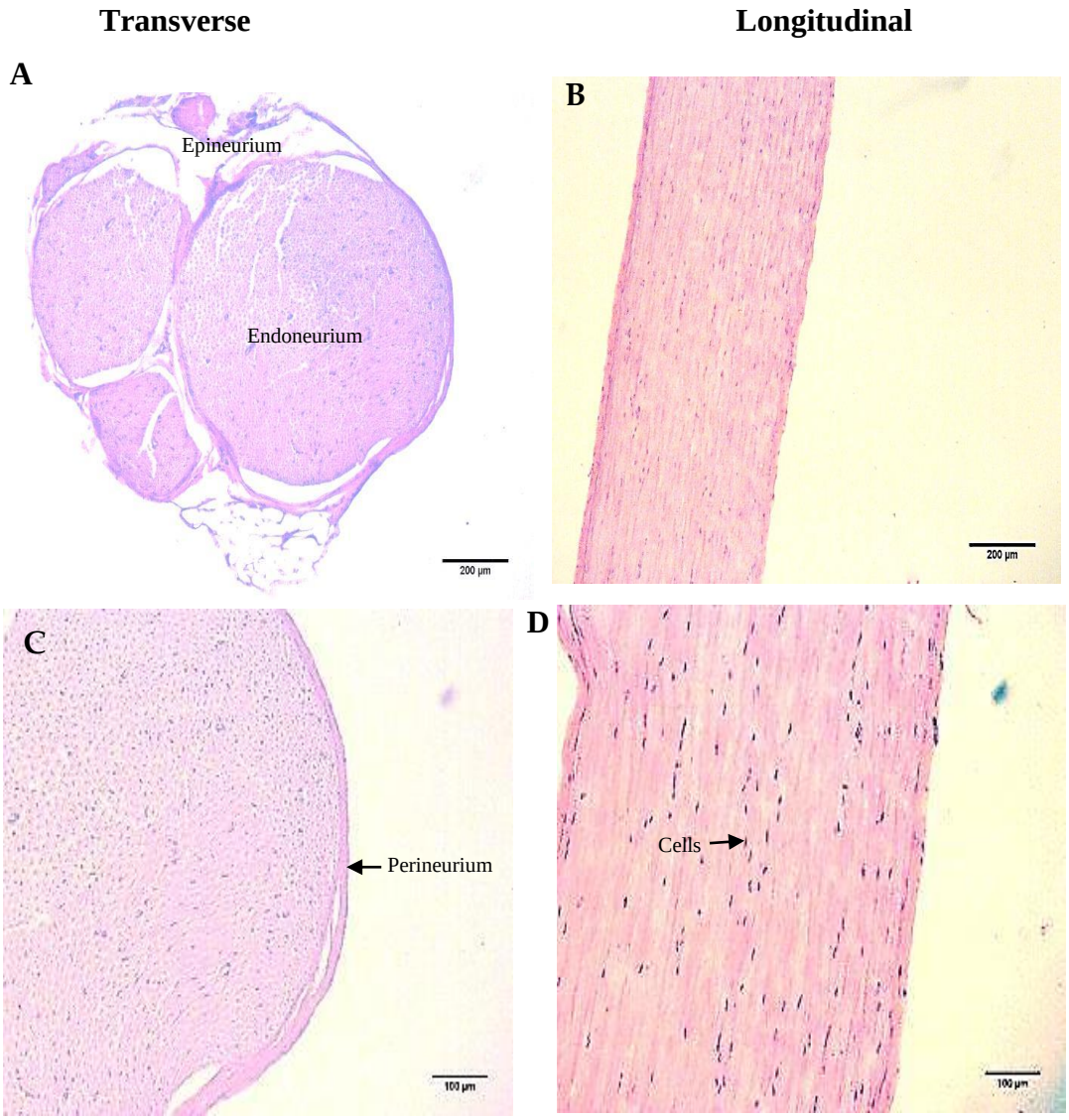


**Figure 3.5 Histoarchitecture of rat sciatic nerve.** Transverse (A & C) and longitudinal (B&D) orientation using haemotoxylin and eosin stain. Transverse sections revealed the rat sciatic nerve fascicles contained an endoneurium and perineurium. Longitudinal sections revealed cells (blue) aligning amongst collagen fibrils. Majority of the cells are located within the perineurium and the endoneurium Scale bars A and B at 200 µm; Scale bars C and D at 100 µm.

### 3.4.3 Quantification of fasicle size and area

The histology data of both porcine and rat nerve were quantified and analysed using Image J by using transverse images to measure the fasicle area. Data showed the porcine sciatic nerve to have an average of 11 fasicles with an average area of 150 ± 34.18mm$^2$, whilst its branches had on average 20 fasicles with an average area of 94.08 ± 12.28 mm$^{2.}$ The sural cutaneous branch had an average of six fasicles with an average area of 68.97 ± 35.69 mm$^2$ and the sural nerve had an average seven fasicles, with an average area of 47.93 ± 6.510 mm$^2$. In terms of fasicle area size the porcine sciatic nerve was significantly larger than the sural nerve. The rat sciatic

nerve had an average of three fasicles with an average area of 157.3 $mm^2$ . This area was similar to the porcine sciatic nerve (Table 3.1).

| **Nerve** | **Average number of fascicles** | **Area of fascicles ($mm^2$)** |
|---|---|---|
| **Porcine sciatic** | 11 | 150.45 ± 34.18 |
| **Porcine sciatic branches** | 20 | 94.08 ± 12.28 |
| **Porcine sural cutaneous branch** | 6 | 68.97 ± 35.69 |
| **Porcine sural** | 7 | 47.93 ± 6.510 |
| **Rat sciatic** | 3 | 157.3 ± 80.16 |

**Table 3.1 The average number and area of fascicles present in porcine and rat peripheral nerves.** Porcine and rat sciatic nerve have the largest fasicle area. The sural nerve has the smallest fasicle area, which is significantlly smaller than the sciatic nerves ($p$<0.05). Porcine sciatic nerve have on average 11 fasicles with an average area of 150 ± 34.18$mm^2$ (n = 3); sciatic branches (pereoneal/tibial nerve) have on average 20 fasicles with an average area of 94.08 ± 12.28 $mm^2$ (n = 3) ; sural cutaneous branch has an average of six fasicles with an average area of 68.97 ± 35.69 $mm^2$ (n =3); sural branch has an average of seven fasicles with an average area of 47.93 ± 6.510 $mm^2$ (n =3) and rat sciatic nerve has an average of three with an average area of 157.3 $mm^2$ (n = 3). Data was analysed using the unpaired Student's *t*-test and is presented as the mean ± 95 % C.I

## 3.5 Discussion

In this study the identification and characterisation of porcine peripheral nerves located in the lower limb is reported. The rat sciatic nerve was also included in the study as a control.

The general nerve branching observed in the porcine peripheral nerves is consistent with similar findings in the peripheral nerve anatomy of humans as well as other mammals such as rat (Sunderland and Ray 1948; Schmalbruch 1986). In addition, the length and dimensions of the porcine nerves were found to be comparable to that of human nerves (Gustafson, Grinberg et al. 2012). The fasicular pattern observed in the porcine nerves was similar to that reported for human studies (Sunderland 1990; Chentanez, Cha-oumphol et al. 2006; Ugrenovic, Jovanovic et al. 2013; Ugrenović 2014). When mapping the branches from the sciatic nerve, the fascicular patterns within the individual nerves have previously been shown to differ in respect to the arrangement, size and number. Sunderland et al. (1948) reported no constant or characteristic pattern in regards to the number and size of the funiculi, which varied greatly from nerve-to-nerve and individual-to-individual at any given level (Sunderland and Ray 1948). Interestingly, a study by Ugrenović et al. (2014) showed a significant difference in the average number of fascicles between the tibial and common peroneal nerve. The common peroneal nerve had a significantly lower number of fascicles; however there was no significant difference in the average value of fascicular area or diameter between the two nerves (Ugrenović 2014).

The internal nerve structure has substantial relevance in terms of the clinical outcome of nerve lesions, as well as the surgical repair of nerve injuries. In direct nerve repair the surgeon aligns the fascicles by matching similar looking ones in the stumps to prevent misalignment in addition to using epineurial blood vessels (Stewart 2003). Similarly in nerve grafting, attention to the fascicular pattern is thought to be of importance in achieving good functional recovery (Stewart 2003). In turn, an appropriately matched nerve graft would lead to a more accurate technical repair, minimal sutures and potentially less scarring.

A study conducted by Burks et al. (2014) highlighted the challenge of insufficient donor nerve graft with a specific focus on human sciatic nerve transection requiring autologous sural nerve graft. The authors reported that a

considerable degree of variability existed in the diameter of the fascicles and cross sectional area of the sural nerve harvested, in comparison with the sciatic nerve. The study also reiterated the fact that small sensory nerves such as the sural nerve do not provide sufficient material for grafting and that allogeneic intercostal nerves (common peroneal or tibial) are preferred (Burks, Levi et al. 2014). This approach was reported by (Mackinnon, Doolabh et al. 2001) where the tibial nerve was reconstructed with allograft tissue .

The sciatic nerve in both porcine and rat possess larger fascicles in comparison to its branches. It was initially demonstrated by Sunderland et al. (1961) that there are more fascicles and larger cross-sectional area of extrafasicular connective tissue present in regions when the nerve passed a joint, such as the sciatic nerve. This led to the later suggestion that this was a protective feature by which vulnerable areas of nerves resisted mechanical injury (Sunderland and Bradley 1961). A study by (Phillips, Smit et al. 2004) also concluded that sciatic nerves exhibited greater strain in the joint region, however it was further concluded that this was a result of the complex tissue architecture rather than fascicle number (Mason and Phillips 2011).

## 3.6 Conclusion

In summary, this study details the anatomy of porcine peripheral nerves in the lower limb. The results demonstrate that porcine nerves are more comparable to human nerves than rat in terms of anatomical structure and size. In addition, the study also highlights anatomical differences of the nerve as it branches. It is therefore suggested that the similarities between porcine and human nerve may allow for the clinical use of porcine nerves as grafts following nerve injury.

# Chapter 4. Optimisation of Methods for the Decellularisation of Porcine Peripheral Nerves

## 4.1 Introduction

Xenogeneic tissues such as porcine can be used as nerve grafts as they provide an ECM which mimics the native nerve tissue as described in Chapter 3. They contain an endoneurial microstructure which can provide the same level of guidance and regenerative support as nerve autografts. In addition, these nerves can also offer the potential for size/length and motor/sensory specificity (Moore, MacEwan et al. 2011).

However when used clinically these grafts possess risks from the immune response from the body due to the presence of foreign cells (Janeway, Travers et al. 1999; Mackinnon, Doolabh et al. 2001; Badylak 2014). Alternatively, the immunogenic components from the graft can be removed through a processing condition called decellularisation, producing a non-immunogenic acellular tissue graft. Acellular grafts still retain the 3D structure and ECM components of the native tissue; however, it can be used clinically without eliciting an immune response. The rationale behind decellularisation are that ECM components are generally conserved amongst species and are tolerated well by recipients (Ratner, Hoffman et al. 2004; Badylak, Freytes et al. 2009).

Xenogeneic nerve grafts such as rat (Hudson, Liu et al. 2004; Kim, Yoo et al. 2004; Yu, Peng et al. 2009; Gao, Zheng et al. 2014); porcine (Zhang, Luo et al. 2010); Macaca fascicularis (Hess, Brenner et al. 2007); Rhesus monkey (Hu, Zhu et al. 2007) have been used extensively in tissue engineering applications. It has been reported that decellularised nerve allografts are capable of returning adequate sensation in nerve defects ranging from 0.5 to 3 cm without infection or rejection (Moore, MacEwan et al. 2011). In another study, Hudson et al 2004 showed the ability of macrophages to migrate within a decellularised tissue and produce growth factors to promote axonal regeneration (Hudson, Zawko et al. 2004).

The aim of any decellularisation protocol is to remove all immunogenic cellular and nuclear material whilst preserving the biochemical and biomechanical properties of the ECM. However, any process that removes cells will ultimately alter the native three dimensional architecture of the ECM.

A number of methods have been documented for the preparation of acellular nerve grafts from donor nerve tissue. The most commonly utilised method for decellularisation of nerve tissue involves physical (Hiles 1972; Gulati 1988; Evans, Mackinnon et al. 1998; Ide, Tohyama et al. 1998), chemical (Sondell, Lundborg et al. 1998; Hudson, Liu et al. 2004) or enzymatic treatments (Wang, Itoh et al. 2015) .

Physical methods used to facilitate decellularisation of nerve tissues include cold preservation (Evans, Mackinnon et al. 1998) thermal (Gulati 1988; Ide, Tohyama et al. 1998) and radiation (Hiles 1972). Prolonged cold preservation of donor nerve tissue resulted in the preservation of native Schwann cell basal laminae and nerve ECM. The drawbacks however were the long processing times (approximately seven weeks) as well as poor mechanical properties of the decellularised graft (Evans, Mackinnon et al. 1998).

Thermal decellularisation subjects the nerve tissue to repeated freeze-thaw cycles, rendering the graft non-immunogenic by lysing cells (Zalewski and Gulati 1982; Gulati and Cole 1994). The process however fails to remove the cell remnants and fractures the basal laminae that surround myelinated and unmyelinated axons. *In vivo* studies have shown that cellular remnants left behind from this process lead to cellular invasion in the form of Schwann cells and macrophages invading the basal lamina to clear away the debris and thereby delaying the regenerative process and further damaging the basal lamina (Pollard and Fitzpatrick 1973; Osawa, Tohyama et al. 1990; Danielsen, Kerns et al. 1995).

Radiation has also been used as a decellularisation technique for nerve tissue. Studies have shown that this process does not damage the tissue morphology (Marmor 1964). Nevertheless similar to thermal decellularisation, cellular debris still remains inside the basal laminae causing cellular invasion post implantation (Hudson, Liu et al. 2004).

Physical decellularisation treatments have the ability to detach cells from the nerves ECM. However, their inabilities to remove cellular debris from the tissue and the destructive effects of freeze-thawing on the nerve ultrastructure makes these processes insufficient. Therefore, to achieve complete and effective decellularisation physical treatments are usually combined with a chemical treatment, which includes the presence of detergents and hyper/hypotonic solutions. Commonly, physical treatments are applied at the beginning of the

decellularisation process to disrupt the cell membrane and lyse the cells and are then followed by the chemical treatments.

Detergents are the predominant chemical treatments used in the decellularisation of nerves (Sondell, Lundborg et al. 1998; Hudson, Liu et al. 2004; Wakimura, Wang et al. 2015). Ionic, non-ionic, and zwitterionic detergents have been shown to be effective in the removal of cellular material by solubilising both cytoplasmic and nuclear cellular membranes. However, these detergents can also denature proteins in the ECM by disrupting protein-protein interactions (Seddon, Curnow et al. 2004; Gilbert, Sellaro et al. 2006). Common ionic detergents that have been used for nerve tissue include sodium dodecyl sulphate (SDS) (Wakimura, Wang et al. 2015), sodium deoxycholate (Wang, Itoh et al. 2015) and Triton X-200 (Hudson, Liu et al. 2004).

A study by Wang et al (2015) used TritonX-100 on its own and as a combination with sodium deoxycholate to decellularise rat sciatic nerve. The results showed that in both treatments there were nerve fibre breakage as well as traces of myelin sheath and cells still present within the tissue (Wang, Itoh et al. 2015). In another study by Wakimura et al (2015) a combination of 1% SDS and Triton X-100 was used to decellularise rabbit median nerves. Results demonstrated an intact structure with the elimination of cells. Further *in vivo* analysis showed limited ED1-positive macrophage invasion in addition to abundant axons and Schwann cells penetrating through the implanted nerves (Wakimura, Wang et al. 2015).

Compared to other detergents SDS is the most effective detergent for removal of cellular material , nuclear remnants, and cytoplasmic proteins (Booth, Korossis et al. 2002; Grauss, Hazekamp et al. 2005; Wilcox, Korossis et al. 2005; Wilshaw, Kearney et al. 2006). A drawback of SDS does however include disruption to the native tissue structure and collagen structure (Gilbert, Sellaro et al. 2006). However studies have found that a low concentration of SDS (0.1 %; w/v) can eliminate cells whilst preserving the native structure of the tissue (Booth, Korossis et al. 2002; Wilcox, Korossis et al. 2005), as well as maintaining the tissues mechanical strength (Korossis, Booth et al. 2002).

Non-ionic detergents such as Triton X-100 have been extensively used due to their mild effects upon tissue structure. Using a combination of Triton X-100 and sodium deoxycholate Sondell et al. (1998) produced an acellular graft that was

shown to support nerve regeneration. Post implantation analysis revealed regenerating axons within the basal lamina tubes and migration of host Schwann cells, which reoccupied the empty basal lamina tubes without excessive signs of inflammation (Sondell, Lundborg et al. 1998) . The grafts however were still not able to match the regeneration rates observed with the autograft, even with the incorporation of Schwann cells (Frerichs, Fansa et al. 2002). It was hypothesised that the inadequate preservation of the basal lamina in the acellular graft was a contributing factor to this failure (Hudson, Zawko et al. 2004). Studies using Triton X-100 have reported a decrease in laminin and fibronectin content (Grauss, Hazekamp et al. 2005) which would attributed to damage of the basal lamina.

A milder chemical decellularisation technique developed by Hudson et al (2004) used zwitterionic detergents in conjunction with Triton X-200; sulfobetaine-10 (SB-10) and Triton X-200/sulfobetaine-16 (SB-16). This process demonstrated superior preservation of native ECM and equivalent levels of decellularisation compared with the Sondell chemical processing technique (Hudson, Liu et al. 2004). *In vivo* analysis of the acellular nerve graft developed by Hudson showed no sign of rejection on the basis of the level of immune cells (T cells and macrophages) in the graft. There was no increase in $CD8^+$ cells (cell surface markers on cytotoxic T cells) when compared with isografts, however there was a slightly higher invasion of macrophages within the acellular graft. A possible cause is that the open basal lamina tubes and the absence of myelin permitted a greater number of macrophages to invade and remain inside the grafts (Hudson, Zawko et al. 2004). Regeneration capacities of the acellular graft showed that the axon density at the midpoints of the acellular graft was indistinguishable from that in isografts and statistically higher than in the thermally decellularised model described by Gulati et al. (1988) and the chemically decellularised model described by Sondell et al. (1998).

The decellularisation process developed by Hudson et al (2004) is now licensed by AxoGen® Inc. which produces Avance®, a clinically approved nerve graft for PNS injury repair. The Avance® nerve graft has shown to be superior over the comercially available NGCs in promoting nerve regeneration (Karabekmez, Duymaz et al. 2009; Whitlock, Tuffaha et al. 2009; Mackinnon 2011). This is most likely attributed to the retention of the nerves ECM and basal lamina which are

known to play important in promoting and guiding axonal growth (Faweett and Keynes 1990; Ide, Osawa et al. 1990; Martini 1994; Hudson, Liu et al. 2004).

Alongside detergents enzymatic treatments are commonly used in the decellularisation process. These include the use of calcium chelating agents and nucleases. Nucleases such as endonucleases catalyse the hydrolysis of the interior bonds of deoxyribonucleotide or ribonucleotide chains whereas exonucleases catalyse the hydrolysis of the terminal bonds which ultimately leads to the degradation of RNA and DNA (Crapo, Gilbert et al. 2011). The effectiveness of enzymatic treatment for the removal of cellular material from the ECM has been studied in a variety of tissues with varied results. Chelating agents such as EDTA and EGTA form a ring-shaped molecular complex that binds and isolates a central metal ion. Divalent cations such as $Ca^{2+}$ and $Mg^{2+}$ are needed for cell attachment to collagen and fibronectin at the Arg-Gly-Asp receptor. By binding the divalent cations present at the cell adhesions to the ECM the chelating agents facilitate in the removal of the cellular material from the tissue.

Hypotonic and hypertonic solutions are commonly used in the decellularisation process. Hypotonic solutions are used to lyse the cells within tissues through osmotic shock with minimal changes in matrix molecules and architecture (Xu, Chan et al. 2007). Hypertonic solutions dissociate DNA from proteins (Cox and Emili 2006). For a maximum osmotic effect, it is common for the tissue to be immersed alternatively in hyper and hypotonic solutions. This treatment however does not remove the cellular remnants from the tissue therefore additional enzymatic or chemical treatments are necessary for the removal of the cellular debris (Crapo, Gilbert et al. 2011).

During the decellularisation process proteases are released from lysed cells which can cause damage to the native ECM ultrastructure. Protease inhibitors such as Aprotinin are therefore added to solutions. Buffered solutions of pH 7 - 8 as well as temperature control and time of exposure to the lysis solutions can also limit protease activity.

Following the completion of the decellularisation process the tissues must be sterilised prior to *in vitro* cell seeding or *in vivo* studies. Sterilisation of biological scaffolds is vital to eliminate endotoxins and viral and bacterial DNA that may be present. Sterilisation methods have included incubation in acids or

solvents, ethylene oxide exposure, gamma irradiation and electron beam irradiation (Hodde and Hiles 2002).

Acid and alkaline treatments solubilise the cytoplasmic component of the cells as well as removing nucleic acids such as RNA and DNA through hydrolytic degradation (Gilbert, Sellaro et al. 2006). Acids such as peracetic (PAA), sulphuric and hydrochloric can effectively disrupt cell membranes and intracellular organelles. PAA is an oxidising agent and an effective chemical sterilant (Pruss, Kao et al. 1999; Hodde and Hiles 2002). PAA also doubles up as a decellularisation agent with the removal of residual nucleic acid (Badylak, Tullius et al. 1995) as well as being an excellent agent for inhibiting viruses (Hodde and Hiles 2002). PAA has minimal effect on the ECM composition and structure as seen with the preservation of several collagen types in a variety of porcine tissue such as small intestinal submucosa (SIS) and the urinary bladder (Hodde, Janis et al. 2007; Gilbert, Wognum et al. 2008). PAA treatment retains many of the native GAGs (hyaluronic acid, heparin, heparin sulphate, chondroitin sulphate A and dermatin sulphate) (Hodde, Badylak et al. 1996) as well as numerous growth factors including transforming growth factor-β, fibroblast growth factor and vascular endothelial growth factor (Voytik‐Harbin, Brightman et al. 1997; Hodde, Record et al. 2001)

Peracetic acid has been associated with oxidative damage to collagen due to their reactivity with oxygen-free radicals. The presence of these compounds have been associated with crosslinks which can affect the mechanical properties of the sterilised ECM (Monboisse and Borel 1992; Brown, Merritt et al. 2002). The microstructure of the collagen fibres have also been reported to be dissimilar after the PAA treatment (Brown, Lindberg et al. 2006). However a study by Hodde et al (2002) found that endothelial cells were still able to adhere to PAA treated porcine small intestinal submucosa (SIS) and urinary bladder matrix (UBM) which suggests that amino acid sequences responsible for cell adhesion remained unaltered by the PAA (Hodde, Record et al. 2002). In addition a study by Freytes et al (2004) showed no significant difference between PAA treated and untreated porcine SIS, UBM and urinary bladder submucosa (UBS) (Freytes, Badylak et al. 2004).

The efficacy of a given decellularisation protocol varies depending on the tissue, composition and density. In the case of denser tissues such as peripheral nerves access for the decellularisation solutions may be more difficult. It is therefore common to immerse the tissues in the solutions whilst being subjected to agitation. Immersion and agitation methods of tissue decellularisation have been well documented in a variety of tissues including heart valves (Meyer, Chiu et al. 2006), tendons(Cartmell and Dunn 2000) and peripheral nerves (Hudson, Liu et al. 2004; Karabekmez, Duymaz et al. 2009). The duration of this method is dependent on tissue thickness and density as well as the detergent used and the intensity of agitation.

It is important to highlight that for each tissue studied, it is necessary to optimise a decellularisation and sterilisation protocol to achieve optimal cell removal without significantly damaging the ECM. Each variable will affect the composition and ultrastructure of the ECM which in turn will influence the host tissues response to the tissue following implantation (Gilbert, Sellaro et al. 2006). The removal of DNA is a vital indicator in determining the efficacy of the decellularisation method. It is possible to quantitatively assess cell components such as double-stranded DNA (dsDNA), single stranded DNA (ssDNA), RNA, mitochondria or membrane associated molecules. Currently there is no value for the level of residual cellular material permitted within an acellular scaffold or what amount of residual material will elicit an immune response, this is almost certainly dependent on the tissue being decellularised. No decellularisation technique can remove 100 % of cell material, even with the most rigorous processing methods (Badylak 2014). Most commercially available biological scaffolds contain trace amounts of remnant DNA, nonetheless the clinical efficacy of these devices have been largely positive (Table 4.1).

| Source Tissue | Source species | Products |
|---|---|---|
| **Dermis** | Porcine | Strattice ™(Lifecell), XenMatrix ™ (Bard Davol) |
| **Dermis** | Bovine | TissueMend ® (Stryker), Veritas ® (Synovis) |
| **Pericardium** | Equine | OrtAdapt ® (Synovis) |
| **Pericardium** | Bovine | CopiOs ® (Zimmer Inc), Perimount ® (Edwards Lifesciences) |
| **Small intestine** | Porcine | Surgisis ® (Cook Biotech), Restore ® (DePuy Orthapaedics), FortaFlex® (Integra LifeSciences) |
| **Urinary bladder** | Porcine | MatriStem® (ACell) |

**Table 4.1 Summary of clinically approved products produced from xenogeneic tissue. Reproduced from Badylack (Badylak 2014)**

Based on findings from *in vivo* studies in which constructive remodelling has been observed with no adverse host or cell responses, a minimum criteria has been developed to describe a decellularised scaffold (Crapo, Gilbert et al. 2011).

- < 50 ng dsDNA per mg ECM dry weight
- < 200 bp DNA fragment length
- Lack of visible nuclear material in tissue sections stained with 4, 6-diamidino-2-phenylindole (DAPI) or haematoxylin and eosin

This Chapter therefore describes the development of a method for the decellularisation of porcine peripheral nerves, based on a previously developed method for arterial matrices (Wilshaw, Rooney et al. 2012). To create the most effective acellular nerve tissue the decellularisation process developed in the present study included a combination of physical, chemical and enzymatic methods.

Freeze-thawing is carried out as the initial physical decellularisation step to detach cells from the ECM. Subsequently chemical and enzymatic treatments such as SDS, EDTA, hypotonic and hypertonic buffers are added to efficiently remove the cells from the tissue. A low concentration of SDS is chosen to remove cellular material and cytoplasmic proteins whilst preserving the native structure. In addition, a nuclease treatment is also added to remove DNA and RNA from the tissue as well as a final sterilisation step using PAA.

## 4.2 Aims and Objectives

**Aims:**

The aim of the study presented in this Chapter was to optimise a process for the decellularisation of porcine peripheral nerves.

**Objectives:**

- To develop a decellularisation method for porcine peripheral nerves that is able to remove the cells and cellular remnants whilst preserving the histioarchitecture and the biomechanical integrity of the ECM.
- To determine which type of peripheral nerve to use as a scaffold
- To characterise the decellularised porcine peripheral nerves histologically
- To assess the efficacy of the decellularisation process by quantifying the amount of DNA left in the nerve

## 4.3 Methods

### 4.3.1 Decellularisation solutions

#### 4.3.1.1 Disinfection solution

This solution was prepared fresh before use and consisted of 100 mL PBS containing 10 µg/mL vancomycin hydrochloride, 100 µg/mL gentamicin sulphate and 50 µg/mL polymyxin B. The volume was made up to 500 mL with PBS.

#### 4.3.1.2 EDTA solution (200 mM)

EDTA (74.4 g) was dissolved in 1 L distilled water and the pH of the solution was adjusted to 7.2 - 7.4 by adding either 6 M hydrochloric acid or sodium hydroxide pellets. The solution was stored at room temperature for up to one month. Aprotinin (1 mL, 10,000 KIU/mL) was added to the solution just before use.

#### 4.3.1.3 PBS EDTA solution (2.7 Mm; 0.1% w/v) containing 10 KIU/mL aprotinin

EDTA (1 g) was added to 1 L PBS and the pH of the solution was adjusted to 7.2 - 7.4 by adding either 6 M hydrochloric acid or sodium hydroxide pellets. The solution was stored at room temperature for up to one month. Aprotinin (1 mL, 10,000 KIU/mL) was added to the solution immediately before use.

#### 4.3.1.4 Hypotonic buffer (10 mM Tris, 2.7 mM EDTA, 10 KIU/mL aprotinin)

Trizma base (1.21 g) and EDTA (1 g) was dissolved in 900 mL distilled water and the pH of the solution was adjusted to 8 - 8.2 by adding either 6 M hydrochloric acid or sodium hydroxide pellets. The solution was made up to 1 L with distilled water and autoclaved. The solution was stored at room temperature for up to one month. Aprotinin (1 mL, 10,000 KIU/mL) was added to the solution immediately before use.

#### 4.3.1.5 Hypertonic buffer (50 mM Tris buffer, 1.5 M sodium chloride)

Trizma base (6.06 g) and sodium chloride (87.66 g) was dissolved in 900 mL distilled water and the pH of the solution was adjusted to 7.5 - 7.7 by adding either 6M hydrochloric acid or sodium hydroxide pellets. The solution was made up to 1 L with distilled water and autoclaved. The solution was stored at room temperature for up to one month.

#### 4.3.1.6 SDS hypotonic buffer (0.1 % w/v SDS, 10 mM Tris, 0.1 % w/v EDTA, 10 KIU/mL aprotinin)

SDS (1 g) was added to 10 mL distilled water to make a 10 % (w/v) stock solution and filter sterilised. The 10 % (w/v) SDS stock solution was added to 990 mL sterile hypotonic buffer. The unused hypotonic SDS buffer was stored for up to one week at 4 °C if it was opened aseptically. Aprotinin (1 mL, 10,000 KIU/mL) was added to the solution just before use

#### 4.3.1.7 Nuclease treatment solution (50 mM Tris buffer, 1 mM $MgCl_2.6H_2O$, 1 U/mL Benzonase)

Trizma base (6.1 g) and magnesium chloride (0.203 g) was dissolved in 100 mL distilled water and the pH of the solution was adjusted to 7.5 - 7.7 by adding either 6M hydrochloric acid or sodium hydroxide pellets. The solution was made up to 1 L with distilled water and autoclaved. On the day of use 4 µL of Benzonase (250 U/µL) was added to the solution under sterile conditions. The nuclease solution must be used within ten minutes of preparation.

#### 4.3.1.8 Peracetic solution (0.1 % v/v)

PAA (40 %, 2.5 mL) was added to 500 mL of PBS. The pH was adjusted to 7.2 - 7.5 by adding 6 M NaOH dropwise. The solution was made fresh just prior to use.

### 4.3.2 Histology

#### 4.3.2.1 Evaluating the decellularisation process

Tissue samples from three decellularised nerves from different animals were fixed with 3.7 % (v/v) formaldehyde and paraffin embedded as described in Section 2. Histological evaluation was performed as described in Section 2.2.4 Paraffin embedded tissue sections of 6 µm were all positioned transversely to study the effects of decellularisation. Haematoxylin and eosin was used to study the tissue architecture and cell distribution. H&E samples were viewed using an upright microscope. Nuclei were imaged using an upright fluorescent microscope using a DAPI filter ($\lambda_{ex}$ = 300 nm / $\lambda_{em}$ = 550 nm)

#### 4.3.2.2 Evaluating the lipid content of native and acellular tissue

Tissue samples from native and acellular nerves were cryo embedded as described in Section 2.2.3.1. Cryo embedded tissue sections of 10 µm were positioned

longitudinally to study the lipid content. Slides were stained with Oil Red O and haematoxylin as described in Section 2.2.4. Oil Red O and haematoxylin were used to study the lipid content and cell distribution. Samples were viewed using an upright microscope.

### 4.3.3 DNA quantification

DNA quantification was used to determine the total remaining DNA in porcine peripheral nerves following decellularisation by comparing the DNA levels in decellularised and fresh tissue. This was for determining the efficacy of the decellurisation process.

#### 4.3.3.1 DNA extraction

DNA was extracted from fresh and decellularised porcine nerves using the QIAgen DNeasy blood and tissue kit. DNA was extracted from tissues from three fresh and three decellularised porcine nerves. For each nerve triplicate samples were taken for DNA extraction.

Samples of the fresh and decellurised porcine nerves were lyophilized to a constant weight prior to DNA quantification assay. Each sample consisting of 100 mg tissue were macerated with a scalpel blade and placed in a sterile 1.5 mL microcentrifuge tube. The samples were then freeze-dried; the mass of each sample was recorded daily until a consistent weight was achieved (approximately 25 mg).

DNA extraction was carried out using the DNeasy blood and tissue kit (QIAgen). Buffer ATL (360 µL) and proteinase K (40 µL), both from the QIAgen kit, were mixed with the macerated freeze dried tissue by vortexing and incubating at 56 °C for three hours or until the tissue was completely digested. Pulse vortexing (5 to 10 seconds) was performed every 30 minutes to disperse the sample. Each sample was vortexed for 15 seconds at the end of the incubation. Buffer AL (400 µL) from the QIAgen kit was added to the sample, and mixed thoroughly immediately by vortexing and 400 µL of ethanol (100 %; v/v) was added, and mixed thoroughly immediately by vortexing.

Each sample was transferred to a separate DNeasy Mini spin column placed in a 2 mL collection tube, and centrifuged at 6,000 × g for one minute. The flow-through was discarded together with the collection tube. The DNeasy Mini spin column was placed in a fresh 2 mL collection tube, and Buffer AW1 (500 µL) was added to the column. The DNeasy membrane at the bottom of the DNeasy Mini

spin column was dried by centrifuging at 15,000 × g for three minutes. The flow-through was discarded together with the collection tube. The DNeasy Mini spin column was placed in a clean 1.5 mL microcentrifuge tube, and Buffer AE (200 µL) was added directly to the centre of the DNeasy membrane. After incubation for one minute, the 1.5 mL microcentrifuge tube was centrifuged for one minute at 6,000 × g to elute. The extracted DNA was in Buffer AE in the flow-through. The DNeasy Mini spin column was discarded. The extracted DNA was subjected to quantification immediately or stored at – 20 °C until needed.

#### 4.3.3.2 DNA quantification by spectrophometry

The concentration of extracted DNA was determined spectrophometrically using a Nanodrop spectrophotometer. Buffer AE (2 µL) was used as a blank. Extracted DNA sample (2 µL) was loaded onto the Nanodrop, and the absorbance was determined at 260 nm. Three readings were taken for each sample, and the mean was considered as the absorbance of the sample. The DNA concentration (ng/µL) in the sample was directly displayed in the Nanodrop software. This concentration was used to calculate the DNA weight/tissue weight (µg/mg) according to:

$$\text{DNA weight/tissue weight (µg/mg)} = \frac{c \times 200}{25 \times 1000}$$

where *C* represents the DNA concentration in the Buffer AE (ng/µL). The volume of the Buffer AE containing extracted DNA was 200 µL. The total weight for each tissue sample was 25 mg. The mean ± 95 % C.I. of the DNA weight/tissue weight (µg/mg) for each region of fresh (n = 3) or decellularised (n = 3) tissue was calculated.

### 4.3.4 Dissection and storage of porcine peripheral nerves

Yorkshire pigs (24 - 26 weeks old) were obtained from a local abattoir (John Penny & Sons, Leeds, United Kingdom) within 24 hours of slaughter. The peripheral nerves dissected from the porcine leg included the femoral, sciatic, tibial, common peroneal and sural nerve. Femoral nerves (10 - 15 mm diameter) were dissected from the anterior compartment of the thigh. Sciatic nerve (10 - 15 mm diameter) was dissected from the posterior compartment of the leg. The sciatic nerve divides into two terminal branches; the tibial (3 - 6 mm diameter) and common peroneal

nerve (2 - 4 mm diameter). The tibial nerve travels in the posterior leg and the peroneal nerve travels in the lateral compartment of the leg. The sural nerve (1 - 1.5 mm diameter) was dissected by a longitudinal incision made from the popliteal fossa along the posterior midline and towards the posterior-inferior aspect of the lateral malleolus. As much excess fat and connective tissue was removed from the samples and the tissues were washed thrice at room temperature, 30 minutes each time in PBS containing 0.1 % (w/v) EDTA and Aprotinin 10 KIU/mL to remove excess blood. Tissues were then cut into individual 5 cm segments, positioned longitudinally to avoid any kinks and stored at - 80 °C on PBS moistened filter paper for future use.

## 4.4 Decellularisation of peripheral nerves

Prior to the decellularisation process the peripheral nerves were subjected to a freeze-thaw cycle and individually placed in 200 mL sterile containers containing 200 mL disinfection solution and incubated for an hour at 37 °C under agitation (containers were placed horizontally) at 120 rpm. Each nerve was subjected to 200 mL of the solutions indicated below. Figure 4.1 summarises the standard decellularisation process. The number of SDS and nuclease cycles along with incubation temperature and agitation speeds was subject to change.

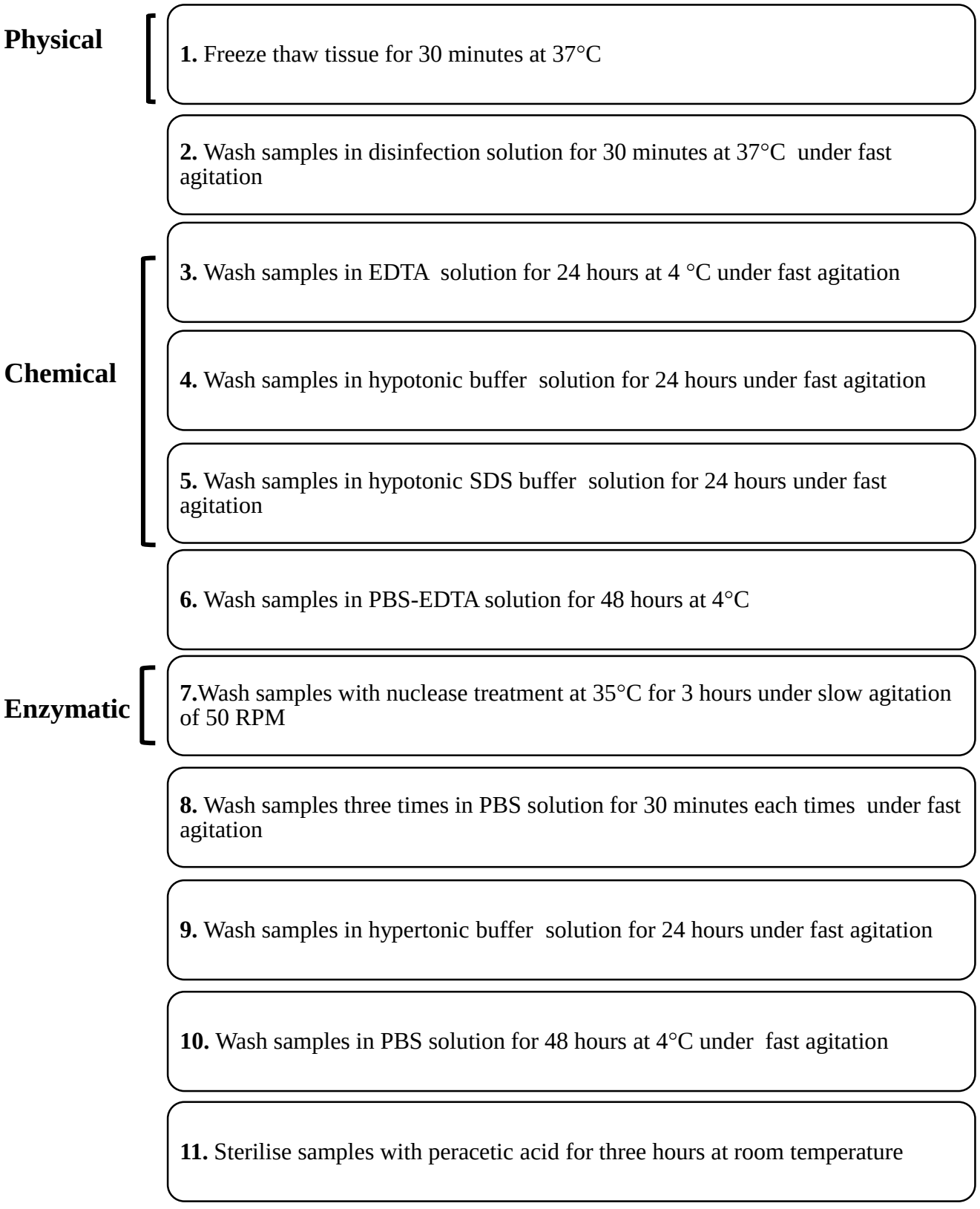


**Figure 4.1 Overview of the key stages involved in the decellularisation process.** The process involves a combination of physical, chemical and enzymatic treatment for efficient cell removal. For some stages the exact temperature and agitation speed are not specified due to subject to change

### 4.4.1 Decellularisation of femoral nerves

Three decellularisation runs were carried out on femoral nerves (n = 3); all agitation was carried out at 120 rpm, apart from the nuclease step which was carried out at 50 rpm. The temperatures of the solutions changed within each run apart from the nuclease step which remained at 37 °C. In the first decellularisation run all steps were carried out at 37 °C unless otherwise stated and the nerves were subjected to two SDS cycles.

After freeze thaw and disinfection, each femoral nerve was washed in 200 mM EDTA solution for 24 hours at 4 °C. The nerves were then subjected to three cycles of hypotonic buffer in the presence of Aprotinin for 24 hours with one of the buffers containing 0.1 % (w/v) SDS. The nerves were then washed with PBS and 0.1 % (w/v) EDTA containing Aprotinin for 48 - 56 hours at 4 °C. The nerves were subjected to one cycles of hypotonic buffer containing 0.1 % (w/v) SDS for 24 hours and were then washed three times in PBS for 30 minutes each time before being further washed in PBS overnight. The following day the nerves were incubated in two nuclease cycles for three hours at 50 rpm agitation for each cycle. Each nerve was then washed three times in PBS at for 30 minutes each time before being further washed in PBS overnight. The nerves were then washed in hypertonic buffer at and incubated for 24 hours with agitation. The nerves were washed three times in PBS, 30 minutes each time at before being sterilised with 0.1 % (v/v) peracetic acid in PBS for three hours at room temperature (20 – 25 °C) with agitation. Nerves were then washed a further three times in sterile PBS for 30 minutes each with agitation and stored in the fridge at 4 °C till needed.

The same procedure was used for the second and third decellurisation methods however in the second run all steps were carried out at 42 °C and the nerves were subjected to three SDS cycles. In the third run all steps were carried out at 45 °C and the nerves were subjected to two SDS cycles. Table 4.2 summarises the decellularisation runs carried out on the femoral nerves.

| Method | Nerve type | SDS cycles | Incubation temp (°C) | Agitation speed (rpm) | Nuclease Cycles |
|---|---|---|---|---|---|
| **1** | Femoral | **2** | **37** | **120** | **2** |
| **2** | Femoral | **3** | **42** | **120** | **2** |
| **3** | Femoral | **2** | **45** | **120** | **2** |

**Table 4.2 Summary of the decellularision runs carried out on the femoral nerves**

#### 4.4.1.1 Results of the decellularised femoral nerves

Characterisation of the femoral nerves decellularised using the methods summarised in Table 4.2 was undertaken by analysing their tissue structure by staining them with haematoxylin & eosin. Presence of cell nuclei within the tissue was detected with DAPI labelling. Decellularisation of femoral nerves using method 1 revealed the presence of cell nuclei within the endoneurium (Figure 4.2 D). Haematoxylin & eosin staining revealed an intact histioarchitecture when compared to native controls (Figures 4.2 A and B). Figure 4.2 B shows the presence of the nerve fascicles with an intact endoneurium and surrounding perineurium. There is a however a loss of surrounding epineurial connective tissue in the decellularised nerve.

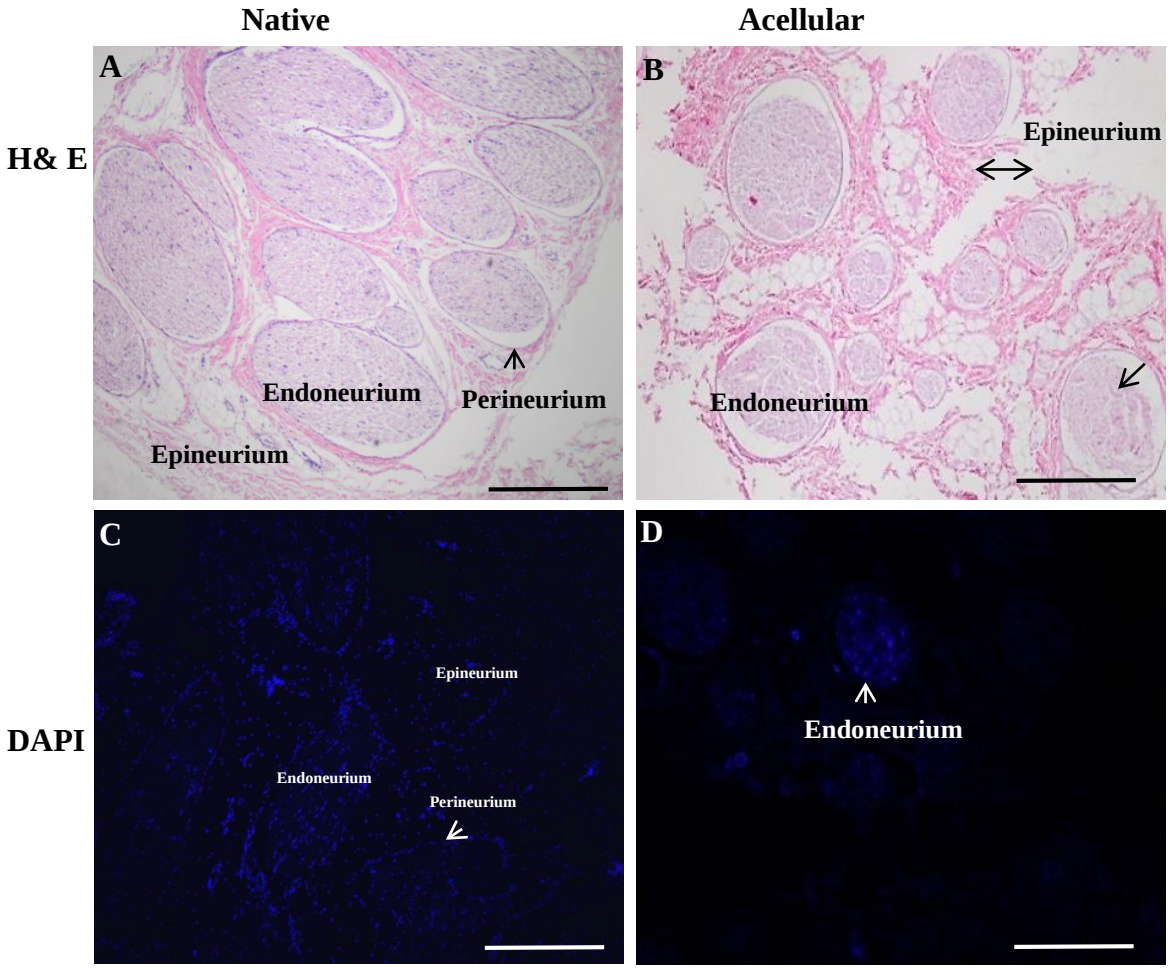


**Figure 4.2. Decellularisation of porcine femoral nerve at 37°C.** Haemotoxylin and eosin (A and B) and DAPI staining (C and D) of native and acellular femoral nerves . H&E of acellular femoral nerve revealed retention of nerve fasicles along with the connective tissue stained in pink and cell nuclei in blue, there was some noticable loss of connective tissue surrounding the the epineurium and within the endoneurium as indicated by the arrows (B). DAPI staining of native nerve shows presence of cells predominatly around the perineurium and within the endoneurium, with some cells present in the epineurium (C). DAPI staining revealed presence of cells in endoneurium seen in blue (D). Scale bar at 500 µm. Nuclei were imaged using an upright fluorescent microscope using a DAPI filter ($\lambda_{ex}$ = 300 nm / $\lambda_{em}$ = 550 nm)

Decellularisation of femoral nerves using method 2 saw no presence of cell nuclei following DAPI labelling (Figure 4.3 B). However, this process resulted in the degradation of the tissue architecture, and its connective tissues. The endoneurium is not as compact and the fascicles have lost parts of the perineurium layer. There is also a notable loss of surrounding epineurial connective tissue (Figure 4.3 A).

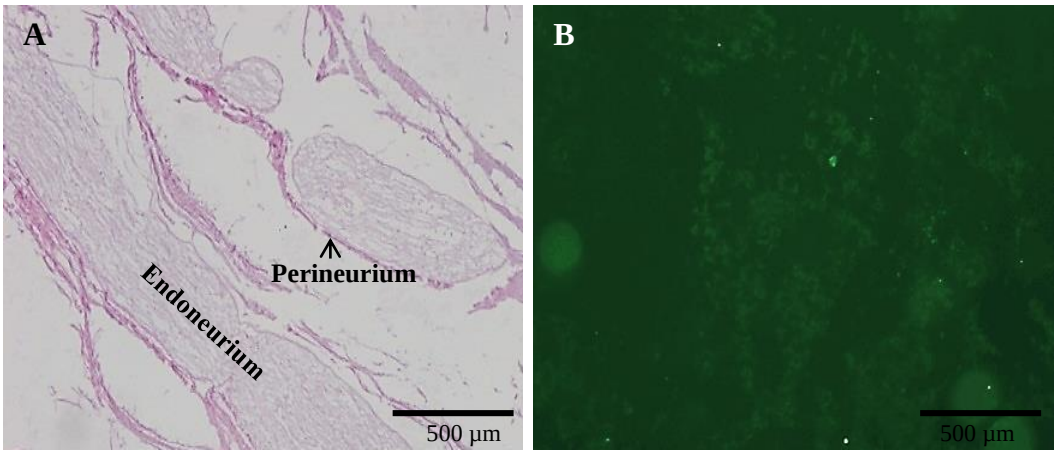


**Figure 4.3. Decellularisation of porcine femoral nerve using increased SDS cycles.** Haemotoxylin and eosin staining showed disruption of collagen fibrils within the endoneurium and loss of surrounding perineurium around the fascicles. There was a notable loss of surrounding epineurial tissues in the acellular femoral nerve (A); DAPI labelling showed no evidence of cell nuclei which is usually seen in blue. The structure of the nerve tissue is seen in green (B). Scale bar at 500 µm. Nuclei were imaged using an upright fluorescent microscope using a DAPI filter ($\lambda_{ex}$ = 300 nm / $\lambda_{em}$ = 550 nm). Structure of tissue in green is the natural autofluorescence of the tissue when imaged under a fluorescent microscope

Decellularisation of femoral nerves using method 3 saw the complete destruction of the nerve architecture revealed by haematoxylin and eosin staining as a result of the increased temperature (Figure 4.4). Further analysis of the tissue was not possible due to the quality of the tissue.

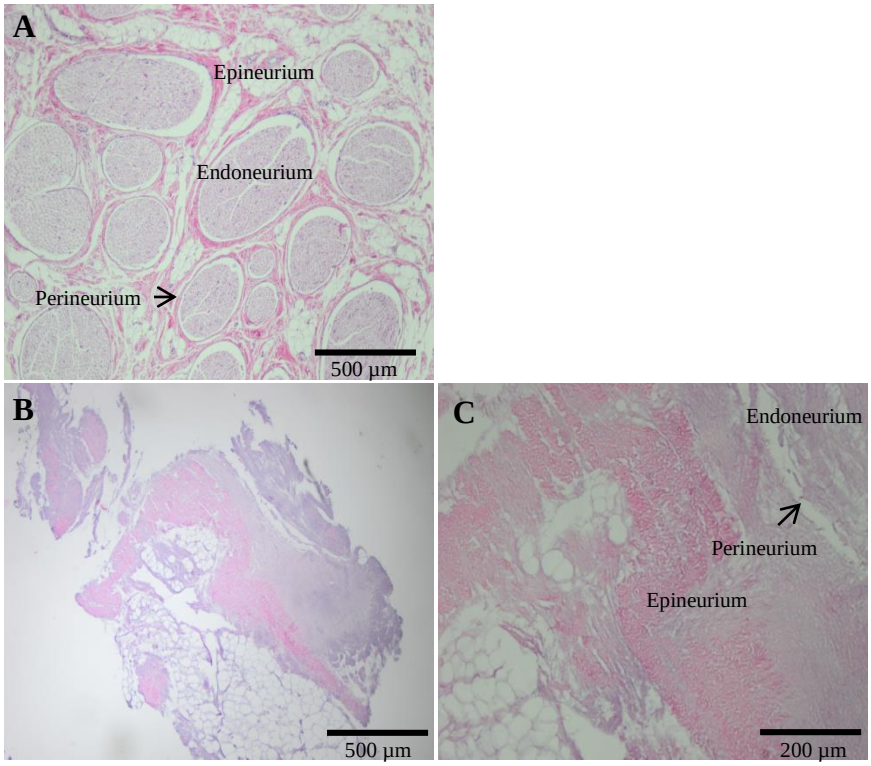


**Figure 4.4. Decellularisation of porcine femoral nerve using increased temperature.** Haematoxylin and eosin labelling of figure B and C show a complete loss of the nerves connective tissue when compared to the native nerves structure (A). Scale bars at 500 µm and 200 µm

## 4.5 Removal of fat from femoral nerve

It was proposed the reason for the poor decellularisation of porcine femoral nerves was due to the large amount of fat present. This fat could be reducing the diffusion of decellularisation solutions throughout the nerves. Sections of native femoral and acellular nerves were stained using Oil Red O, to locate regions of fat and adipocytes. The Oil Red O stain revealed a large presence of fat globules within the internal structure of the nerves, which stained a reddish-orange colour (Figure 4.5 A). In the acellular nerve there was a notable loss of lipids (Figure 4.5 B). Following decellularisation macroscopic observations indicated a large volume of external fat and connective tissue still surrounding the nerves (Figure 4.5 C).

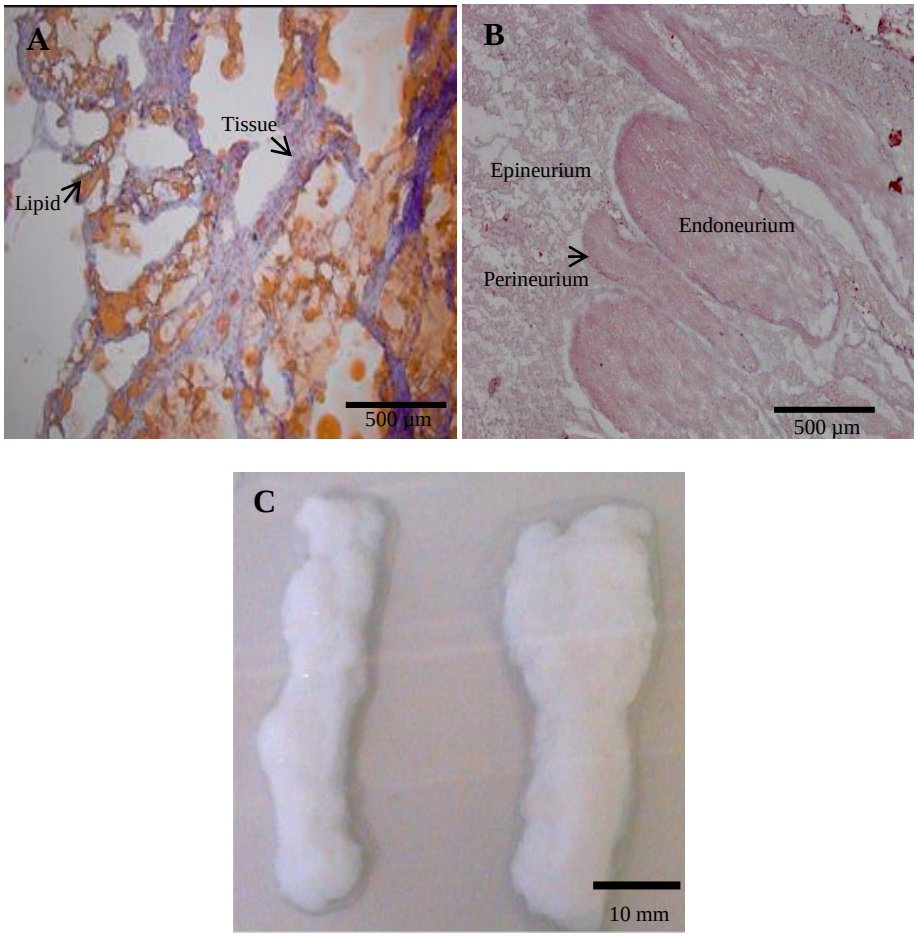


**Figure 4.5. Femoral nerve contained a large amount of adipose tissue.** Internal structure of native femoral nerve stained with Oil Red O revealed large globules of lipid (red) surrounding the tissue (blue) (A). Internal structure of decellularised femoral nerve stained with Oil Red O showing loss of lipids after decellularisation (B). An acellular femoral nerve showing large amount of external fat and connective still present (C). Scale bar at 500µm and 10 mm.

An investigation was carried out to evaluate a method to remove the fat from femoral nerves prior to decellularisation. Femoral nerves were submerged for two hours in individual containers containing 200 mL of hexane, acetone or chloromethanol (2:1 ratio) under agitation at 120 rpm. Each sample was washed three times using PBS-EDTA solution for 15 minutes. Sections of each solvent treated nerve were evaluated histologically. Haematoxylin & eosin staining demonstrated all three solvents had a destructive effect on the tissue structure, albeit less so in the acetone solution (Figure 4.6).

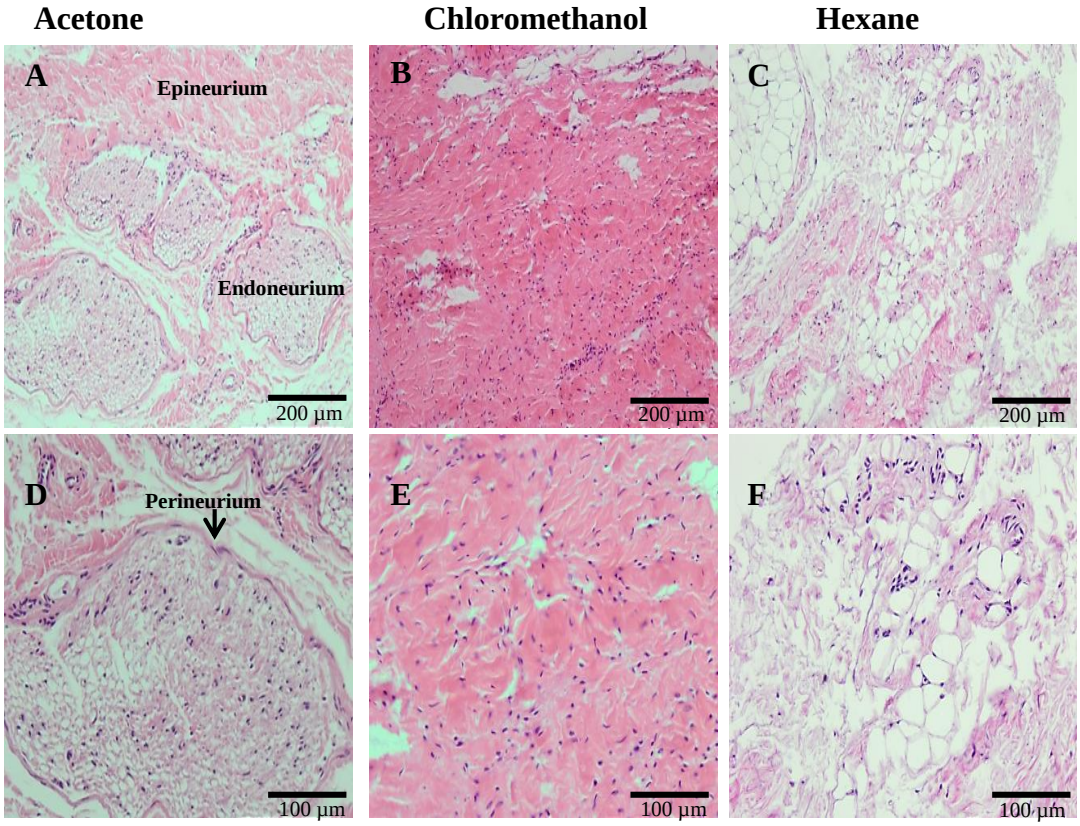


**Figure 4.6. Removal of fat from femoral nerves.** Nerves immersed in acetone (A and D) show retention of structure, however nerve fascicles have lost their shape. Nerves immersed in chloromethanol (B and E) and hexane (C and F) show complete destruction of tissue architecture. Tissue structure shown in pink and cell nuclei in blue. Figures A-C at x10 magnification and D-F at x20 magnification Scale bar at 100 µm and 200 µm.

## 4.6 Decellularisation of sciatic branches and sural nerves

Due to difficulties in the decellularisation of porcine femoral nerves, the sciatic branches (tibial and peroneal) and sural nerves were used. All steps of the following decellularisation processes were carried out at 42 °C and the nuclease step carried out at 37 °C unless otherwise stated.

### 4.6.1 Method for the decellularised sciatic branches and sural nerves

After freeze thaw and disinfection, the sural and sciatic branches nerves were washed in 200 mM EDTA solution for 24 hours at 4 °C. The nerves were then subjected to three cycles of hypotonic buffer in the presence of aprotinin at 42 °C for 24 hours with one of the buffers containing 0.1 % (w/v) SDS. The nerves were then washed with PBS and 0.1 % (w/v) EDTA containing aprotinin for 48 - 56 hours at 4 °C. The nerves were subjected to one cycles of hypotonic buffer containing 0.1 % (w/v) SDS for 24 hours and were then washed three times in PBS at 42 °C for 30 minutes each time before being further washed in PBS overnight.

The following day the nerves were incubated in two nuclease cycles for three hours at 37 °C at 50 rpm agitation for each cycle. Each nerve was then washed three times in PBS at 42 °C for 30 minutes each time before being further washed in PBS overnight. The nerves were then washed in hypertonic buffer at 42 °C and incubated for 24 hours with agitation. The nerves were washed three times in PBS, 30 minutes each time at 37 °C before being sterilised with 0.1 % (v/v) peracetic acid in PBS for three hours at room temperature (20 - 25°C) with agitation. Nerves were then washed a further three times in sterile PBS at 37°C for 30 minutes each with agitation and stored in the fridge at 4 °C.

In method 4 the nerves were subjected to two cycles of SDS and in method 5 three cycles of SDS was applied to the nerve samples. Table 4.3 summarises the variables for decellularisation method 4 and 5.

| Method | Nerve type | SDS cycles | Incubation temp (°C) | Agitation speed (rpm) | Nuclease Cycles |
|---|---|---|---|---|---|
| **4** | Sural | 2 | 42 | 240 | 2 |
| | Sciatic branches | 2 | 42 | 240 | 2 |
| **5** | Sural | 3 | 42 | 240 | 2 |
| | Sciatic branches | 3 | 42 | 240 | 2 |

**Table 4.3 Summary of the decellularisation runs carried out on the sural and sciatic branches**

### 4.6.2 Results of the decellularised sciatic branches and sural nerves

Haematoxylin & eosin staining of decellularised sural nerve and sciatic branches showed retention of the nerve fascicles and connective tissue when both decellularisation processes were applied. The use of SDS does cause damage to the connective tissues; however, this was noticeable less with the two SDS cycles. There was more pronounced damage and loss of connective tissue in the endoneurium and surrounding epineurium tissue when a three SDS cycle process was used (Figures 4.7 G and H). Under higher magnification it was also discovered that there were fewer and less compact collagen fibres within the endoneurium after three SDS washes (Figure 4.7 (I). Despite the fact that two different nerve types were used (sciatic nerve branches and sural nerve) no cell nuclei were visible in

either nerve type for both decellularisation protocols (Figure 4.8 and 4.10). This demonstrates that the decellularisation process can efficiently remove cells for nerves of all sizes

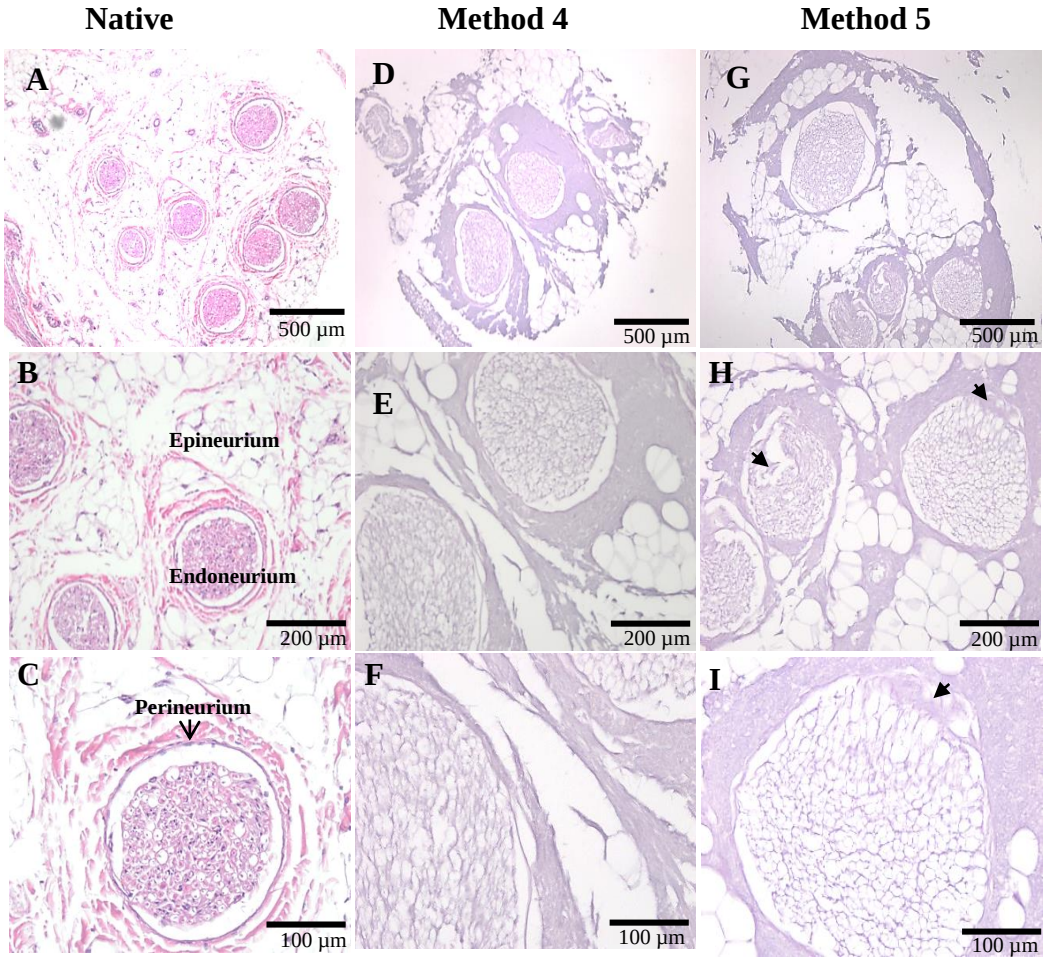


**Figure 4.7 Decellularisation of sural nerve with two and three cycles of SDS.** Haematoxylin and eosin of native sural nerves (A-C); Method 4 shows retention of nerve structure and connective tissue in the acellular sural nerves after decellularisation with two SDS cycles (D-F); Method 5 shows retention of nerve structure and connective tissue in the acellular sural nerves after decellularisation with three SDS cycles (G-I). There was noticeable damage to the nerves endoneurium as indicated by the arrows (H) as well as loss of collagen within the endoneurium (I). Scale bar at 500 µm, 200 µm and 100 µm respectively.

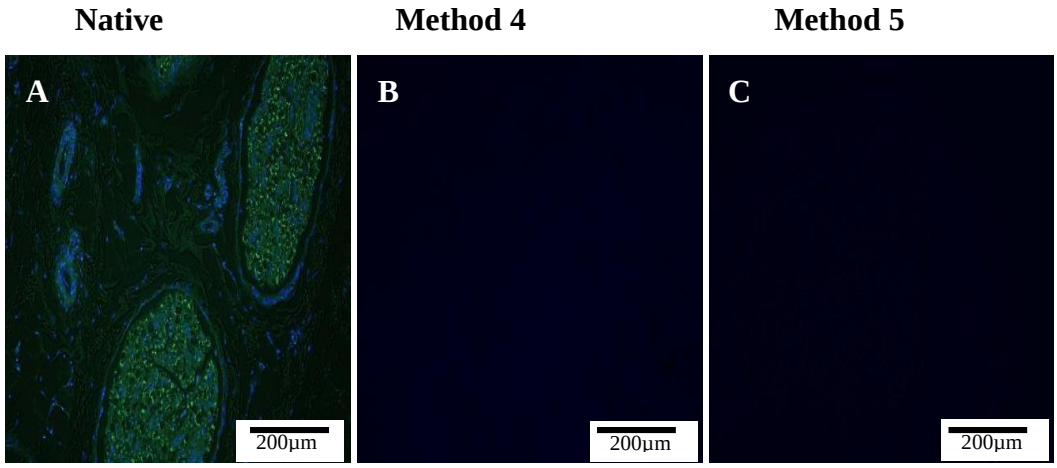


**Figure 4.8. Cells removed in both decellularisation runs.** DAPI labelling showed no evidence of nuclei in both decellurisation runs (B & C) when compared to the native nerve (A). Tissue structure shown in green and cell nuclei in blue. Nuclei were imaged using an upright fluorescent microscope using a DAPI filter ($\lambda_{ex}$ = 300 nm / $\lambda_{em}$ = 550 nm). Structure of tissue in green in the natural autofluorescence of the tissue when imaged under fluorescent microscope. Scale bar at 200µm

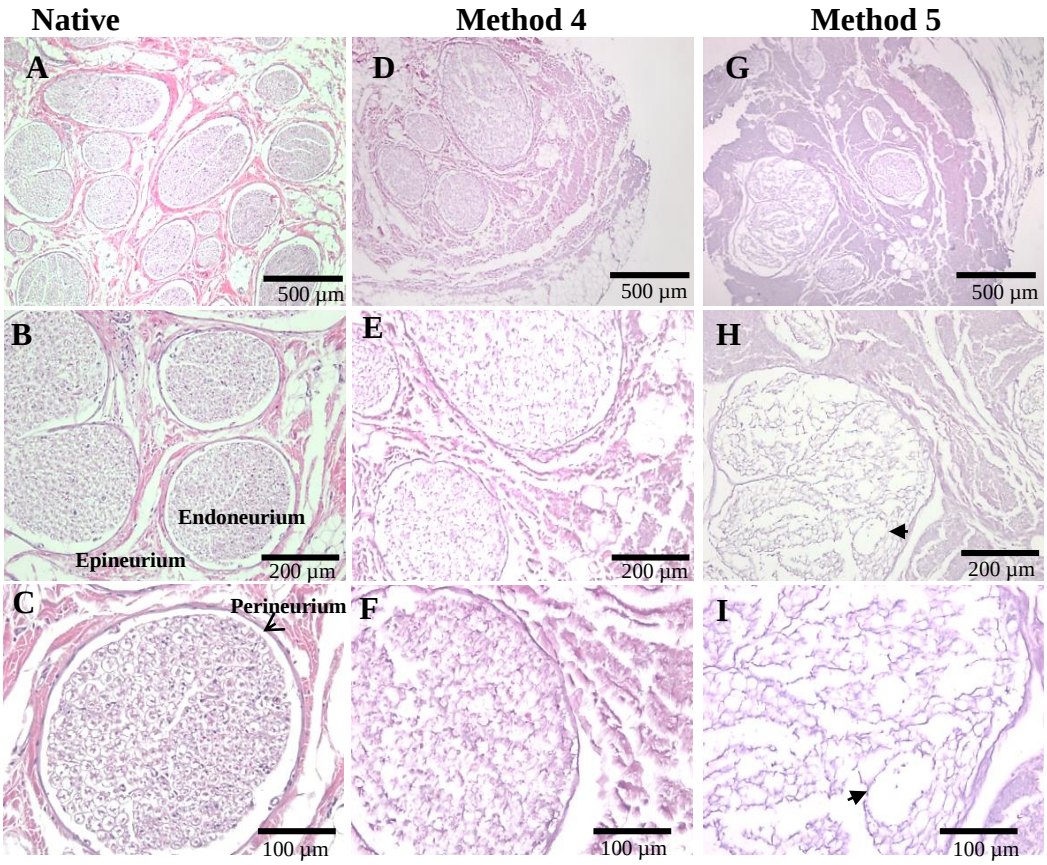


**Figure 4.9 Decellularisation of sciatic branches with two and three cycles of SDS.** Haematoxylin and eosin of native sciatic branches (A-C); Method 4 shows retention of nerve structure and connective tissue in the acellular sciatic branches after decellularisation with two SDS cycles (D-F); Method 5 shows retention of nerve structure and connective tissue in the acellular sciatic branches after decellularisation with three SDS cycles (G-I). There was noticeable damage to the nerves structure as indicated by the arrow (H) as well as loss of collagen within the endoneurium (I). Scale bar at 500 µm, 200 µm and 100 µm respectively.

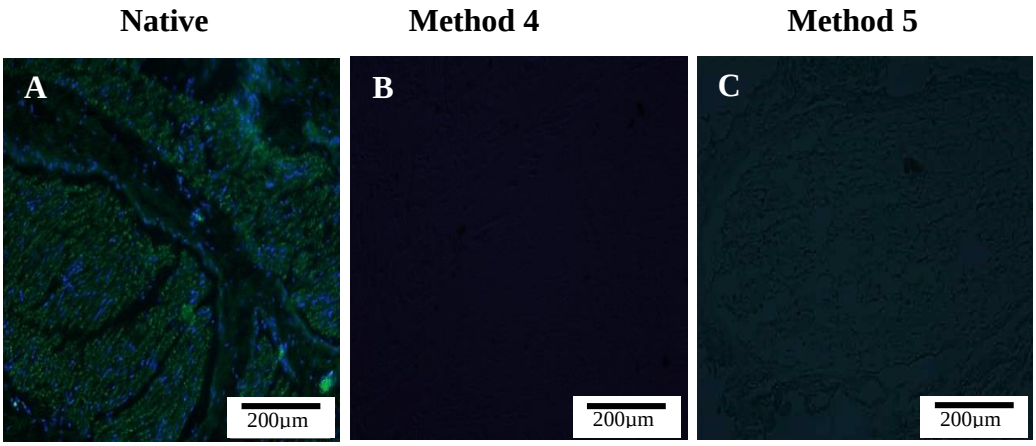


**Figure 4.10. Cells removed in both decellularisation runs. DAPI labelling shows no evidence of nuclei in both decellurisation runs (B&C) when compared to the native nerve (A).** Tissue structure shown in green and cell nuclei in blue. Nuclei were imaged using an upright fluorescent microscope using a DAPI filter ($\lambda_{ex}$ = 300 nm / $\lambda_{em}$ = 550 nm). Structure of tissue in green in the natural autofluorescence of the tissue when imaged under fluorescent microscope. Scale bar at 200µm

The DNA was extracted from native and acellular porcine sciatic branches using a commercially available kit and quantified using spectrophotometry at 260 nm. The results revealed a significant reduction in the sciatic branches (n = 3) when both decellularisation processes were applied (Figure 4.11). There was an 84 % (w/w) DNA reduction using two cycles of SDS and an 88 % (w/w) reduction using three cycles of SDS when compared to fresh samples ($p<0.05$, Students *t*-test). The sural nerve could not be analysed due to the difficulty in obtaining a large enough sample size to quantify.

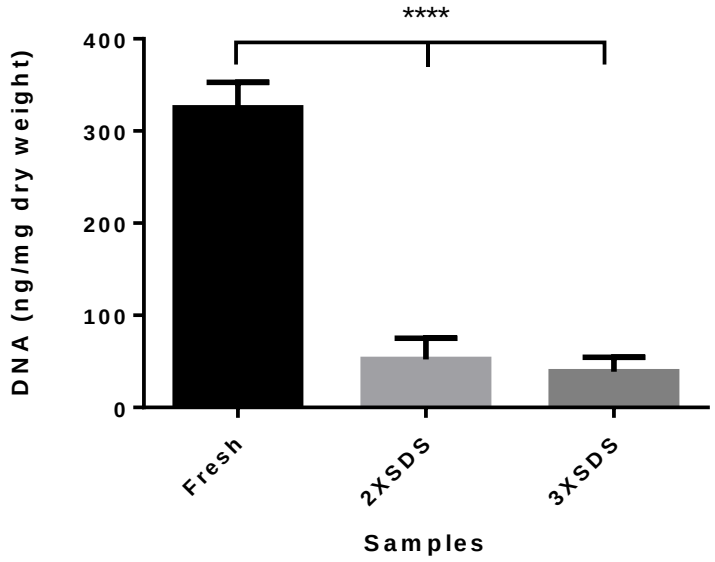


**Figure 4.11. DNA content of fresh and decellularised porcine sciatic branches determined by Nanodrop spectrophotometry.** A significant reduction of 84% using two cycles of SDS and 88% reduction using three cycles of SDS compared to fresh tissue. Data was analysed using the unpaired Student's *t*-test and is presented as the mean (n =3) ± 95 % C.I ($p<0.0001$****)

## 4.7 Optimising the decellularisation of sciatic branches

The previous results indicated that both the sural and sciatic branches have the capacity to be decellularised however further optimisation was required to reduce to DNA content within the tissue whilst maintaining its structure. Two decellularisation process were applied to samples of nerve, in both processes the nuclease cycles were doubled, however one was subjected to one SDS cycle whilst the other to two SDS cycles. The sciatic branches were chosen as the predominant nerves to be used throughout the study due to ease of procurement.

### 4.7.1 Method for the optimised acellular sciatic branches

After freeze thaw and disinfection, the sciatic branches nerves were washed in 200 mM EDTA solution for 24 hours at 4 °C. The nerves were then subjected to three cycles of hypotonic buffer in the presence of aprotinin at 42 °C for 24 hours with one of the buffers containing 0.1 % (w/v) SDS. The nerves were then washed with PBS and 0.1 % (w/v) EDTA containing aprotinin for 48 - 56 hours at 4 °C. The nerves were subjected to one cycles of hypotonic buffer containing 0.1 % (w/v) SDS for 24 hours and were then washed three times in PBS at 42 °C for 30 minutes each time before being further washed in PBS overnight. The following day the nerves were incubated in two nuclease cycles for three hours at 37 °C at 50 rpm agitation for each cycle. The nerves were then washed overnight in PBS at 42 °C. The following day the nerves were again incubated in two nuclease cycles for three hours at 37 °C at 50 rpm agitation for each cycle. Each nerve was then washed

three times in PBS at 42 °C for 30 minutes each time before being further washed in PBS overnight. The nerves were then washed in hypertonic buffer at 42 °C and incubated for 24 hours with agitation. The nerves were washed three times in PBS, 30 minutes each time at 37 °C before being sterilised with 0.1 % (v/v) peracetic acid in PBS for three hours at room temperature (20 - 25°C) with agitation. Nerves were then washed a further three times in sterile PBS at 37°C for 30 minutes each with agitation and stored in the fridge at 4 °C.

In method 6 the nerves were subjected to one cycle of SDS and in method 7 two cycles of SDS was applied to the nerve samples. Table 4.4 summarises the variables for decellularisation method 6 and 7.

| **Method** | **Nerve type** | **SDS cycles** | **Incubation temp (°C)** | **Agitation speed (rpm)** | **Nuclease Cycles** |
|---|---|---|---|---|---|
| **6** | Sciatic branch | **1** | **42** | **240** | **4** |
| **7** | Sciatic branch | **2** | **42** | **240** | **4** |

**Table 4.4 Summary of the decellularisation runs carried out on the sciatic branches.**

### 4.7.2 Results of the optimised decellularisation for the sciatic branches

Haematoxylin & eosin staining revealed that both processes preserved the native nerve structure with intact fascicles, perineurium and epineurial connective tissue (Figure 4.12). Higher magnification of fascicles revealed damage to collagen within the endoneurium when method 7 was used (Figure 4.12 F) compared to method 6 (Figure 4.12 G). This showed that method 6 was more effective in retaining the native nerve structure. DAPI revealed no cell nuclei or whole cells in both methods (Figure 4.13). This result provided evidence of removal of cells from porcine sciatic branches after both decellularisation runs.

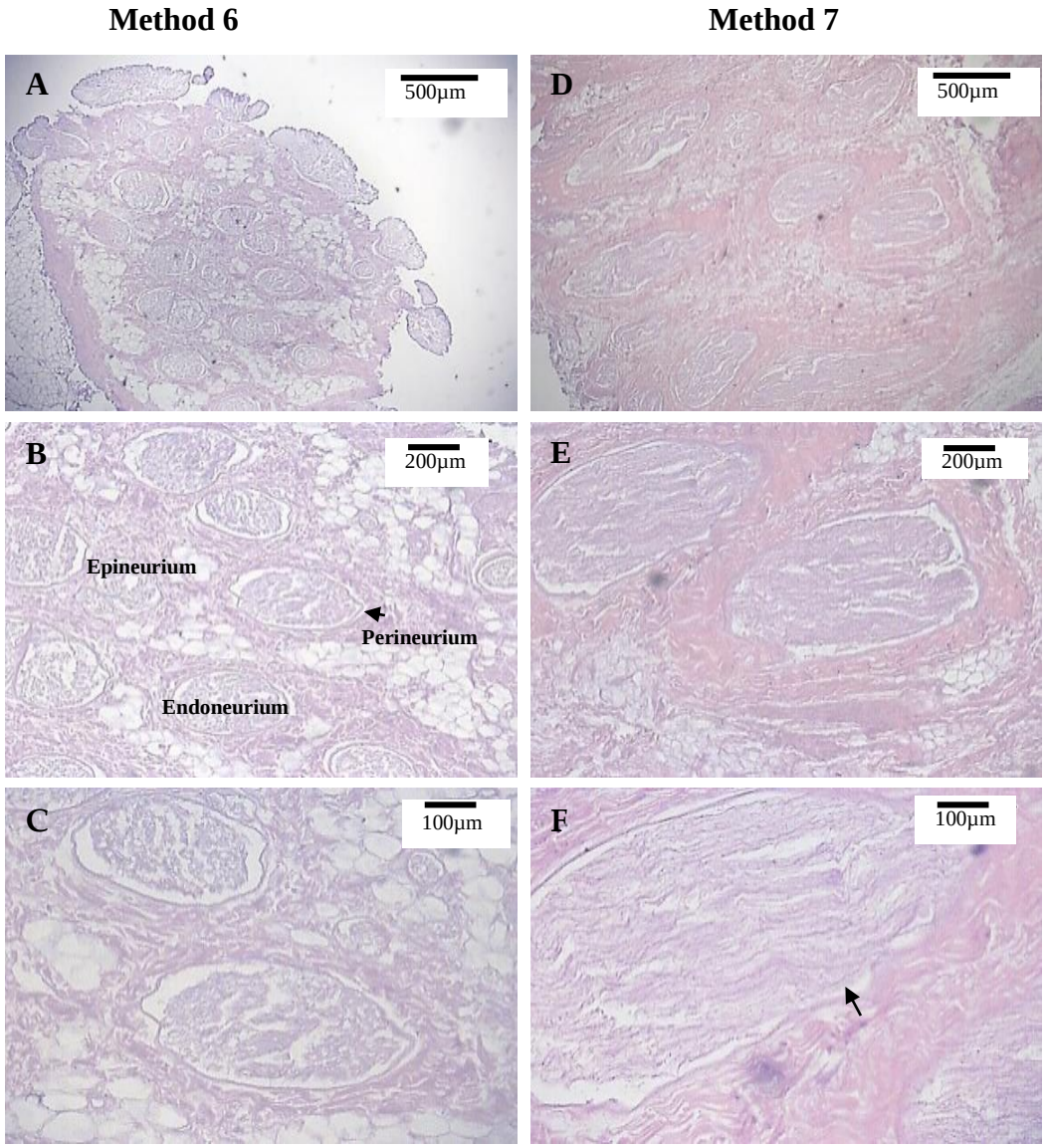


**Figure 4.12 Decellularisation of sciatic branches with one and two cycles of SDS and extra nuclease wash.** Method 6 showed good retention of nerve structure and connective tissues in the acellular sciatic branches after decellularisation with two SDS cycles (A-C); Method 7 showed retention of nerve structure and connective tissue in the acellular sciatic branches after decellularisation with three SDS cycles (D-F), however there was notable damage to the collagen in the endoneurium indicated by the arrow (F). Scale bar at 500 µm, 200 µm and 100 µm respectively.

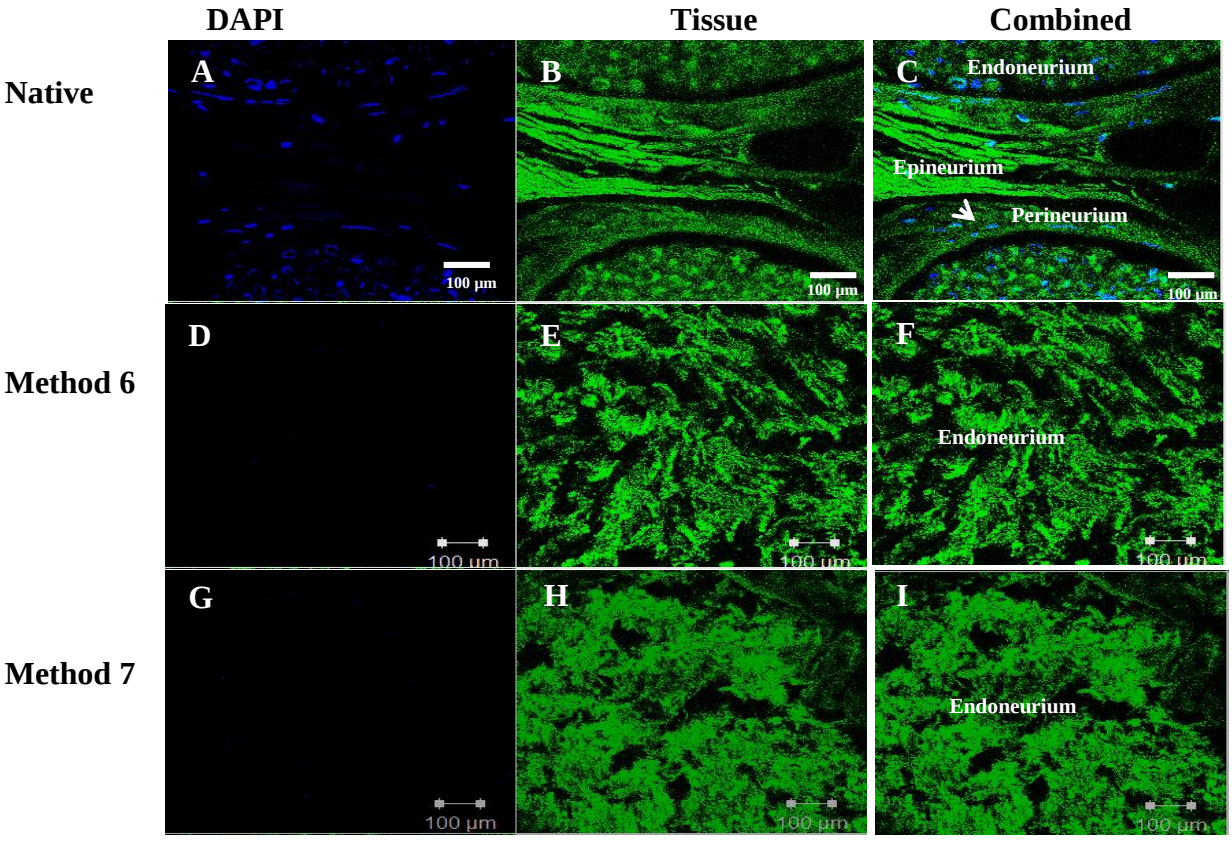


**Figure 4.13. Cells removed in both decellularisation runs.** DAPI labelling showed no evidence of nuclei in Method 6 using one SDS cycle (D-F) and Method 7 using two SDS cycles (G-I) when compared to the native nerve which has cells within the endoneurium and around the perineurium(A-C). Each image shows the transverse sections of the nerve fascicles. Tissue structure shown in green and cell nuclei in blue. Nuclei were imaged using an upright fluorescent microscope using a DAPI filter ($\lambda_{ex}$ = 300 nm / $\lambda_{em}$ = 550 nm). Structure of tissue in green in the natural autofluorescence of the tissue when imaged under fluorescent microscope. Scale bar at 100µm

Quantification of DNA extracted from native and acellular porcine sciatic branches revealed a significant reduction in the sciatic branches (n = 3) in both decellularisation processes (Figure 4.14). There was a 95 % DNA reduction using one cycle of SDS and a 94 % reduction using two cycles of SDS, when compared to native samples ($p < 0.0001$, Students *t*-test).

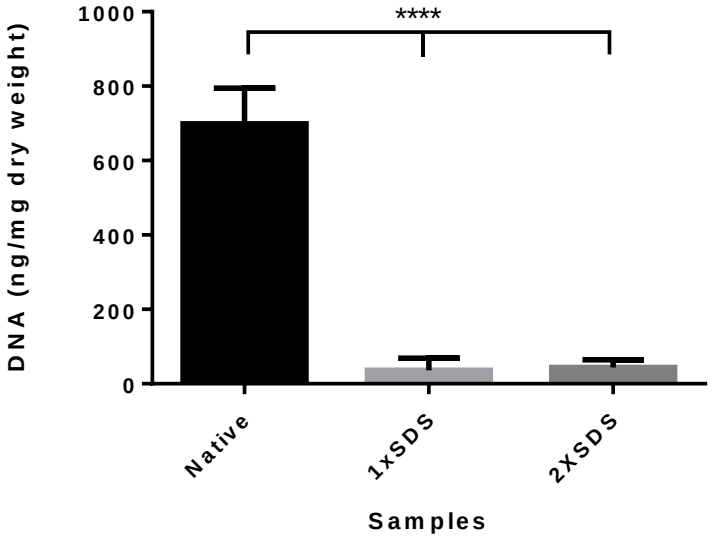


**Figure 4.14. DNA content of native and acellular porcine sciatic branches determined by Nanodrop spectrophotometry.** The DNA was extracted from the tissue using a DNeasy blood and tissue kit. The extracted DNA samples were loaded onto a Nanodrop and read at an absorbance of 260 nm. Results showed a significant reduction of 95% using one cycle of SDS and 94% reduction using two cycles of SDS compared to native tissue. Data was analysed using an unpaired students *t*-test and is presented as the mean (n =3) ± 95 % C.I ($p < 0.0001$****)

### 4.7.3 Summary of the decellularisation method development for porcine peripheral nerves

In this study three types of peripheral nerves (femoral, sural and sciatic branches) were assessed using seven methods. Each method used the steps shown in Figure 4.1; however, the variables included a change in nerve type, temperature, agitation speed as well as the number of SDS and nuclease cycles. Table 4.5 summarises the experimental variables for each decellularisation run and the effects on the nerve tissue. Table 4.6 summarises the amount of DNA removed from methods 4 - 7.

| Method | Nerve type | SDS cycles | Incubation temp (°C) | Agitation speed (rpm) | Nuclease Cycles | Results |
|---|---|---|---|---|---|---|
| **1** | Femoral | 2 | 37 | 120 | 2 | Cells found in the endoneurium |
| **2** | Femoral | 3 | 42 | 120 | 2 | Cells removed but structure was damaged |
| **3** | Femoral | 2 | 45 | 120 | 2 | Complete destruction of tissue |
| **4** | Sural | 2 | 42 | 240 | 2 | Retention of structure and DAPI staining revealed no cells |
| | Sciatic branches | 2 | 42 | 240 | 2 | Retention of structure. DNA assay revealed 84 % cell reduction |
| **5** | Sural | 3 | 42 | 240 | 2 | Retention of structure albeit more damage due to increased SDS cycle. |
| | Sciatic branches | 3 | 42 | 240 | 2 | Retention of structure albeit more damage due to increased SDS cycle. DNA assay revealed 88 % cell reduction |
| **6** | Sciatic branches | 1 | 42 | 240 | 4 | Retention of structure. DNA assay revealed 95 % cell reduction |
| **7** | Sciatic branches | 2 | 42 | 240 | 4 | Retention of structure albeit more damage due to increased SDS cycle. DNA assay revealed 94 % cell reduction |

**Table 4.5. Summary of experimental variables investigated to optimise peripheral nerve decellularisation**

| Method | DNA content of fresh tissue ($ng.mg^{-1}$) | DNA content of decellularised tissue ($ng.mg^{-1}$) | Percentage of DNA removed (%) |
|---|---|---|---|
| **4** | 325 ± 27.61 | 52.07±7.75 | 84 % |
| **5** | 325 ± 27.61 | 38.84±6.95 | 88 % |
| **6** | 698.40 ± 95.73 | 36.53 ± 10.72 | 95 % |
| **7** | 698.40 ± 95.73 | 43.85±7.03 | 94 % |

**Table 4.6 Summary of DNA removal from decellularisation processes.** DNA content of native (n = 6) and acellular (n = 6) porcine sciatic branches determined by Nanodrop spectrophotometry at 260 nm (mean ± 95 % C.I.) and percentage of DNA removal after decellularisation.

## 4.8 Discussion

The aim of the work presented in this Chapter was to develop a process for the decellularisation of porcine peripheral nerve, which eliminated the cellular content within the tissue whilst retaining the native histioarchitecture.

The decellularisation procedure developed used a combination of chemical and enzymatic treatments, based on the process developed by Wilshaw et al (2012) and modified for porcine peripheral nerve (Wilshaw, Rooney et al. 2012) . The first step of the process was a single freeze-thaw cycle to open up the tissue ECM, increasing the susceptibility of subsequent decellularisation reagents. The nerves were disinfected and then exposed to a solution of 200 mM EDTA. EDTA inhibits matrix metalloproteases as well as chelating divalent metal ions (in particular such as $Ca^{2+}$), which disrupts cell attachment to the ECM by interfering with the integrin secondary structure and consequent binding (McFetridge, Daniel et al. 2004).

This was followed by sequential incubation in hypotonic Tris buffer to lyse the neuronal and glial (Schwann) cells and 0.1 % (w/v) SDS in hypotonic buffer. SDS is widely considered to be an excellent decellularisation agent effectively removes DNA remnants and cytoplasmic proteins by solubilising the lipid bi-layer of the cells and forming micelles around the cell membrane and its proteins. SDS has been shown to retain the structure of the nerves important ECM components such as the basal lamina, laminin and fibronectin (Wakimura, Wang et al. 2015; Wang, Itoh et al. 2015).

A nuclease step was incorporated with the addition of Benzonase, a nuclease which degrades both DNA and RNA followed by a wash in hypertonic buffer which was used to further remove cellular proteins. The activation of proteases in natural tissues during decellularisation can lead to extensive autolysis of ECM proteins and can cause major damage to the structure and function of the scaffold (Bodnar *et al.*, 1986; Courtman *et al.*, 1994; Pachence, 1996, Walles *et al.*, 2003). Aprotinin, a serine protease inhibitor was therefore incorporated to preserve the ECM components in all stages of decellularisation apart from prior to and during nuclease treatment in order to not compromise the action of nuclease enzymes.

Sterilisation of the tissue was carried out using 0.1 % (v/v) peracetic acid for three hours followed by extensive washing in PBS to remove residual SDS.

Peracetic acid is a commonly used disinfection agent, widely used to disinfect surgical instruments due to excellent anti-viral properties (Rutala and Weber 2004) in addition to doubling up as a decellularisation agent (Gilbert, Sellaro et al. 2006).

The femoral nerve was the first nerve to be identified due to its large size and easy location within the porcine leg. All three decellularisation methods for the femoral nerve were limited in their ability to eliminate the cell content, whilst preserving the tissue architecture. Method 1, a decellularisation protocol developed for porcine carotid arteries used a mild treatment which retained the nerves native structure; however, the presence of cells was still seen in the nerves endoneurium. Method 2 was based on the decellularisation of bovine carotid arteries saw an elimination of cells from the tissue however the increase in SDS cycles severely damaged the nerve fascicles. Method 3 saw the complete destruction of the tissue, most likely due to the increase in the temperature.

Throughout all the decellularisation runs carried out on the femoral nerve the decellularised femoral nerves still contained a large amount of external fat and connective surrounding the tissue which may have prevented the chemical and enzymatic treatments from fully penetrating into the tissue structure. Adipose tissue in general plays a functional role in protecting nerves. Nerves which are subjected to high pressure and strain such as the femoral and sciatic nerves contain a higher portion of adipose tissue to protect the nerve by cushioning the fasciculi (Sunderland 1945). Native and decellularised nerves were stained with Oil Red O to deduce whether internal lipids within the tissue were also preventing the nerve from being successful decellularised. Histological characterisation of the native nerve showed large deposits of lipids shown in orange; however, for the decellularised nerve there were no signs of lipids. The removal of lipids after decellularisation have been shown in porcine adipose tissue (Brown, Freund et al. 2011) and adult and rat omentum (Porzionato, Sfriso et al. 2013).

To try and eliminate the external fat from the femoral nerve the tissues were immersed in alcohols as they are known to remove the insoluble lipids from tissue (Flynn 2010; Brown, Freund et al. 2011). Femoral tissues were immersed into three different alcohol solvents which included chloromethanol, acetone and hexane. These solvents have all been used in previous decellularised studies to remove lipid in biological tissues such as porcine dermis, cartilage and omentum (Baldoni,

Bolognani et al. 1994; Yang, John et al. 2007; Lumpkins, Pierre et al. 2008; Prasertsung, Kanokpanont et al. 2008; Montoya and McFetridge 2009).

Chloromethanol is formed from a chloroform-methanol mixture. The chloroform extracts mainly neutral lipids such as triglycerides whilst methanol extracts cell-membrane lipids such phospholipids, glycoproteins and cholesterol (Ferraz, Fiuza et al. 2004). Acetone which is polar solvent selectively removes hydrophobic lipids (Bancroft and Gamble 2008) whilst hexane which in non-polar solvent also removes neutral lipids such as triglycerides (Ferraz, Fiuza et al. 2004).From our results all of these solvents damage the ECM of the nerve tissue. Chloromethanol and hexane completely destroy the nerves ECM structure whilst the acetone is less damaging to the structure. Previous studies have reported damage to the ECM ultrastructure (Cole 1984) as well as precipitation of proteins (Jamur and Oliver 2010) using these alcohols. The use of alcohol solvents to eliminate to external lipid content of the femoral nerve tissue proved unsuccessful. The solvents damaged the internal structures of the nerves making them inadequate as a nerve graft.

From these previous experiments it was deduced that the optimal temperature for nerves to be decellularised is at 42 °C and that it may be more feasible to choose a nerve which did not contain so much surrounding connective and fat tissue. The study focus subsequently shifted towards using smaller peripheral nerves such as sural nerve and the branches of the sciatic nerve. Sural nerves have been used as an autograft in patients and decellularised xenogeneic sural through cold preservation (Hess, Brenner et al. 2007) and peroneal/tibial nerves through chemical extraction (Hu, Zhu et al. 2007) have been used as scaffolds in tissue engineering applications.

Methods 4 & 5 comprised of incubating the sural and peroneal / tibial nerves (sciatic branches) at 42 °C with increased agitation. In method 4 the nerves were subjected to two cycles of SDS whilst in method 5 they were subjected to three. Histological evaluation showed retention of the fascicles and the connective tissues for both methods. Nonetheless damage to the fascicles as well as loss of collagen within the endoneurium was more evident for method 5; this was not unexpected as SDS can cause damage to ECM components such as collagen. The quantification assay does show a slightly lower DNA content in method 5, most likely attributed by the extra SDS cycle. Nevertheless, when considering the

damage SDS does to the structure as well as the increased chance of residual SDS being retained in the tissue it was decided that increasing the SDS cycles was not an efficient way of removing cells whilst trying to maintain the nerves histioarchitecture.

Methods 6 & 7 solely concentrated on the sciatic branches due to ease of procurement and availability. The nuclease cycle was doubled for both processes and the SDS cycles were reduced to one and two respectively. Haematoxylin and eosin and DAPI stained images showed no evidence of cell presence in the decellularised tissue, indicating the removal of cells. Haematoxylin and eosin staining showed that both decellularisation runs managed to retain the native nerve structure. In both processes the fascicles as well as the connective tissues were maintained. Evidence of damage was more evident in the nerves subjected to two cycles of SDS which caused more extensive damage to the collagen within the endoneurium. This may be due to the cells being predominantly located within the endoneurium.

Both methods achieved the criteria defined by Crapo et al (2011) in terms of removal of cells from the tissue and a 95 % DNA reduction was made possible with just one SDS cycle. This DNA reduction value is comparable to the Sondell method and Hudson method whose overall reduction in cell content was 98 % (Sondell, Lundborg et al. 1998) and 97 % (Hudson, Liu et al. 2004), respectively. It is important to note that the Hudson study was carried out on rat sciatic nerve and analysed for removal of cellular protein whilst our study used porcine nerves and quantified total DNA content (single and double stranded DNA) in the tissue. Further characterisation of the decellularised sciatic branches according to Method 6 will be discussed in the subsequent chapter. This will include the effects our decellularisation process has on the nerves ECM and how it compares to other methods.

## 4.9 Conclusions

A decellularisation method for porcine peripheral nerves was developed based on the original method described by Wilshaw *et al.* (2012). Several methods were tried and tested on different segments of peripheral nerves found in the lower limb. It was deduced that sural and sciatic branches (peroneal/tibial) can be successfully decellularised. The sciatic branches were however chosen solely as the nerves to be used throughout the study for consistency. The sciatic branches were selected due to their size, ease of procurement and the availability of the tissue. Unlike the femoral and sciatic nerve, the sciatic branches are smaller and contain less surrounding adipose tissue which makes it easier for the decellularisation solutions to penetrate into the tissue and remove the cells. The study has also demonstrated that porcine sural nerve may also be efficiently decellularised. Nonetheless there is a limited amount of sural tissue which can be obtained from the porcine leg, making it difficult to use for certain experimental analysis such as DNA quantification.

The optimised decellularisation process (Method 6) consists of the nerves being subjected to four nuclease cycles and one SDS cycle at a temperature of 42 °C with agitation. Histological characterisation revealed overall better retention of the nerve fascicles, along with its connective tissues, most likely due to the use of only one SDS cycle. The DNA quantification assay revealed a 95 % DNA reduction, which adheres to the decellularisation criteria as well as being comparable to the established Sondell and Hudson protocol. Further evaluation of the decellularisation method will be discussed in Chapter 5.

# Chapter 5. Characterisation of Native and Acellular Porcine Peripheral Nerves

## 5.1 Introduction

A successful decellularisation process should be able to produce an acellular scaffold which retains its native architecture and be devoid of cells. A decellularisation process has the capacity to alter the native histioarchitecture, biocompatibility, strength and composition of the extracellular matrix (ECM) and its components. Therefore, if being used clinically it is vital to assess the effect of the process by undertaking biological characterisation and mechanical testing of the acellular nerve and comparing it to its native counterpart.

Peripheral nerves consist of a three dimensional ECM and basal lamina. These are the non-cellular components of the nerve tissue that along with Schwann cells and axons comprise the endoneurium and form nerve fascicles. The ECM is a highly organised dynamic three dimensional network which is the product of resident cells (i.e. Schwann cells) such as proteins, glycoproteins and proteoglycans. The ECM provides structural support for tissues, cell layers and individual cells as well as fundamental cell processes such as cell growth, adhesion, migration, proliferation, differentiation and gene expression (Gao, Wang et al. 2013) by sensing different environmental stimuli and providing specific inputs to the surrounding cells. In addition, the ECM captures and releases a wide range of growth factors. In the peripheral nervous system (PNS) the three dimensional ultrastructure, surface topology and composition of the ECM provide precise guidance for axonal regeneration.

The basal lamina is a Schwann cell product consisting of continuous laminin tubes (~10 μm diameter) embedded within the ECM. The basal lamina also contains important components such as fibronectin, collagen and proteoglycans, all of which help promote axonal outgrowth (Weinstein 1999). In peripheral nerve tissue, the important ECM components include collagen types - I, III and IV, laminin, fibronectin and chondroitin sulphate proteoglycans (CSPGs) (Gao, Wang et al. 2013).

Collagen is a structural protein and is the main ECM constituent found in all three connective tissue layers within the PNS. Collagen type I and III together

constitute approximately 49 % of total protein in the nerves (Bunge, Bunge et al. 1989). The collagenous matrix surrounds and protects individual axons and their Schwann cell sheaths from trauma (Lundborg 2004). In the PNS, two classes of collagen molecules are expressed; fibril forming collagens (types-I, III, and V) and basement membrane collagen (type-IV) (Koopmans, Hasse et al. 2009). Collagen I, the most predominant collagen in the human body, is localised primarily in the epineurium whilst collagen III is located within the endoneurium and perineurium.

Whilst the bulk of fibril forming collagen is synthesized by fibroblasts, Schwann cells and perineurial cells secrete the non-fibrillar type IV collagen of basal lamina. Collagen IV is an important structural component of basement membranes, integrating ECM proteins such as laminin and perlican into a stable supramolecular aggregate (Hudson, Reeders et al. 1993), lining the outer aspect of endoneurial capillaries as well as surrounding the processes of Schwann cells and perineurial cells (Alovskaya, Alekseeva et al. 2007).

Laminins are glycoproteins, existing within the endoneurium and perineurium of the peripheral nerve (Palm and Furcht 1983), forming a major structural element of the basement membrane, the basal lamina (Timpl 1996). They are produced by Schwann cells and are distributed along the cell surface in a continuous band. Evidence suggests that Schwann cells require an organised basal lamina to properly ensheath and myelinate axons (Obremski, Johnson et al. 1993). Laminin plays many roles within the PNS including promoting neurite outgrowth and survival (Edgar, Timpl et al. 1984) such as laminin-2 ($\alpha 2\beta 1\gamma 1$) and laminin-8 ($\alpha 2\beta 1\gamma 1$) which are important for postnatal nerve development and are upregulated for axonal regeneration after injury (Wallquist, Patarroyo et al. 2002). Laminin also provides attachment sites for cells via cell surface proteins (Palm and Furcht 1983) (Henry and Campbell 1996) as well as providing attachment points for axons to extend and exert forces on the ECM (Laura, Leipzig et al. 2008). In addition, laminin act as a ligand for cell receptors (e.g. integrins), thereby initiating signals that influence cell behaviour and survival (Schwartz 2001). Cellular studies have also revealed laminin enhances neuronal cell survival (Edgar, Timpl et al. 1984) and guide growth cones (Dodd and Jessell 1988). A study conducted by Lein 1992 also showed that laminin had the ability to enhance axonal growth using hippocampal neurons in culture (Lein, Banker et al. 1992).

Fibronectin is a cell surface associated glycoprotein produced by Schwann cells, predominantly located in the perineurium. It contains different functional domains that directly bind onto various molecules such as fibrin, collagen and heparin (White and Muro 2011) as well as two domains that support cell adhesion. One is the central cell-binding domain that is recognized by a variety of cell types via the integrin alpha 5 beta 1. The second is located in the alternatively spliced type III connecting segment (IIICS) (Komoriya, Green et al. 1991). In the PNS neurons can extend neurites on the two domains (Humphries, Akiyama et al. 1988). Fibronectin plays a role in peripheral nerve repair as they promote Schwann cell growth and motility (Baron-Van Evercooren, Kleinman et al. 1982; Ahmed, Underwood et al. 2003).

CSPGs are proteoglycans consisting of a protein core and a chondroitin sulphate side chain which are produced by Schwann cells. In the PNS they exist mainly in the basal lamina and ECM surrounding collagen fibrils (Aquino, Margolis et al. 1984). These proteoglycans have been implicated in the regulation of axonal growth, however it has been found that CSPGs bind to and inhibit the neurite-promoting activity of laminin. It has been observed that after a nerve injury there are markedly upregulated levels of inhibitory CSPGs levels which accumulate in the endoneurial tissue surrounding the Schwann cell basal laminae (Zuo, Hernandez et al. 1998); consequently CSPGs play a negative role in nerve regeneration.

The decellularisation process can alter the ECM composition as well as the components of the nerve. The solutions used in the process such as sodium dodecyl sulphate (SDS) have been associated with ultrastructure disruption and GAG depletion (Kasimir, Rieder et al. 2003; Gilbert, Sellaro et al. 2006; Ott, Clippinger et al. 2010), whilst peracetic acid (PAA) treatment has been show to disrupt the collagen structure (Lomas, Jennings et al. 2004). It is therefore important to try and retain the significant ECM components. By doing so the acellular nerve can provide a suitable environment for cellular growth and nerve regeneration.

The biocompatibility of any acellular scaffold is important whether it is to be used as a clinical graft or *in vitro* model. Solutions used in the decellularisation process such as SDS detergent, EDTA, aprotinin and the PAA are known to be cytotoxic (Koulaouzidou, Margelos et al. 1999; Newby, Barr et al. 2000; Sagripanti and Bonifacino 2000). Therefore, to ensure that the reagents used in the

decellularisation protocol were adequately removed from the tissue *in vitro* cytotoxicity testing is carried out.

Under normal physiological conditions nerves are exposed to various mechanical forces. These include tensile, compressive or shear stress or as a combination of stresses (Figure 5.1). Uniaxial tensile testing is a standard method used in the evaluation of the mechanical properties of biological tissues (Kwan, Wall et al. 1992; Millesi, Zoch et al. 1995; Borschel, Kia et al. 2003; Phillips, Smit et al. 2004).

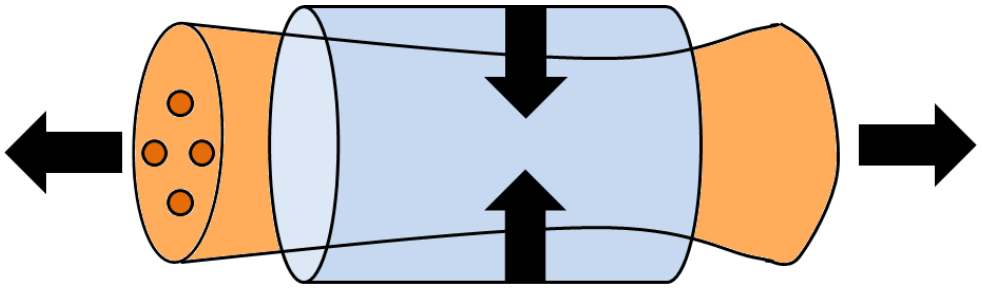

**Figure 5.1. Physical stresses placed on peripheral nerve. Tensile stress applied longitudinally to the peripheral nerve creates an elongation of the nerve (and an increase in strain). The transverse contraction that occurs during this elongation is greatest at the middle of the section undergoing tensile stress. Reproduced from Topp and Boyd (2006)**

The mechanical behaviour of a nerve segment under longitudinal tensile force can be described by a standard stress-strain curve. The typical stress-strain behaviour of peripheral nerves has been illustrated in Section 2. When a load is first applied to a resting nerve the nerve lengthens markedly relative to the applied load, this is known as the "toe region" of the curve. As the tensile load increases the nerve elongates at a steady rate, demonstrated by the linear region of the stress-strain curve. This elongation is due to extension of the epineurium and straightening of the funiculi and of the nerve fibres. Such elongation is "physiological" in the sense that it does not affect the nerve fibres (Haftek 1970). The slope of this portion of the curve is a measure of the resistance of the nerve to deformation and is known as the Young's Modulus or modulus of elasticity. A steep slope indicates that the nerve has more stiffness and less elasticity whilst a shallower slope shows that the nerve is more compliant.

At a certain point the amount of applied load starts to permanently deform particular elements of the nerve. This ultimate stress or ultimate strain represents the transition between the recoverable (elastic) strain and plastic (permanent) deformation areas of the stress-strain curve. In the plastic region of the curve the nerve reaches its ultimate elongation and undergoes mechanical failure (Topp and Boyd 2006).

Minor increases in tensile load create significant elongation of the nerve because of the failure of the infrastructure of the nerve, including perineurial components. There are fewer intact structural elements to provide resistance and at this point the nerve behaves like a viscous material (Haftek 1970).

Decellularisation solutions applied to biological tissues have been shown to affect the mechanical properties of the ECM (Courtman, Pereira et al. 1994; Palsson BO 2004). In terms of nerve repair any change in biomechanical properties can impede the regeneration of the nerve. Properties such as stiffness must be equivalent with their native counterpart so as to resist *in vivo* physiological loads during nerve regeneration. In addition, the nerve scaffold must be flexible to allow bending without kinking. It is important to have a balance between stiffness and flexibility as scaffolds that are too stiff can easily become dislocated and scaffolds which are too flexible fail to support axonal regeneration (So and Xu 2015). It is therefore important to study the effect these solutions have on the biomechanical properties of the acellular tissue. This can be achieved by uniaxial tensile testing the acellular nerve and comparing them with their native counterpart.

The acellular porcine peripheral nerves used in all of the studies in this chapter were produced using decellularisation Method 6 (described in Section 4.3). In this chapter the acellular nerves were assessed in terms of their retention of key ECM components, *in vitro* biocompatibility and mechanical integrity.

## 5.2 Aims and objectives

**Aims:**

The aim of this Chapter was to investigate the effects of a newly developed decellularisation process on porcine peripheral nerves

**Objectives:**

- To determine the effects of decellularisation on the presence of specific ECM proteins by comparison with native porcine peripheral nerves
- To determine the biocompatibility of the acellular scaffold using *in vitro* techniques
- To determine the effects of decellularisation on the biomechanical properties by comparison with native porcine peripheral nerves

## 5.3Methods

Decellularisation of porcine sciatic branches (peroneal and tibial nerves) nerves was performed according to the methodology described in in Section 4.3 (Method 7). The sciatic branches (5cm) and sural nerve (3cm) were subject to decellularisation (n =3) and were used for histology. Acellular sciatic branches (n =3) were also used for immunohistochemistry, biochemical and contact cytotoxicity analysis. The peroneal (10cm) and tibial (10cm) were subject to decellularisation (n =3) and were used for mechanical testing.

### 5.3.1 Histological staining

Specific histological stains were used to determine the histioarchitecture of the decellularised porcine peripheral nerves and locate specific ECM components. Native and acellular nerves were fixed with 3.7 % (v/v) formaldehyde for 24 hours and embedded into paraffin wax as described in Section 2.2. Tissue sections of 6 - 10 μm were prepared transversely and collected onto glass slides. The following stains were used: Picro Sirius red / Miller's elastin stain, a single stain, was used to identify the distribution of collagen and elastin in the tissue. Reticulin stain for collagen III and Alcian blue PAS stain to localise GAG`s in tissue. The slides were viewed using an upright microscope under either Khöler or polarised illumination.

### 5.3.2 Biochemical assays

Samples of native (n = 6) and acellular (n= 6) porcine sciatic branches were lyophilized to a constant weight prior to biochemical assay collagen and sulphated GAG content. Each sample consisting of 100 mg tissue were macerated with a scalpel blade and placed in a sterile 1.5 mL microcentrifuge tube. The samples were then freeze-dried; the mass of each sample was recorded daily until a consistent weight was achieved (approximately 25 mg).

#### 5.3.2.1 Glycosaminoglycan (GAG) quantification of porcine peripheral nerves

A modified GAG assay according to (Farndale, Buttle et al. 1986) was used to quantify the amount of sulphated GAGs present in tissue following decellularisation. The assay is based on changes in the absorption spectrum of the cationic dye 1,9-dimethylmethylene blue (DMB dye) when bound to sulfated GAGs to form a complex (Farndale, Buttle et al. 1986). The amount of GAGs

present was determined by comparing the proteoglycan levels in the native tissue to the acellular tissue.

Papain was used to digest lyophilized samples by adding 5 mL of 50 U. mL-1 papain digestion solutions (1250 Units of papain in 25 mL of digestion buffer; 5 mM L-cysteine hydrochloride; 5 mM $Na_2EDTA$).

Samples were incubated for 36 - 48 hours in an oven at 60 °C and diluted 1:50 in GAG assay buffer (68.5 mL of 0.1 M sodium di-hydrogen orthophosphate and 31.5 mL 0.1 M di-sodium hydrogen orthophosphate). The pH was adjusted to 6.8 so that the absorbance of the unknown falls within the linear region of the standard curve.

GAG assay standards were prepared by diluting the primary standard (10 mg Chondroitin sulphate B in 10 mL GAG assay buffer) to known concentrations:

| **Standard concentration (µg. mL$^{-1}$)** | **Volume of primary standard (µL)** | **Volume of buffer (µL)** |
|---|---|---|
| **200** | 40 | 160 |
| **150** | 30 | 170 |
| **100** | 12 | 180 |
| **50** | 10 | 190 |
| **25** | 5 | 195 |
| **12.5** | 5 | 395 |
| **6.25** | 5 | 795 |
| **3.125** | 5 | 1595 |
| **0** | 0 | 250 |

**Table 5.1 Table of GAG assay standards**

40µL of each standard, blank (GAG assay buffer only) or tissue samples were added to a clear flat-bottomed 96 well plate and 250 µL of DMB dye solution (0.008 mg 1,9 dimethylene blue in 2.5 mL ethanol, 1 mL of formic acid and 1 g of sodium formate; volume made up to 500 mL using distilled water and pH adjusted to 3.0) was added to each well and rocked slowly for two minutes on a plate rocker. Sample optical density was measured using a micro plate spectrophotometer at 525 nm. The blank values (GAG assay buffer) were subtracted from all standards and tissue samples and a standard curve of chondroitin sulphate B concentration against

absorbance was created using GraphPad Prism. The unknown values were interpolated using a linear regression of the standard curve.

#### 5.3.2.2 Quantification of hydroxyproline content in porcine peripheral nerves

A hydroxyproline assay was carried out to determine the total remaining collagen remaining in tissue following decellularisation by comparing the hydroxyproline (amino acid found in collagen tripeptide) levels in native and acellular nerves. The procedure adopted was based on the method described by Woessner and subsequently modified by (Edwards and O'Brien 1980). This assay is centered on the oxidation of hydroxyproline by chloramine - T (sodium *N*-chloro-*p*-toluene sulfonamide) which reacts with *p*-dimethylaminobenzaldehyde to form a chromophore that can be measured at 570 nm (Stegemann and Stalder 1967).

Prior to the assay the tissue samples were hydrolysed (hydrolysis of peptide bound hydroxyproline) in 5 mL of 6 M hydrochloric acid at 120 ˚C for four hours. For the assay a series of known concentrations was made up using primary and secondary standards. The primary standard was prepared by adding 25 mg trans-4-hydroxyproline in 25 mL assay buffer (13.3 g citric acid, 3.2 mL glacial acetic acid, 32 g sodium acetate, 9.1 g sodium hydroxide and 80 mL propan-1-ol in 400 mL distilled water with pH adjusted to 6.0 - 6.5 using 6 M HCL). The secondary standard was prepared by diluting 1 mL of the primary standard in 9 mL assay buffer.

| Standard concentration (µg. mL$^{-1}$) | Volume of secondary standard (µL) | Volume of buffer (µL) |
|---|---|---|
| 30 | 750 | 1750 |
| 25 | 625 | 1875 |
| 20 | 500 | 2000 |
| 15 | 375 | 2125 |
| 10 | 250 | 2250 |
| 8 | 200 | 2300 |
| 6 | 150 | 2350 |
| 4 | 100 | 2400 |
| 2 | 50 | 2450 |
| 0 | 0 | 2500 |

**Table 5.2 Table of hydroxyproline assay standards**

50 µL of each standard and acid hydrolysed test solutions (diluted 1:20 in assay buffer so that readings fall within the range of the assay) were added to a clear flat-bottomed 96 well plate. 100 µL Chloramine T solution (1.41 g chloramine T in 100 mL distilled water) was added to each well and the plate was shaken for 5 minutes at 60 rpm on a shaker. 100uL Ehrlich's reagent (7.5 g *p*-dimethylaminobenzaldehyde), 30.0 mL propan-1-ol, 13.4 mL 60 %; v/v perechloric acid and 6.6 mL distilled water) was added to each well and the plate was incubated at 60 ˚C for 45 minutes. The optical density of each well was determined at 570 nm using a micro plate spectrophotometer, which measured the optical densities. The blank values (assay buffer) were subtracted from all standards and tissue samples and a standard curve of hydroxyproline concentration against absorbance was determined by interpolation from a trans-4-hydroxy-L-proline standard curve. The total collagen content was calculated by using a hydroxyproline to collagen ratio of 1: 7.69 (Ignat'eva, Danilov et al. 2007).

### 5.3.3 Immunohistochemical evaluation of acellular peripheral nerves

Laminin and fibronectin proteins were localised using fluorescent immunolabelling. (Table 5.3). Native and acellular nerve samples were fixed using 3.7 % (v/v) formalin and embedded into paraffin wax; each sample was sectioned at 6 - 10 µm. Sections were permeabilised with 0.1 % (v/v) Triton X-100 diluted in

PBS for 20 minutes. Samples were then incubated with 7.5 % (w/v) bovine serum albumin diluted in PBS at room temperature for an hour, followed by washing once with 1 % (w/v) BSA in PBS. Tissue samples were incubated with primary antibody (diluted to appropriate concentration with 1% BSA) at 4 °C overnight in a humidified chamber. The following day the samples were washed three times with PBS, five minutes each time and then incubated with secondary FITC conjugated anti-rabbit antibody at room temperature in the dark for one hour. Each section was then washed three times with PBS for five minutes and counterstained with 300 nM DAPI in PBS and incubated for twenty minutes in the dark at room temperature. Sections were then washed three times with PBS for five minutes and imaged using a Zeiss LSM510 META upright confocal microscope (xenon arc lamp to excite FITC ($\lambda_{ex}$ = 495 nm / $\lambda_{em}$ = 515 nm). Nuclei were visualised at $\lambda_{ex}$ = 300 nm / $\lambda_{em}$ = 510 nm. Secondary antibody alone served as a negative control to rule out non-specific antibody binding

| **Antigen** | **Clone** | **Working dilution** |
|---|---|---|
| Rabbit anti-laminin antibody | Polyclonal | 1°Ab 1:50<br>2°Ab 1:100 |
| Rabbit anti-fibronectin antibody | Polyclonal | 1°Ab 1:400<br>2°Ab 1:100 |

**Table 5.3. Table of antibodies and working dilutions used throughout the study. 1°Ab = primary antibody; 2°Ab = secondary antibody**

### 5.3.4 Biomechanical evaluation of native and acellular porcine peripheral nerves

The biomechanical properties of native and acellular porcine sciatic branches (peroneal and tibial nerves) were evaluated using uniaxial tensile testing. Native porcine peroneal nerves (n = 5) and tibial nerves (n = 10) and acellular peroneal nerves (n = 3) and tibial nerves (n = 4) were tested under uniaxial tensile loading to failure in order to characterised their stress-strain behaviour. All peroneal nerves tested ranged from 5 - 7 mm in width and tibial nerves ranged 6 - 7 mm in width.

All specimens were 10 mm in length (initial gauge length). Tissue specimens were taken from three different animals within each test group. The methodology followed during uniaxial tensile testing was described in Section 2.2.6. The mean stress-strain curves for each group were generated using the Origin 8.0 software package.

### 5.3.5 In vitro biocompatibility

In order to determine the biocompatibility of the decellularised tissues *in vitro*, decellularised peripheral nerves were assessed using a qualitative contact cytotoxicity assay. For the assay, two types of cells were used: human dermal fibroblasts and primary rat Schwann cells. Human dermal fibroblasts cells were isolated from donor skin of abdominoplasty or breast reduction donated from patients of the Royal Hallamshire Hospital, Sheffield. Primary Schwann cells were isolated and cultured *in vitro* from freshly dissociated adult rat nerve following a protocol developed by (Kaewkhaw, Scutt et al. 2012). These cells resurrected from frozen, cultured and passaged as described in Section 2.2.5. Human dermal fibroblasts at passage eight and primary rat Schwann cells at passage five were used for contact cytotoxicity assay.

#### 5.3.5.1 Contact cytotoxicity assay

Three acellular nerve tissue samples (approximately 5 $mm^2$) were attached to the center of six-well tissue culture plates using rat-tail collagen (neutralised using sterile 0.1 M sodium hydroxide) and left for 15 minutes at room temperature to allow the gel set. A drop of cyanoacrylate contact adhesive was placed in the centre of control wells (n = 3). This was used as a positive control, as it has been demonstrated to produce a cytotoxic response. Collagen gel (20 μL) was added to the centre of the wells and neutralised with 10 μL of 0.1 M sterile NaOH (n =3). This served as a negative control as rat-tail collagen gel is biocompatible. All the wells containing samples, positive and negative controls were washed three times using sterile PBS, each for ten minutes. Human dermal fibroblasts and primary Schwann cells were seeded into each well at a density of $5x10^5$ cells per well and incubated at 37 °C in 5 % $CO_2$ (v/v) for 48 hours. Following incubation, the culture medium was discarded and the wells were gently washed with PBS containing calcium and magnesium and fixed with 3.7 % (v/v) formaldehyde for ten minutes.

Each well was stained with Giemsa solution (2 mL per well) for five minutes. Each well was gently rinsed with tap water until running clear and left to air dry. The plates were examined under Khöler illumination and any changes in cell morphology and density were recorded.

## 5.4 Results

### 5.4.1 Histological evaluation of acellular porcine peripheral nerves

Samples of native and acellular nerves were stained using general and specific histological stains to evaluate the gross effects of the decellularisation process on the histioarchitecture of porcine sciatic branches and sural nerves. Nerve sections were stained with Picro Sirius red (Figures 5.2 and 5.3), Miller's elastin (Figures 5.4 and 5.5) and Alcian blue PAS (Figures 5.6 and 5.7). In terms of ECM staining there was no apparent difference between native and acellular sural nerve and sciatic branches.

Picro Sirius red is a strong anionic dye which stains collagen by reacting via its sulphuric acid groups, with basic groups present in the collagen molecule. The elongated dye molecules are attached to the collagen fibre in such a way that their long axes are parallel. This parallel relationship between dye and collagen results in an enhanced birefringency. It has been hypothesised that staining with Sirius Red, when combined with enhancement of birefringency, may be considered specific for collagen (Junqueira, Bignolas et al. 1979). The Picro stains thicker collagen fibres red-orange and thinner newly formed fibres appear green, when viewed under polarized illumination.

Following staining using Picro Sirius red (Figures 5.2 and 5.3) it was observed that acellular nerves retained a large portion of the collagen fibres within the endoneurium, perineuiurm and epineurium when compared to native controls. There was no evidence of elastic fibres (blue/black stained fibres) in the native or acellular nerves when stained using Miller's elastin stain (Figures 5.4 and 5.5).

Following staining using Alcian blue GAGs were found to be located predominatly within the endoneurium and perinerium (stained purple; Figures 5.6 and 5.7). Following decellularistaion the distribution of GAGs remained the same as native nerves samples, however the staining intesnity was lower when compared to native nerve (Figures 5.6 and 5.7).

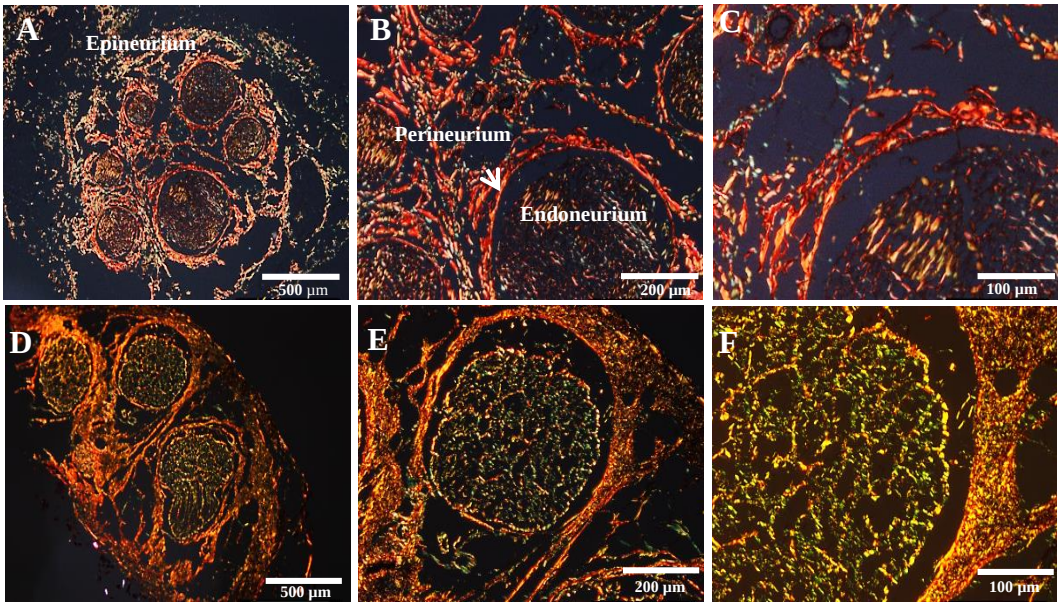


**Figure 5.2 Transverse sections of acellular porcine sural nerve stained with Picro Sirius red.** (A-C) Native sural nerve; (D-F) acellular sural nerve. Acellular nerves retained a large portion of the collagen fibres within the endoneurium, perineuiurm and epineurium when compared to native tissue. Thicker collagen fibres stained red-orange are seen predominatly within the epineurium. Thinner fibres stained green are located within the endoneurium and are more prominent in the acellular nerves. Sections imaged under polarized illumination. Scale bars at 500 µm, 200µm and 100 µm respectively.

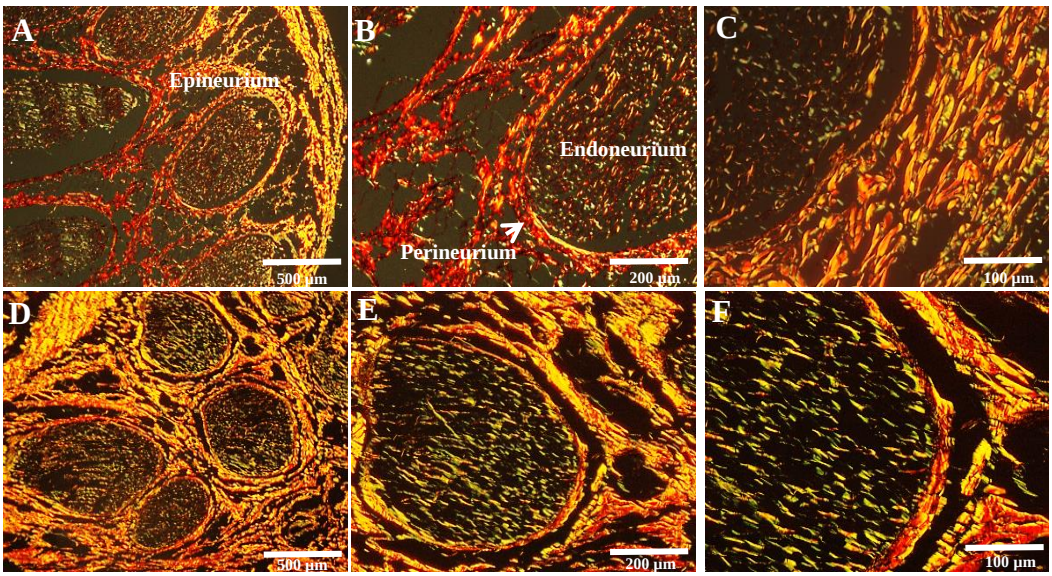


**Figure 5.3 Transverse sections of acellular porcine sciatic branches stained with Picro Sirius red.** (A-C) Native nerve; (D-F) acellular sural nerve. Acellular nerves retained a large portion of the collagen fibres within the endoneurium, perineuiurm and epineurium when compared to native tissue. Thicker collagen fibres stained red-orange are predominatly within the epineurium. Thinner fibres stained green are located within the endoneurium and are more prominent in the acellular nerves. Sections imaged under polarized illumination. Endo = endoneurium. Scale bars at 500 µm, 200µm and 100 µm respectively.

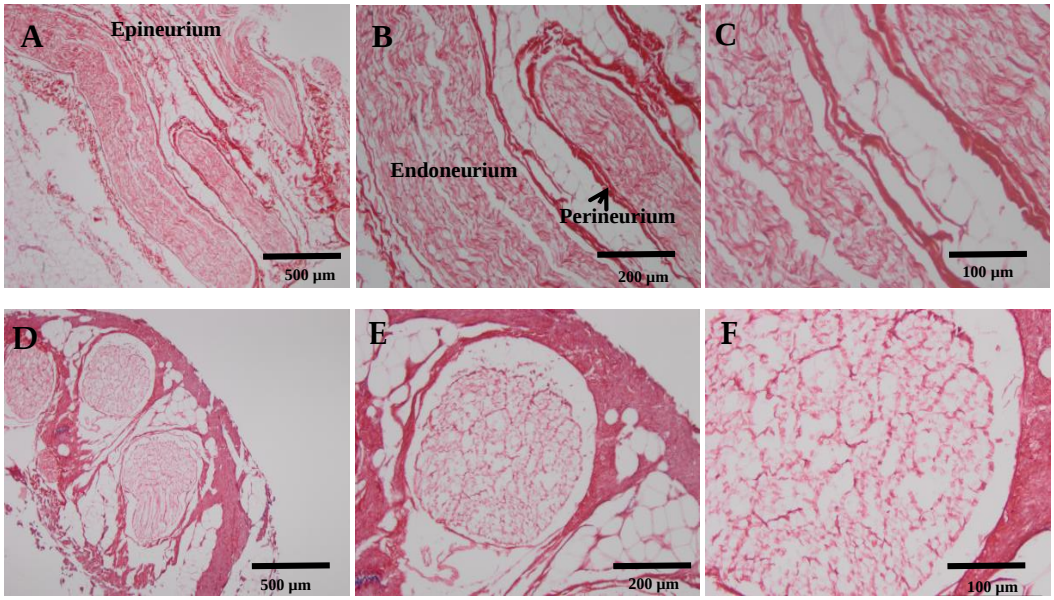


**Figure 5.4 Sections of decellularised porcine sural nerves stained with Miller's elastin. (A-C)** Native sural nerve; (D-F) acellular sural nerve. No elastin (blue/black stain) was detected within the connective tissues of the native or acellular nerves. Scale bars at 500 µm, 200µm and 100 µm respectively

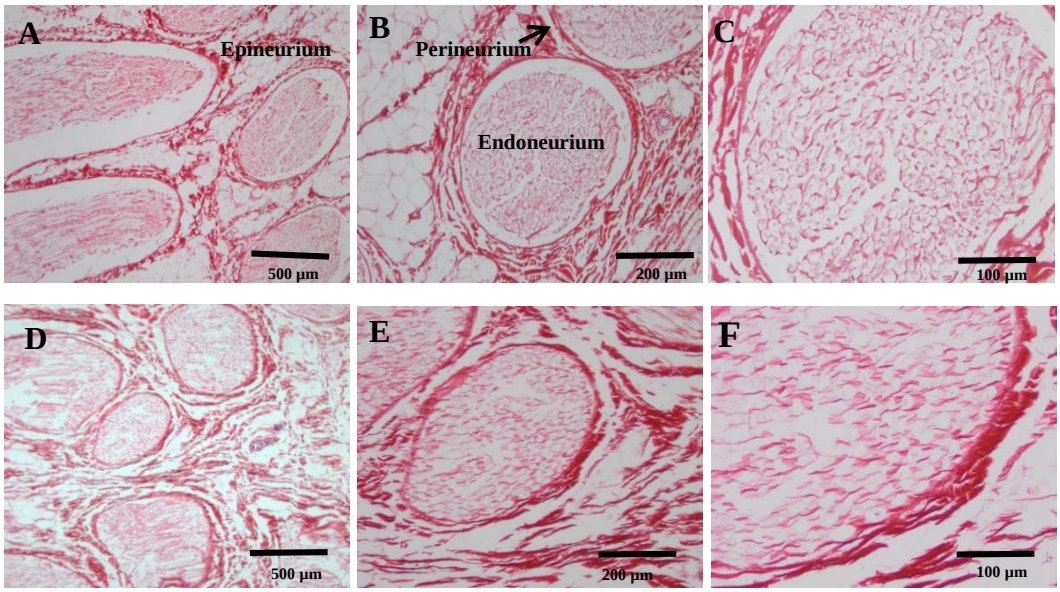


**Figure 5.5 Sections of decellularised porcine sciatic branches stained with Miller's elastin.** (A-C) Native nerve; (D-F) acellular nerve. No elastin (blue/black stain) was detected within the connective tissues of the native or acellular nerves. Scale bars at 500 µm, 200µm and 100 µm respectively

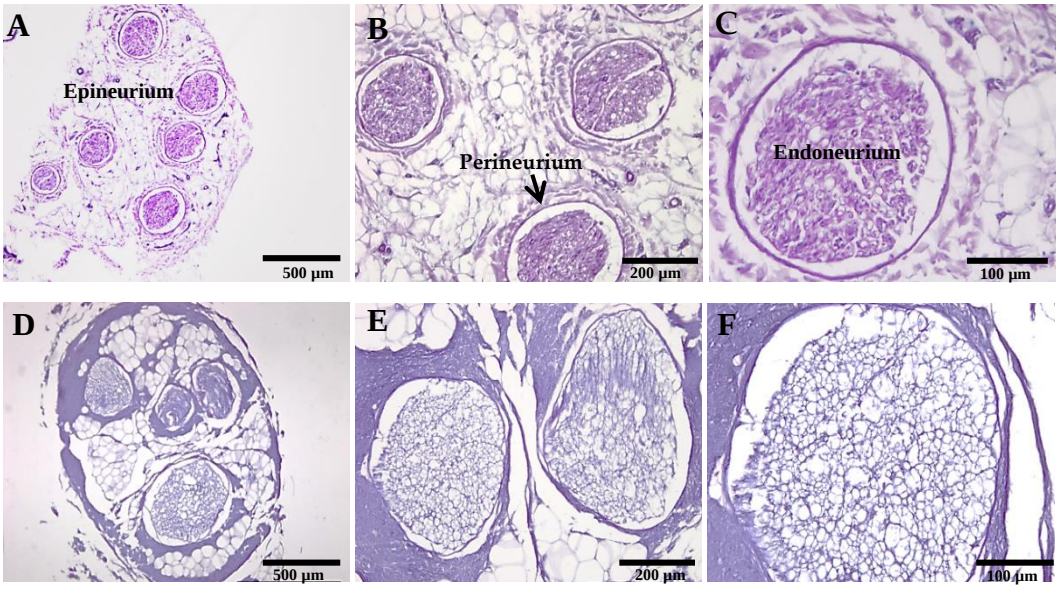


**Figure 5.6 Transverse sections of decellularised porcine sural nerves stained with Alcian blue PAS.** (A-C) Native sural nerve; (D-F) acellular sural nerve. Glycosaminoglycan's are detected predominantly within the endoneurium and perineurium in the native and acellular nerve, however when compared to native controls this staining was less intense in the acellular nerve. Scale bars at 500 µm, 200µm and 100 µm respectively.

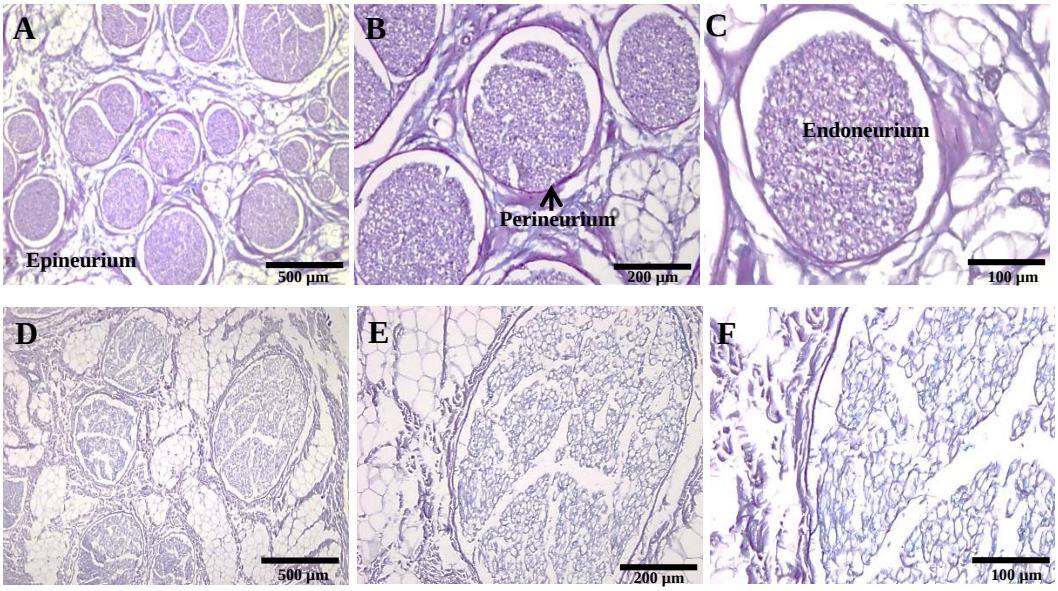


**Figure 5.7 Transverse sections of decellularised porcine sciatic branches stained with Alcian blue PAS.** (A-C) Native nerve; (D-F) acellular nerve. Glycosaminoglycan's are detected predominantly within the endoneurium and perineurium in the native and acellular nerve, however when compared to native controls this staining was less intense in the acellular nerve. Scale bars at 500 µm, 200µm and 100 µm respectively.

Sections of native and acellular porcine sciatic branches were stained using a reticulin stain to highlight reticular or collagen type III fibres, which were observed as black structures or fibres. Following staining collagen type III was found to be predominantly localised within the nerve fascicles (perineurium) and endoneurium (Figure 5.8). There was a similar distribution of collagen type III observed in sections of acellular porcine sciatic branches, however when compared to native controls this staining was less intense (Figure 5.8).

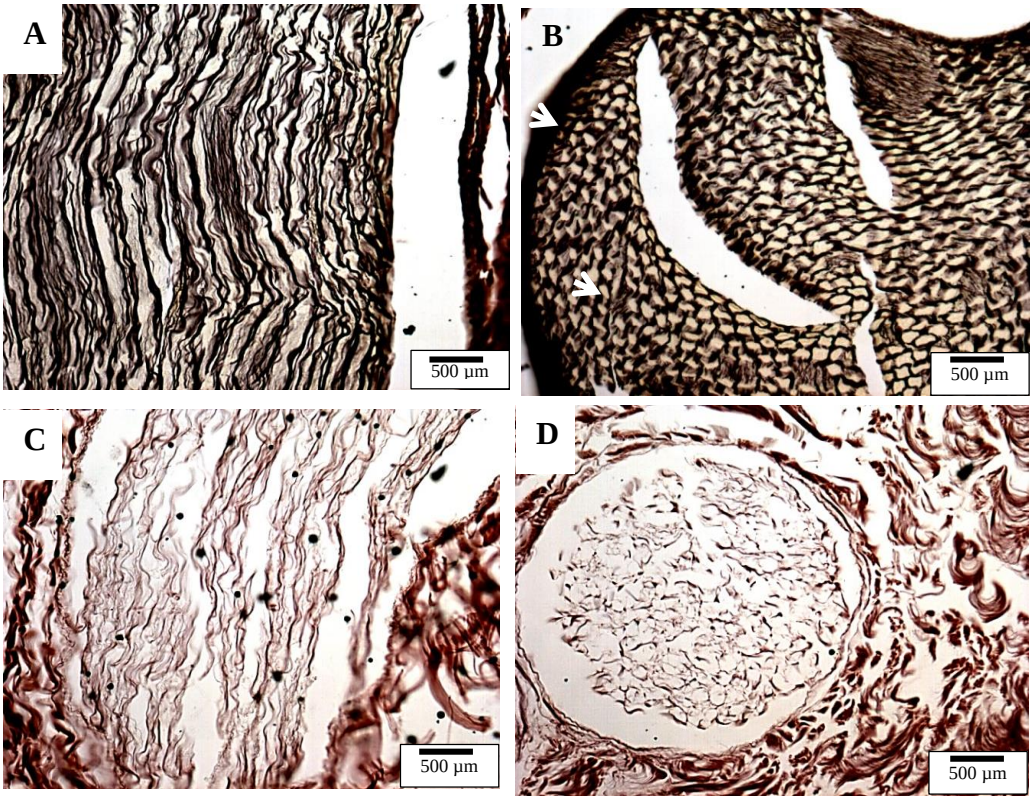


**Figure 5.8 Longitudinal and transverse sections of acellular porcine sciatic branches stained for collagen III fibres.** Intense black stain show collagen III localised around the perineurium and within the endoneurium in the native nerve as indicated by the arrows (A-B). A less intense black stain is shown in the acellular sciatic branches (C-D). Scale bar at 500 µm.

### 5.4.2 Biochemical analysis of native and decellularised porcine sciatic branches

Samples of native and acellular porcine sciatic branches were lyophilized to a constant weight prior to quantification of collagen and sulphated sugars as described in Section 5.3.3.

#### 5.4.2.1 Sulphated sugar assay

The amount of sulphated GAGs extracted from native and decellularised porcine sciatic branches was quantified using a sulphated sugar assay. The assay produced a liner relationship between absorbance at 525 nm and GAG content (Figure 5.9). The results shown in Figure 5.10 showed a significant 33 % reduction in sulphated GAGs after decellularisation.

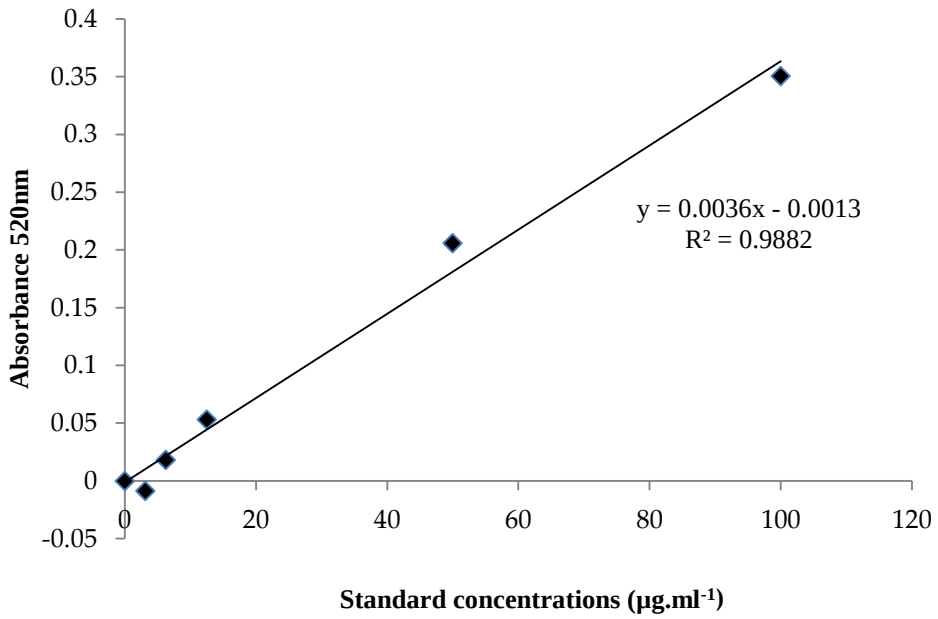


**Figure 5.9 Standard curve for glycosaminoglycan (GAG) assays**

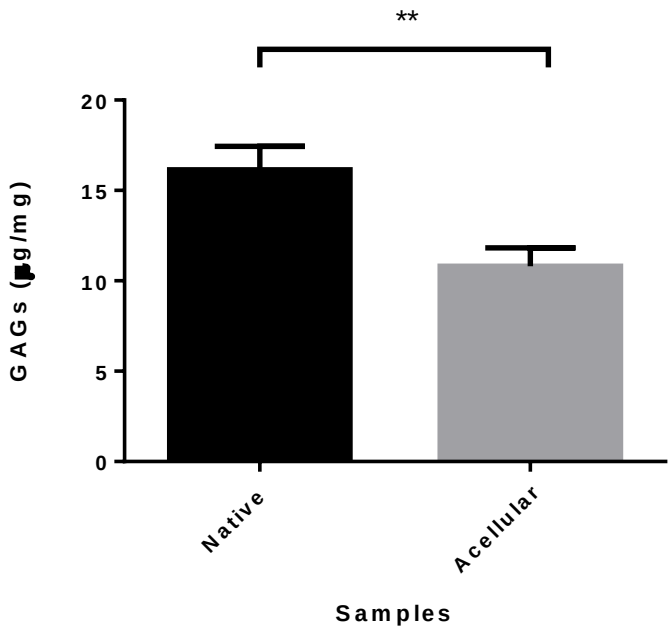


**Figure 5.10 Sulphated proteoglycan content of native and acellular porcine sciatic branches determined by glycosaminoglycan (GAG) quantification assay at 525 nm.** There is a significant reduction in GAG content after the decellularisation process. Native nerves have an average GAG content of 16.15 ± 1.30 µg/mg (n=6); acellular nerves have an average GAG content of 10.81 ± 1.02 µg/mg (n=6). Data was analysed using a student's *t*-test and is presented as the mean ± 95 % C.I ($p<0.0052$**)

### 5.4.2.2 Hydroxyproline assay

The collagen content of native and decellularised porcine sciatic branches was quantified using a hydroxyproline assay; these values were multiplied by 7.69 to calculate total collagen content. The hydroxyproline assay produced a liner relationship between absorbance at 570 nm and hydroxyproline content (Figure 5.11). Native porcine nerves were found to contain 1212 ± 194.8 µg/mg collagen and decellularised 1124 ± 100.70 µg/mg (Figure 5.12). This represented a 6.7 % decrease in collagen after decellularisation. This was not found to be statistically significant.

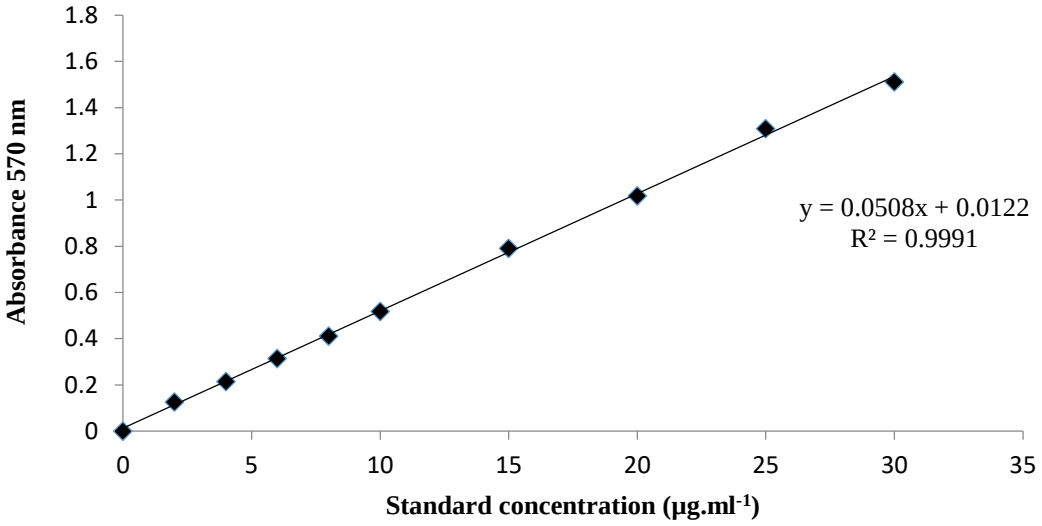


**Figure 5.11 Standard curve for hydroxyproline assays**

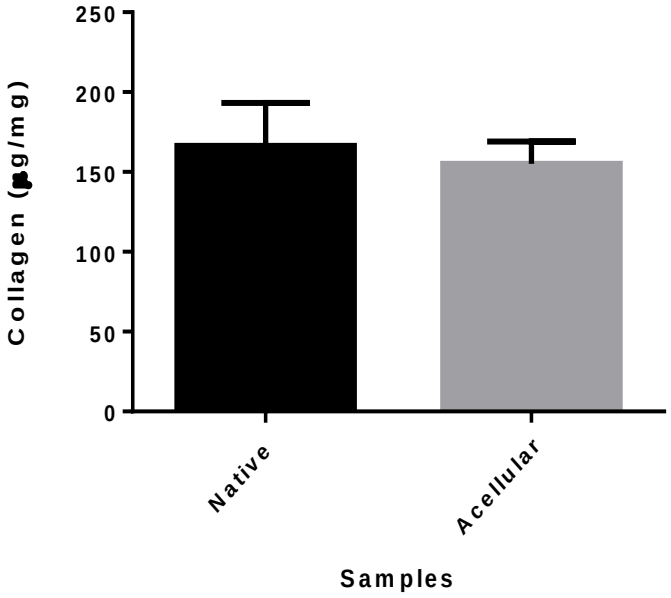


**Figure 5.12 Collagen content of native and acellular porcine sciatic branches determined by a hydroxyproline assay at 570 nm.** There was a slight reduction in collagen after the decellularisation process. Native nerves have an average collagen content of 1206 ± 195.50 µg/mg (n=6); acellular nerves have an average collagen content of 1124 ± 100.70 µg/mg (n=6). Data was analysed using a student's *t*-test and is presented as the mean ± 95 % C.I

### 5.4.3 Immunofluorescent evaluation of native and decellularised porcine sciatic branches

Antibody labelling was used to localise specific proteins in porcine sciatic branches. By comparing the images of the native and acellular samples, it was possible to determine if there was any change in specific extracellular matrix components. A FITC conjugated secondary antibody was used to visualise primary antibodies used to label laminin and fibronectin. Samples were imaged using an upright Zeiss LSM510 META confocal microscope (xenon arc lamp to excite FITC at $\lambda_{ex}$ = 495 nm / $\lambda_{em}$ = 515 nm). Nuclei were visualised using ($\lambda_{ex}$ = 300nm / $\lambda_{em}$ = 550nm).

#### 5.4.3.1 Immunolabelling for laminin

The images of porcine sciatic branches labelled with antibody specific to laminin are shown in Figure 5.13. Immunofluorescent labelling of native porcine sciatic nerve branches demonstrated laminin to be located around areas known to contain the basal lamina. These include the circumference around each Schwann cell/neuron unit (myelinated or ensheathed) within the endoneurium, the lamellar perineurial sheaths and the outer walls of blood vessels. The staining pattern was similar in samples of acellular sciatic nerve branches (Figure 5.13)

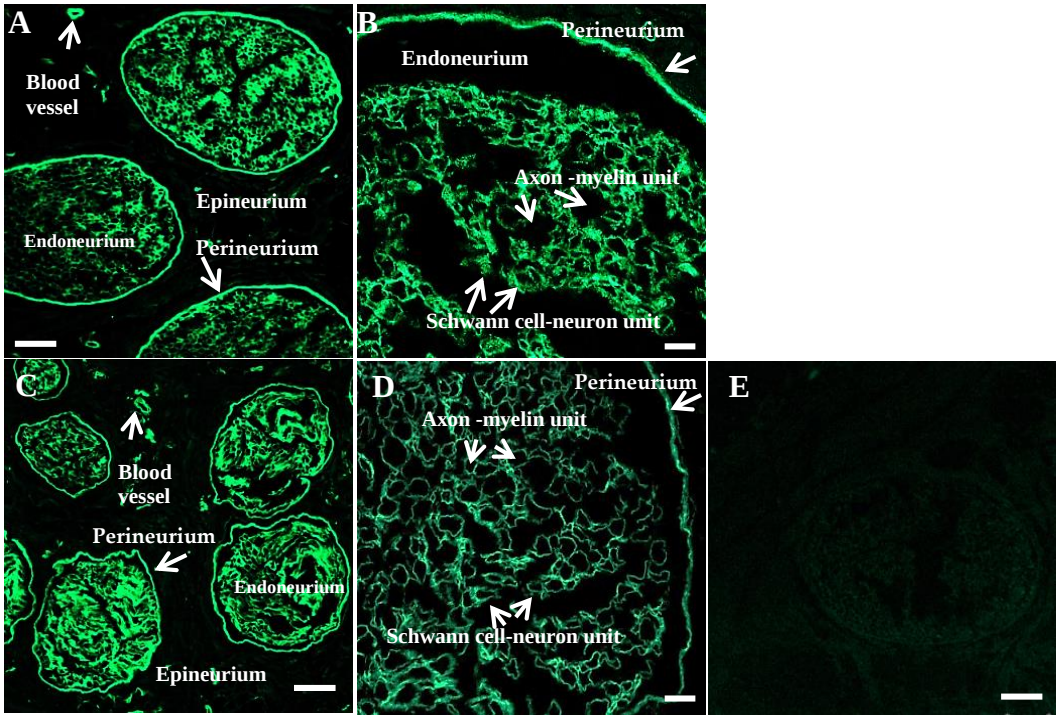


**Figure 5.13 Representative histological images from the central region of native and acellular porcine peripheral nerves labelled using a monoclonal antibody against laminin.** Antibodies to laminin delineate a discrete ring around each Schwann cell/neuron unit in the endoneurium (B and D), the lamellar structure of the perineurium (A-D) and around blood vessels (A and B). Unstained round areas are spaces occupied by axon/myelin units as indicated by the arrows (A and D). Images (C - D) show retention of laminin within the endoneurium and around the perineurium of the fascicle following decellularisation. The ring-like appearance of the open tubes in the native nerve (A-B) as well as the acellular nerves (C-D) suggests preservation of the basal lamina. Image E is a negative control for the antibodies raised against laminin. For the negative control the sample was stained with only the FITC conjugated secondary antibody. Scale bar at 20 µm for images B and D and 100 µm for images A, C and E.

### 5.4.3.2 Immunolabelling for fibronectin

The images of porcine sciatic branches labelled with antibody specific to fibronectin are shown in Figure 5.14. Immunofluorescent labelling of native porcine sciatic nerve branches indicated presence of fibronectin within the endoneurium and epineurium. The lamellar perineurial sheaths and the outer walls of blood vessels also indicated a strong presence of fibronectin. The staining pattern was similar in samples of acellular sciatic nerve branches (Figure 5.14)

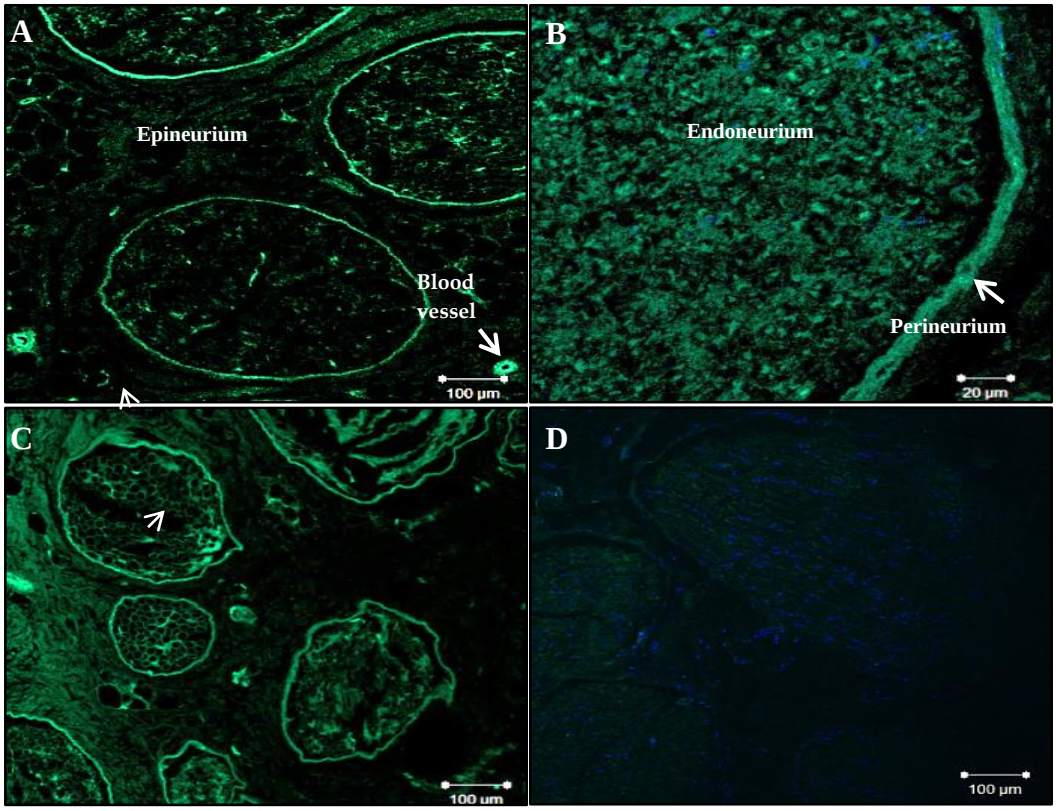


**Figure 5.14 Representative histological images from the central region of native and acellular porcine peripheral nerves labelled using a monoclonal antibody against fibronectin.** Antibodies to fibronectin delineate a discrete ring around each Schwann cell/neuron unit in the endoneurium (B-C), the lamellar structure of the perineurium (B), the epineurium and around blood vessels within the epineurium (A and C). Unstained round areas are spaces occupied by axon/myelin units (C). Image C shows retention of fibronectin within the epineurium, endoneurium and around the perineurium of the fascicle following decellularisation. The ring-like appearance of the open tubes in the native nerves endoneurium (A-B) as well as the acellular nerves as indicated by the arrows (C) suggests preservation of fibronectin within the connective tissues following decellularisation. Image D is a negative control for the antibodies raised against fibronectin. For the negative control the sample was stained with only the FITC conjugated secondary antibody and DAPI. Scale bar at 20 µm and 100 µm.

### 5.4.4 *In vitro* biocompatibility assays

A contact cytotoxicity assay was used to evaluate the *in vitro* biocompatibility of the acellular porcine sciatic branches. The effect of the acellular tissue on proliferation and morphology of human dermal fibroblasts and primary rat Schwann cells was evaluated.

Cells were cultured directly in contact with the samples of decellularised nerve, collagen type I and cyanoacrylate contact adhesive (Figure 5.15. There was no evidence of cells found in a circular area around the cyanoacrylate contact adhesive (positive control; Figure 5.15 E). Collagen gel (negative control) had no effect on either cell type, both dermal fibroblasts and Schwann cells grew up to and

in contact with the collagen gel and exhibited normal morphologies (Figure 5.15 B).

Both cell types were found to grow up to and in contact with the samples of acellular nerve (Figure 5.15 A-D). The acellular nerves had no effect on cell growth or morphology for both cell types. No differences were observed between the morphology of cells cultured with the acellular porcine sciatic branches and cells cultured with the collagen gel.

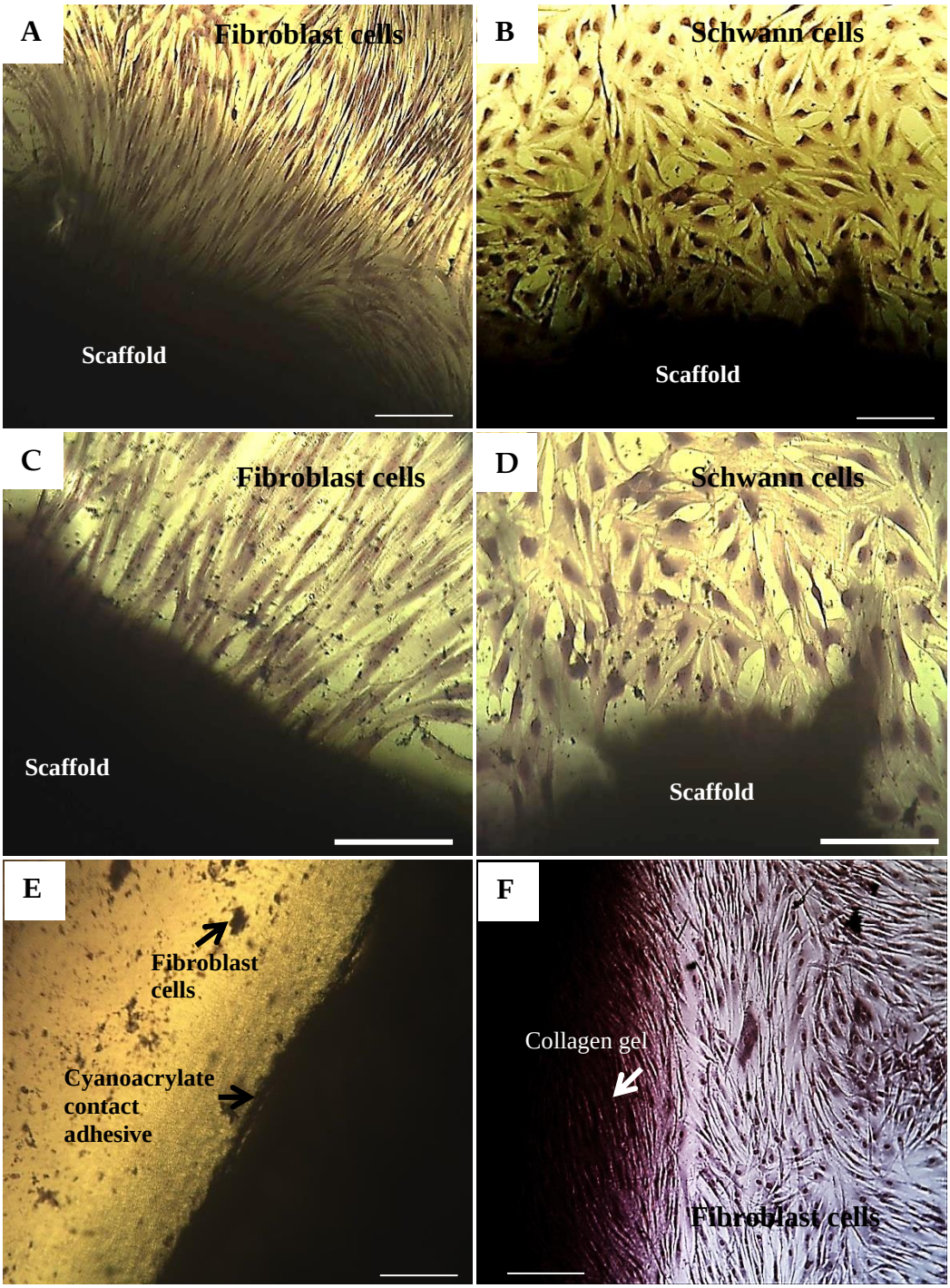


**Figure 5.15 Contact cytotoxicity assays of acellular porcine nerve scaffolds following 48 hours' culture with human fibroblasts and primary rat Schwann cells.** (A and C) acellular scaffold with fibroblasts; fibroblasts are observed growing up to and in contact with the scaffolds as well as retaining their elongated spindle shaped morphology under higher magnification (C) suggesting that the scaffold is not cytotoxic to fibroblasts; scale bar at 100 µm and 200 µm respectively; (B and D) acellular scaffold with Schwann cells; Schwann cells are observed growing up to and in contact with the scaffolds as well as retaining their bi- or tripolar elongated morphology suggesting that the scaffold is not cytotoxic to Schwann cells; scale bar at 100 µm and 200 µm respectively; (E) Cyanoacrylate contact adhesive (positive control) shows clumps of necrotic fibroblast cells as indicated by the arrows due to cytotoxic effect of the cyanoacrylate adhesive , scale bar at 100 µm; (F) Image F shows fibroblast cells growing up to and in contact with the collagen gel (negative control), scale bar at 100 µm.

### 5.4.5 Biomechanics of native and acellular porcine sciatic branches

The biomechanical properties of the tissues were assessed under uniaxial tensile loading to failure in order to assess the effect of the decellularisation treatment on the mechanical behaviour of the porcine peroneal and tibial nerves.

#### 5.4.5.1 Biomechanical characterisation of the porcine sciatic branches

The stress-strain behaviours of native and acellular peroneal and tibial nerves are illustrated in Table 5.4. The table shows that the peroneal and tibial nerves ultimate tensile strength (UTS), strain and Young's modulus (YM) had increased after decellularisation. There was a significant increase in UTS for both the acellular peroneal and tibial nerve when compared to native (control) tissue. There was also a significant increase in strain for the acellular tibial nerve when compared to control.

| **Nerve** | **Young's Modulus (MPa)** | **Ultimate tensile strength (MPa)** | **Strain at ultimate tensile strength** |
|---|---|---|---|
| Native peroneal | 7.75 ± 0.56, n=5 | 1.23 ± 0.056, n=5* | 0.23 ± 0.036, n=5 |
| Acellular peroneal | 8.03 ± 0.81, n=3 | 1.81 ± 0.30, n=3 | 0.43 ± 0.10, n=3 |
| Native tibial | 7.43 ± 0.53, n=10 | 0.87 ± 0.09, n=10* | 0.16 ± 0.01, n=10* |
| Acellular tibial | 8.45 ± 0.36, n=4 | 2.69 ± 0.51, n=4 | 0.36 ± 0.09, n=4 |

**Table 5.4 Biomechanical evaluation of native and acellular porcine nerves.** Mechanical analysis showed a significant increase in UTS in both the acellular peroneal (1.81 MPa) and tibial nerve (2.69 MPa) when compared to their native nerve counterparts (native peroneal nerve; 1.23 MPa and tibial nerve; 0.87 MPa). There was a significant increase in strain at UTS for the acellular tibial nerve (0.36) when compared to its native counterpart (0.16). All data is expressed as mean (peroneal nerve n = 8; tibial nerve n = 11; acellular peroneal n = 3; and tibial nerve n = 4). Data was analysed using the Students *t*-test and is presented as the mean ± 95 % C.I (*$p<0.05$).

## 5.5 Discussion

In this Chapter, the biological characteristics of acellular porcine peripheral nerves were evaluated and compared to native controls. The decellularisation method used to obtain the acellular tissue in this chapter was referred to as 'Method 7' in Chapter 4. Histological, immunohistochemical and biochemical characterisation of the native and acellular nerve was used to demonstrate that the decellularisation process can retain the nerves native endoneurial structure and important ECM components. This study further revealed that acellular nerves are not cytotoxic to cells and that the nerves retain its mechanical properties.

Collagen is an important structural ECM component of the peripheral nerve (Seyer, Kang et al. 1977; Bunge, Bunge et al. 1989). Previous decellularisation studies have reported that SDS is more effective in removing cell residues from tissues compared to other detergents such as Triton X-100, however it tends to be more disruptive to the ECM ultrastructure and collagen fibres (Kasimir, Rieder et al. 2003; Gilbert, Sellaro et al. 2006; Gratzer, Harrison et al. 2006; Ott, Clippinger et al. 2010). By decreasing the SDS cycle and using a low concentration of SDS as described in Chapter 5, the histological stain using Picro Sirius red showed that the nerves collagen fibres and structure were maintained. Unlike previous chemical processes which have left the nerve with an unpreserved ECM (Hall 1986; Sondell, Lundborg et al. 1998; Krekoski, Neubauer et al. 2001) the acellular tissue in this study retained its ultrastructure along with its connective tissue layers (epineurium, endoneurium and perineurium) and intact fascicles. Tissue preservation has also been noted with other SDS treated tissues (Elder, Eleswarapu et al. 2009; Wilshaw, Rooney et al. 2012; Wang, Itoh et al. 2016).

Histological staining also revealed a reduction in the intensity of the reticulin staining of collagen III; nevertheless, a quantification assay demonstrated that SDS does not significantly reduce the overall collagen content. Previous decellularisation studies using SDS have also demonstrated the preservation of collagen content including collagens type I and IV which construct the basal lamina tubes in peripheral nerves (Kheir, Stapleton et al. 2011; Xu, Xu et al. 2014; Wang, Itoh et al. 2016).

Alcian Blue staining and GAG assay demonstrated a significant reduction of sulphated proteoglycans within the decellularised nerves. The removal in GAGs has been noted in other SDS based decellularisation processes (Kheir, Stapleton et

al. 2011; Xu, Xu et al. 2014). The absence of GAGs reduces the restriction on water flow and causes a reduction in the water retention of the tissue, which also facilitates the diffusion of decellularisation solutions to remove soluble cellular components (Gilbert, Sellaro et al. 2006).

The importance of GAGs in terms of nerve regeneration is relatively unknown. Hyaluronic acid the predominant GAG found in the PNS (Chandrasekaran and Bachhawat 1969) assists with fibrin organization, which may facilitate a pathway for cellular and axonal ingrowth during the acellular fibrin matrix phase of peripheral nerve regeneration (Wang, Nemeth et al. 1998). Chondroitin sulphate GAGs however inhibits the neurite promoting activity of laminin, and therefore may have a negative role in nerve regeneration (Zuo, Hernandez et al. 1998). A study by Krekoski (2001) treated acellular rat sciatic nerve grafts with chondroitinase ABC that inactivated CS-GAG chains and observed an enhancement in the growth promoting properties of the acellular scaffold (Krekoski, Neubauer et al. 2001). Therefore, the removal of sulphated GAGs may actually be beneficial in terms of its regeneration capacity.

Millers Elastin staining indicated no presence of elastin in either the native or decellularised nerves. A reason for this may be due to the fact that both collagen and elastin cross-stain with the traditional histochemical techniques such as Weigert and Verhoeff-VanGiesson, therefore making it more difficult to distinguishing the presence of elastin from collagen. Through immunolabelling Tassler (1994) was able to locate small amounts of elastin in the epineurium, endoneurium and perineurium, adjacent to the collagen fibres (Tassler, Dellon et al. 1994).

Immunohistochemical staining of the acellular nerves revealed the retention of the basal lamina, tubes of structural proteins comprised of collagen, laminin and fibronectin that surround the axons. The basal lamina is an important component of the nerve as both laminin and fibronectin play essential roles in nerve regeneration (Gao, Wang et al. 2013). Research has also shown that bands of Bünger cannot be formed by Schwann cell without the basement membrane. This implies that the ECM may play a more important role than Schwann cell in nerve regeneration (Donzelli, Maiuri et al. 2006). Other nerve decellularisation methods including thermal (Ide, Tohyama et al. 1998) and chemical (Sondell, Lundborg et al. 1998) processes have been known to fracture and damage the basal lamina. The

Sondell method which uses Triton X-100 has shown to decrease the laminin and fibronectin content (Grauss, Hazekamp et al. 2005). In contrary SDS studies have been shown to retain the basal lamina, laminin and fibronectin (Wakimura, Wang et al. 2015; Wang, Itoh et al. 2015).

The importance of an intact basal lamina was highlighted in the nerve study which compared two well-known detergents based decellularisation processes. The Hudson method, which used zwitterionic detergents (SB-10 and SB-16 in combination with Triton X-200), produced acellular nerve grafts which retained the basal lamina more effectively than the Sondell method which used Triton X-100. As a result the Hudson graft displayed higher axon densities and stronger regeneration potential than the Sondell graft (Hudson, Liu et al. 2004). A separate study also showed the Hudson acellular nerve graft outperforming NeuraGen® (an FDA-approved and commercially available type I collagen NGC) (Hudson, Liu et al. 2004). The study proposed that the presence of intact basal lamina within the acellular nerve graft contributes to the enhanced regenerating capacity to support axonal growth (Whitlock, Tuffaha et al. 2009). The method developed by Hudson et al. (2004) is currently licensed by AxoGen® Inc. to produce Avance®, the only commercially available acellular nerve graft.

Residual SDS can be retained in decellularised tissues, and has been suggested in previous studies that it can potentially be cytotoxic to cells (Cartmell and Dunn 2004; Rieder, Kasimir et al. 2004). Therefore, a biocompatibility assay was performed. Both fibroblast and Schwann cells were observed microscopically and found to proliferate up and in contact with the scaffold. Both cell types maintained membrane integrity, native phenotype and there was no sign of cell lysis, indicating that the tissue was not cytotoxic. Other studies using SDS based treatments to treat tissues have reported on similar findings (Wilshaw, Rooney et al. 2012; Luo, Korossis et al. 2014)

Biomechanical testing of the native and decellularised nerve was undertaken to see if there was any change in the nerves mechanical properties as loss of GAGs has been associated with a reduction in the ultimate tensile strength of the tissue (Partington, Mordan et al. 2013). The biomechanical result showed an increase in Young's modulus, UTS and strain at UTS. There was no significant difference in the Young's modulus; however, there was significance in the UTS for both the decellularised peroneal and tibial nerves, as well as strain for the tibial

nerves when compared to their native counterparts. These results were found to be similar in other decellularisation studies (Stapleton, Ingram et al. 2008; Williams, Liao et al. 2009; Abdelgaied, Stanley et al. 2015). As previously discussed, elastin and collagen fibres contribute to the mechanical properties native nerves (Tassler, Dellon et al. 1994; Mason and Phillips 2011). During the decellularisation process the tissue becomes 'looser' due to cell removal and the collagen fibre network starts to uncrimp (Williams, Liao et al. 2009). Uncrimping or relaxation of the collagen fibres has been associated with increased stiffness in soft tissues (Freed and Doehring 2005). In addition increased fibre mobility due to the less compact nature of the acellular tissue allow collagen fibres to reorient easily towards the direction of applied strain, which would also lead to increased stiffness (Williams, Liao et al. 2009).

Peripheral nerves have visco-elastic properties and are able to respond to a normal range of motion of the joints (Tassler, Dellon et al. 1994). It was first suggested that the visco-elastic properties of the nerves were due to the elastin fibres found within the connective tissue supporting elements (Sunderland 1968). However, the relatively small percentage of elastin fibres found in the nerve suggests that the visco-elastic properties of the peripheral nerve may also be due not only to elastin but to collagen as well. When viewed at a molecular level it was noted that collagen fibres were arranged in such a way to allow some degree of longitudinal stretch (Ushiki and Ide 1990). It is thought that this specialised arrangement of layers of collagen fibres is likely to be the underlying structural component, in conjunction with fluid pressure, which provides the nerve with its viscoelasticity (Phillips, Smit et al. 2004). It was postulated by Tassler et al. (2004) that elastin plays a role in the first phase of the stress-strain curve (strain less than 20 %) and collagen thereafter, making collagen the predominant molecule responsible for the elasticity of the nerve (Tassler, Dellon et al. 1994).

## 5.6 Conclusion

Porcine peripheral nerves were successfully decellularised using a low concentration SDS and hypotonic buffers. Qualitative and quantitative analysis of the ECM revealed preservation of important ECM components including collagen, laminin and fibronectin, however there was a significant loss of GAGs observed by quantitative analysis. *In vitro* contact cytotoxicity assays demonstrated the acellular nerves were not cytotoxic to human dermal fibroblasts and primary rat Schwann cells fibroblasts. Biomechanical evaluation of the acellular nerves revealed a slight increase in the YM's, UTL and strain, however the decellularisation process did not decrease the mechanical properties of the nerves.

The retention of the ECM components and its biomechanical properties translates to suitable acellular graft which can be used for *in vivo* or *in vitro* analysis. For clinical purposes the acellular nerve grafts would be easy to handle and suture due to the retention of their structure and mechanical properties, in addition to the well preserved ECM and basal lamina structure, making it an ideal environment for axonal regeneration. The retention of laminin and fibronectin within the basal lamina tubes also provides a suitable environment for the introduction of Schwann cells into the acellular graft, by providing cell adhesion sites as well as stimulating cell growth. In summary, the decellularised porcine peripheral nerve scaffold demonstrated good retention of ECM components as well as biocompatibility and biomechanical properties. The use of the acellular graft, both as an *in vitro* and *in vivo* model with and without the inclusion of Schwann cells will be discussed in subsequent chapters.

# Chapter 6. An Ultrastructural Study on Porcine Peroneal and Tibial Nerve

## 6.1 Introduction

The tibial and peroneal nerves are two terminal branches of the porcine sciatic nerve, the largest nerve in the lower limb. The tibial nerve is the larger of the branches and provides motor innervation to the muscles of the posterior compartment of the leg, and sensory innervation to the posterior aspect of the leg. The peroneal nerve provides motor innervation to the muscles of the lateral compartment of the leg, which innervates the foot, and sensory innervation to the distal section and dorsum of the foot (McCrory, Bell et al. 2002).

Under normal physiological conditions nerves are exposed to various mechanical stresses. Each peripheral nerve consists of connective tissues (endoneurium, perineurium and epineurium), which encase the nerve bundle to ensure flexibility as well as protecting the nerve fibres from stretch and compression forces during body movement. When the nerve undergoes elongation, pressure produced in the endoneurium will resist the resulting transverse contraction and contribute to the stiffness of the nerve when stretched (Millesi, Zoch et al. 1995; Layton and Sastry 2004). The perineurium is the primary contributor to the nerve's tensile strength and elasticity. The collagen fibrils as well as the elastic fibres are orientated in circumferential, oblique and longitudinal orientations which together provide multidirectional tensile strength to the fascicles, making the perineurium the load bearing portion of the nerve (Topp and Boyd 2006). The epineurium is composed of collagen, elastin and adipose tissues. Is the last layer to be affected by an increase in tensile stress and is generally maintained after the other layers have been compromised (Rydevik, Kwan et al. 1990; Kwan, Wall et al. 1992). It has been suggested that the collagen fibres in the epineurium provide resistance to stretch (Campbell, Samlan et al. 2013), while the adipose protects against compression (Sunderland 1965).

Our previous study on the characterisation of porcine peripheral nerves reported that the porcine peroneal nerve has a higher ultimate tensile strength value in comparison to the porcine tibial nerve when undergoing mechanical testing (Zilic, Garner et al. 2015). In the posterior femoral region, the tibial nerve continues in the direction of the sciatic nerve towards the popliteal fossa. In contrast, the peroneal nerve changes direction and descends laterally to the neck of the fibula.

Consequently, it is believed that the peroneal nerve tolerates a greater tensile strength during the leg movement than the tibial nerve due to the anatomical position (Ugrenović 2014).

Studies have shown that the ultrastructure of the connective tissues and associated ECM components play important roles in the biomechanics of peripheral nerves. Research has shown that the mechanical properties may be attributed by various factors such as the number and arrangement of fascicles (Sunderland and Bradley 1961), the internal fluid pressure maintained by the perineurium (Low, Marchand et al. 1977), ECM components such as collagen and elastin (Ushiki and Ide 1990; Tassler, Dellon et al. 1994) and variance in collagen fibril diameter within the connective tissue (Parry, Barnes et al. 1978; Mason and Phillips 2011).

Developing a clear understanding of the biomechanical features of peripheral nerves is important in tissue engineering applications where xenogeneic nerves are increasingly being investigated for clinical application (Gutmann and Sanders 1943; Osawa, Tohyama et al. 1990; Hudson, Liu et al. 2004; Whitlock, Tuffaha et al. 2009; Zhang, Luo et al. 2010). Identifying the maximum tension which nerves can withstand and understanding the origin of their mechanical resilience is of great importance to improving the outcome of surgical nerve repairs. Nerve graft coaptations are tension free by design; however *in situ* stress is always present in peripheral nerves and varies with joint position (Sunderland and Bradley 1961). Properties such as suture holding ability to maintain a mechanically robust interface with the native nerve stump are critical for axon regeneration (Borschel, Kia et al. 2003).

As the mechanical properties of the nerve tissue are known to depend on a variety of factors it is difficult to give a precise role to any one component. Our previous study reported that collagen was the predominant extracellular matrix protein in porcine nerve, and so its role in the mechanical property of nerve may be more discernible. Alterations in the mechanical properties of nerves, such as increased stiffness have been associated with an increase in the diameter of collagen fibrils in the endoneurium of diabetic rat models (Muona, Jaakkola et al. 1989). Furthermore, the association between collagen fibril diameter and the functional properties of tissues is well established elsewhere in tissues such as tendons, ligaments and skin (Ottani, Raspanti et al. 2001). It has been postulated

that if the tissue consists of smaller diameter sized collagen fibrils then it is designed to be a more compliant material, and consequently large collagen fibrils are predicted to have a greater tensile strength than smaller fibrils (Parry, Barnes et al. 1978).

## 6.2 Aims and objectives

**Aims:**

The aim of this Chapter was to evaluate the ultrastructure of porcine peroneal and tibial nerves and investigate if differences in ultrastructure explain experimentally derived differences in mechanical properties. The study focused on the connective tissue of the endoneurium, perineurium and epineurium.

**Objectives:**

- Histologically determine the size, number and area of nerve fascicles and surrounding epineurium tissue.
- Analyse size, number and area of the fascicles and surrounding epineurium tissue through histological staining and image analysis.
- Quantify the diameter and density of collagen fibrils in transverse sections of the peroneal and tibial nerves using transmission electron microscopy (TEM).

## 6.3 Materials and methods

### 6.3.1 Dissection of peroneal and tibial nerves

Large White Yorkshire pigs (24-26 weeks old) were sourced from a local abattoir and hind legs obtained within 2-3 hours of slaughter. Legs were stored at 4°C between slaughter and delivery to the laboratory. Upon arrival, peripheral nerves were immediately dissected from the porcine leg. Dissection of the nerves from each leg took approximately 20 minutes. Once dissected, nerves were immediately fixed in 10 % (v/v) neutral buffered formalin (NBF) for histological analysis or 2 % paraformaldehyde and 2 % (w/v) glutaraldehyde in 0.2 M phosphate buffer for TEM analysis.

The tibial and common peroneal were isolated and dissected, with initial reference to the anatomy of human nervous system anatomy of the lower leg. The sciatic nerve was dissected from the posterior compartment of the leg. The sciatic nerve divided into two terminal branches; the tibial and common peroneal nerve. The tibial nerve was observed to travel in the posterior section of the leg and the peroneal nerve in the lateral section. Excess fat and connective tissue was removed from the nerve samples and tissues washed three times in phosphate buffered saline solution containing 0.1 % (w/v) ethylene diamine tetra acetic acid (EDTA) to remove excess blood and tissue fluid.

For histological and electron microscopy, three peroneal and three tibial nerves were used. Thus, in total six nerves were harvested from three porcine legs. The number of individual measurements in total for each characterisation method is given below, for each nerve.

### 6.3.2 Characterisation of tibial and peroneal nerves

Native porcine nerve tissue was cut into 1 cm segments, dissected from either end of the nerve (n=3) and fixed in 10 % (v/v) neutral buffered formalin (NBF) for 24 hours. Paraffin embedded samples were then processed as described in Section 2.2.3.

#### 6.3.2.1 Haematoxylin and eosin staining of peripheral nerves

Transverse sections (6 µm) of each nerve sample were stained with haematoxylin & eosin was undertaken to evaluate the histioarchitecture and nerve fascicular pattern. Samples were viewed using an Olympus BX51 microscope and images

captured using an Olympus XC50 digital camera (with Olympus Soft Imaging Solutions software). The number and size of the nerve fascicles present within each peripheral nerve was analysed using ImageJ (NIH, USA).

#### 6.3.2.2 Fixation and embedding nerves for TEM analysis

Prior to excision, nerves were marked and measured then following excision they were maintained at their *in situ* length on a piece of card during fixation. Peroneal and tibial nerves were fixed at room temperature for four hours in 2 % paraformaldehyde and 2 % (w/v) glutaraldehyde in 0.2 M phosphate buffer. Each nerve (5 mm in length) was post fixed in 1 % (w/v) osmium tetroxide in 0.1 M phosphate buffer for 1 hour at room temperature. Nerve samples were dehydrated using increasing concentrations of acetone (30 %, 50 %, 70 % and 90 % (v/v) acetone in distilled water for 20 minutes each and in three changes of 100 % (v/v) acetone for ten minutes each). The samples were left in a 50:50 mix of acetone and Epon 812 resin for 12 hours then embedded in Epoxy resin (after Luft 1961). Semi-thin sections were cut at 2 μm and stained with 1 % toluidine blue in 2 % borax solution for one minute to confirm transverse tissue orientation under a light microscope. Ultrathin sections of 70 nm were cut using a Leica Ultracut UCT ultramicrotome. Sections were mounted onto copper grids and stained with 4 % uranyl acetate (UAc) solution under dark conditions for 30 minutes. Three changes of double distilled water ($ddH_20$) were used to wash the excess UAc from the tissue and excess $ddH_2O$ then removed by blotting the backs of the copper grids with filter paper. The sections were stained with Reynold's lead citrate solution for ten minutes under carbon dioxide free conditions (achieved by adding a small number of sodium hydroxide granules to an enclosed staining environment). The grids were then rinsed with a final three changes of $ddH_2O$ to remove excess stain and the sections were left to dry before imaging.

#### 6.3.2.3 Collagen fibril diameter analysis

Images were captured at x4800 magnification using a FEI Tecnai G2 Spirit transmission electron microscope with attached 11 MP digital camera. The diameters of 150 collagen fibrils were sampled from the endoneurium, 150 from the epineurium and 50 from the perineurium of peroneal and tibial nerves. Images were captured around the circumference of the epineurium and of the perineurium until a quarter of the circumference was fully mapped. Five images were captured

from the endoneurium, and 150 fibrils were measured from each image using a standardised approach to obtain images from equivalent positions in each nerve region. The largest fibril diameter was measured using ImageJ software.

#### 6.3.2.4 Perineurium thickness

Transmission electron micrographs were taken of nerves at x 1900 magnification. For each sample, ten perineurium measurements were sampled from the circumference of the nerve, with the typical anatomy of the perineurium providing morphological identification enabling measurements to be made.

#### 6.3.2.4 Data Analysis

All numerical values are shown as mean values ± 95 % confidence limits. Data was displayed as box and whisker plots. Statistical significance was assessed by the T-method and *P*-values of <0.05 were considered significant.

## 6.4 Results

### 6.4.1 Histioarchitecture and fascicular pattern of peroneal and tibial nerves

Qualitative characterisation of transverse porcine peroneal and tibial nerve sections stained using haematoxylin and eosin showed that the tibial nerve (Figure 6.1 1A) was significantly larger and contained more fascicles than the peroneal nerve (Figure 1B).

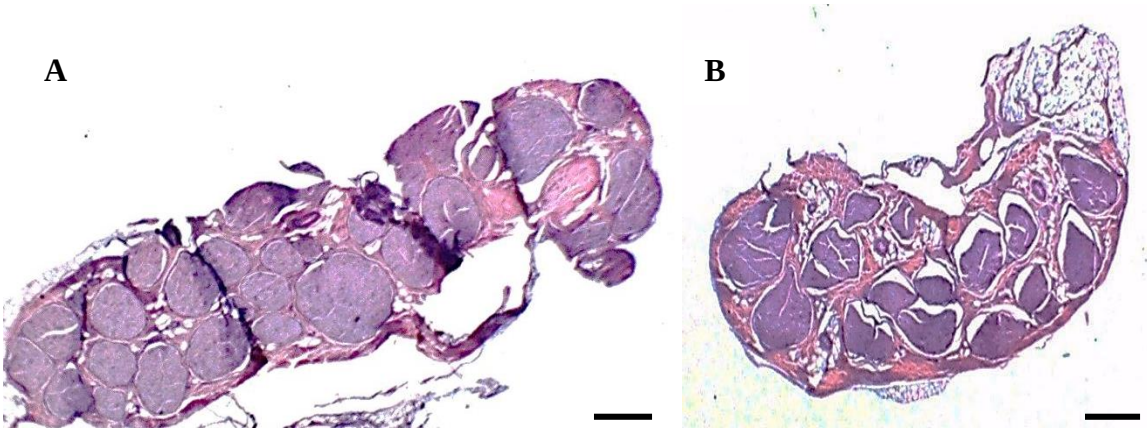


**Figure 6.1. Histioarchitecture of porcine tibial and peroneal nerves.** Haematoxylin and eosin staining of transverse nerve sections. The tibial nerve (A) is larger and contains more fascicles than the peroneal nerve (B) nerve. Scale bar at 500 µm.

Quantitative analysis using Image J revealed that the tibial nerve contained a significantly larger proportion of nerve fascicles, with tibial nerves having on average 37 fascicles per section in contrast to the peroneal nerve, which had an average 13 fascicles (Figure 6.2 A). The average fascicle size for the tibial nerves was 84,717 ± 3,839 $\mu m^2$. The average size for the peroneal nerve was 76,450 ± 6,198 $\mu m^2$ (Figure 6. 2 B), this was not statistically different.

The tibial nerve was shown to have a significantly larger fascicular and non-fascicular area in comparison to the peroneal nerve (Figure 6. 2 C and D). The tibial nerve had an average fascicular area of 28,069 ± 5,959 $\mu m^2$, whilst the peroneal had an average fascicular area of 9,214 ± 1,037 $\mu m^2$. The average non-fascicular area of the tibial nerve was 24,130 ± 3,855 $\mu m^2$ and the peroneal average area was 8,869 ± 9678 $\mu m^2$. Overall, the peroneal nerve had approximately 49 % non-fascicular tissue whilst the tibial nerves had 47 % non-fascicular tissue, in relation to the total area of the nerve. Table 6.1 summarises the fascicular pattern and area of the peroneal and tibial nerves.

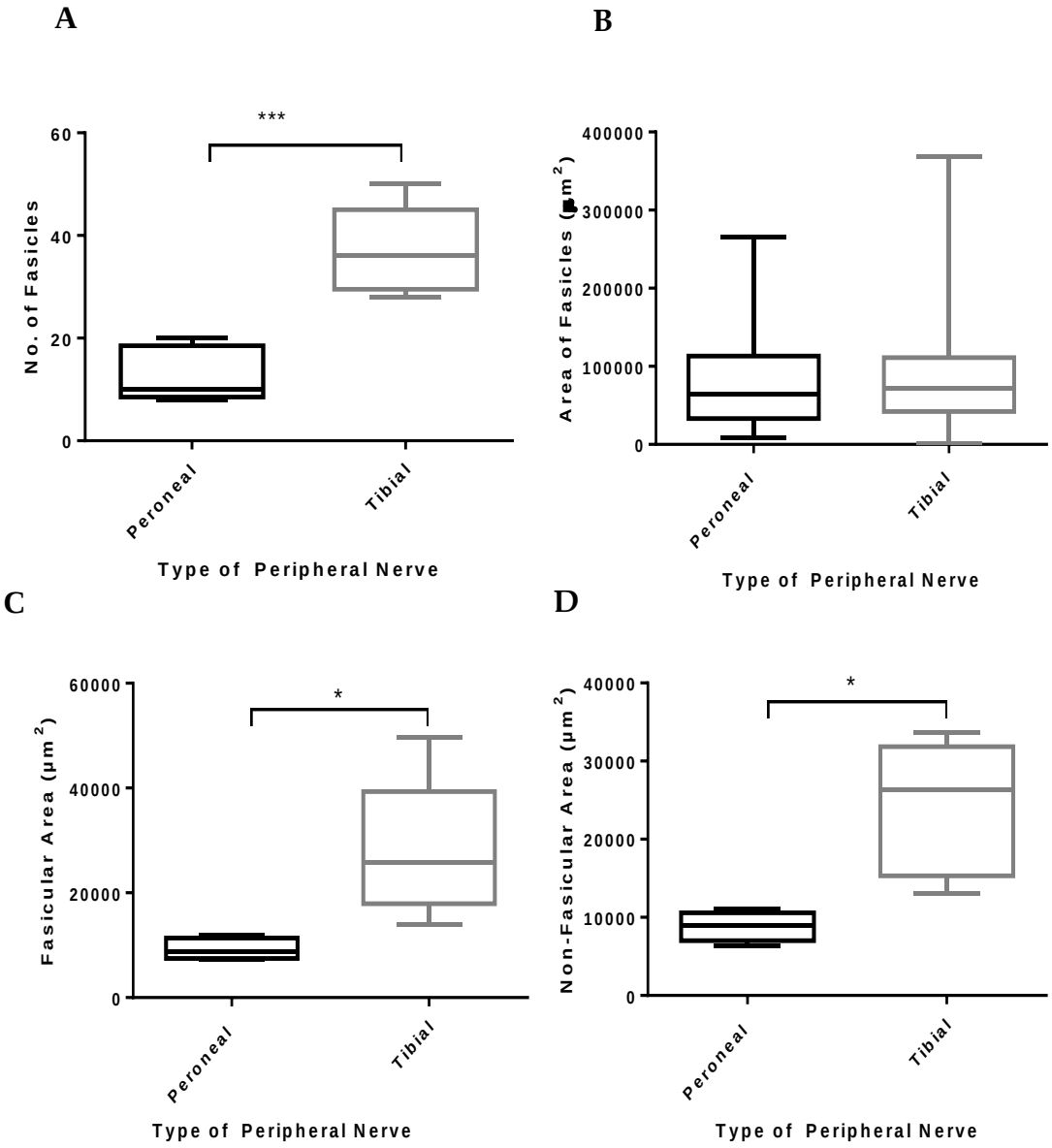


**Figure. 6.2 Analysis of collagen fibrils in porcine common peroneal and tibial nerve connective tissue.** (A) Box and whisker plots summarising the distribution of collagen fibril diameters in common peroneal and tibial nerve. 150 fibrils measured in epineurium, endoneurium and 50 fibrils measured in perineurium. The number of collagen fibrils was counted from three common peroneal and three tibial nerves. The mean collagen fibril diameter found in the tibial epineurium was 108.90 ± 1.7 nm whilst for the common peroneal nerve was 88.59 ± 1.3 nm. The mean collagen fibril diameter found in the tibial nerve endoneurium was 84.20 ± 0.8 nm and for the common peroneal nerve, 63.87 ± 0.3 nm. The mean for the collagen fibrils found in the perineurium for the tibial nerve was 63.98 ± 0.6 nm and for the common peroneal nerve was 65.04 ± 0.4 nm. (B) Box and whisker plots summarising the thickness of perineurium in common peroneal and tibial nerve. The tibial nerve had an average thickness of 7 µm, which was approximately 11 cells thick. The perineurium within the common peroneal nerve had an average thickness of 10 µm and was approximately 9 cells thick. Box and whisker plots summarise the number of collagen fibrils found in epineurium (C) and endoneurium (D). The number of collagen fibrils was counted in three 580 x380 nm areas sampled from endoneurium, epineurium and perineurium micrographs of common peroneal and tibial nerves in three common peroneal and three tibial nerves. An average of 645.0 ± 102.5/µm2 fibres were found in the epineurium of the peroneal nerve and 849.4 ± 64.3/µm2 within the tibial nerve (C). An average of 854.4 ± 67.4/µm2 fibres were found in the endoneurium of the common peroneal nerve and 806.6 ± 32.5/µm2 within the tibial nerve. Data are means ± SEM (n =3) *p< 0.05

| | Peroneal Nerve | Tibial Nerve | p-value |
|---|---|---|---|
| **Fascicle number** | 12.80 ± 2.396 | 37.00 ± 3.847 | < 0.0007 |
| **Fascicle area (μm)$^2$** | 76450 ± 6198 | 84,717 ± 3,839 | 0.278 |
| **Fascicular area(μm)$^2$** | 9,214 ± 1,037 | 28,069 ± 5,959 | < 0.0279 |
| **Non-fascicular area(μm)$^2$** | 8,869 ± 968 | 24,130 ± 3,855 | < 0.0110 |

**Table 6.1. Summary of fascicular pattern and area of porcine peroneal and tibial nerves.** Tibial nerve contained a significantly larger proportion of nerve fascicles, with an average of 37 fascicles in contrast to the peroneal nerve, which had an average 13 fascicles. The average size of fascicles was slightly larger in the tibial nerves with an average size of 84,717 ± 3,839 μm$^2$ whilst the peroneal had an average size 76,450 ± 6,198 μm$^2$, this was not statistically different. The tibial nerve has a significantly larger fascicular and non-fascicular area in comparison to the peroneal nerve. The tibial nerve had an average fascicular area of 28,069 ± 5,959 μm$^2$, whilst the peroneal had an average fascicular area of 9,214 ± 1,037 μm$^2$. The average non-fascicular area of the tibial nerve was 24,130 ± 3,855 μm$^2$ and the peroneal average area was 8,869 ± 9678 μm$^2$. Data are presented as means ± SEM (n =3)

### 6.4.3 Collagen fibril analysis

Analysis of collagen fibrils located within the connective tissues of the endoneurium, perineurium and epineurium was undertaken using TEM. In addition, the size and thickness of the perineurium was measured using image J (Figure 6. 3).

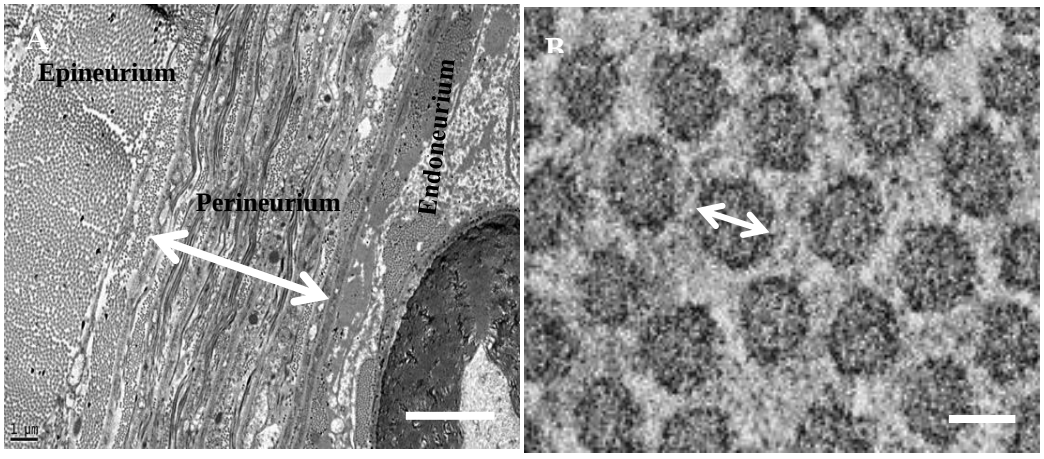


**Figure 6.3. Measurement of perineurium and collagen fibril diameter by TEM.** The perineurium is an area of dense connective tissue situated between the endoneurium and epineurium in the peripheral nerve. The white arrow shows a typical measurement of perineurium thickness (A). Collagen fibrils from transmission electron micrographs were measured using ImageJ software. The white arrow represents a typical fibril diameter measurement (B). Scale bars at (A) 1 μm and (B) 200 nm.

TEM analysis of the porcine nerves revealed the location of collagen fibrils in the endoneurium, epineurium, and to lesser extent the perineurium (Figure 6.4). TEM images and analyses revealed that the tibial nerve contained significantly larger collagen fibrils within the epineurium and endoneurium (Figure 6.5 A). The mean collagen fibril diameter found in the tibial epineurium was 108.90 ± 1.7 nm whilst for the peroneal nerve it was 88.59 ± 1.3 nm. The mean collagen fibril diameter found in the tibial nerve endoneurium was 84.20 ± 0.8 nm and for the peroneal nerve, 63.87 ± 0.3nm. The peroneal nerve contained slightly larger collagen fibrils within the perineurium with an average mean of 65.04 ± 0.4 nm compared to the tibial nerve which was 63.98 ± 0.6 nm; however, this was not statistically significant.

The perineurium of both the peroneal and tibial nerve was measured in terms of size and perineurial cell thickness (Fig. 6.5 B). The tibial nerve had a thicker perineurium with an average thickness of 7 µm, which was approximately 11 cells thick. In contrast, the perineurium within the peroneal nerve had an average thickness of 10 µm and was approximately 9 cells thick. This was not statistically significant (t test). The density of collagen fibrils located within the epineurium and endoneurium of both nerves was analysed by TEM and Image J (Figs. 6.5 C and D). On average, the tibial nerve contained 849.4 ± 64.27 fibrils within the epineurium and 806.6 ± 32.49 within the endoneurium. The peroneal nerve on average contained 645.0 ± 102.5 fibrils within the epineurium and 854.4 ± 67.41, this was not statistically significant. Table 6.2 summarises the TEM analysis of the porcine nerves.

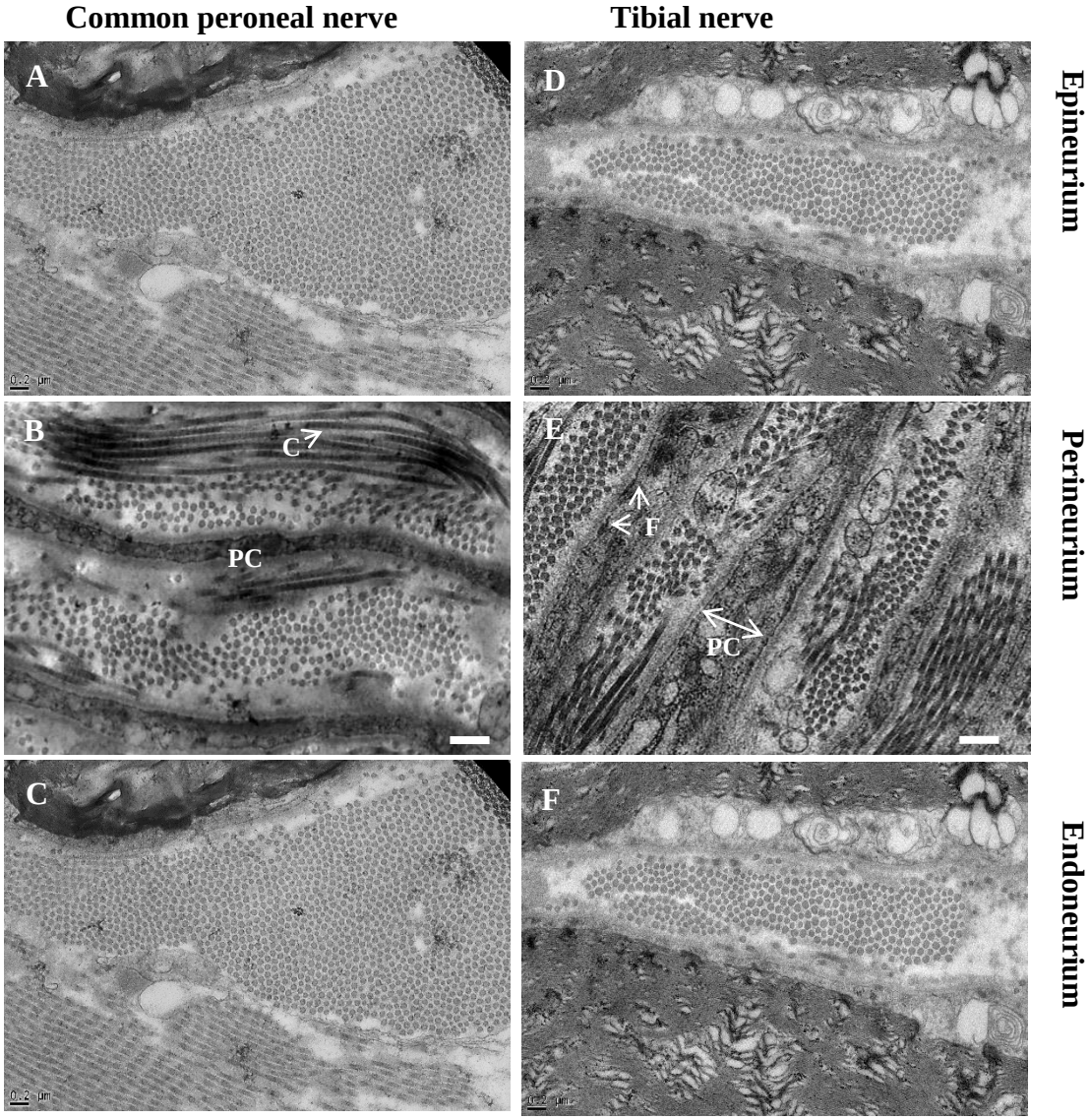


**Figure 6.4. TEM of collagen fibrils in porcine common peroneal and tibial nerve.** Transmission electron micrographs showing collagen fibrils in the epineurium, perineurium and endoneurium in common peroneal (A-C) and tibial nerves (D-F). The perineurium consists of flattened perineurial cells (PC), circumferentially orientated collagen fibrils (C) and fibroblasts (F). Scale bar at 0.2 µm.

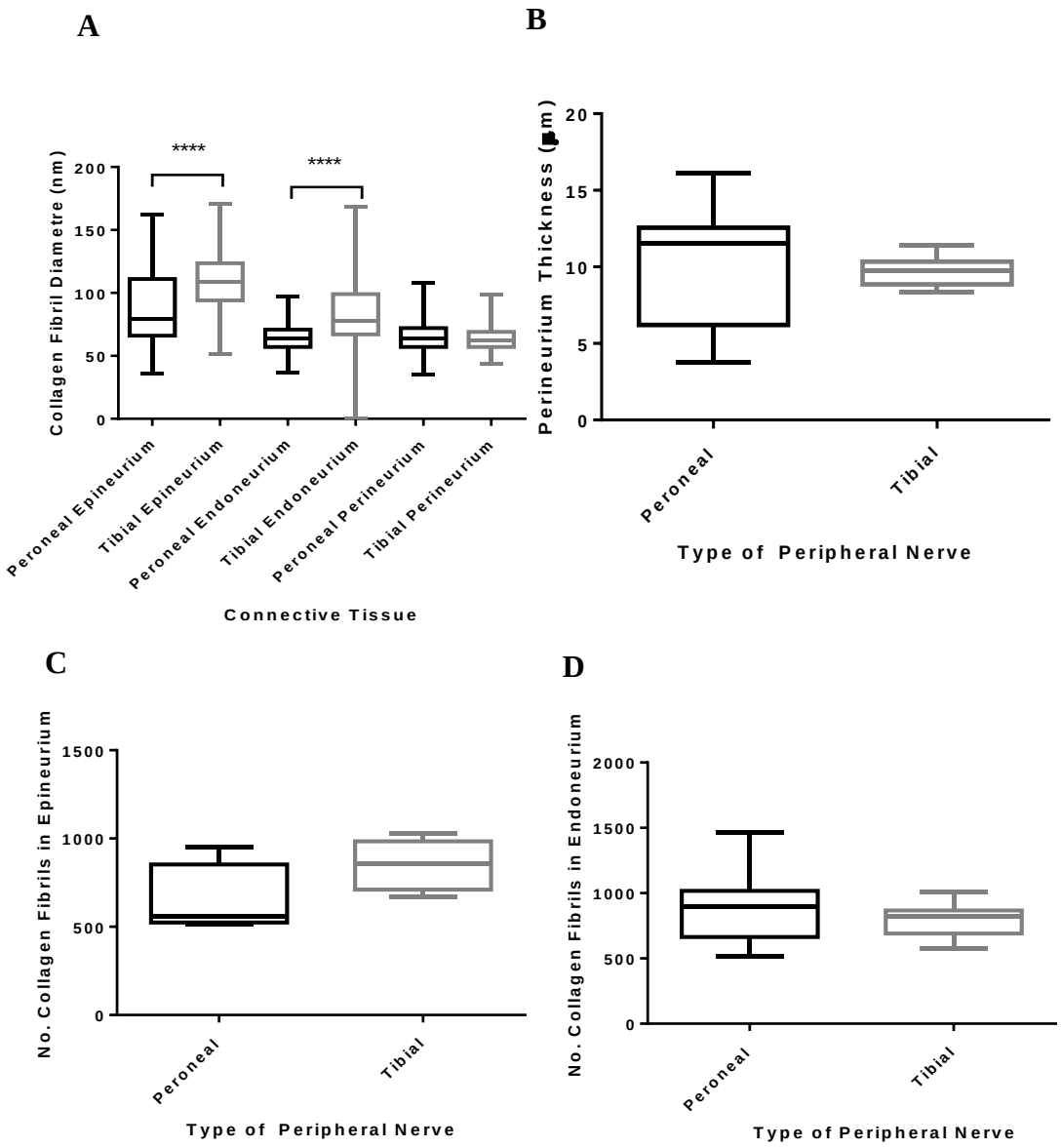


**Fig. 6.5. Analysis of collagen fibrils in porcine common peroneal and tibial nerve connective tissue.** (A) Box and whisker plots summarising the distribution of collagen fibril diameters in common peroneal and tibial nerve. 150 fibrils measured in epineurium, endoneurium and 50 fibrils measured in perineurium. The number of collagen fibrils was counted from three common peroneal and three tibial nerves. The mean collagen fibril diameter found in the tibial epineurium was 108.90 ± 1.7 nm whilst for the common peroneal nerve was 88.59 ± 1.3 nm. The mean collagen fibril diameter found in the tibial nerve endoneurium was 84.20 ± 0.8 nm and for the common peroneal nerve, 63.87 ± 0.3 nm. The mean for the collagen fibrils found in the perineurium for the tibial nerve was 63.98 ± 0.6 nm and for the common peroneal nerve was 65.04 ± 0.4 nm. (B) Box and whisker plots summarising the thickness of perineurium in common peroneal and tibial nerve. The tibial nerve had an average thickness of 7 µm, which was approximately 11 cells thick. The perineurium within the common peroneal nerve had an average thickness of 10 µm and was approximately 9 cells thick. Box and whisker plots summarise the number of collagen fibrils found in epineurium (C) and endoneurium (D). The number of collagen fibrils was counted in three 580 x380 nm areas sampled from endoneurium, epineurium and perineurium micrographs of common peroneal and tibial nerves in three common peroneal and three tibial nerves. An average of 645.0 ± 102.5/µm$^2$ fibres were found in the epineurium of the peroneal nerve and 849.4 ± 64.3/µm$^2$ within the tibial nerve (C). An average of 854.4 ± 67.4/µm$^2$ fibres were found in the endoneurium of the common peroneal nerve and 806.6 ± 32.5/µm$^2$ within the tibial nerve. Data are means ± SEM (n =3) *$p$< 0.05

| | Common Peroneal Nerve | Tibial Nerve | p-value |
|---|---|---|---|
| **Fascicle number** | 12.80 ± 2.396 | 37.00 ± 3.847 | < 0.05 |
| **Fascicle area (μm)$^2$** | 76450 ± 6198 | 84,717 ± 3,839 | 0.278 |
| **Fascicular area (μm)$^2$** | 9,214 ± 1,037 | 28,069 ± 5,959 | < 0.05 |
| **Non-fascicular area (μm)$^2$** | 8,869± 968 | 24,130 ± 3,855 | < 0.05 |

**Table 6.2. Summary of perineurium size and collagen fibril analysis within porcine peroneal and tibial nerves**

## 6.5 Discussion

In this Chapter we investigated the endoneurium, perineurium and epineurium connective tissue of porcine peroneal and tibial nerves in order to evaluate if their structure can account for the difference in their reported mechanical strength. In our previous study we determined porcine peroneal nerves to have significantly larger ultimate tensile stress value of 1.23 ± 0.13 MPa when compared to porcine tibial nerves which had an average value of 0.87 ± 0.29 MPa (Zilic, Garner et al. 2015).

We found that the porcine tibial nerve had a significantly larger number of fascicles, total fascicular and non-fascicular area, in comparison to the peroneal nerve. The average fascicular area was however similar for both the peroneal and tibial nerves. These findings resonate with previous fascicular studies carried out on the peroneal and tibial nerves (Sunderland and Ray 1948); (Ugrenović 2014). The average fascicular pattern regarding number and size in the porcine peroneal and tibial nerve closely match comparable human nerves (Ugrenović 2014). This concurs with the conclusions from our previous study, that porcine peripheral nerves in the lower limb are anatomically similar to human nerves (Zilic, Garner et al. 2015).

Our previous study reported on the peroneal nerve possessing a higher ultimate tensile strength in comparison to the tibial nerve (Zilic, Garner et al. 2015). Herein, a detailed analysis was undertaken to understand which component of the tissue contributed to the differences in tensile strength of the nerves. Collagen is reported as a contributing factor to the viscoelastic properties of nerve under loading (Ushiki & Ide 1990). Our previous study revealed that the majority of the peroneal nerve is composed of collagen type I (as the predominant collagen),

located in the epineurium. In this study we identified collagen type III localised within the endoneurium and perineurium, which agrees to previous findings (Luque, Angulo et al. 1983; Kaemmer, Bozkurt et al. 2010)

Analysis of the collagen fibrils within the three connective layers of both nerve types revealed the collagen fibres, which have the largest diameter, are found in the epineurium, whilst both the endoneurium and perineurium contained similar sized albeit smaller collagen fibrils. Further analysis showed no difference in the density of fibrils within the endoneurium and epineurium of the two nerves. Information regarding the dimensions of collagen fibrils in porcine tissue is limited, however this pattern correlates with other peripheral nerve studies performed on xenogeneic models such as rabbit (Thomas 1963) and rat sciatic nerve (Mason and Phillips 2011) as well as human brachial plexus (Gamble and Eames 1964), noting that the overall sizes varies from species to species. Investigation into the thickness of the perineurium in both nerves revealed the peroneal nerve to possess a thicker perineurium sheath than the tibial nerve. This links to previous studies which state that as the number of fascicles increases within a nerve, the width of the perineurium decreases (Piña-Oviedo and Ortiz-Hidalgo 2008).

Evaluation of the collagen fibrils between the two nerves revealed the peroneal nerve to contain significantly smaller collagen fibrils when compared to the tibial nerve. Studies have correlated smaller collagen fibril diameter with more compliant tissues (Parry, Barnes et al. 1978); (BINKLEY and PEAT 1986; Mason and Phillips 2011). However, in regards to their anatomical position the tibial nerve is found to be more compliant and less susceptible to injury than the peroneal nerve (Rossi 2014). The tibial nerve has a singular and loose fixation site, as opposed to the peroneal nerve which has dual fixation at the sciatic notch proximally, and the fibular neck distally (Murovic 2009). Consequently, traction of the sciatic nerve results in more damage to the peroneal nerve as it is stretched between two points, whereas for the tibial nerve, displacement can be dissipated over a greater length of (Sunderland 1953). This may also be a reason why the ultimate tensile strength was found to be greater in the peroneal nerve, as its anatomical course means it has to withstand more stress under loading.

## 6.6 Conclusion

This study found that porcine tibial nerves are significantly larger than the peroneal nerves in terms of fascicle number, fascicular area and total fascicular area. Previously, we showed these nerves to be primarily composed of collagen, and we identified collagen type III present within the endoneurium and perineurium. TEM analysis of the porcine nerves revealed larger fibril diameters located within the epineurium and smaller diameters within the endoneurium and perineurium. The tibial nerve was found to possess significantly larger collagen fibril diameters when compared to the peroneal nerve. That the peroneal nerve possess smaller fibrils than the tibial nerve, yet has a greater ultimate tensile strength, does not correlate with previous studies (Parry, Barnes et al. 1978; Ottani, Raspanti et al. 2001) . However other investigations suggest that collagen fibril diameter alone cannot predict the structural properties of the tissues (Bay, Howell et al. 1993; Derwin and Soslowsky 1999). Researchers have shown that other factors besides collagen fibril diameter distribution are important for mechanical integrity and strength of the nerve such as endoneurial fluid pressure and nerve vasculature (Low, Marchand et al. 1977; Myers, Murakami et al. 1986). Our leading explanation as to the difference based on current data suggests that the mechanical properties of nerves cannot be determined exclusively by their fascicle size or collagen fibril diameter, but supports further investigation in to the relationship between structure and biomechanical properties of nerve.

# Chapter 7. Repopulation of Acellular Nerve Scaffold with Cells

## 7.1 Introduction

Inclusion of neuronal support cells such as Schwann cells into nerves grafts have been shown to be vital for effective nerve regeneration. Although the exact underlying mechanism through which Schwann cells and damaged axons communicate is relatively unknown, studies have highlighted the close relationship between Schwann cells and axons as a "regenerating unit" (Morris, Hudson et al. 1972; Brushart 2011).

Following nerve injury Schwann cells undergo a phenotypic change from myelinating to growth supportive in order to direct and support regenerating axons towards the distal nerve stump. This phenotype switch is associated with the up-regulation of several growth associated genes including neurotrophic factors, cell adhesion molecules and receptors (Rodrigues, Rodrigues et al. 2012). These molecules help support axonal migration and recruit further cells such as macrophages, mast cells and activated endothelial cells into the injury site (Hall 2005; Walsh and Midha 2009). Activated Schwann cells also provide a supportive environment by producing collagen and laminin which results in Schwann cell proliferation and the formation of longitudinally orientated strands (known as bands of Büngner) that guide the regrowing axons (Bunge 1994).

If axonal contact is not re-established or the gap length increases, Schwann cell migration, proliferation and alignment decreases and the growth supportive environment cannot be maintained. This is due to the denervated Schwann cells losing their ability to interact with regenerating axons and express regeneration-assisting genes. As the capacity of the denervated distal nerve to support axonal regeneration is dependent on proliferating Schwann cells, this translates to poor reinnervation outcomes (Walsh and Midha 2009). In an attempt to aid the regenerative cellular response to injury and to help stimulate nerve regeneration across long peripheral nerve defects, cellular based therapies are considered essential for nerve repair.

Schwann cells have been used in synthetic and biological nerve guide conduits (NGC's) to improve functional recovery, regeneration and remyelination of injured peripheral nerves. There have been a number of studies which have used

Schwann cells as part of a nerve graft. Such cell based studies have demonstrated an increase in nerve regeneration and enhanced axonal regeneration rate (Guenard, Kleitman et al. 1992; Mosahebi, Woodward et al. 2001; Evans, Brandt et al. 2002; Udina, Rodriguez et al. 2004; Nilsson, Dahlin et al. 2005; Stang, Fansa et al. 2005).

*In vivo* studies using acellular nerve tissue repopulated with cells have been undertaken with great success (Hess, Brenner et al. 2007; Tulla, Huhtala et al. 2007; Zhang, Luo et al. 2010). However, understanding the molecular, biochemical, and biological changes that occur *in vivo* during reinnervation such as the influence of Schwann cells and the impact of local pro-inflammatory cytokines is difficult, due to the inherent complexity of the regeneration process (Gingras, Bergeron et al. 2003).

*In vitro* models have value in a number of areas, serving as an investigational platform for studies including developmental biology, disease studies and the design of devices and scaffolds for peripheral nerve repair (Daud, Pawar et al. 2012). With a three dimensional nerve model there is degree of experimental control which is not possible *in vivo.* Factors such as cell source, cell orientation and delivery of exogenous compounds can be delivered in a controlled manner to a three dimensional system which has a similar microenvironment to that found *in vivo* (Cullen, Wolf et al. 2011).

Current nerve studies involve the use of collagen gels and sponges which have shown to support axon ingrowth and Schwann cell proliferation (Allodi, Guzmán-Lenis et al. 2011) as well as myelination (Gingras, Beaulieu et al. 2008). A study by Daud et al. (2012) developed a three dimensional *in vitro* peripheral nerve model using aligned electrospun polycaprolactone fibre scaffolds showed aligned neurite formation with dorsal root ganglion explants and co-localisation of Schwann cells with the neurites (Daud, Pawar et al. 2012). However, there is very little research currently in three dimensional *in vitro* peripheral nerve model using acellular scaffolds. This is in contrast to other tissues such as skin, where extensive work has been conducted (MacNeil 2007).

In order to create a three dimensional acellular model there are various factors that need to be considered. Acellular nerves are comprised of dense collagenous tissue, which makes it more difficult to populate with cells. Current methods of introducing cells into acellular scaffolds include opening up the collagenous matrix by ultrasonification (Ingram, Korossis et al. 2007) or by

injecting cells directly using a syringe into the ends of a graft (Brenner et al 2005; Fox et al 2005; Hess et al 2007).

The migration and survival of the cells within the scaffold is dependent on the maintenance of nutrient diffusion throughout the scaffold (Sun, Norton et al. 2005). For Schwann cell culture it is likely that continuous perfusion with medium will better support metabolic activity rather than changing the medium every few days (Sun, Norton et al. 2008). In situ peripheral nerve cells receive constant nutrients from blood vessels which are located within the epineurium with smaller branches of these blood vessels penetrating into the perineurium. In addition, with long-term culture of seeded scaffolds that requires repetitive handling (e.g. changing medium every few days) can increase the risk of contamination.

Therefore, to introduce continuous perfusion to scaffolds in sterile environment bioreactors can be implemented for the reproducible production of tissue-engineered nerve for both experimental and clinical use. Bioreactors have been used extensively in nerve tissue engineering applications for growing functional cells and tissues for transplantation, as well for controlled *in vitro* studies (Kallos and Behie 1999; Hadlock, Sundback et al. 2000; Lin, O'Shaughnessy et al. 2004; Sun, Norton et al. 2008; Cullen, Wolf et al. 2011; Murray-Dunning, McArthur et al. 2011). These systems can help establish spatially uniform cell distributions on 3D scaffolds as well as maintaining desired concentrations of gases and nutrients in the culture medium, which are important step towards the development of functional grafts (Korossis, Bolland et al. 2005; Chen and Hu 2006).

There have been many different types of bioreactors that have been used for growing neuronal cells and for tissue engineered nerve applications such as suspension bioreactors (Kallos and Behie 1999), NASA designed rotating wall vessel bioreactors (Lin, O'Shaughnessy et al. 2004) and a micro-perfusion bioreactor (Cullen, Wolf et al. 2011). Previous studies have successfully developed simple closed loop perfusion system (Hadlock, Sundback et al. 2000; Sun, Norton et al. 2008; Murray-Dunning, McArthur et al. 2011).

A study on perfusion by Sun et al. (2008) established a simple closed loop bioreactor system to introduce and culture Schwann cells on longitudinally aligned microfibers of viscose rayon and polystyrene model materials. It was discovered that a continuous medium flow of 0.8 $mL.H^{-1}$ increased total cell number by 2.5-

fold verses static culture. In addition, results from the perfused conditions showed a nine-fold increase in cell viability as well as cellular adhesion and alignment on the longitudinal axis (Sun, Norton et al. 2008). This study showed that perfusion was a factor in cell viability and proliferation. In addition, the study also showed that the use of a bioreactor can permit a quick and systematic evaluation for the introduction, growth and evaluation of support cells *in vitro*.

Therefore, in this study focus was on the development of a three dimensional *in vitro* nerve model using acellular nerve tissue. The acellular model was used as a basis for the study of perfused flow within the tissue for the introduction of Schwann cells using a simple closed loop perfusion system.

## 7.2 Aims and objectives

**Aims:**

The aim of this chapter was to determine the conditions for the introduction of primary rat Schwann cells into acellular porcine peripheral nerves that would be appropriate both for experimental and clinical use. The reseeded nerves were then compared under static and perfused conditions.

**Objectives:**

- Taking a systematic approach determine methodology for introducing cells into the acellular scaffold. RN22 Schwann cells were used initially at the developmental stage, and then replaced with primary rat Schwann cells once the seeding technique was established;
- To develop a bioreactor for the reseeded tissue which will provide continuous flow of medium to the recellularised nerve tissue;
- Localise cells within the tissue using histological methods – hematoxylin and eosin, nuclei (DAPI) and CellTracker™;
- Identification of primary Schwann cells within re-seeded acellular nerve tissue by Immunolabelling for S100β, Glial Fibrillary Acidic Protein (GFAP) and p75 nerve growth factor receptor (NGFR) markers;
- To determine viability and function of Schwann cells seeded onto the acellular nerve scaffold.

## 7.3 Methods

### 7.3.1 Cell culture medium for RN22

The standard cell culture medium used for RN22 Schwann cells was Dulbecco's modified Eagle's medium (DMEM) containing 10 % (v/v) FCS, 100 U. $mL^{-1}$ penicillin / 100 µg. $mL^{-1}$ streptomycin, 0.25 µg. $mL^{-1}$ amphotericin and 2 mM L-glutamine. The culture medium was stored at 4 °C for up a month.

### 7.3.2 Cell culture medium for primary rat Schwann cells

The standard cell culture medium used for primary rat Schwann cells was MEM–D-valine containing 10 % (v/v) FCS, 100 U. $mL^{-1}$ penicillin, 100 µg. $mL^{-1}$ streptomycin, 0.25 µg. $mL^{-1}$ amphotericin, 5 µM forskolin and 2 mM L-glutamine. The culture medium was stored at 4°C for up a month.

### 7.3.3 Labelling Schwann cells with CellTracker™ Red CMPTX dye

CellTracker™ fluorescent probes can be used to visualise cells by fluorescence microscopy. These probes pass freely through cell membranes. Once inside the cells these mildly thiol-reactive probes undergo a glutathione S-transferase-mediated reaction to produce membrane-impermeable glutathione-fluorescent dye compounds that are retained inside the cells for at least 24 hours after loading and can be passed onto daughter cells. The probes contain amino groups, so can be cross-linked using formaldehyde for sample storage and analysis.

The red CellTracker™ solution was prepared by dissolving 50 µg of CellTracker™ in 7 µL DMSO. This was then added to 7 mL of the required cell medium. The medium from either RN22 or primary rat Schwann cells was removed from the flask and washed once with 5 mL PBS. The CellTracker™ solution was then added to the flask and incubated for 45 minutes in 37 °C in 5 % $CO_2$ (v/v). The flask was subsequently washed three times using 10 mL of PBS to remove excess cell tracker. Normal cell seeding as described in Section 2.2.5 was then undertaken.

### 7.3.4 Histology

Histology was used to determine the localisation of cells within the repopulated acellular nerves. Repopulated acellular nerves (n=3) were fixed with 3.7 % (v/v) formaldehyde for 24 hours. Histological evaluation was performed as described in Section 2.2. Native and acellular nerves were processed for tissue architecture and cell distribution analysis. Paraffin embedded tissue sections of 10 μm were prepared transversely and longitudinally. The slides were stained with haematoxylin and eosin and labelled with DAPI and CellTracker ™ to enable the identification of tissue structure as well as the cell nuclei and cell distribution. Hematoxylin and eosin stained sections were viewed by light microscopy. Cell nuclei and cell distribution samples were viewed under a Zeiss LSM510 META upright confocal microscope. DAPI nuclei were visualised at $\lambda_{ex}$ = 300 nm / $\lambda_{em}$ = 510 nm and CellTracker ™ Red at $\lambda_{ex}$ = 577 nm / $\lambda_{em}$ = 602 nm.

### 7.3.5 Immunolabelling seeded Schwann cells within acellular nerve tissue

Schwann cells in two dimensional culture and within the three dimensional acellular construct were fluorescently immunolabelled for the Schwann cell protein markers S100β, GFAP and p75 NGFR. Acellular nerve samples and primary Schwann cells tissue grown in two dimensional cultures were fixed using 3.7 % (v/v) formalin and embedded into paraffin wax; each sample was sectioned at 6 - 10 μm. Sections were permeabilised with 0.1 % (v/v) Triton X-100 diluted in PBS for 20 minutes. Samples were then incubated with 7.5 % (w/v) bovine serum albumin diluted in PBS at room temperature for an hour, followed by washing once with 1 % (w/v) BSA in PBS. Tissue samples were incubated with primary antibody (diluted to appropriate concentration with 1 % BSA) at 4 °C overnight in a humidified chamber. The following day the samples were washed three times with PBS, five minutes each time and then incubated with secondary FITC conjugated anti-rabbit antibody at room temperature in the dark for one hour. Each section was then washed three times with PBS for five minutes and counterstained with 300 nM DAPI in PBS and incubated for twenty minutes in the dark at room temperature. Sections were then washed three times with PBS for five minutes and imaged using a Zeiss LSM510 META upright confocal microscope (xenon arc lamp to excite FITC ($\lambda_{ex}$ = 495 nm / $\lambda_{em}$ = 515 nm). Nuclei were visualised at $\lambda_{ex}$ =

300 nm / $\lambda_{em}$ = 510 nm. Secondary antibody alone served as a negative control to rule out non-specific antibody binding

| Antigen | Isotype | Clone | Working dilution |
|---|---|---|---|
| Anti-S100 astrocyte marker ab868 | IgG | Rabbit Polyclonal | 1°Ab 1:250<br>2°Ab 1:200 |
| Anti-GFAP delta primary antibody ab28926 | IgG | Rabbit Polyclonal | 1°Ab 1:250<br>2°Ab 1:200 |
| Anti-p75 NGF receptor antibody | IgG | Rabbit Polyclonal | 1°Ab 1:50<br>2°Ab1:100 |

**Table 7.1. Table of antibodies and working dilutions used throughout the study**

### 7.3.6 Determination of Schwann cell viability

#### MTT Assay

The MTT assay is a colorimetric method for assessing cell viability. MTT (3-(4,5dimethylthiazol-2-yl)-2,5- diphenyltetrazolium bromide) is a yellow water soluble tetrazolium salt. The MTT acts as an artificial hydrogen acceptor substrate for mitochondrially-located dehydrogenase enzymes (NAD (P) H-dependent cellular oxidoreductase) in living cells. Reduction of MTT is converted to insoluble purple formazan crystals by cleavage of the tetrazolium ring by the dehydrogenous enzymes. The insoluble purple formazan can be solubilised using acidified isopropanol.

RN22 Schwann cells were seeded and grown in 24 well plates. Culture medium was removed and 1 mL of MTT solution was added to each well. The MTT solution was made by dissolving 0.5 mg MTT in 1 mL PBS and filter sterilized before use. The plate was left to incubate for 1 hour at 37 °C / 5 % $CO_2$ (v/v). The MTT solution was removed from the well and 400 µL acidified isopropanol added to elute the stain. The acidified isopropanol was made by adding 25 µL of 6 M HCL to 20 mL isopropanol. Once all the stain had been eluted (after approximately 15 minutes), 150 µL of solution was transferred to a clear 96 well plate (triplicates of each sample) and optical density determined at a wavelength of 540 nm with a reference filter at 630 nm.

**Alamar Blue Assay**

Alamar Blue is a cell viability assay reagent which contains the cell permeable dye resazurin. Resazurin (7-hydroxy-10-oxidophenoxazin-10-ium-3-one) is a water soluble non-fluorescent blue dye which is reduced to the pink-coloured and highly fluorescent resorufin. The resazurin dye is highly dichromatic and acts as an intermediate electron acceptor. Resazurin undergoes the colorimetric change in response to cellular metabolic reduction usually in the presence of mitochondrial reductases NADPH dehydrogenase or NADH dehydrogensase. As the resazurin dye accepts electrons, it changes from the oxidized, non-fluorescent, blue state to the reduced, fluorescent, pink state. The intensity of fluorescence produced is proportional to the number of living cells (Rampersad 2012).

Schwann cells were seeded and grown in 24 well plates. Medium was removed from the well and 1 mL of Alamar blue working solution was added. The Alamar blue working solution was prepared by diluting the Alamar blue stock solution (12.6 mg resazurin salt powder diluted in 50 mL distilled water and filter sterilize) 1 in 10 with culture medium to obtain a 0.1 mM working solution. The samples were incubated for four hours in 37 °C/5 % $CO_2$ (v/v). 200 µL of the reduced pink resorufin solution was then pipetted into a clear 96 well plate (triplicates of each sample) and read at a wavelength of 540 nm with a reference filter of 630 nm.

### 7.3.7 Bioreactor setup

The perfused bioreactor system comprised of a 1-litre Duran bottle with three connections drilled into the bottle cap. Two of the connections were used for the inlet and outlet tubes. These tubes were PharMed® BPT tubes with an internal diameter of 3.1 mm. One end of the PharMed® BPT tube was inserted into the inlet connection and the tube was pulled downwards until it skimmed the bottom surface of the Duran bottle. The other end of the tube was then lengthened with more PharMed® BPT tubing (approximately one metre in length) which were connected via male luer connectors and passed through the Masterflex peristaltic pump and into the outlet connection to allow media to flow in and out in a closed looped system. In the outlet connection the tube was pulled half way down towards the bottom surface of the Duran bottle. Enough space was left to allow the nerve scaffold to be attached onto the outlet tube. The third connection was for the air

filter to allow gaseous exchange. The air filter was comprised of a Nalgene ™ syringe filter (25 mm diameter) attached onto the PharMed® BPT tube. A picture and design of the bioreactor setup is shown in Figure 7.1.

To sterilise the bioreactor system the Duran bottle along with the connected tubes were autoclaved. Once sterilised the syringe filter and media was added to the bioreactor system in a sterile hood.

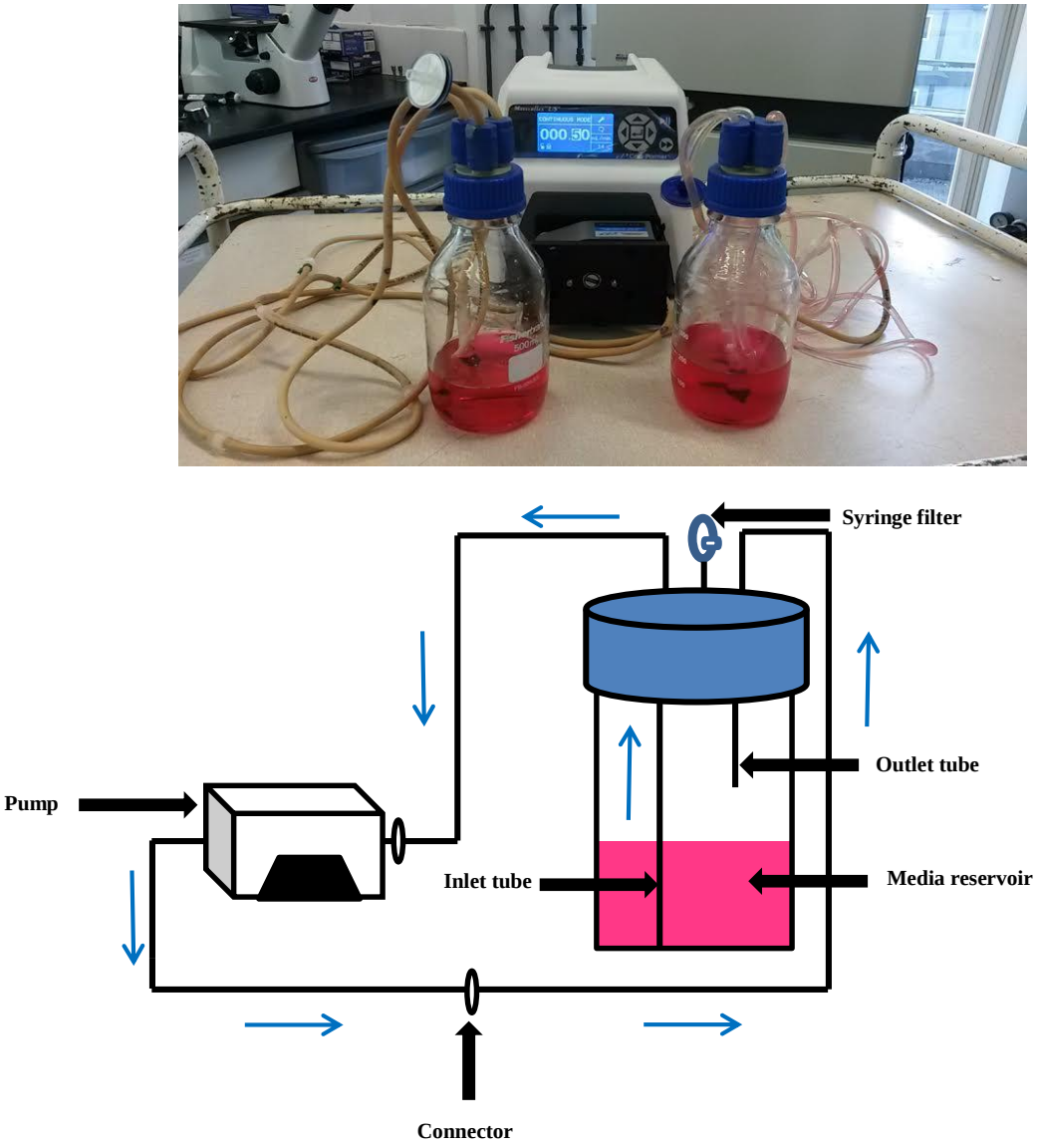


Figure 7.1. Bioreactor setup. Bioreactor is comprised of a Duran bottle with inlet, outlet and air filter connections. The inlet and outlet tubes are connected to a peristaltic pump in a series circuit. The pump allows the media to flow into the inlet tube and come back out the outlet tube in a closed loop system. The flow of media is shown by the direction of the blue arrows.

## 7.4 Introduction Schwann cells into acellular porcine nerve scaffolds

Several experimental techniques were undertaken to reseed acellular nerve scaffolds with Schwann cells. Following each seeding iteration, the reseeded scaffolds (n =3) were placed under static and perfused conditions. Under static conditions the reseeded scaffolds were placed in a 90 mm petri dish immersed in medium (5-10 mL). Under perfused conditions the reseeded scaffold was placed in the bioreactor system as described in Figure 7.1.

RN22 Schwann cells were used in the initial experimental procedures to reintroduce cells back into the porcine acellular scaffolds. RN22 cells are an immature rat Schwannoma cell line, which are relatively easy to maintain, divide relatively quickly and can be used up to passages of typically 100.

### 7.4.1 Method 1- introduction of RN22 Schwann cells into cannulated nerve scaffolds

To introduce RN22 Schwann cells into the acellular nerve scaffolds, a 2 cm acellular scaffold was cannulated by inserting a cannula (24-gauge x 75mm x50) through the nerve and suturing (4-0 sutures) into place (Figure 7.2). The cannulated nerve sample was then sterilised in 0.1 % (v/v) peracetic acid for three hours under agitation. Under sterile conditions the nerve sample was immersed with 10 % (v/v) DMEM overnight. $1x10^6$ cells were resuspended in 100 µL medium and injected into the scaffold with a 1 mL syringe.

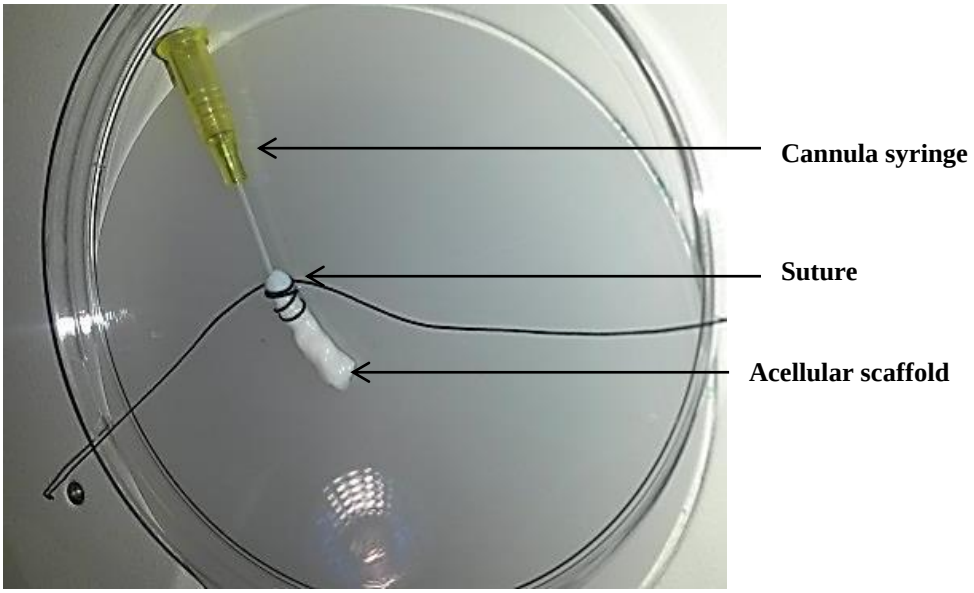


**Figure 7.2 Cannulation of acellular nerve for reintroduction of cells**. Acellular scaffold sutured to a cannula syringe with a 24-gauge needle.

The recellularised scaffolds were left either under static condition or under perfused flow. For the perfused conditions Figure 7.3 shows a schematic diagram of how the cannulated scaffold was attached to the outlet tube within the bioreactor.

For static conditions the reseeded cannulated scaffolds were left in a Petri dish immersed in medium and incubated at 37 °C in 5 % $CO_2$ (v/v) for three days. Reseeded scaffolds that needed to be perfused were left overnight for cells to adhere and placed in the bioreactor the following day as shown in Figure 7.1. The bioreactor was placed inside an incubator 37 °C in 5 % $CO_2$ (v/v). Medium was perfused through the tissue at a rate of 30 $mL.min^{-1}$ for 48 hours.

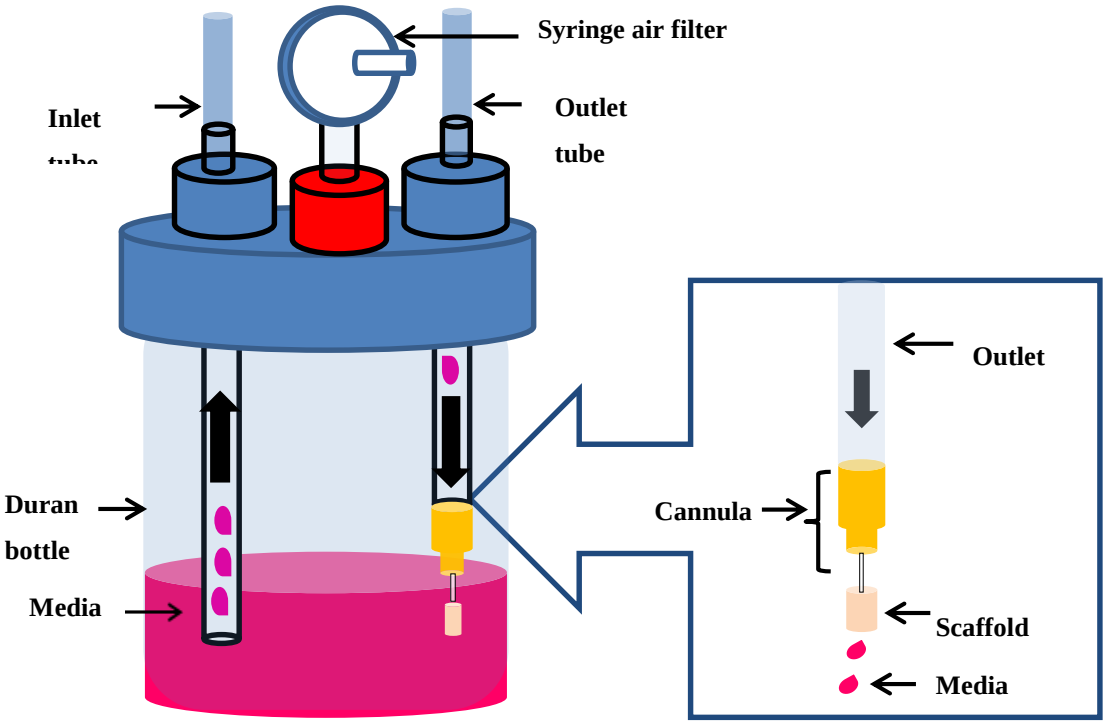


Figure 7.3. Schematic diagram of cannulated nerve scaffold attached inside the bioreactor. Bioreactor consists of a Duran bottle with an outlet and inlet tube for media to flow through and air syringe filter for gaseous exchange. Nerve scaffold is attached to outlet tube via cannula syringe and media flows towards the scaffold.

### 7.4.2 Results for Method 1

Histological analysis of the recellularised scaffold under static conditions showed no presence of cells apart from the region where cells were initially introduced. Clumps of RN22 Schwann cells can be observed within the epineurium, around the edge of the tissue with no signs of migration (Figure 7.4)

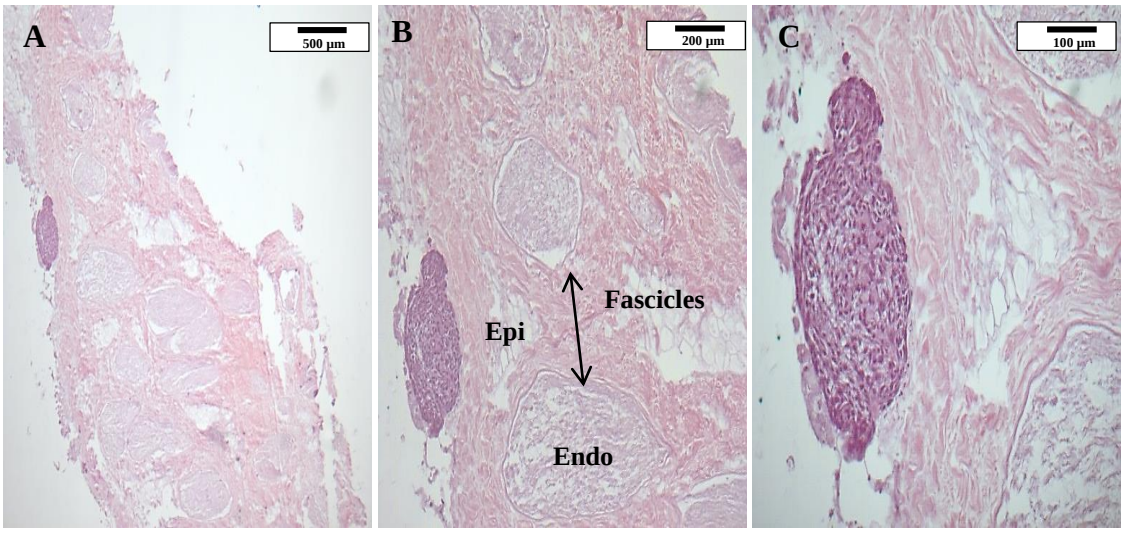


Figure 7.4 Reseeded acellular scaffold under static conditions at day three. Hematoxylin and eosin of RN22 Schwann cells within acellular porcine nerve tissue. Transverse section of proximal nerve shows cells located within the epineurium, clumped together at the edge of the scaffold. Scale bar at 500 µm, 200 µm and 100 µm respectively. Tissue structure seen in pink and cells in purple. Endo = endoneurium; Epi = epineurium.

Results for the perfused conditions showed that similarly to the static conditions a majority of the cells were located predominantly around the edges of the tissue, at the site of the injection. In addition, the results showed cells distributed around the perineurium and within the endoneurium of the nerve fascicles as indicated by the arrows (Figure 7.5). This indicates that perfusion may have a positive effect on cell distribution.

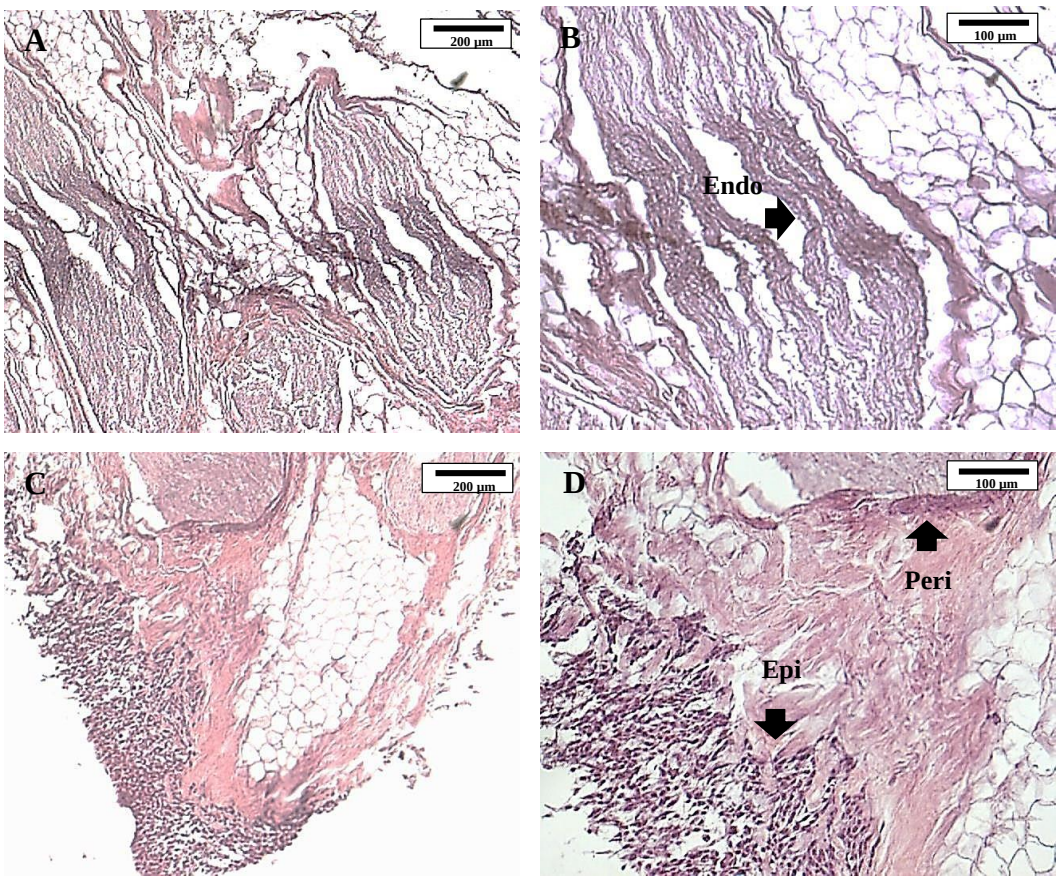


Figure 7.5 Reseeded acellular scaffolds under perfused conditions at day three. Hematoxylin and eosin staining show presence of RN22 Schwann cells within transverse tissue sections. Black arrows show cells within endoneurium (B), epineurium and surrounding the perineurium (D) Endo = endoneurium; Epi = epineurium; Peri = perineurium. Scale bar at 200 µm and 100 µm. Tissue structure seen in pink and cells in purple.

Hematoxylin and eosin staining of cells seeded scaffolds (Figure 7.4 and 7.5) demonstrated could be introduced into acellular scaffolds via cannulation. However, this method was unable to distribute cells through the entire tissue.

### 7.4.2.1 Method 2 -introduction of RN22 Schwann cells into nerve scaffolds via syringe pump

A syringe pump seeding system was developed to introduce cells into scaffolds (Figure 7.6). Prior to reseeding, the RN22 Schwann cell population was labelled with CellTracker (as described in Section 7.3.3). RN22 Schwann cells (1 x$10^6$) were suspended in 1 mL of standard medium and drawn up into a 1 mL syringe. Under sterile conditions the syringe was then placed on a syringe pump and 1 cm length of scaffold was placed inside a sterile 1.5 cm PharMed® BPT tube (I.D 3.1 mm) which was then attached to the end of the syringe. The cells were injected

through the syringe into the proximal end of the scaffold. Once half the cell suspension was injected the distal portion of the scaffold was placed towards the syringe. This was to ensure that cells were introduced to the entire scaffold. The pump was set to a rate of 40 µL.min$^{-1}$.

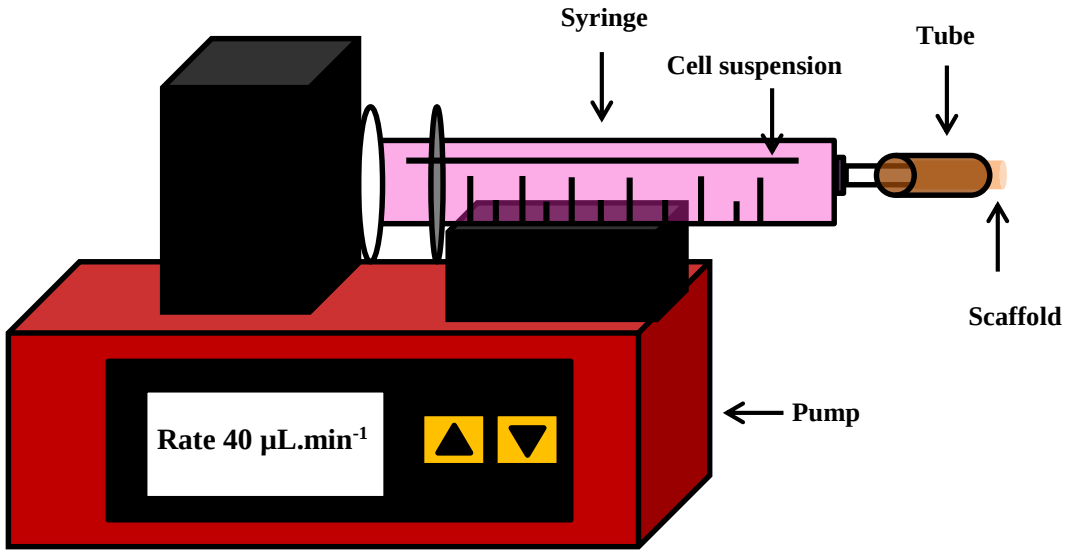


**Figure 7.6. Reseeding cells into nerve scaffold using a syringe pump**. RN22 Schwann cell suspension was injected into the scaffold encased within a tube using a syringe and motor pump set at a rate of 40µL.min$^{-1}$.

The recellularised scaffolds were incubated either under static condition or under perfused flow as shown in Figure 7.1. For the static samples the reseeded scaffolds were left in petri dishes immersed in media for three days at 37 °C in 5 % $CO_2$ (v/v). For the perfused samples cells the reseeded scaffolds were left overnight to adhere. The following day the samples were attached to the bioreactor (Figure 7.7).

Figure 7.7 shows a schematic diagram of how the reseeded scaffold was attached to the outlet tube within the bioreactor. The reseeded scaffold was placed in a 3 mm silicone tube with two luer connectors with a male adapter placed on the top and bottom. The top connectors attached the scaffold and the tube to the outlet tube, allowing medium to flow through, whilst the bottom connector allowed the medium to pass through. A polymer mesh filter was placed at the bottom of the tube to prevent the scaffold from being pushed into the bottom connector. The bioreactor was placed inside an incubator 37 °C in 5 % $CO_2$ (v/v). Media was perfused through the tissue at a rate of 0.5 mL.min$^{-1}$ for 48 hours.

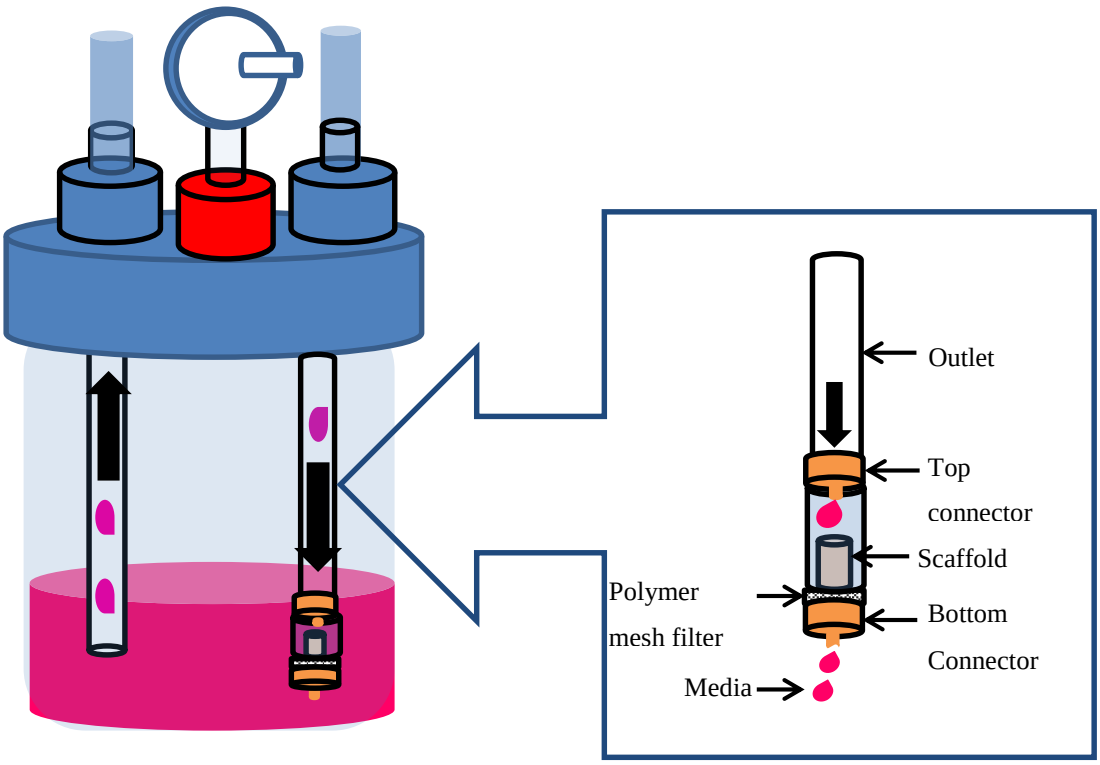


**Figure 7.7 Schematic diagram describing how nerve scaffold was attached inside the bioreactor**. The bioreactor consisted of a Duran bottle with an outlet and inlet tube for medium to flow through and an air syringe filter for gaseous exchange. The reseeded scaffold was placed in a 3 cm silicon tube with a top connector attaching to the outlet tube to allow medium in to and through the scaffold and a bottom connector to allow medium to pass through. The polymer mesh filter kept the scaffold within the tube.

### 7.4.2.2 Results for Method 2

Figures 7.8 and 7.9 illustrate that Schwann cells can be detected by epifluorescence microscopy in acellular porcine nerve when using the motor pump device. Under static conditions the cells were observed to perfuse through the proximal and middle regions of the scaffold (Figure 7.8). However, no cells were located in the distal region.

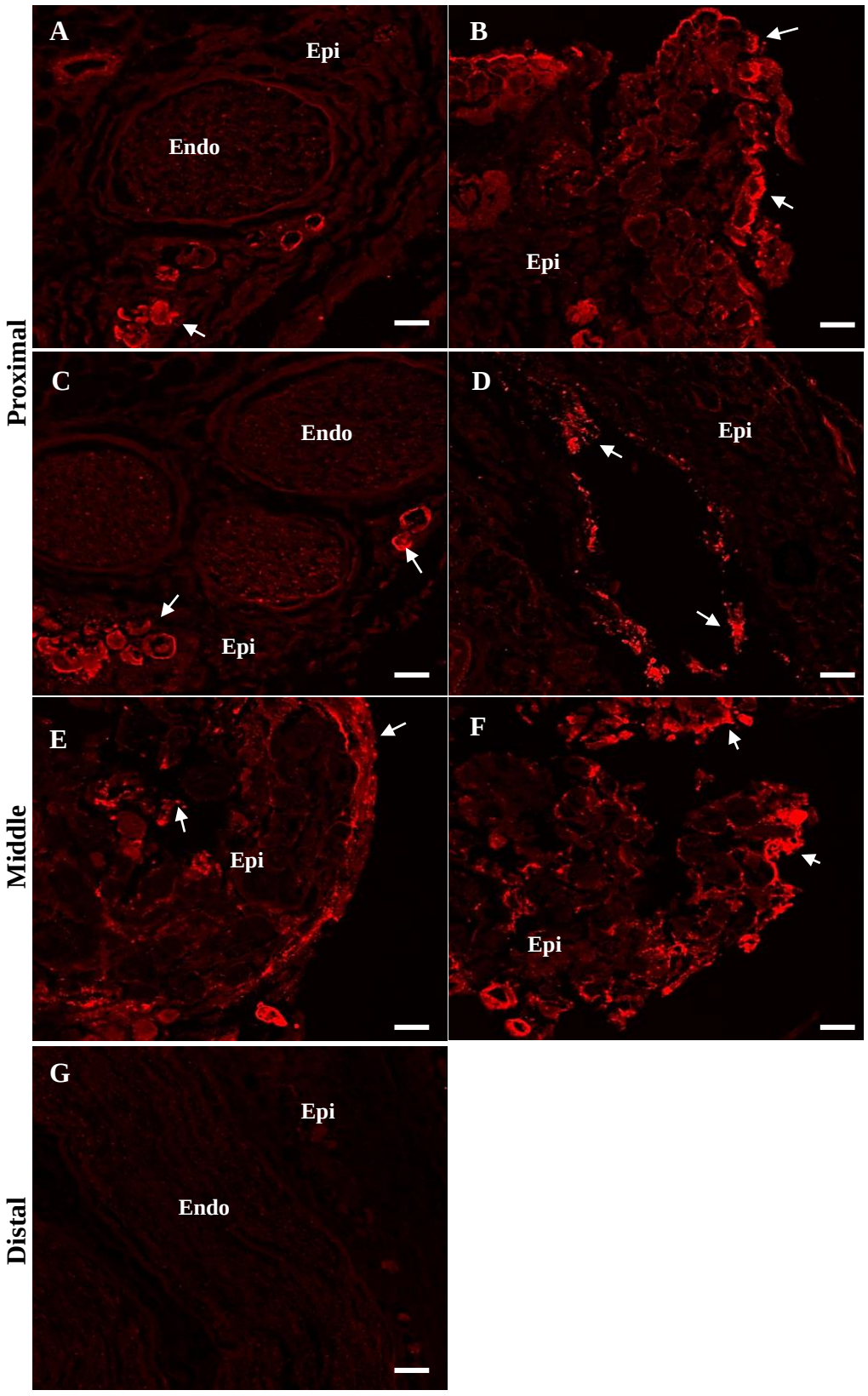


**Figure 7.8 Reseeded CellTracker red labelled RN22 Schwann cells grown under static conditions at day three**. RN22 Schwann cells were detected primarily surrounding the edges of the epineurium and some cells residing within epineurium in the proximal (A-D) and middle sections (E-F) of the nerve as indicated by the arrows. No cells were detected in the distal region (G). Endo = endoneurium; Epi = epineurium. Scale bar at 100 µm.

Under perfusion Schwann cells were located throughout the entire scaffold, and were observed within all three connective tissue layers (Figure 7.9). The proximal section of the scaffold under perfusion shows that the cells were located within the endoneurium of the nerve fascicles as well as surrounding the perineurium (Figure 7.9 A-C) unlike the static conditions where the cells were predominantly located within the epineurium (Figure 7.8 A-D). Furthermore, under perfused conditions there is a larger portion of cells observed in the distal region (Figure 7.9 F-H) when compared to the static results (G) which suggests that perfusion helps cells migrate throughout the entire scaffold.

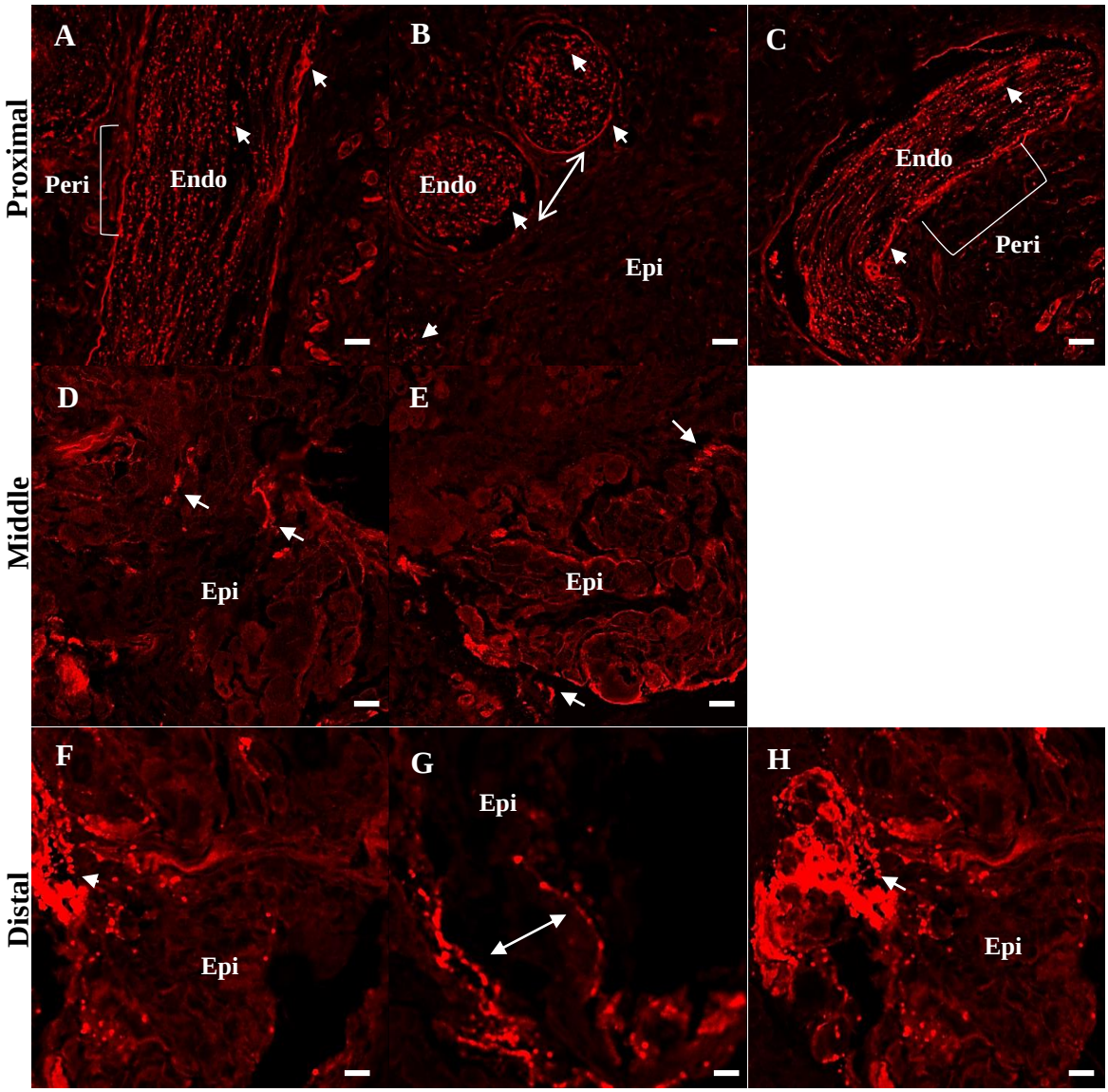


**Figure 7.9 Reseeded CellTracker red labelled RN22 Schwann cells under perfused conditions at day three**. RN22 Schwann cells are seen within the endoneurium, surrounding the perineurium and within the epineurium in the proximal region (A-C); in the epineurium in the middle (D-E) and distal (F-H) regions of the nerve as indicated by the arrows. Endo = endoneurium; Epi = epineurium; Peri = perineurium. Scale bar at 100 µm.

### 7.4.3 Method 3-introduction of primary Schwann cells into nerve scaffolds via syringe pump

The seeding method devised using a syringe pump and RN22 Schwann cells was observed by histology and epifluorescence microscopy to introduce cells throughout the whole acellular porcine scaffold. Thus, RN22 cells were replaced with primary rat Schwann cells to investigate if primary cells could be re-introduced into an acellular scaffold. The scaffold was left under static and perfused condition to investigate whether perfused conditions had a similar effect on primary Schwann cells in terms of migrating throughout the entire scaffold as observed with the RN22 cells in Method 2.

Acellular scaffolds were seeded with primary Schwann cells ($1x10^6$ cells/50 µL) via the motor syringe pump (1 mL). Cells were injected via both ends and left under static or under perfused flow as shown in Figure 7.1. Reseeded statically cultured samples were left in petri dishes immersed in media for three days at 37 °C in 5 % $CO_2$ (v/v). For the perfused samples cells the reseeded scaffolds were left overnight to adhere. The following day each sample was attached to the bioreactor as shown in Figure 7.7. Medium was perfused through the tissue at a rate of 0.5 mL/min for 48 hours. Thereafter, the samples were processed for histology with longitudinal and transverse sections taken from the same block/sample. Cell Tracker and DAPI were used to verify the location of cells.

#### 7.4.3.1 Results for Method 3

Figure 7.10 shows the primary Schwann cells under static conditions. The cells were located predominantly within the epineurium. A large portion of cells were seen in the proximal section of the nerve and to a lesser extent in the middle and distal portion. Figure 7.11 shows the cells under perfusion. As was observed for the static samples, the majority of cells were located in the proximal and middle sections and to a lesser extent in the distal portion. The cells were found to be within the middle and near the edge of the epineurium (Figure 7.11).

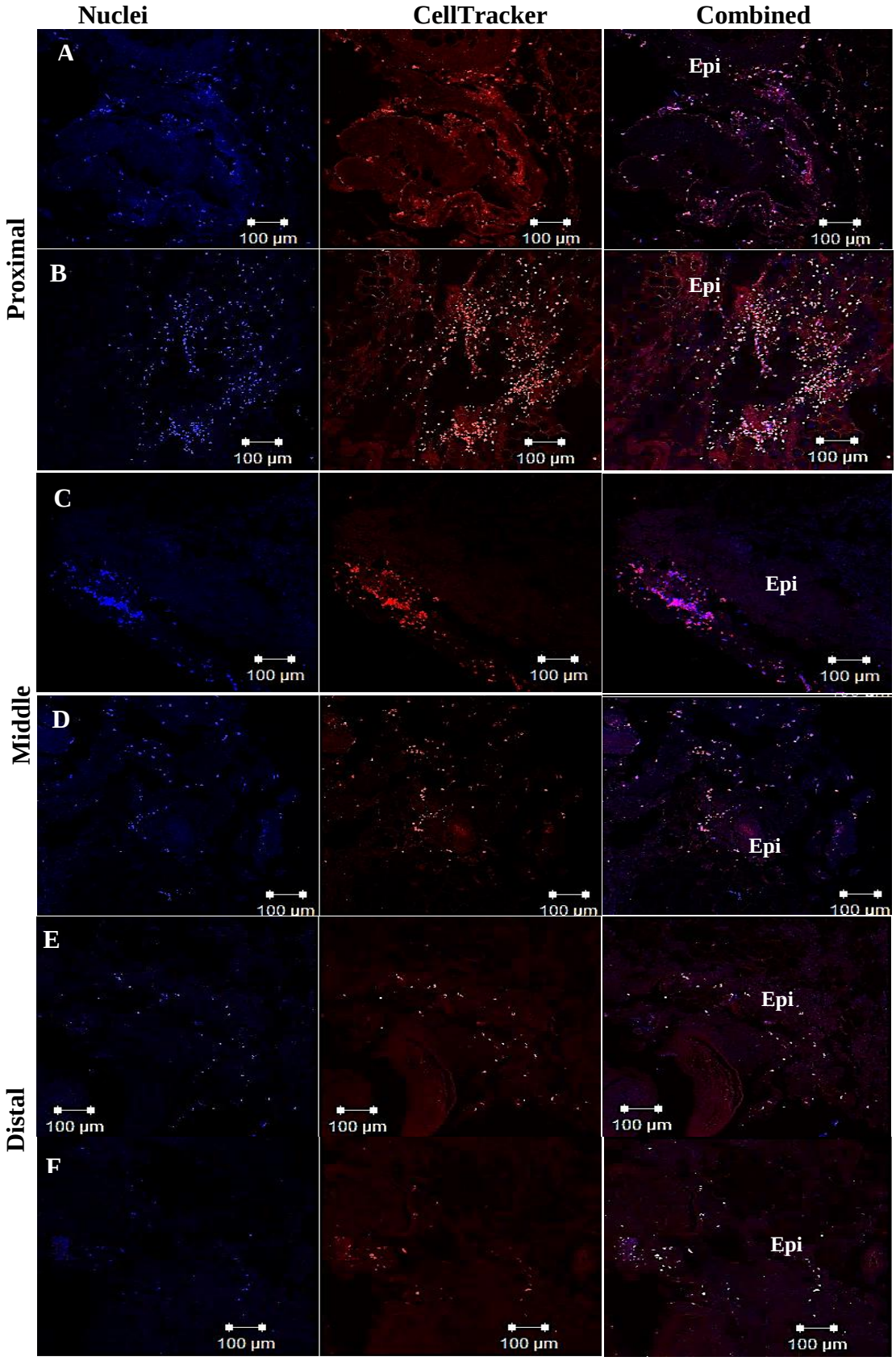


**Figure 7.10 Primary rat Schwann cells introduced into porcine acellular nerve by the motor pump method at day three under static conditions**. CellTracker and nuclei (DAPI) labelled cells. Schwann cells were detected in the epineurium and were observed to a greater extent in proximal (A-B) and middle (C-D) sections of the nerve. Fewer cells were observed in the distal (E-F) sections of the nerve. CellTracker labelled Schwann cells are in red, cell nuclei are blue. Epi = epineurium. Scale bar at 100µm.

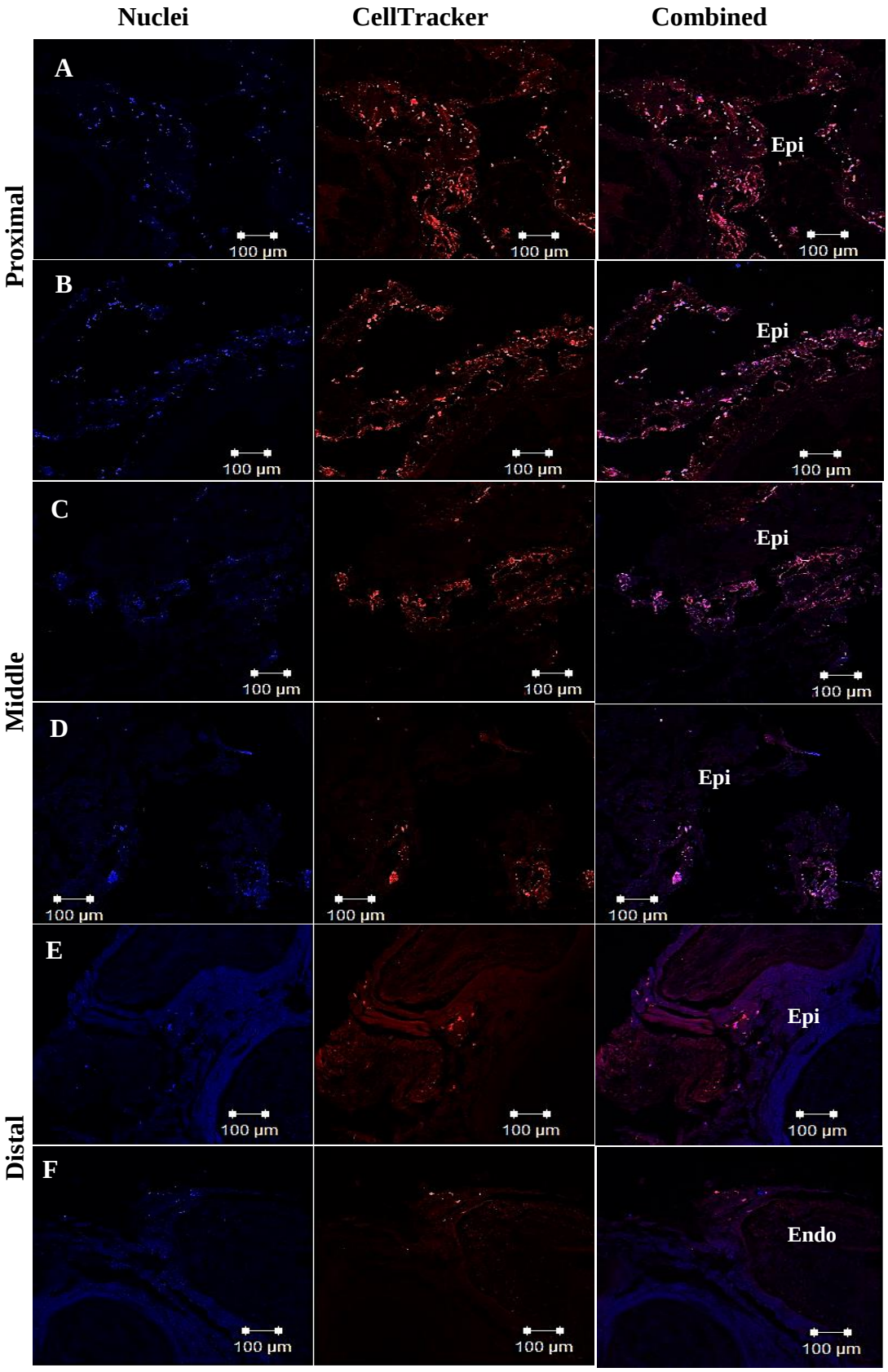


**Figure 7.11 Primary rat Schwann cells introduced in to porcine acellular nerve by the motor pump method at day three under perfused conditions**. CellTracker and nuclei (DAPI) labelled cells. Schwann cells were observed to a greater extent in proximal (A-B) and middle (C-D) sections of the nerve. Fewer cells were observed in the distal (E) sections of the nerve. CellTracker labelled Schwann cells are in red, cell nuclei are blue. Endo = endoneurium; Epi = epineurium. Scale bar at 100µm.

### 7.4.4 Method 4-introduction of primary Schwann cells into nerve scaffolds via Hamilton syringe

The motor pump seeding technique was noted on being able to introduce cells through the entire scaffold; however, a large portion of cells were lost during the seeding process as there was a notable leakage of cell suspension in the gap between the syringe and the nerve scaffold. This system was therefore refined to include the use of a Hamilton syringe with a 26-gauge needle (0.41 mm in diameter) to allow direct injection of Schwann cells into the scaffold.

A Hamilton syringe was used to inject $1x10^6$ Schwann cells resuspended in 60 µL media underneath the epineurium of the nerve. Cells were injected in equal volumes (approximately 10 µL) at three evenly spaced points on both sides of the nerve in order to create minimal damage and observed under a dissection microscope (Figure 7.12).

The recellularised scaffolds were placed into static or perfused flow culture conditions as shown in Figure 7.1. Samples placed into static culture were initially immersed in media for three days at 37 °C in 5 % $CO_2$ (v/v). For the perfused samples cells the reseeded scaffolds were left overnight to adhere. The following day the samples were aseptically transferred to the perfusion bioreactor as shown in Figure 7.7. Medium was perfused through the tissue at a rate of 0.5 mL/min for 48 hours. Thereafter, each sample was processed for histology, with longitudinal and transverse sections taken from the same block/sample. CellTracker and DAPI were used to locate cells within the scaffold.

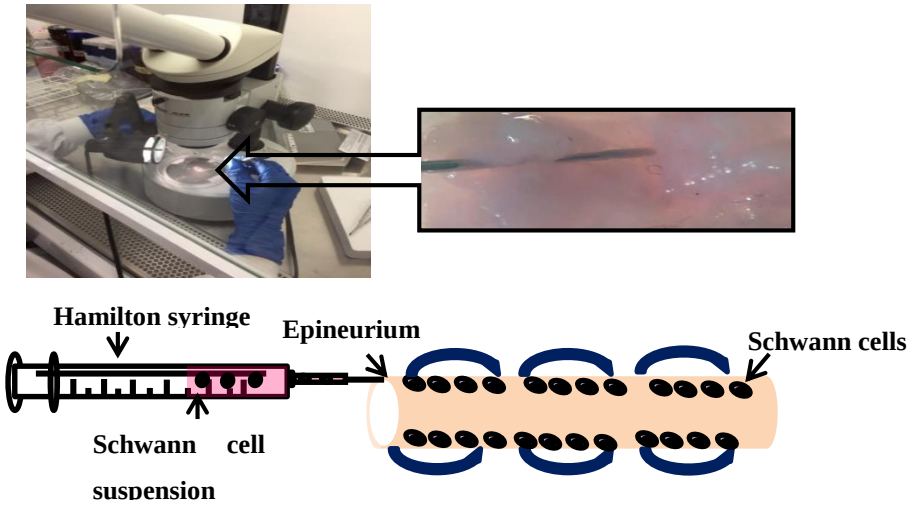


**Figure 7.12 Seeding primary Schwann cells using Hamilton syringe and dissection microscope**. Schwann cells were seeded directly underneath the epineurium of the nerve at three evenly spaced points on both sides of the nerve as indicated by the arrow for minimal damage using a Hamilton syringe with a 26-gauge needle and a dissection microscope.

### 7.4.4.1 Results for Method 4

#### 7.4.4.1.1 Viability of primary Schwann cells post injection with a Hamilton syringe

Due to the small diameter of the Hamilton syringe, there was concern that the shear force of the needle could potentially damage the Schwann cells, and in turn, have a damaging effect on cell viability when injected into the scaffold. Therefore, a viability assay using Alamar blue was undertaken. A 50 µL cell suspension was injected into a six well plate using the Hamilton syringe and as a control 50 µL of cell suspension using a 200 mL pipette was also plated.

The viability assay demonstrated that Schwann cell viability was affected post injection (Figure 7.13). There was a significant decrease in cell after 48 hours, however the cell number significantly increase by day five (120 hours).

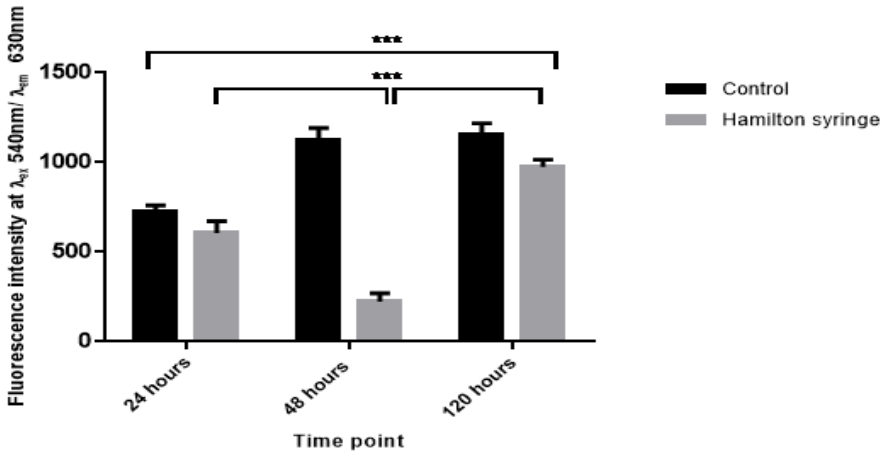


**Figure 7.13. Graph showing Schwann cell viability post Hamilton syringe injection**. Alamar blue assay shows viability of primary Schwann cells. There was a significant decrease of cells at 48 hours post injection but the viability significantly increased by 120 hours. There was a significant difference in the cell number between 24 hours and 120 hours. 24 hours; control 728.5 ± 10.55 RFU and syringe injected 606.8 ± 22.06 RFU. 48 hours; control 1122 ± 23.78 and syringe injected 224.9 ± 15.15 RFU. 120 hours; control 1161 ± 19.74 RFU and syringe injected 976.1 ± 13.30 RFU. Data was repeated three times in triplicates and analysed using an unpaired Students *t*-test and is presented as SD (n = 3) ± 95 % C.I ($p < 0.0002$***) RFU = relative fluorescent units

#### 7.4.4.2.2 Introduction of primary Schwann cells into nerve scaffolds via Hamilton syringe

Figure 7.14 and 7.15 illustrates that the use of a Hamilton syringe to introduce Schwann cells underneath the nerve epineurium was a suitable method. The figures show a distribution of cells throughout the entire nerve with no indication of damage to the nerve structure as a result of the injection. In terms of cell distribution, the majority of the cells under static and perfused conditions were located within the epineurium. Figure 7.14 A and E revealed the presence of cells around the fascicles, surrounding the perineurium.

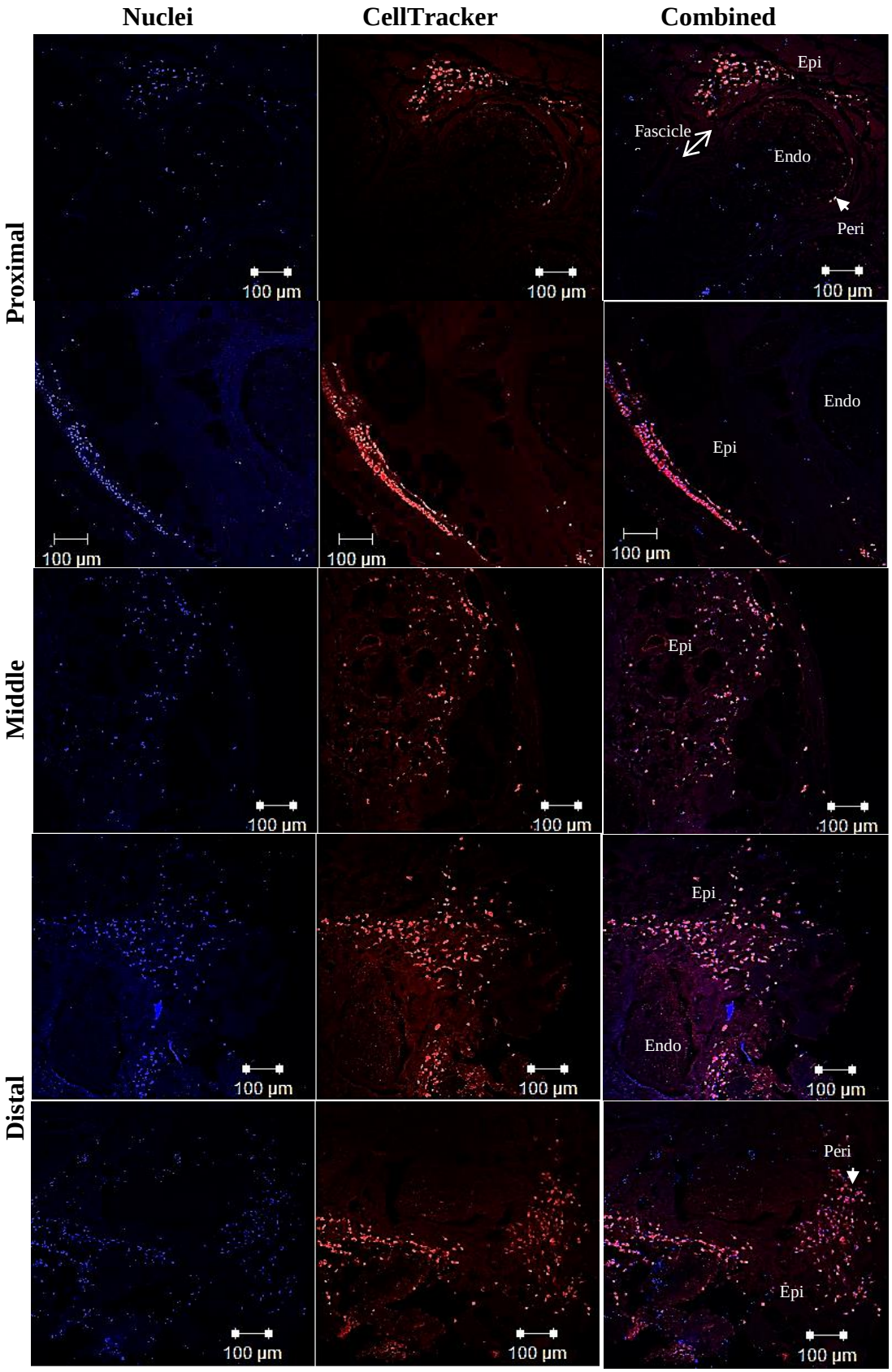


**Figure 7.14 CellTracker and DAPI labelled reseeded Schwann cells via Hamilton syringe under static conditions at day three**. Schwann cells were seen in proximal (A) middle (B-C) and distal (D-E) sections of the nerve. Cells are predominantly located within the epineurium but some cells are seen around the perineurium as indicated by the arrows. CellTracker labelled Schwann cells are seen in bright red, cell nuclei are seen in blue. Endo = endoneurium; Epi = epineurium; Peri = perineurium. Scale bar at 100µm.

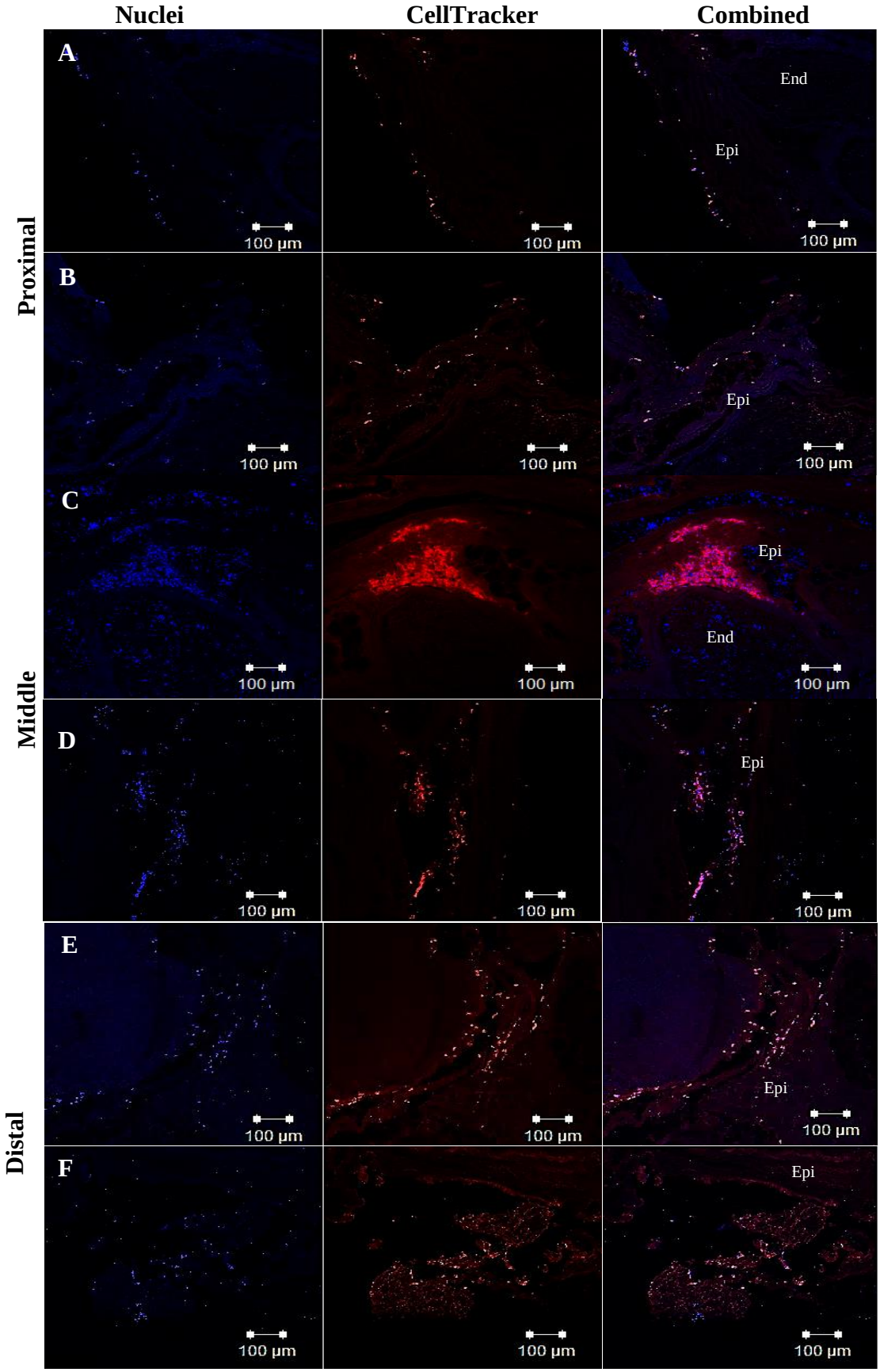


**Figure 7.15 CellTracker and DAPI labelled reseeded Schwann cells via Hamilton syringe under perfused conditions at day three.** Schwann cells were seen in proximal (A-B), middle (C-D) and distal (E-F) sections of the nerve. Cells were predominantly located within the epineurium. CellTracker labelled Schwann cells were bright red, cell nuclei in blue. Endo = endoneurium; Epi = epineurium. Scale bar at 100µm.

### 7.4.5 Analysis of recellularised acellular nerve scaffolds

The Hamilton syringe method (method 5) was concluded to be the most effective method for introducing primary Schwann cells into the acellular scaffold. Cells were seeded at three time points (1, 3 and 7 days) under static and perfused culture conditions to determine the viability over the time course and whether the cells proliferate.

#### 7.4.5.1 Results

#### 7.4.5.1 Analysis of cellular migratory pattern under static and perfused conditions

Histological analysis of the reseeded scaffolds showed the presence of cells throughout the entire scaffold under both static and perfused conditions (Figure 7.16-7.21). The majority of the cells were clumped together, however higher magnification revealed that cells were located around the perineurium, as seen in Figure 7.16 (I); 7.17 (J) and 7.21 (C). Some cells were also seen entering the endoneurium, as illustrated in Figure 7.18 (E) and Figure 7.20 (I).

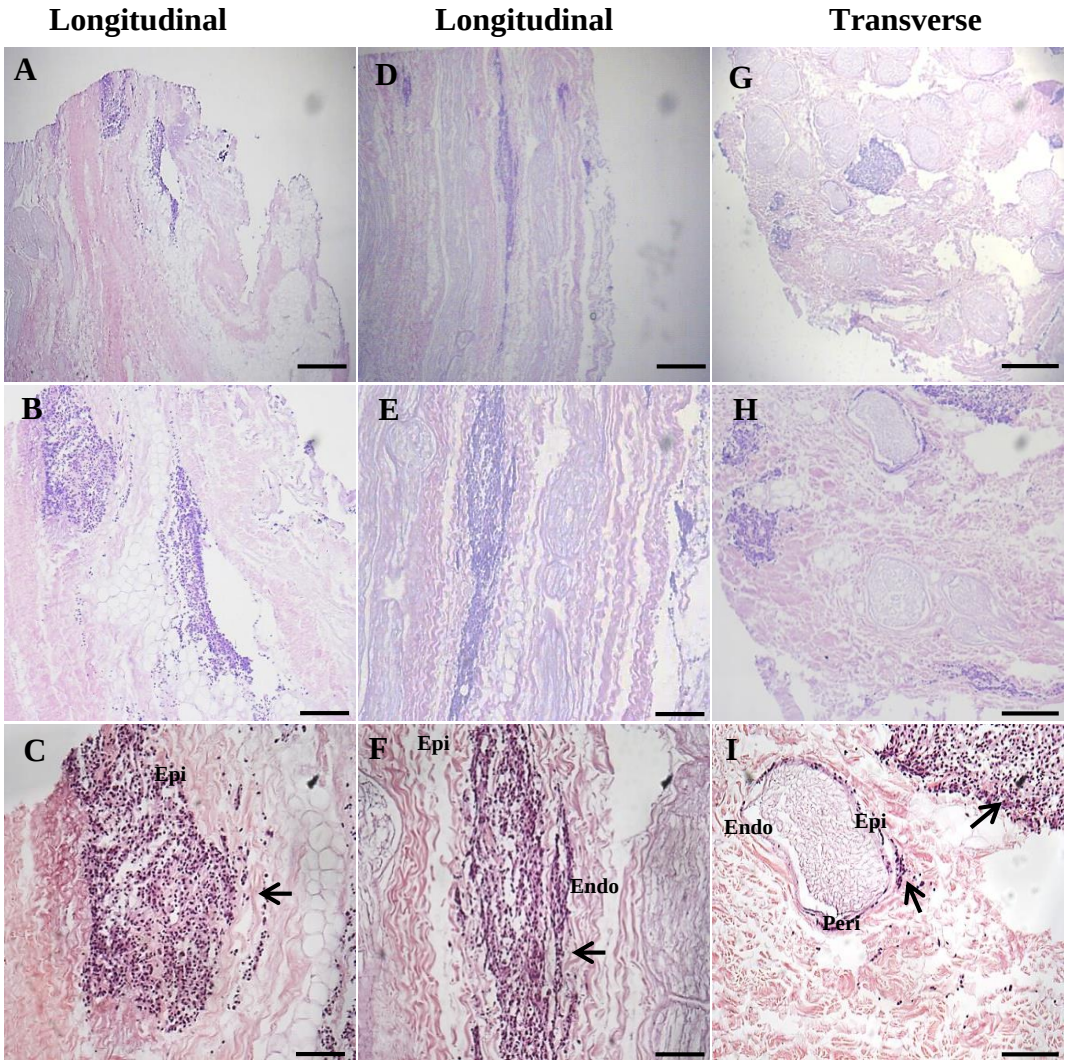


**Figure 7.16 Reseeded Schwann cells via Hamilton syringe under static conditions at day one.** Longitudinal (A-F) and transverse (G-I) recellularised nerves sections stained with haematoxylin and eosin. Longitudinal sections reveal the presence of cells within the epineurium as indicated by the arrows (C and F). Transverse sections (G-I) show cells within the epineurium and surrounding the perineurium indicated by the arrows (I). Endo = endoneurium; Epi = epineurium; Peri = perineurium. Scale bar at 500µm (A, D and G), 200µm (B, E and H) and 100µm (C, F and I) respectively.

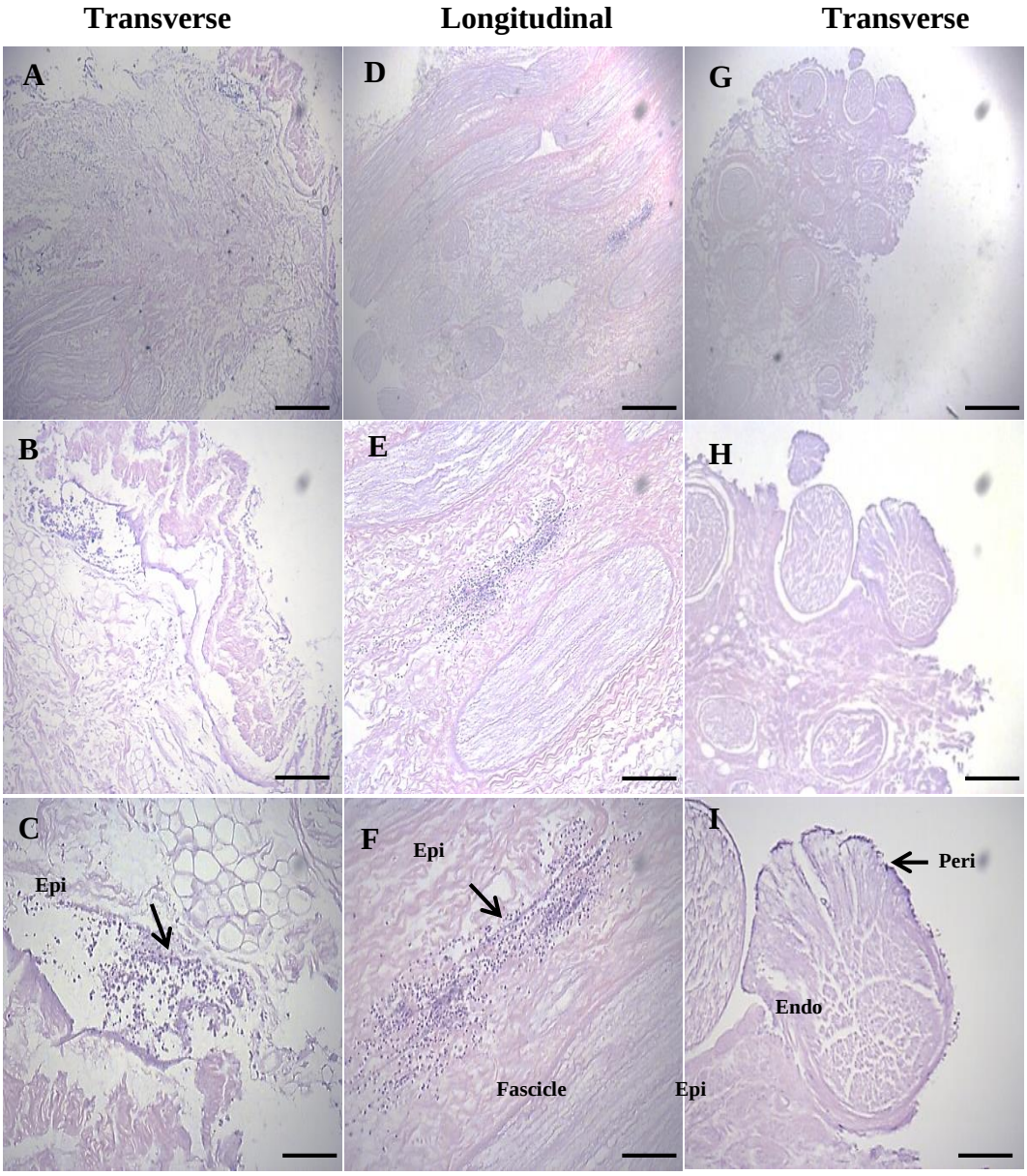


**Figure 7.17 Reseeded Schwann cells via Hamilton syringe under static conditions at day three.** Transverse and longitudinal recellularised nerves sections stained with haematoxylin and eosin. Longitudinal section (D-F) reveals presence of cells within the epineurium as indicated by the arrow (F). Transverse sections show cells within the epineurium (C) and surrounding the perineurium (I) as indicated by the arrows. Endo = endoneurium; Epi = epineurium; Peri = perineurium. Scale bar at 500µm (A, D and G), 200µm (B, E and H) and 100µm (C, F and I).

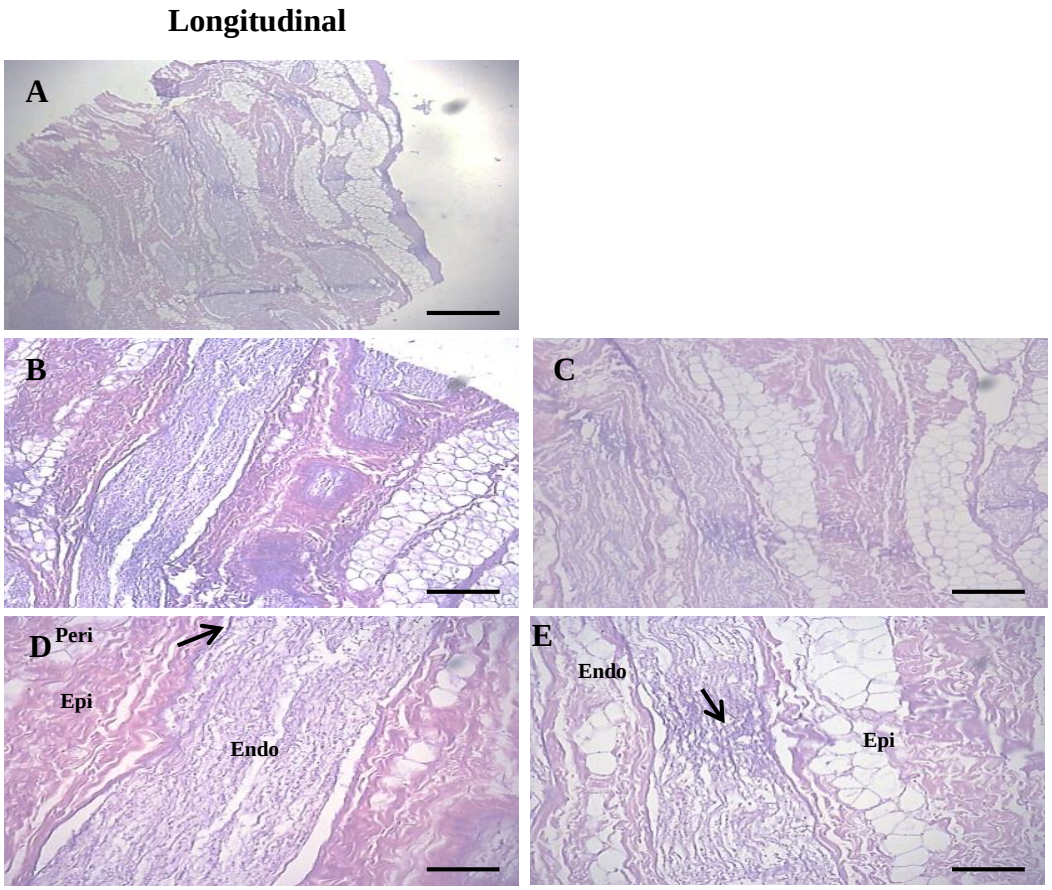


**Figure 7.18 Reseeded Schwann cells via Hamilton syringe under static conditions at day seven. Longitudinal recellularised nerves sections stained with haematoxylin and eosin. Longitudinal** sections reveal presence of cells around the perineurium (D) and within the endoneurium (E) as indicated by the arrows. Endo = endoneurium; Epi = epineurium; Peri = perineurium. Scale bar at 500µm (A), 200µm (B-C) and 100µm (D-E).

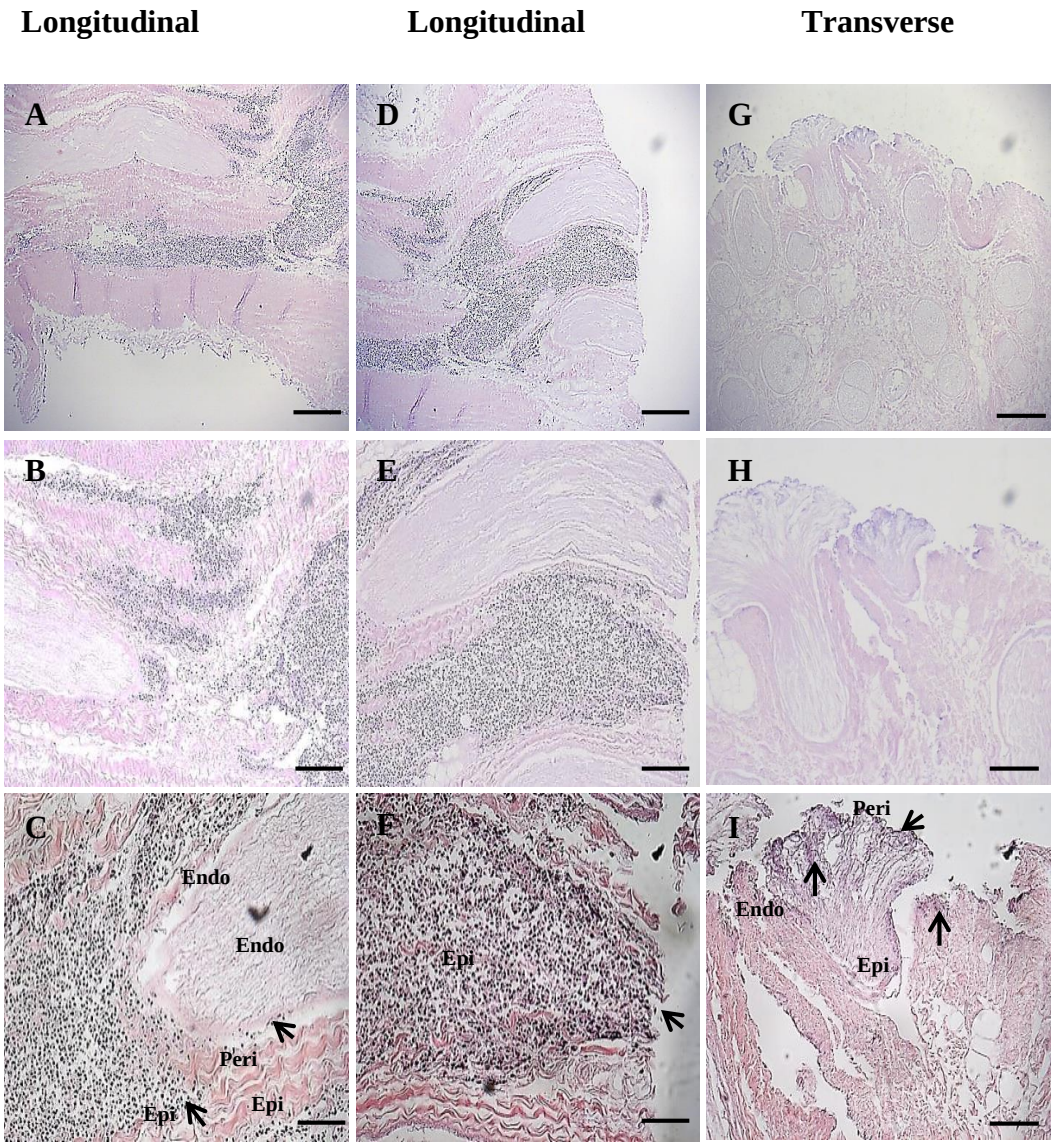


**Figure 7.19 Reseeded Schwann cells via Hamilton syringe under perfused conditions at day one.** Transverse and longitudinal recellularised nerves sections stained with haematoxylin and eosin. Longitudinal sections (A-F) reveal presence of cells surrounding the epineurium (C, F and I), and surrounding the perineurium (C) as indicated by the arrows. Transverse sections (G-I) show cells surrounding the perineurium and entering the endoneurium indicated by the arrows (I). Endo = endoneurium; Epi = epineurium; Peri = perineurium. Scale bar at 500µm (A, D and G), 200µm (B, E and H) and 100µm (C, F and I).

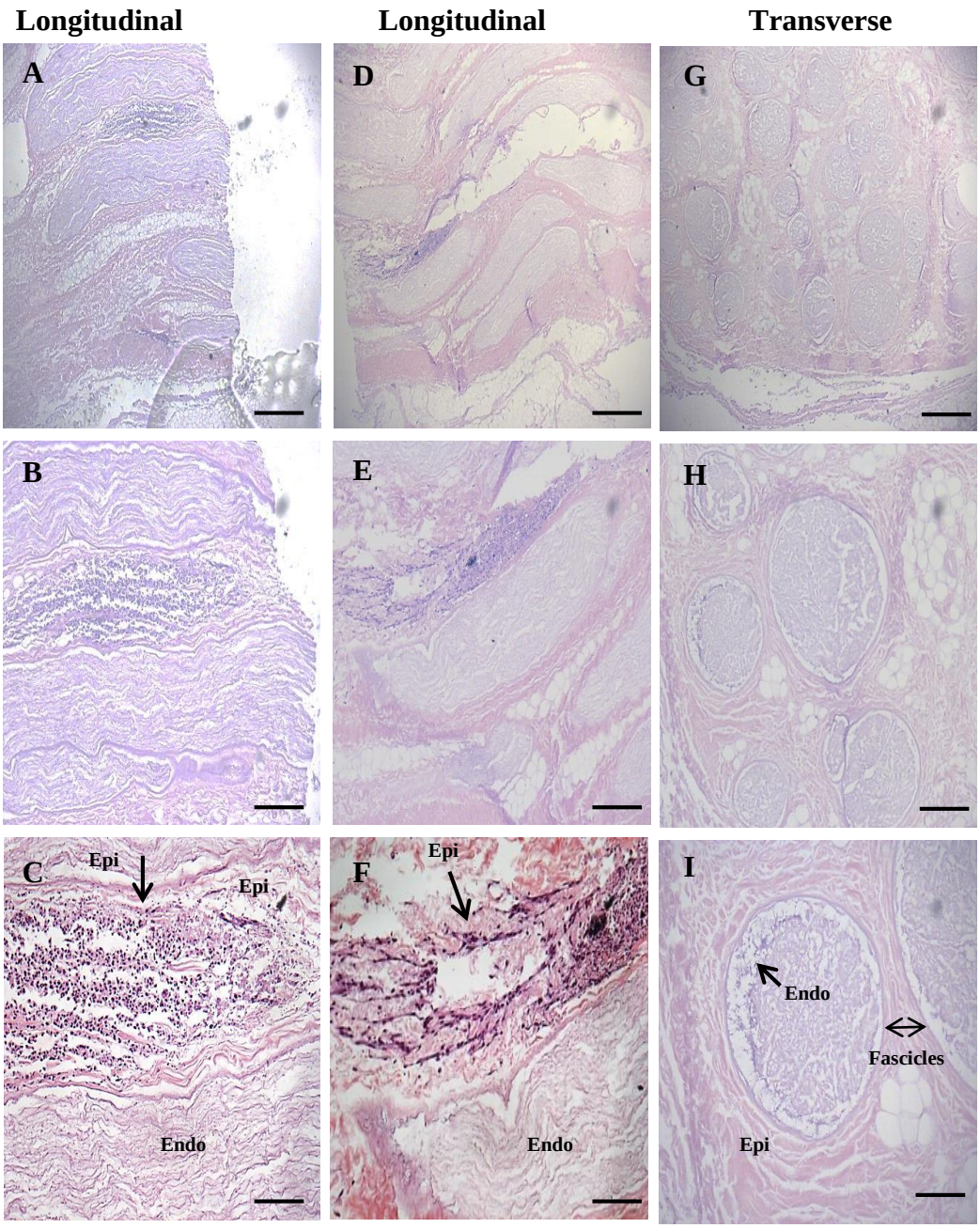


**Figure 7.20 Reseeded Schwann cells via Hamilton syringe under perfused conditions at day three.** Transverse and longitudinal recellularised nerves sections stained with haematoxylin and eosin. Longitudinal sections (A-F) reveal large presence of cells within the epineurium (C and F) as indicated by the arrows. Transverse sections (G-I) show cells entering the endoneurium of the nerve fascicle (I). Endo = endoneurium; Epi = epineurium; Peri = perineurium. Scale bar = 500µm (A, D and G), 200µm (B, E and H) and 100µm (C, F and I).

**Longitudinal**

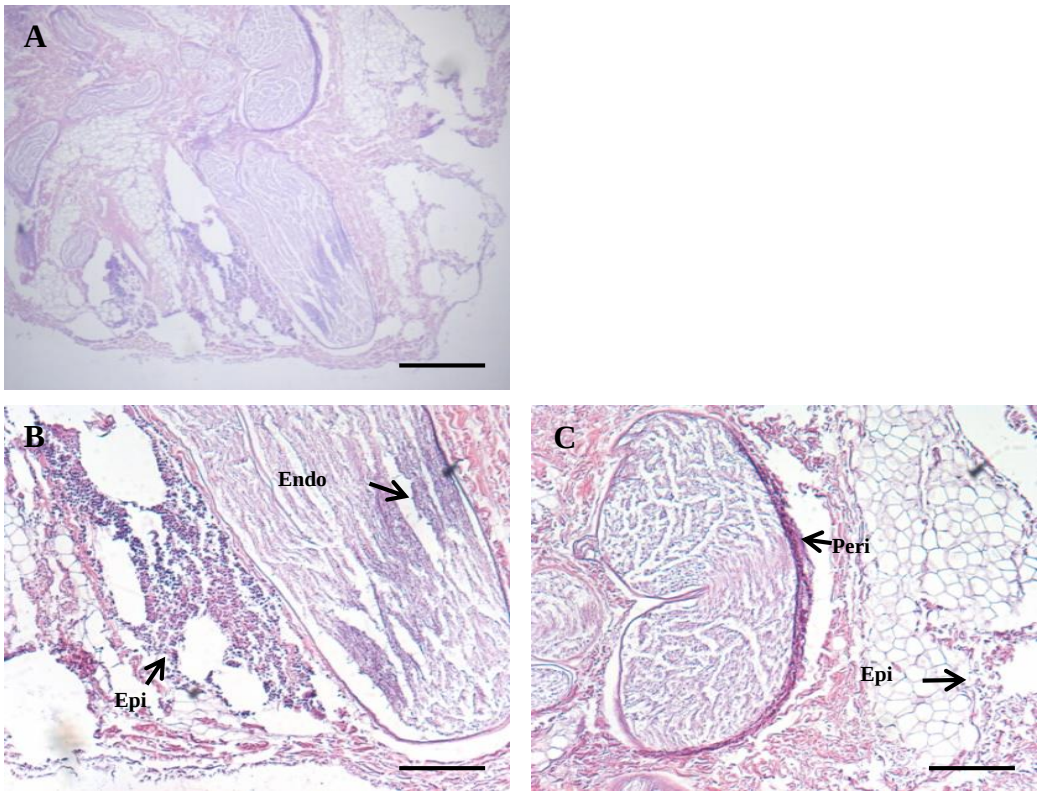


**Figure 7.21 Reseeded Schwann cells via Hamilton syringe under perfused conditions at day seven.** Longitudinal recellularised nerves sections stained with haematoxylin and eosin. Longitudinal sections revealed presence of cells within the epineurium and endoneurium (B-C). The sections also showed cells surrounding the perineurium of the fascicle indicated by the arrows (C). Endo = endoneurium; Epi = epineurium; Peri = perineurium. Scale bar = 500µm (A) and 200µm (B-C).

To assess the viability of the cells within the scaffold over seven days a cell viability analysis was undertaken (by MTT). The viability assay was inconclusive (Figure 7.22). It was noted that when the MTT solution was placed on the samples, both the recellularised and acellular samples turned purple on the outer (Figure 7.22 B) and inner surfaces of the nerve (Figure 7.22 C), in addition the acidified isopropanol could not elute all of the dye from the samples. Therefore, the MTT assay was concluded as an inaccurate technique for measuring cell viability of these samples.

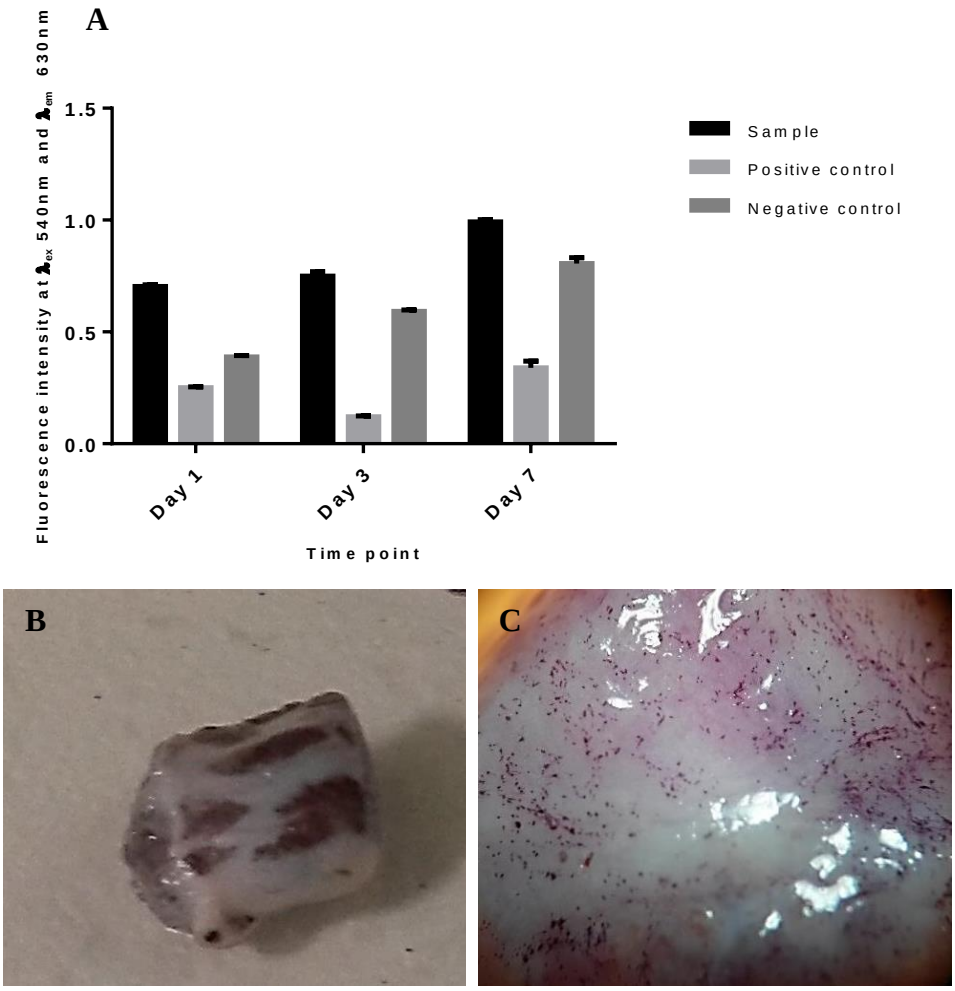


**Figure 7.22 Schwann cell viability within recellularised nerves under static conditions.** Graph (A) shows both the recellularised and decellularised scaffolds fluorescence readings increased from day 1 to day 7. Mean fluorescent reading of sample day one = 0.70; day three = 0.75; day seven = 0.99. Mean fluorescent reading of positive control day one = 0.25; day three = 0.12; day seven = 0.34. Mean fluorescent reading of negative control day one = 0.39; day three = 0.59; day seven = 0. 81. (B and C) Image of decellularised scaffold reducing the MTT reagent (seen in purple) which could have attributed to the high fluorescence reading observed in the scaffold. Image B shows the retention of the MTT reagent on the outer surface of the nerve whilst Image C reveals inner surface of the nerve which also shows retention of the MTT reagent. Data was analysed using two-way ANOVA presented as the mean (n =3) ± SD

A DNA quantification assay was undertaken as an indicator of the amount of DNA present within the scaffolds (as described in Section 5.3.3). This assay gave a more accurate reading to the DNA content as the controls (acellular scaffold) remained significantly lower than the receullarised scaffolds over the duration (Figure 7.24 A). Under static conditions the DNA content significantly increased from day 1 to day 3 indicating that cells were proliferating within the scaffold. By day 7 however there was a dramatic decrease in the DNA number (Figure 7.24 B). The low number of DNA suggests that the cells within the scaffold had ceased to proliferate; this may have been due to lack of media/nutrients reaching the cells. Under perfused conditions (0.5 $mL.min^{-1}$) there was a similar trend. However, more of a gradual increase of DNA was detected from day one and day three; with a slight decrease by day seven (Figure 7.24 C). This suggests that perfusion helps maintain cell proliferation within the scaffold. The slight decrease by day 7 may have been due to the limited space within the scaffold.

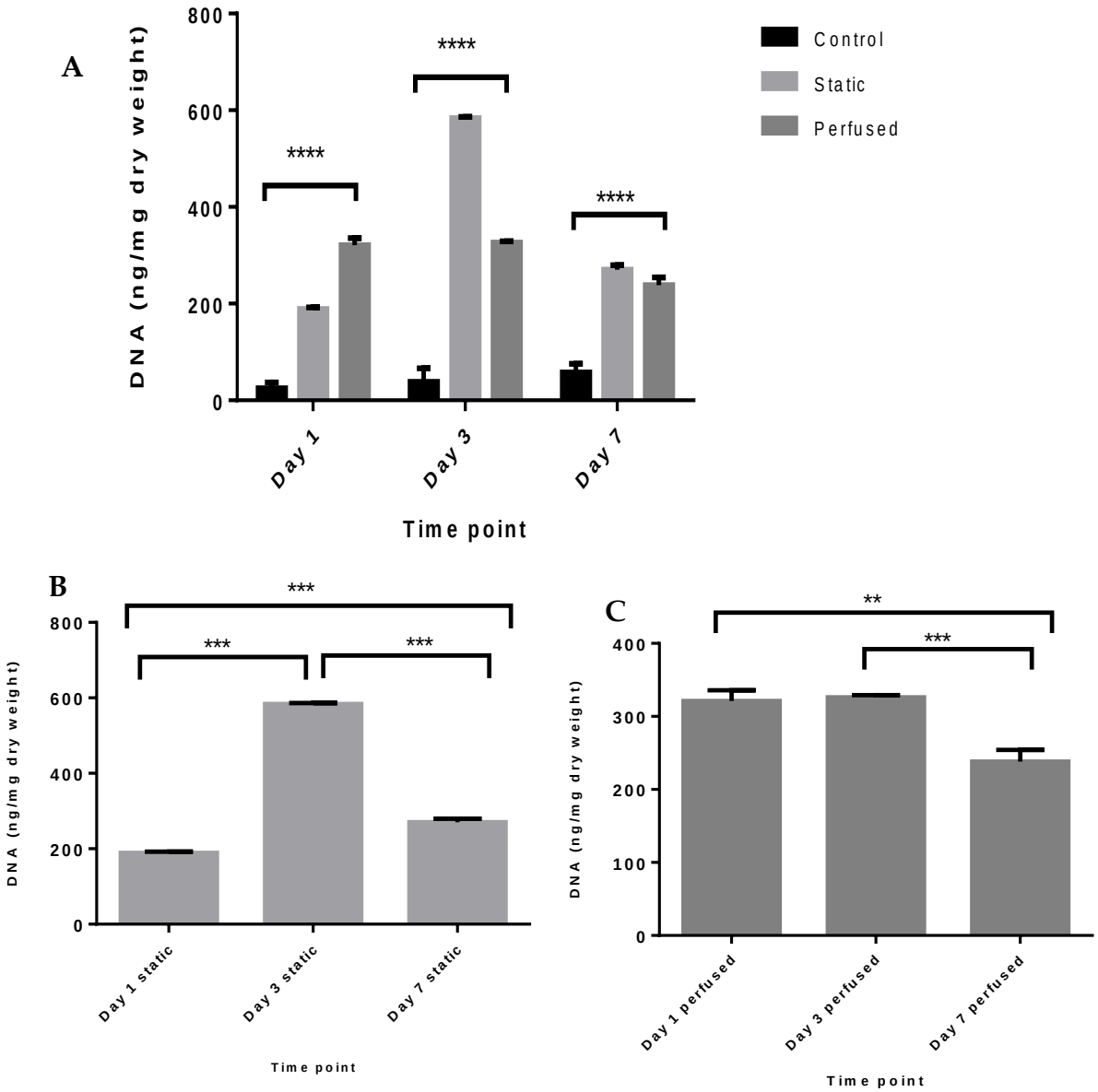


**Figure 7.23. Graph showing DNA content in reseeded scaffolds under static and perfused conditions**. Primary Schwann cells-introduced scaffolds under static and perfused conditions showed a significant increase in DNA when compared to the control (decellularised scaffold) *($p<0.0001$). Under static conditions there was a significant increase in DNA from day 1 to day 3 in the recellularised nerves and a significant decrease in DNA from day 3 to 7 *($p<0.0001$). Overall there was a significant change in DNA content from day 1 to day 7 under static conditions*($p<0.0002$). Under perfused conditions there was no significant increase from day 1 to 3 however there was a significant decrease in DNA from day 1 to day 7 in the recellularised nerves*($p<0.0002$) Overall there was a significant change in DNA content from day 1 to day 7 under perfused conditions *($p<0.0027$). Mean DNA content under static conditions, day 1 = 189 ng/mg; day 3 = 583 ng/mg; day 7 = 189 ng/mg. Mean value under perfused conditions, day 1 = 321 ng/mg; day 3 = 326 ng/mg; day 7 = 238 ng/mg. Control decellularised sample day 1 = 25 ng/mg; day 3 = 38 ng/mg; day 7 = 57 ng/mg. Data was analysed using two-way ANOVA and unpaired Students *t*-test presented as the mean (n =3) ± SD

#### 7.4.5.3 Analysis of cellular phenotype under static and perfused conditions

Following static or perfused culture each scaffold was processed from normal histology and immunolabelled with the Schwann cell markers S100β (calcium-binding protein), GFAP (cytoskeleton component) and p75 NGFR (neurotrophin). Schwann cells cultured on tissue culture plastic served as positive controls for antibody labelling, in each case DAPI was used as a counter stain (Figure 7.24 & 7.25). Cultured Schwann cells labelled positively for S100β (green), p75 NGFR (red) and GFAP (yellow; Figure 7.24). Omission of a primary antibody served as a negative control (Figure 7.25).

Figures 7.24 and 7.25 show the positive and negative controls for the proteins expressed by the Schwann cells; each control was counterstained with DAPI to show the cell nuclei seen in blue. Figure 7.24 shows the positive controls (Schwann cells grown on tissue culture plastic grown) and expression of S100β (green), p75 NGFR (red) and GFAP (yellow), which indicated the presence of Schwann cells. Figure 7.25 shows the acellular scaffolds reseeded with cells which have been incubated with only the secondary antibody (omission of the primary antibody step), serving as a negative control. This was to show the level of background fluorescence (nonspecific binding) arising from the secondary antibody under identical illumination.

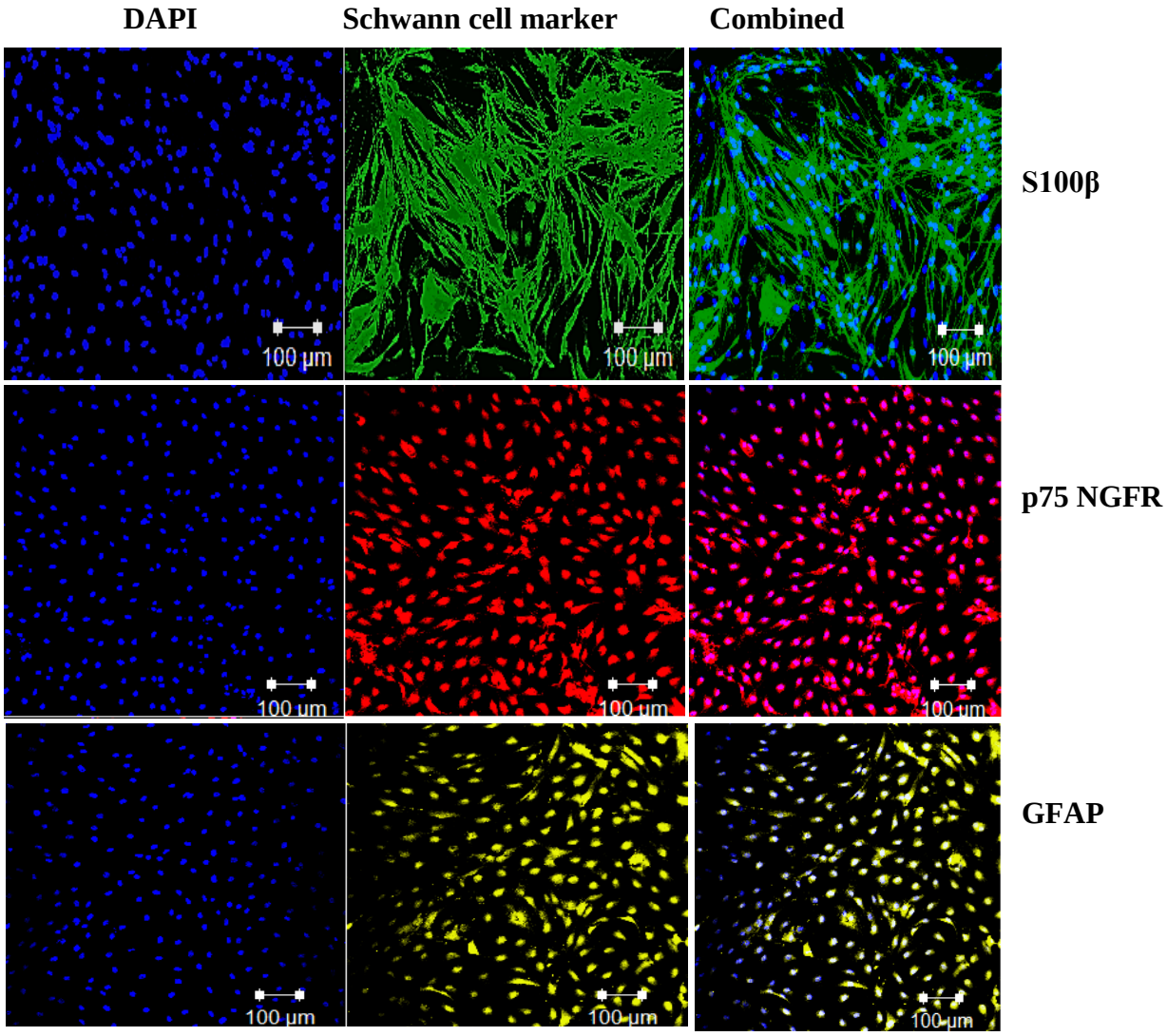


**Figure 7.24. Schwann cells immunolabelled for S100β, P75 and GFAP grown on polystyrene (positive control).** Schwann cells grown on tissue culture plastic were immunolabelled for S100β (green); p75 NGFR (red); GFAP (yellow). The majority of cells stained positive for all three markers, which confirmed the cells as having a Schwann cell phenotype. Cells were counterstained with DAPI to show cell nuclei (blue). Scale bar at 100µm

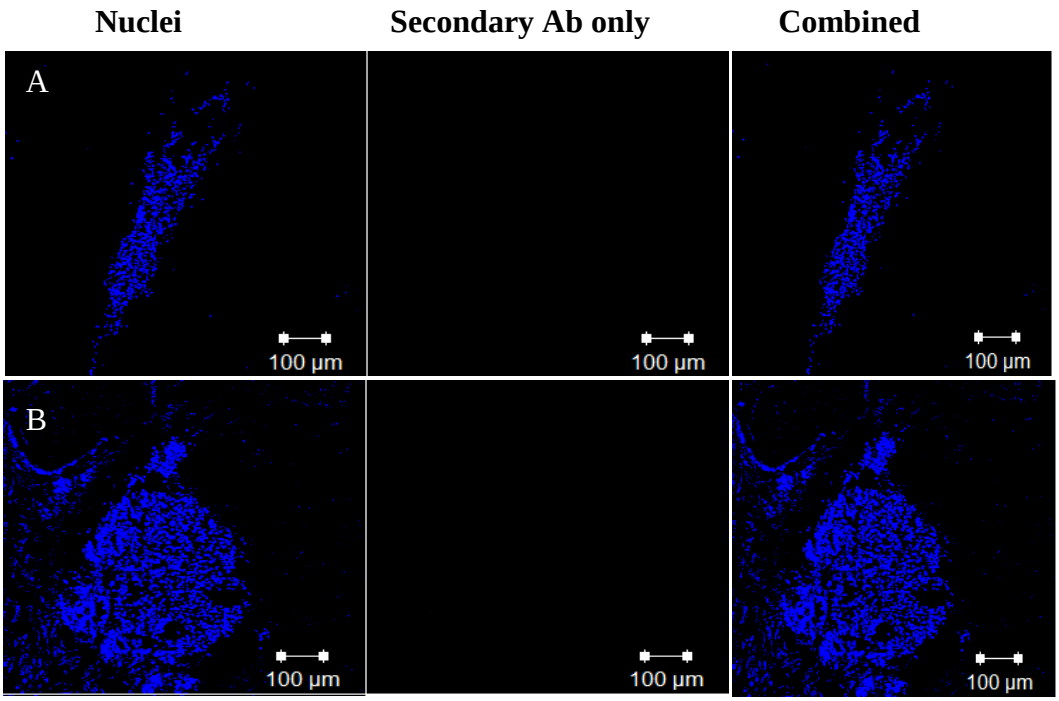


**Figure 7.25. Schwann cells incubated with secondary antibody alone (negative control).** Schwann cells introduced in to porcine acellular nerve showed no indication of non-specific binding of the secondary antibody at different concentrations (A and B). Cells were counterstained with DAPI to shown cell nuclei (blue). Scale bar at 100µm

Figures 7.26 - 7.31 illustrates confocal micrographs of porcine acellular scaffolds seeded with primary Schwann cells and cultured under static and perfused conditions for one, three and seven days. The cells were found to be located predominantly within the epineurium and some around the perineurium (Figure 7.26) within the proximal, middle and distal sections of the nerve. The recellularised samples expressed all three Schwann cell markers (p75 NGFR, S100β and GFAP). These markers are important for cell proliferation; migration, myelination and cell adhesion. These results demonstrate that the nerve scaffold provides a suitable environment in which primary Schwann cells are able to retain their phenotypic markers, when cultured in both static and perfused conditions.

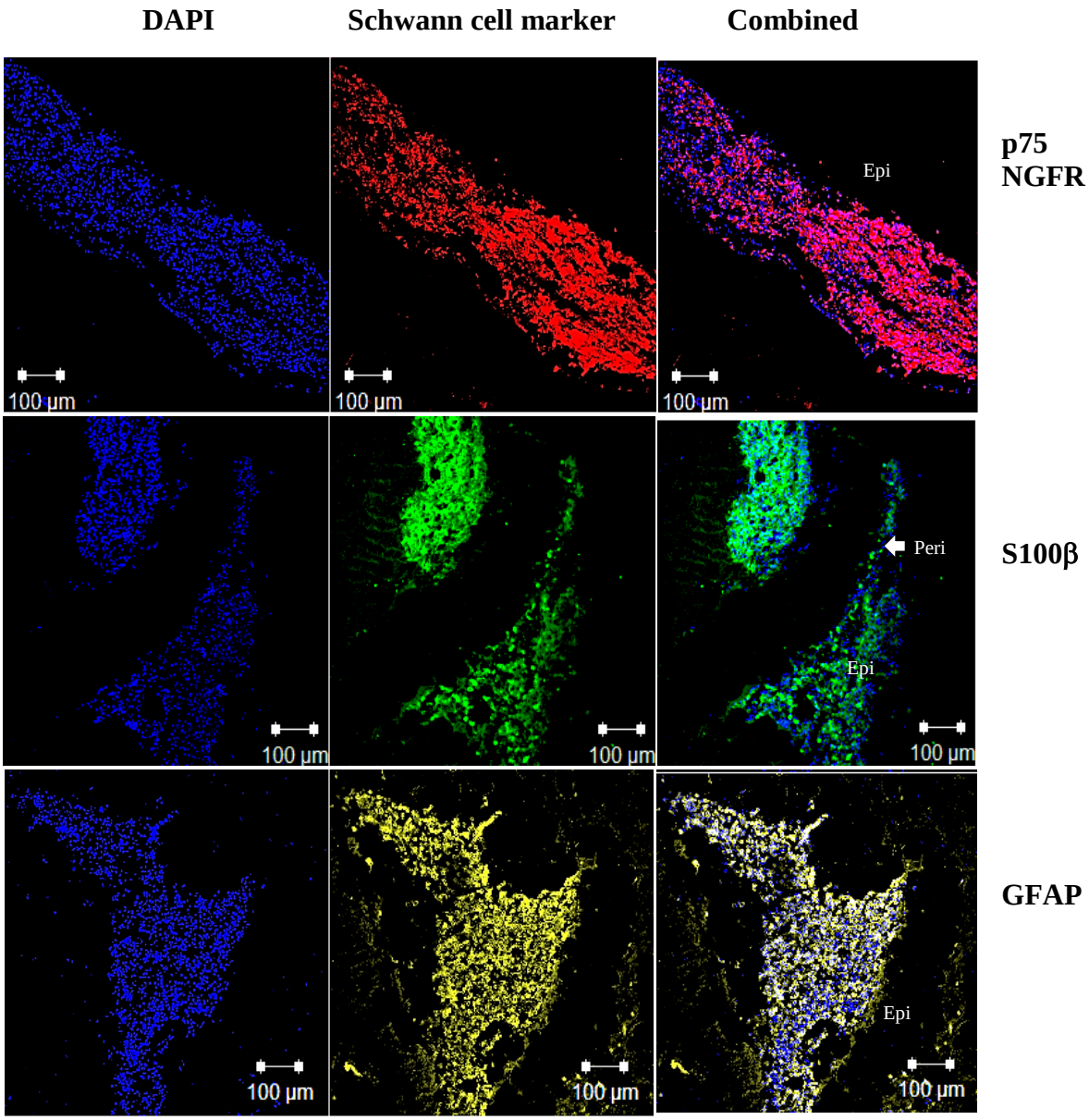


**Figure 7.26. Reseeded acellular scaffold at day one under static conditions**. Schwann cells immunolabelled for p75 NGFR (red); S100β (green) and GFAP (yellow). Recellularised cells, which were located within the epineurium and around the perineurium within the proximal section of the nerve stained positive for all three Schwann cell markers. Cells were counterstained with DAPI to shown cell nuclei (blue). Scale bar at 100µm.

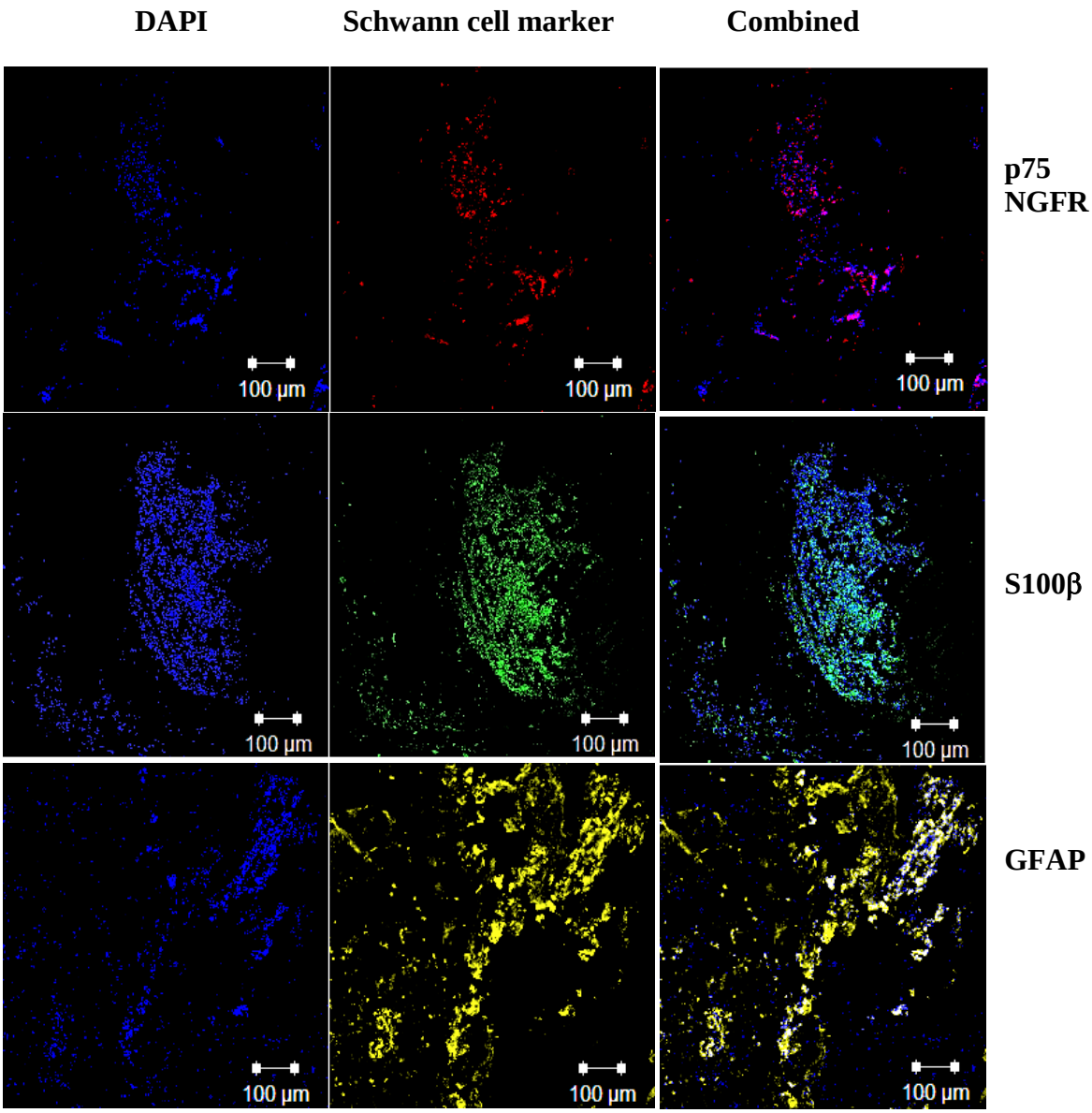


**Figure 7.27. Reseeded acellular scaffold at day 3 under static conditions.** Schwann cells immunolabelled for p75 NGFR (red); S100β (green) and GFAP (yellow). Recellularised cells within the epineurium of the middle section of the nerve stained positive for all three Schwann cell markers. Cells were counterstained with DAPI to shown cell nuclei (blue). Scale bar at 100µm.

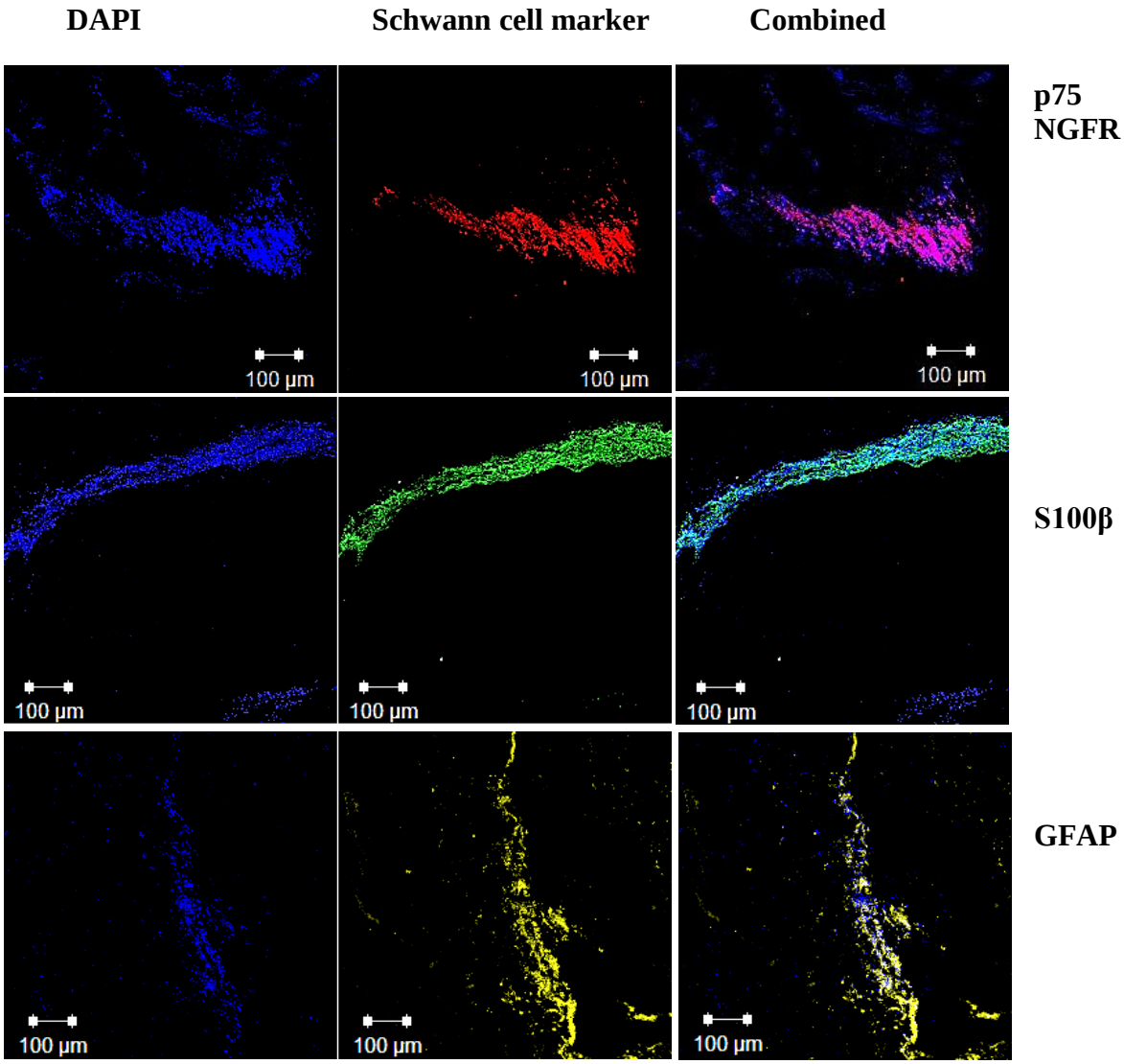


**Figure 7.28. Reseeded acellular scaffold at day 7 under static conditions.** Schwann cells immunolabelled for p75 NGFR (red); S100β (green) and GFAP (yellow). Recellularised cells within the epineurium of the distal section of the nerve stained positive for all three Schwann cell markers. Cells were counterstained with DAPI to shown cell nuclei (blue). Scale bar at 100µm.

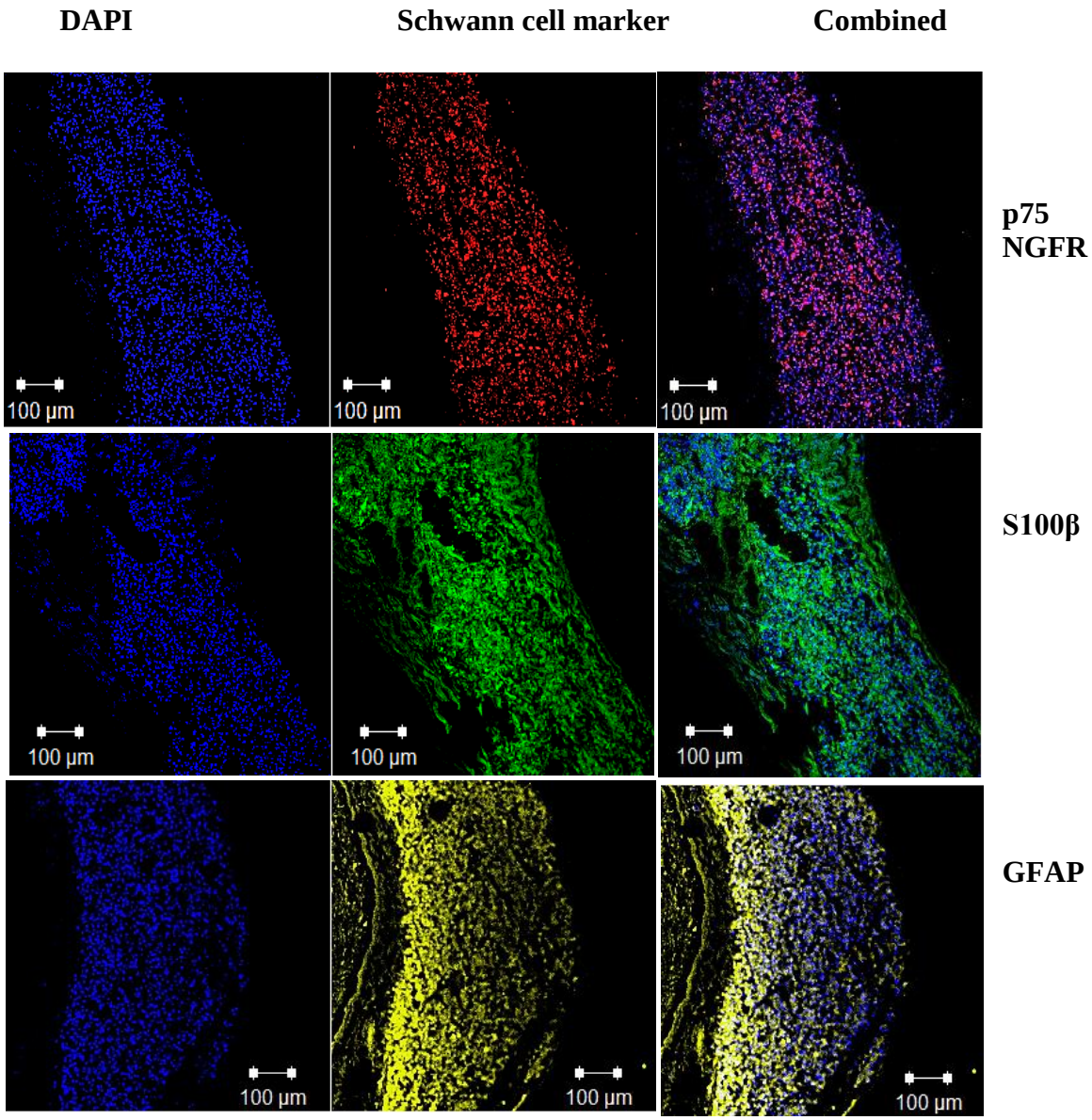


**Figure 7.29. Reseeded acellular scaffold at day 1 under perfused conditions**. Schwann cells immunolabelled for p75 NGFR (red); S100β (green) and GFAP (yellow). Recellularised cells within the epineurium of the proximal section of the nerve stained positive for all three Schwann cell markers. Cells were counterstained with DAPI to shown cell nuclei (blue). Scale bar at 100µm.

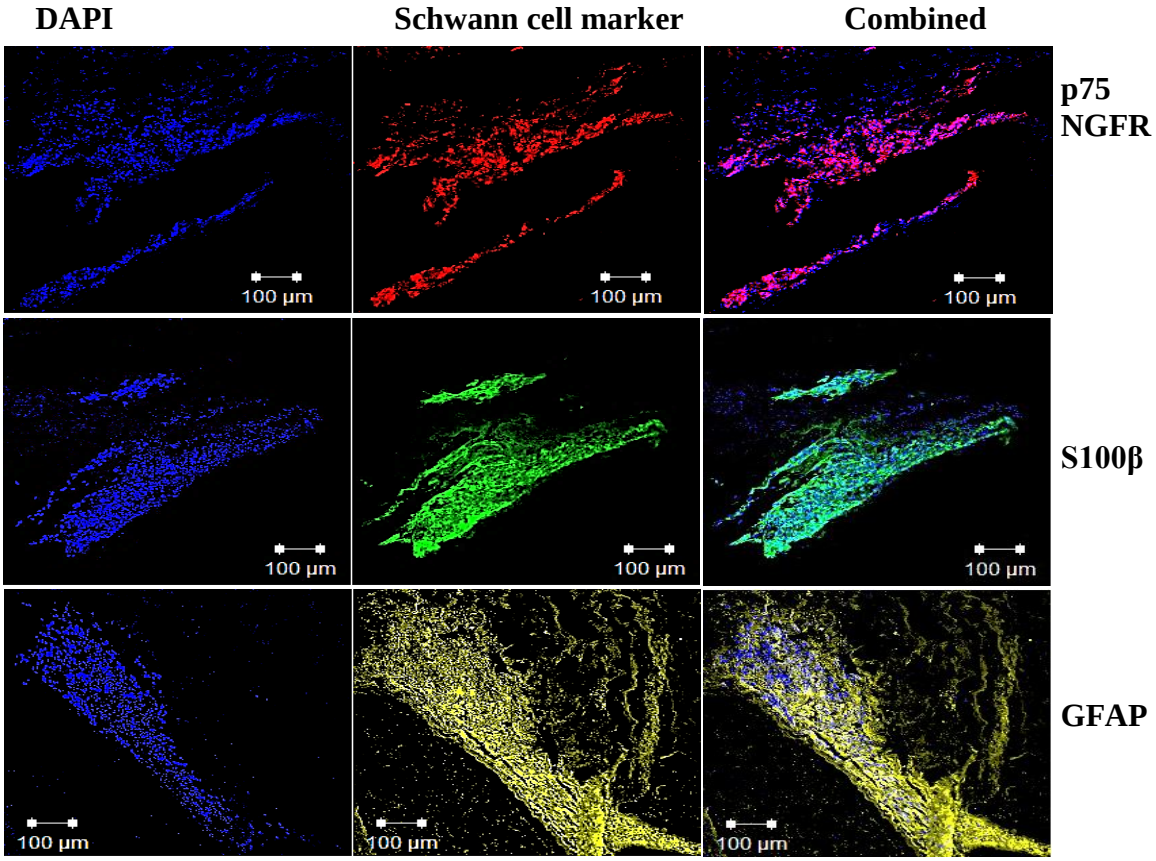


**Figure 7.30. Reseeded acellular scaffold at day three under perfused conditions.** Schwann cells immunolabelled for p75 NGFR (red); S100β (green) and GFAP (yellow). Recellularised cells within the epineurium of the middle portion of the nerve stained positive for all three Schwann cell markers. Cells were counterstained with DAPI to shown cell nuclei (blue). Scale bar at100µm.

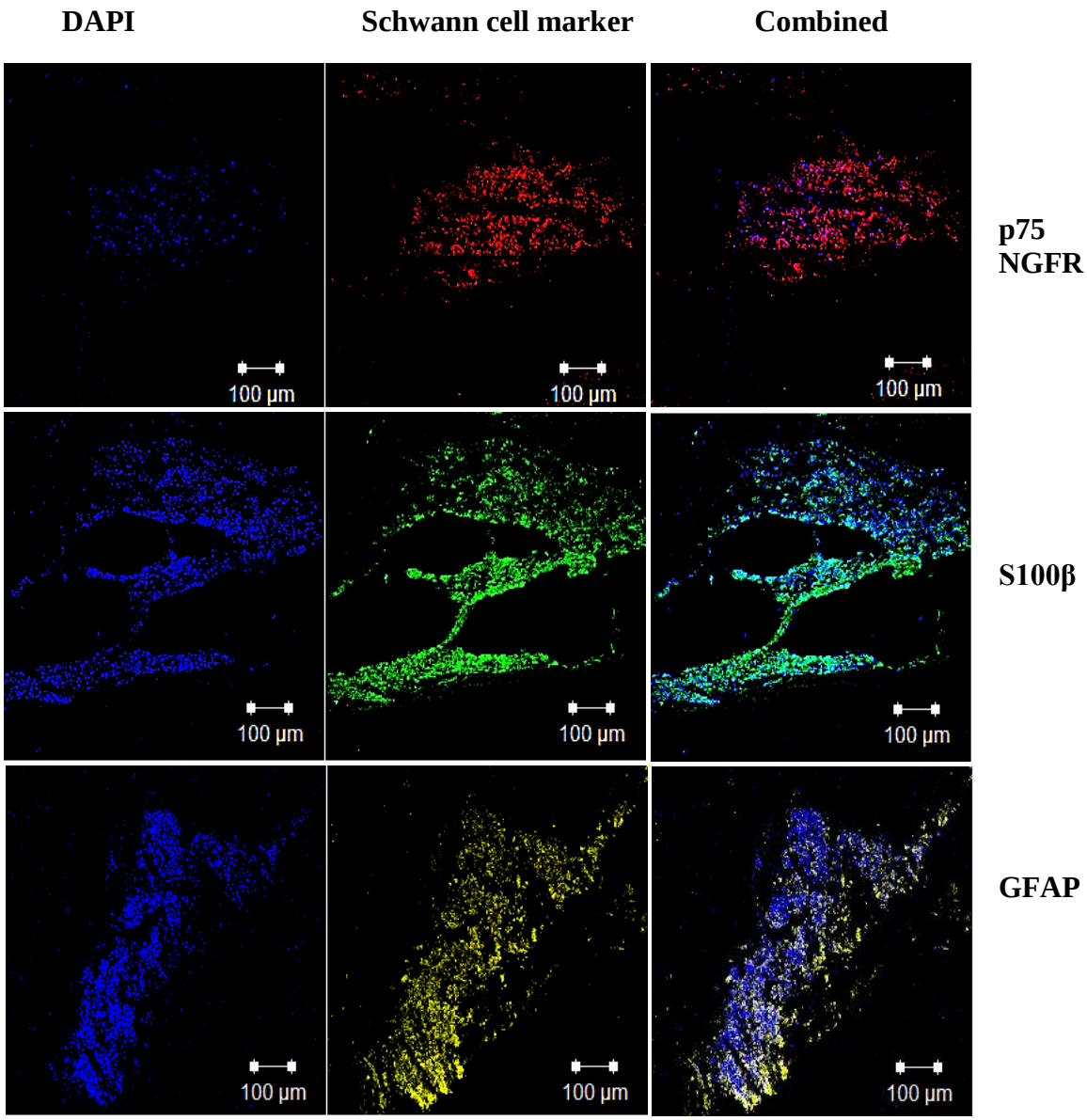


**Figure 7.31. Reseeded acellular scaffold at day seven under perfused conditions.** Schwann cells immunolabelled for p75 NGFR(red); S100β (green) and GFAP (yellow). Recellularised cells within the epineurium of the distal region of the nerve stained positive for all three Schwann cell markers. Cells were counterstained with DAPI to shown cell nuclei (blue). Scale bar at 100µm.

## 7.5 Discussion

This Chapter describes an investigation into recellularising acellular porcine nerve scaffolds using RN22 Schwann cells, and subsequently primary rat Schwann cells. Reseeded scaffolds were placed in a closed loop bioreactor system to investigate if Schwann cells would grow more efficiently under perfused conditions. The cells were under constant perfusion at a maximum flow rate of 0.5 $mL.min^{-1}$. A low flow rate was chosen, based upon previous work reporting that the viability of Schwann cells increased 2.5-fold under low flow conditions compared to static conditions (Sun, Norton et al. 2008).

The first aim of the study was to create an efficient seeding technique in which Schwann cells could be delivered directly into the acellular scaffold, infiltrating throughout the entire nerve. Early attempts of reseeding cells included cannulating the nerve and injecting through a cannula. This however proved to be ineffective as histological analysis showed Schwann cells clumped at the point of insertion, with no presence towards the rest of the scaffold. Reseeded scaffolds under perfusion also showed cells predominantly around the edges of the tissue, where cells were initially introduced. However, there were signs of cells located around the perineurium and within the endoneurium of the nerve fascicles. This showed that perfusion may play an important role in cellular migration following introduction.

In an attempt to introduce Schwann cells throughout the entire scaffold, the seeding technique was modified, by injecting cells ($1x10^6$/mL) to the proximal and distal ends using a syringe pump. Schwann cells were also pre-labelled with CellTracker for tracking their location within the scaffold. Under static conditions there was evidence of Schwann cells within the proximal and middle sections; however, no cells were observed at the distal end. The lack of cells in the distal end may be due to a low number of cells being delivered to the distal end or the cell suspension leaking from the nerve end. In the perfused system the cells were observed to be present throughout the entire scaffold, which suggested that perfusion and migration were associated.

After demonstrating the efficacy of using a syringe pump to seed RN22 Schwann cells throughout the scaffold, normal primary rat Schwann cells were then employed using similar conditions. A slight alteration was made where the Schwann cells were resuspended in a smaller volume ($1x10^6$ / 50 µL). As the

previous problem with this technique was the extended time it took to seed the cells into the scaffold which may have caused cell death during the seeding process. Data showed that cells were present throughout the scaffold under both static and perfused conditions. However, under both conditions, there was not a homogeneous distribution of cells and the majority were located within the proximal and middle sections.

A study by Jesuraj et al. (2011) established a systematic approach to seeding Schwann cells in cold preserved acellular grafts. The authors found that a sub-epineurial injection with a Hamilton syringe resulted in the highest viability of cells, and the least damage to the epineurium (Jesuraj, Santosa et al. 2011). To inject Schwann cells underneath the epineurium a needle should be used the dimensions of which are small enough to penetrate the epineurium connective tissue, and large enough to enable Schwann cells to pass through without damage. The average size of a Schwann cell can be assumed as approximately <50 µm in diameter, and therefore a 26-gauge needle (0.41 mm outer diameter / 0.26 mm inner diameter / 0.10 mm wall thickness) was selected.

Prior to commencing the tissue experiment, Schwann cells were injected into 24 well plates using a Hamilton syringe and cultured for five days to establish if cell damage arose. Previous cell injection procedures have resulted in reduced cell viability, with viabilities as low as 1 %–32 % post-transplantation (Zhang, Methot et al. 2001).

A viability assay was subsequently undertaken on the injected cells and it was found that there was a significant decrease in cell viability 48 hours post injection. Research has shown that cell damage may occur during ejection because of the sheer stress forces placed upon cells during this procedure. When flowing through a needle, cells experience three types of mechanical forces, that can lead to cell disruption; a pressure drop across the cell, shearing forces attributed to linear shear flow, and stretching forces due to extensional flow (Aguado, Mulyasasmita et al. 2011). Forces at the transition point between syringe and needle can also damage cells. In a syringe-based injection system, the inner diameter of a syringe is typically larger than that of the needle, so cells experience an increase in linear velocity as they pass into the needle. This generates an extensional force that has been suggested as the main contributing factor to cell injury during injection (Amer, White et al. 2015). The cell viability had significantly increased by day five

post injection. The improved viability may be due to cellular repair mechanisms being activated, which suggests that cell recovery is possible in a favourable environment. In addition, cells may have undergone exponential growth by this time point (Amer, White et al. 2015).

Using this method, a syringe was used and Schwann cells inserted along the full length of the nerve segment underneath the epineurium. Cells were injected in equal volumes at three evenly spaced points (Walsh, Biernaskie et al. 2009; Jesuraj, Santosa et al. 2011; Jesuraj, Santosa et al. 2011; Jia, Wang et al. 2012; Fan, Yu et al. 2014). Histological analysis confirmed that the injected cells were arranged along the longitudinal acellular nerve graft, however some cells albeit in smaller quantities were also found in transverse sections. A much larger number of Schwann cells were revealed to be present in both perfused and static conditions using this method of injection with the Hamilton syringe. It was also interesting to observe through haematoxylin and eosin stained sections that the cells were located around the perineurium, as well as entering the endoneurium, akin to a native anatomy of peripheral nerve.

An MTT assay was undertaken to assess the viability of the cells within the scaffolds. The results were inconclusive as the negative controls (using decellularised scaffold) along with the cell-introduced showed high false positive readings at each time point. Evidence exists that the MTT reduction is also catalysed by a number of non-mitochondrial enzymes. It has been demonstrated that the endoplasmic reticulum (Berridge and Tan 1993), cytosol (Goodwin, Holt et al. 1996) and plasma membranes (Bernas and Dobrucki 2000) can also participate in the reduction of MTT (Bernas and Dobrucki 2002). During the decellularisation process, not all the cellular remnants such as nuclear material and cytoplasmic debris can be removed from the tissue (Crapo, Gilbert et al. 2011), with the consequent retention of released enzymes which maintain activity when bound to the extracellular proteins, and may consequently contribute to the reduction of MTT in the decellularised scaffolds. MTS and Alamar blue assays also showed similar false positive artefacts.

As an alternative, a DNA quantification assay was carried out on the recellularised tissue samples. A DNA quantification assay measures the amount of DNA present in the tissue. The amount of DNA present in each tissue was quantified; an increase in DNA within the tissue would signify an increase in cell

number. Results showed that under both static and perfused conditions the DNA content increased from day one to day three and then decreased towards day seven. The decline in cell number by day seven could be attributed to numerous factors. Previous studies have shown that when $10^6$ Schwann cells were injected only 10 % remained within the graft (Jesuraj, Santosa et al. 2011). The failure to transfer all the cells may be either due to the death of the cells post injection, or via Schwann cells leaking from grafts post injection. When 1 $x10^5$ Schwann cells were injected there was a 40 % successful transfer (Jesuraj, Santosa et al. 2011). Nonetheless previous studies with $1x10^5$ Schwann cells injected in the acellular graft had shown little effect on peripheral nerve regeneration (Fox, Schwetye et al. 2005), whilst injection with $1x10^6$ Schwann cells enhanced regeneration (Brenner, Lowe et al. 2005). Therefore, it is possible that a lower cell density may be more beneficial for the design of an investigational *in vitro* model, and a higher Schwann cell density for *in vivo* / clinical applications. Although in both static and perfused conditions there was a decrease in DNA by day 7, under perfused conditions the decrease in number was far less and more gradual than when compared under static conditions. This suggests that a controlled medium flow rate was more effective in maintaining cell viability (Sun, Norton et al. 2008). For future reference cell viability assays specifically designed for 3 D culture such as CellTiter-Glo ® which measures the amount of ATP in metabolically active cells may be a more effective way of assessing cell viability within biological tissue.

The cell seeded scaffolds were labelled using antibodies against the following Schwann cell markers: GFAP, S100β and p75 NGFR. GFAP is a major cytoskeletal component. In addition to playing a structural role, it has also been implicated in cytoskeletal reorganization, myelination maintenance and cell adhesion (Eng, Ghirnikar et al. 2000). The S100β protein stimulates cell proliferation and migration, while simultaneously inhibiting apoptosis and differentiation (Selinfreund, Barger et al. 1991). The p75 nerve growth factor receptor plays a role in Schwann cell migration and myelination during development, apoptosis, as well as axonal regeneration (Barrett and Bartlett 1994). The cell introduced scaffolds labelled positively for all three markers, under static and perfused conditions. This confirmed that the Schwann cells maintained their phenotype within the acellular nerve.

## 7.6 Conclusions

In conclusion, this study has evaluated a number of methods to seed Schwann cells into an acellular nerve scaffold, the data indicates the optimal method to be using a Hamilton syringe and injecting cells underneath the epineurium. Histological analysis using haematoxylin and eosin, DAPI and CellTracker reveal cells throughout the entire scaffold. Immunolabelling of reseeded Schwann cells within the acellular scaffold show expression of GFAP, S100β and p75. DNA quantification assay showed that Schwann cells proliferated up to day three and this started to decrease by day seven. This may be a shift from cells proliferating to differentiating, given the positive markers immunolabelled for Schwann cell differentiation.

This study also shows the potential of using the recellularised nerve graft as an *in vitro* model. Using a simple closed loop bioreactor system, the recellularised nerve grafts were subjected to perfusion to assess cell viability. The study revealed that the Schwann cells under perfusion maintained their phenotype and had a lower rate of cell death when compared to static conditions. This suggests that constant medium flow plays a positive role in cell viability.

The *in vitro* nerve model can provide a platform for further study in directing the accurate organisation of Schwann cells within an acellular nerve matrix. In addition the model can also be used to acquire a body of preliminary data on aspects including the signalling pathways activated by new molecules/drugs, (Armstrong, Wiberg et al. 2008; Magnaghi, Parducz et al. 2010; Gnavi, Blasio et al. 2014) and cell behaviour changes due to environmental alterations induced by physical agents such as magnetic fields, mechanical forces and electrical stimuli (Chafik, Bear et al. 2003; Gamboa, Gutiérrez et al. 2007; Koppes, Nordberg et al. 2013).

The use of primary cell models can be used to answer complex questions related to peripheral nerve regeneration processes, as they are the best representation of cells found in *vivo.* Therefore, the data obtained from these *in vitro* models are more likely to predict the phenomena occurring in vivo during nerve regeneration than cell line-based models (Geuna, Raimondo et al. 2015).

Furthermore the *in vitro* model can progress to the introduction of different cell types such as adipose derived stem cells (di Summa, Kalbermatten et al. 2011; Kaewkhaw, Scutt et al. 2011), genetically modified Schwann cells (Lavdas,

Franceschini et al. 2006) and macrophages (Franzen, Schoenen et al. 1998) . Alongside cells other exogenous factors such as neurotrophins can also be introduced into the nerve model, as neurotrophins such as Nerve Growth Factor (NGF) promote the growth, survival and differentiation of cells (Schmidt and Leach 2003).

The *in vitro* nerve model does provide an environment which can help reseeded primary Schwann cells mimic the cell–cell interactions and cell–ECM interactions observed *in vivo.* However, the model lacks the complex vascular systems that support tissues *in vivo* for oxygenation, nutrients, and waste removal. Cells grown in 3D culture perform these functions only by diffusion. This in turn will present a problem in maintaining cells over a long period of time in vitro. Therefore, for long term maintenance an *in vivo* environment would be more favourable for Schwann cells.

Using the combined approach of an acellular scaffold with the inclusion of cells is a valuable tool for the preliminary screening of a number of elements. The *in vitro* model permits a systematic controlled evaluation of novel acellular grafts where promising results can be studied in further detail using *in vivo* injury models. An *in vivo* study using acellular nerve grafts with / without the inclusion of primary Schwann cells is described in Chapter 8.

# Chapter 8 *In Vivo* Analysis of the Regenerative Capacity of Acellular Nerve Scaffolds

## 8.1 Introduction

When inflicted with an injury the peripheral nerve has the ability to regenerate naturally. If the nerve gap injury is less than 5-10 mm spontaneous axonal regeneration will occur. In humans nerve regeneration occurs at a rate of 3-4 mm per day after crush and 2-3 mm per day if the nerve is transected (Stoll and Müller 1999). If, however, the gap size is greater than 5-10 mm regeneration is infrequent, misdirected and often results in poor functional recovery (Pfister, Gordon et al. 2011). For longer nerve gaps the current "gold standard" treatment is autologous grafting; using donor sensory nerve tissue harvested from another site in the body to replace the injured tissue. Limitations using this method include donor site morbidity and chronic pain the autologous clinical functional recovery rates is only 80 % (Schmidt and Leach 2003). It is commonly accepted that physical guidance of axons is a vital component of nerve repair and regeneration. Current research focuses on "entubulating" opposing nerve stumps of the severed nerve in an autograft tube known as a Nerve Guidance Conduit (NGC) (Kehoe, Zhang et al. 2011). These conduits can be used for defects of 20 mm - 25 mm and eliminates the need to graft.

The Food and Drug Administration (FDA) and Conformit Europe (CE) have approved a relatively small number of guidance conduits for clinical repair of peripheral nerves. In clinical trials, NGCs have been reported to have a comparable efficacy to autologous grafting in defects up to 20 mm (Meek and Coert 2008). However, limitations of conduits include the production of acidic degradation products and high rates of degradation which have been observed in Neurotube®; high rigidity reported in Neurolac®, and caused needle breakages when suturing the NGC in place. Also, the slow degradation rate of NeuraGen® (up to 48 months *in vivo*) can lead to nerve compression (Meek and Coert 2008). For nerve defects greater than 30 mm, autografts are still considered as the gold standard, as NGCs are not considered as effective for these gap sizes.

It has been hypothesised that the limited efficacy of NGCs in promoting nerve regeneration over longer distances is due to the lack of a suitable surface topography (Spivey, Khaing et al. 2012). As previously mentioned, the nerve basal

lamina and ECM components such as collagen, laminin and fibronectin play important roles in both the development and repair of the PNS, including neurite formation (Davis, Varon et al. 1985, Spivey, Khaing et al. 2012). The ECM has an ability to influence cell morphology, phenotype and function through cell-substrate interactions, as well as promoting cell-cell interactions. The basal lamina forms a close relationship with the regenerating nerve fibres, and a study by Ide et al. (1983) concluded that the basal lamina provides a pathway not only for the initial axonal elongation but also for the maintenance and maturation of regenerating axons (Ide, Tohyama et al. 1983).

Chapters four and five have described in detail the creation of acellular nerve grafts using low concentration SDS, hypotonic buffers and nuclease enzymes. These grafts replicated the nerve architecture at a subcellular level as well as retaining important ECM components. AxoGen is the only company to have a clinically approved acellular human nerve graft on the market, Avance® Nerve Graft. Current research suggests that Avance® Nerve Graft implants increases reinnervation and improves clinical outcome when compared to commercial available NGCs (Whitlock, Tuffaha et al. 2009). A multicentre study demonstrated that out of all the commercially available nerve products the Avance® Nerve Graft was the only one that had the ability to support repair in motor, sensory and mixed nerve types, as well as having the ability to repair both short (5 - 14 mm), medium (15 - 29 mm) and long (30 - 50 mm) nerve gaps, making it comparable to an autograft (Brooks, Weber et al. 2012). Despite success, the Avance® Nerve Graft does have limitations, in particular the supply of human nerves for decellularisation, the risk of product supply and disease transmission, which limits clinical potential (Zilic, Garner et al. 2015).

Previous *in vivo* studies have shown that inclusion of Schwann cells into acellular grafts have shown improved regeneration. In these studies, significant regeneration was observed in terms of structural and functional repair as well as the formation of bands of Bünger (Hess, Brenner et al. 2007, Hu, Zhu et al. 2007, Zhang, Luo et al. 2010). This chapter describes a three week *in vivo* animal study using acellular and reseeded acellular porcine nerve grafts in an 11mm rat sciatic nerve gap model. Acellular nerves were decellularised using a combination of chemical and enzymatic treatments, based on the process developed by Wilshaw et al. (2012) and modified for porcine peripheral nerve (Zilic, Wilshaw et al. 2016) .

Acellular nerves were then recellularised with primary rat Schwann cells as described in Section 7.4.4.2.

## 8.2 Aims and objectives

**Aim:**

To evaluate the host cellular response to acellular and recellularised acellular sural nerves as a graft in a rat sciatic nerve gap model.

**Objectives:**

- Implant six acellular, nerve grafts versus six acellular nerve grafts reseeded with primary Schwann cells, into a 11 mm rat sciatic nerve injury model

- Use Micro CT to analyse the internal structure of the autologous and acellular nerve grafts post implantation

- Immunolabel grafts with axonal marker PGP9.5 to analyse the regenerating axons within acellular and recellularised nerve grafts

## 8.2 Methods

### 8.2.1 Sural nerve harvesting and decellularisation

Three sural nerves were obtained from large white Yorkshire pigs (24 - 26 weeks old) within 24 hours of slaughter. Each sural nerve was dissected by a longitudinal incision made from the popliteal fossa along the posterior midline and towards the posterior-inferior aspect of the lateral malleolus. Excess fat and connective tissue was removed from the nerve samples and tissues washed three times in PBS containing 0.1 % (w/v) EDTA to remove excess blood. Each individual sural nerve was cut into 10 cm segments and stored at -80 °C on PBS moistened filter paper for future use. The diameter of the sural nerve was approximately 1.4 mm. From each individual sural nerve 4 x 2 cm nerve segments were cut from the proximal segment of each nerve, giving a total of 12 nerve segments altogether. The sural nerve segments were then decellularised according to the methodology described in in Section 6.3 (Method 7).

### 8.2.2 Reseeding primary Schwann cells into acellular graft

Six of the acellular scaffolds were incubated with DMEM with 10% (v/v) FCS overnight before being reseeded with primary rat Schwann cells the following day. A suspension of $1x10^6$ cells suspended in 20 µL of media was injected into the epineurium of the sural nerve using a Hamilton syringe as described in Section 7.4.4.2. The recellularised scaffolds were allowed to adhere overnight at 37° C /5% $CO_2$ before being implanted the following day.

### 8.2.3 *In vivo* surgical procedure

The *in vivo* work was carried out collaboratively with Dr James Phillips, UCL, UK. All the surgery was carried out by Dr James Phillips under Home Office approved procedures (project licence PPL 70/7557 to Dr James Phillips) and the rats were sacrificed according to a Schedule 1 method. All work was conducted in keeping with The Animals Scientific Procedures Act (1986), United Kingdom. Young, adult female Wistar rats (weighing 200 - 230 g) were anesthetized by inhalational of isofluorane (Abbott Laboratories). The left sciatic nerve of the rat was exposed and a section was removed to leave an 11 mm gap. Under an operating microscope (Zeiss), the proximal and distal nerve stumps of the transected nerve were secured within the 11 mm long, porcine acellular or recellularised scaffold (n = 6) using

two epineurial sutures (10-0 Ethilon) at the proximal end and one at the distal end. The muscle was closed using 3-0 sutures and the skin was closed using staples with antibiotic wound powder generously applied around the stapled area. The rats were returned to normal housing for three weeks postoperatively. Autologous grafting (n = 6); 11 mm of sciatic nerve was excised, reversed, and sutured with 10-0 Ethilon epineurial sutures. Each animal was housed in normal housing for three weeks after surgery and exposed to 12-hour light/ dark cycles, with food and water. After three weeks, all animals were euthanized and each scaffold harvested together with a 2 mm excess length of nerve both proximally and distally. Paraformaldehyde (3.7 %; w/v) was used to fix the tissue for 24 hours. Tissues were processed and wax embedded as described in Section 2.2.3. Paraffin embedded tissue sections of 15 μm were prepared longitudinally on slides for analysis.

### 8.2.4 Micro CT of nerve tissues

Micro-computed tomography or "micro-CT" can be used to image the internal structures of 3D specimens at a high resolution, in a non-destructive manner. The micro-CT uses a micro-focus x-ray source, which illuminates the object and a planar x-ray detector collects magnified projection images. Whilst the object rotates hundreds of angular views are acquired and the computer synthesises a stack of virtual cross section slices through the object. Using the cross section slices it is then possible to interpolate sections along different planes to examine the internal structure. Micro CT of nerve tissues was carried out by Dr Adam Glen, University of Sheffield, UK. Micro CT was performed on a Skyscan 1272 (Bruker, Belgium) by securing samples in a polypropylene tube and scanned at 50 kV/200 μA (0.7° increments over 360°). Images were reconstructed, analysed and rendered with Nrecon (v 1.6.9.8 Bruker, Belgium), CT analyzer (v 1.14.4.1 Bruker, Belgium) and CTvol (v2.2.3.0 Bruker, Belgium).

### 8.2.5 Immunolabelling nerve tissue

Prior to staining, paraffin embedded samples were dewaxed, dehydrated and rehydrated as described in Section 2.2.3. The tissue sections were then permeabilsed in a 0.1 % (v/v) Triton X-100/PBS solution for one hour at room temperature. After three washes in PBS (five minutes each wash) samples were incubated with 7.5 % (w/v) BSA/PBS blocking serum for one hour at room temperature. Sections were then incubated with the primary antibody, axonal marker PGP9.5 (rabbit polyclonal 1:200 dilution) at 4 °C overnight. The following day, samples were washed twice in PBS for five minutes and incubated with a FITC-conjugated secondary antibody (anti-rabbit IgG 1:100 dilution) for one hour in the dark at room temperature. After further washes in PBS, samples were counterstained with 300 nM DAPI in PBS and incubated for twenty minutes in the dark at room temperature. Sections are then washed three times with PBS for five minutes and imaged using a Zeiss LSM510 META upright confocal microscope (xenon arc lamp to excite FITC ($\lambda_{ex}$ = 495 nm / $\lambda_{em}$ = 515 nm).

Images of the samples were "stitched together" to create a full length image of the nerve graft using Photoshop. The distance of the regenerating axons from the proximal to the distal end of the nerve were measured and quantified using Image J.

## 8.3 Results

### 8.3.1 Macroscopic observation of xenografts

At the time of tissue harvest, grafts were found to be intact in all groups, and there was no visual evidence of infection, inflammation, or problematic scar tissue. Macroscopically, autografts resembled an intact nerve; however, the porcine grafts had noticeably reduced in size and appeared translucent in colour (Figure 8.1).

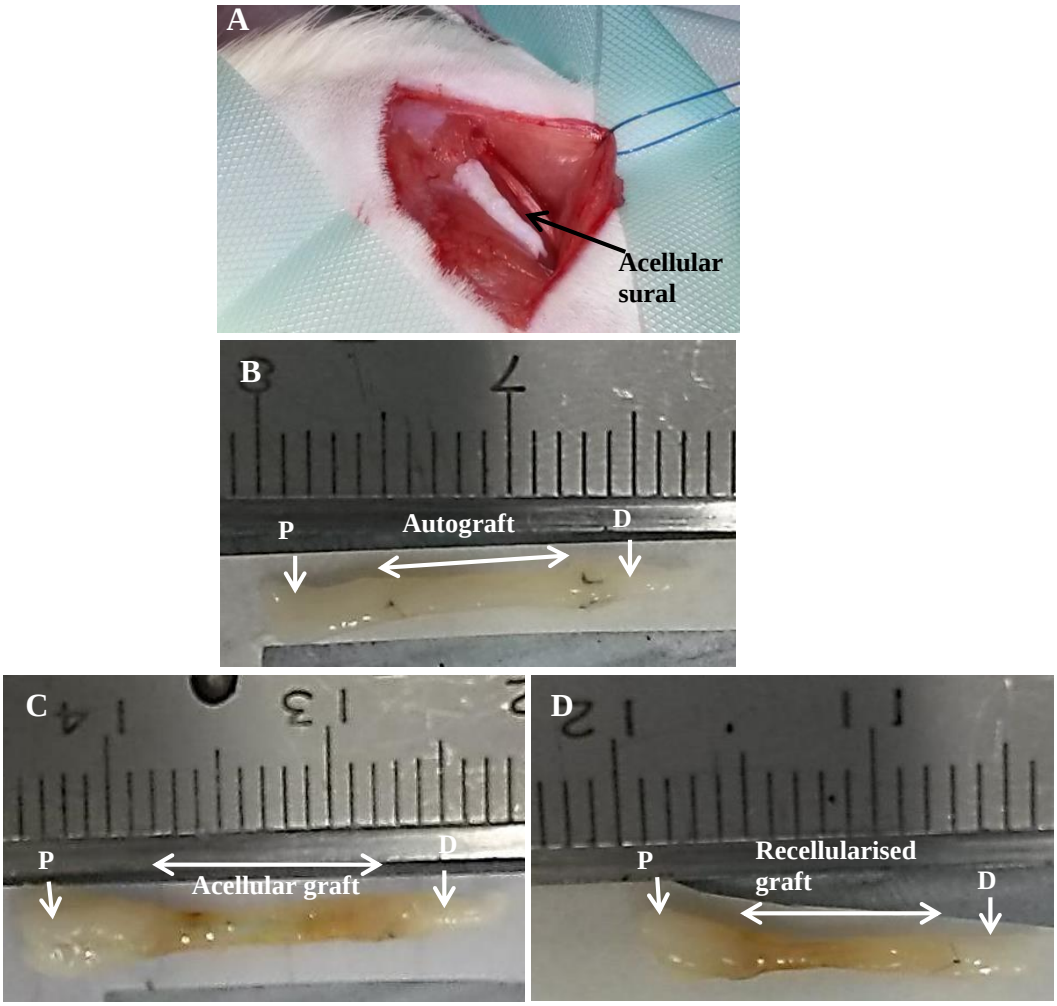


**Figure 8.1. Macroscopic evaluation of nerve grafts implanted in a rat sciatic nerve injury model.** A; bridge-grafted acellular sural nerve. B-DD; autograft, acellular and recellularised nerve three weeks after implantation. The autograft resembles an intact nerve; however, the acellular and recellularised nerve appeared to be reduced in size and translucent in colour. P = proximal; D = distal.

### 8.3.2 Micro CT of grafts

Micro-CT images of explanted nerve samples revealed well defined structures of the nerve fascicles at the proximal ends of the samples, and to a lesser extent in the distal end (Figures 8.2 and 8.3). The micro-CT of autologous nerve showed a homogenous and intact structure (Figure 8.2) whilst the acellular nerve showed evidence of a disordered structure with what reappeared to be differing tissue density (Figure 8.3).

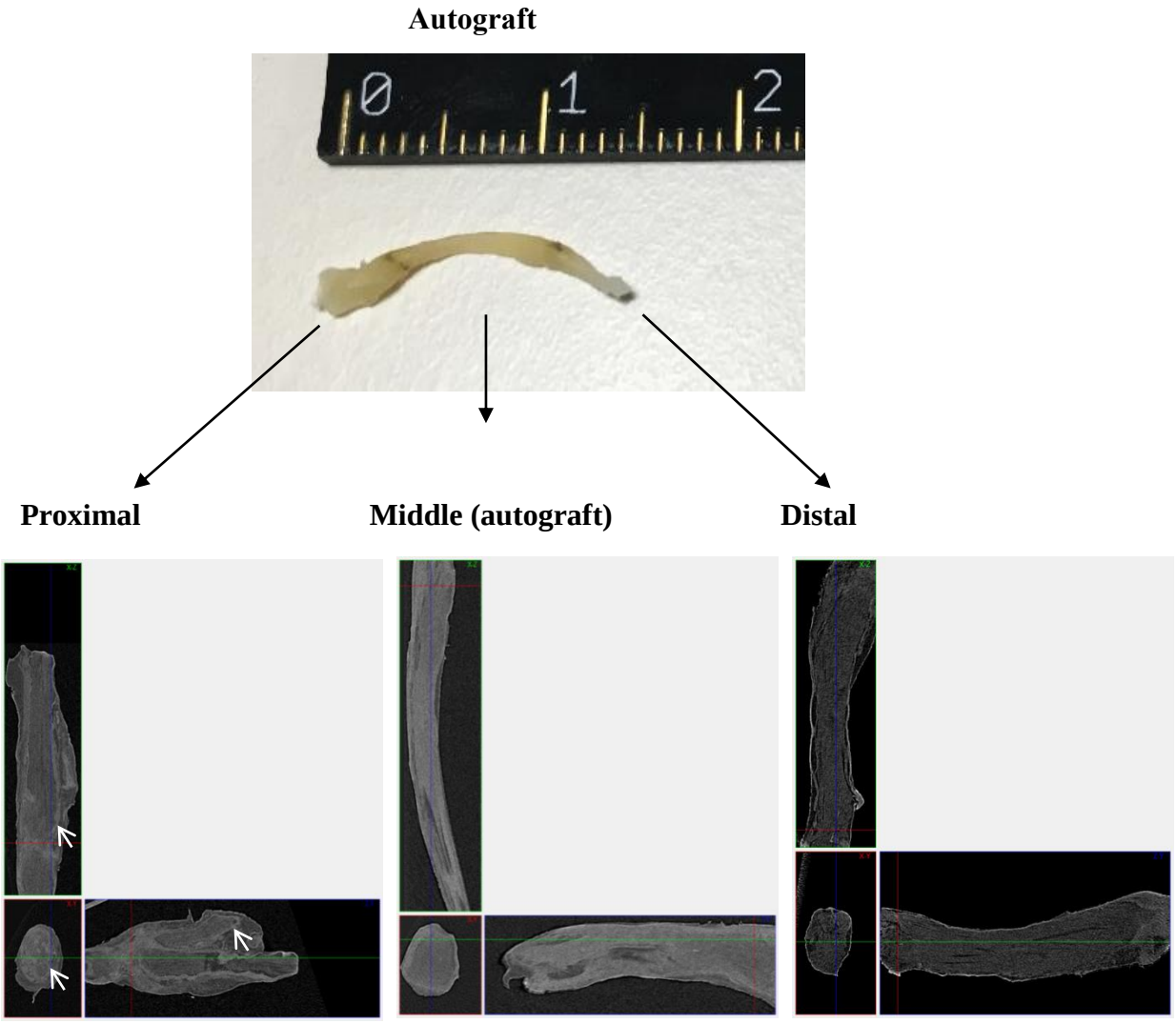


**Figure 8.2 Micro CT images of sciatic nerve autograft post implantation.** Black arrows indicate the approximate locations of scans relative to position within the sciatic nerve. The coordinate planes are the XZ –plane (green), XY-plane (red) and ZY-plane (blue) which displays longitudinal and transverse sections of the nerve. The proximal ends show well-defined and clear macro structures of the nerve fascicles, as indicated by the white arrows. There was little structure observed in the central portion, where the autograft was situated and the distal end of the nerve.

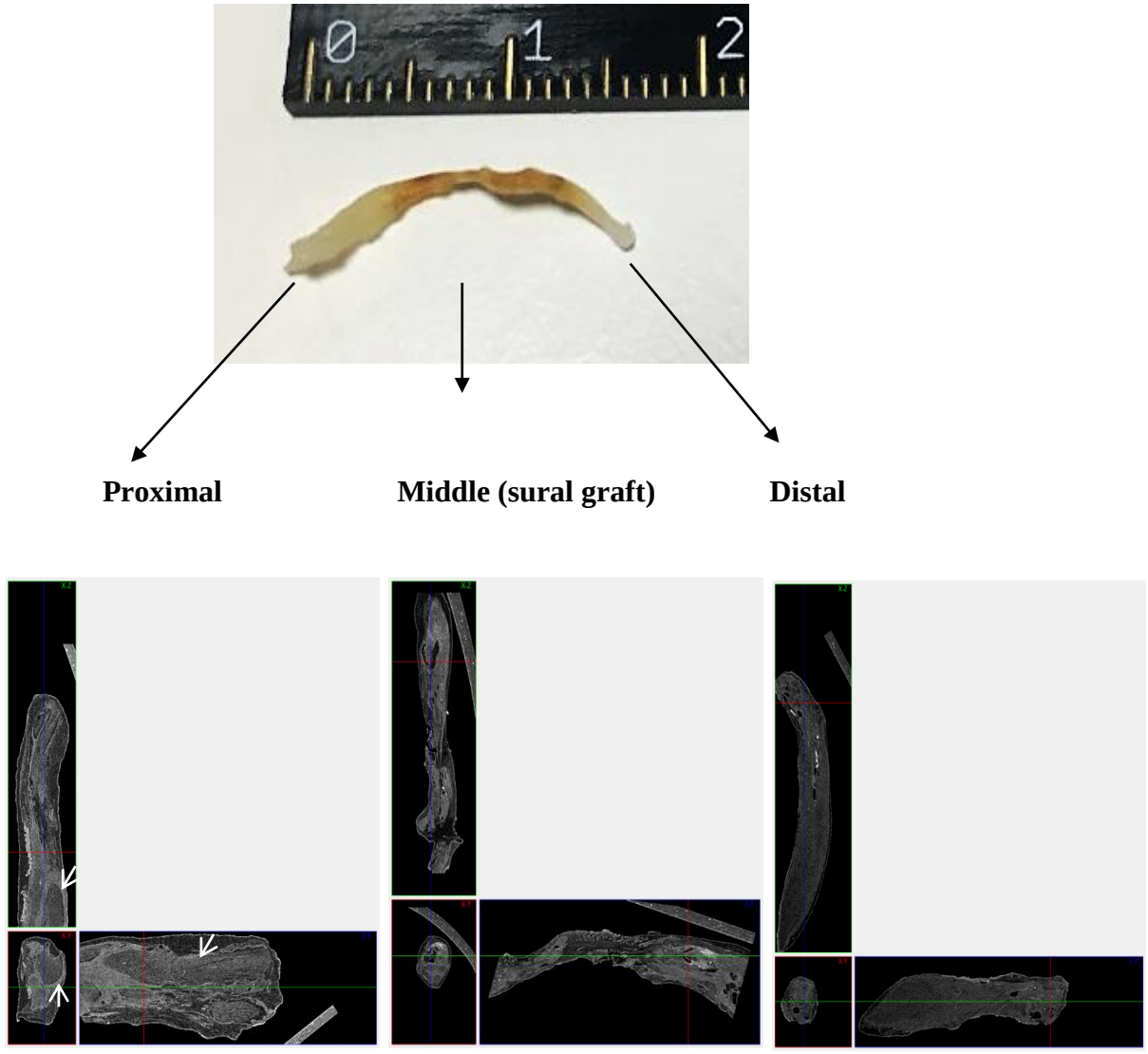


**Figure 8.3 Micro CT images of acellular sural nerve post implantation.** Black arrows indicate the approximate locations of scans relative to position within the sciatic nerve. The coordinate planes are the XZ–plane (green), XY-plane (red) and ZY-plane (blue) which displays longitudinal and transverse sections of the nerve. The proximal ends show well-defined and clear macro structures of the nerve fascicles, as indicated by the white arrows. A disordered structure is observed in the central portion, where the acellular graft is situated and little structure is observed at the distal end of the nerve.

### 8.3.3 Immunolabelling nerve grafts with PGP9.5

The autologous, acellular and reseeded grafts were labelled for PGP9.5, an axonal marker to investigate if the regenerating axons had bridged the injured gap. The axon distribution within the autologous graft was found to be evenly spread throughout the entire graft (Figure 8.4 A). Acellular and recellularised nerve grafts revealed the presence of regenerating axons; however, the axon distribution was not as continuous as observed in the autologous graft (Figure 8.4 B). In some of the allogeneic grafts only the proximal and central part of the grafts were filled with axons; fewer axons were present in the distal part of the grafts (Figure 8.4 C).

Quantification of the regenerating axons from the proximal end of the nerve to the tip of the PGP9.5 immunolabelled axons demonstrated that nerve regeneration was significantly greater in the autologous grafts with an average regenerating distance of 14 mm. The axon regeneration distance within acellular and recellularised nerve grafts were similar. The acellular nerve had a slightly greater regenerating distance of 8.5 mm whilst the recellularised graft had an average of 7.1mm. There was no significant difference between the two porcine grafts (Figure 8.4).

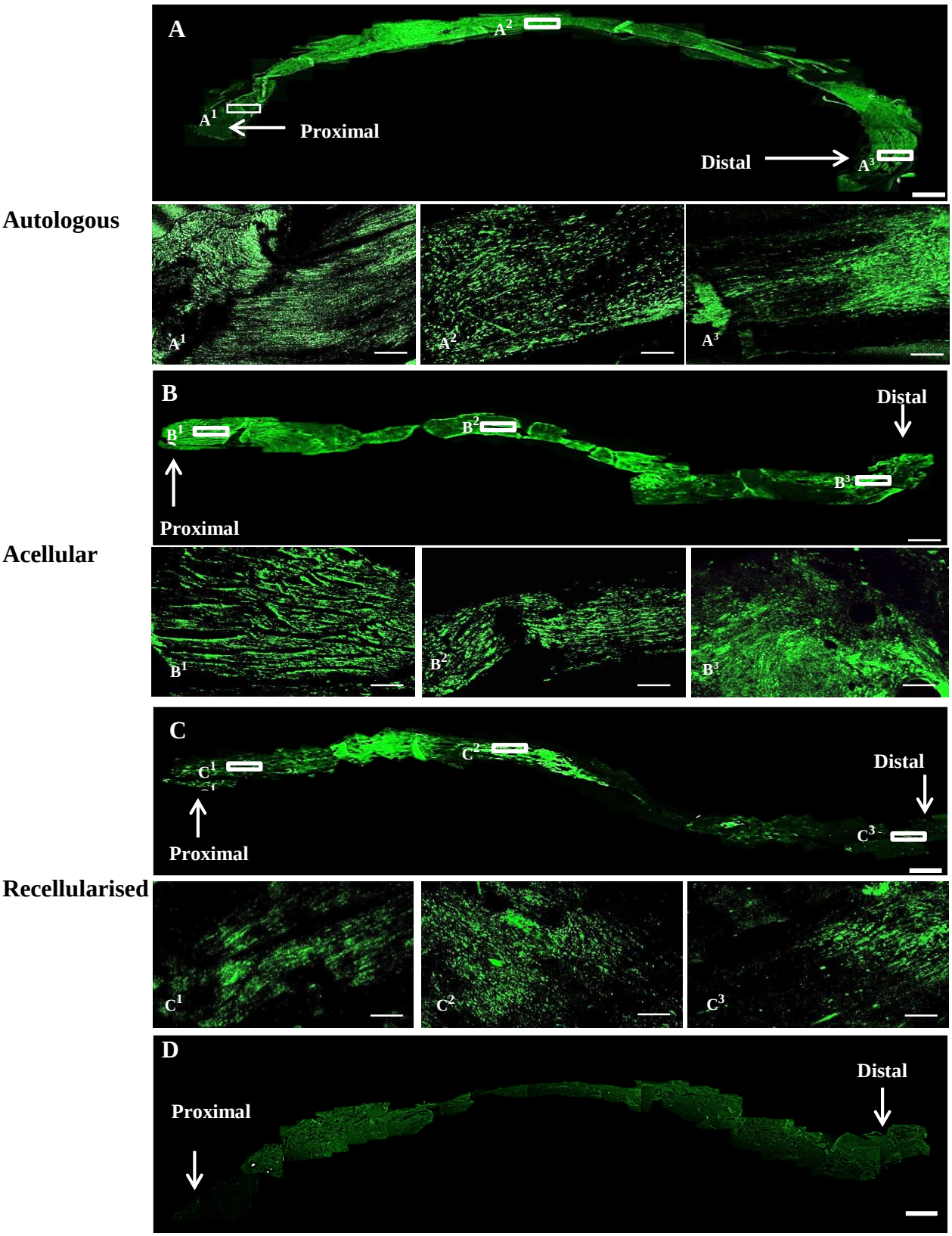


**Figure 8.4. Axonal immunolabelling of nerve grafts.** Overlapping (tiled) images showing the increased area of PGP9.5 label of regenerating nerves in acellular (B) and reseeded (C) sural grafts compared with autologous grafts (A). The images showed an increased area of PGP9.5 labelled regenerating axons in the autologous, acellular and recellularised scaffolds. (D) Nerve labelled with secondary antibody only to illustrate specificity. $A^1$–$A^3$, $B^1$–$B^3$ and $C^1$–$C^3$are magnifications of the corresponding boxed areas in A, B and C, respectively. Scale bar at 1 mm for A-D; scale bar at 100 µm for $A_1$-$C_1$

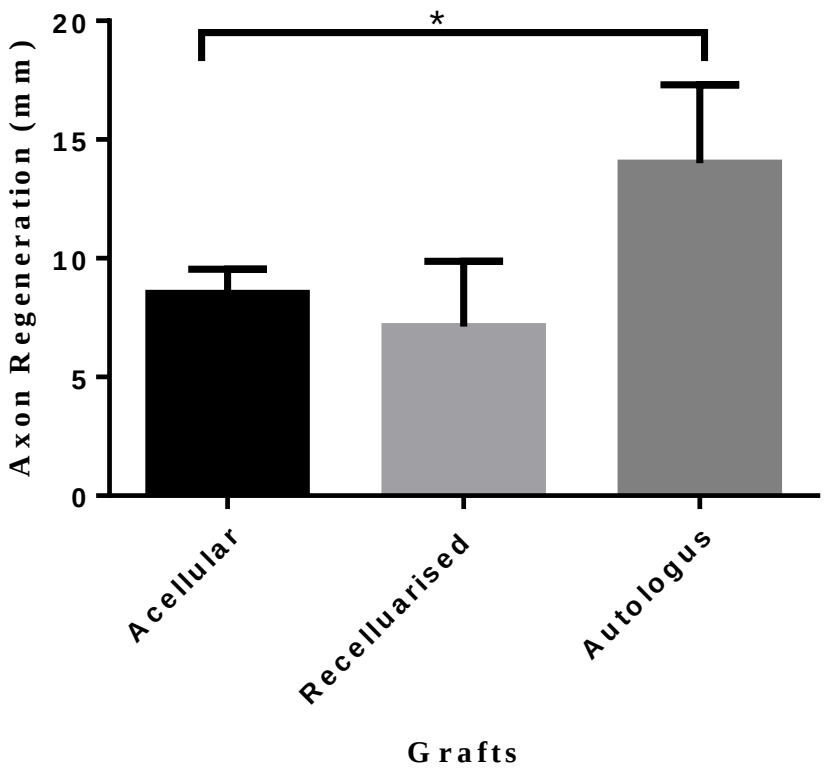


**Figure 8.5. Quantification of axonal regeneration within nerve grafts.** Measurement of regenerating axons from proximal section to the furthest PGP9.5 tip. The autologous nerve had significantly higher axon regeneration with a mean distance of 14 mm (n=5) when compared to the acellular and recellularised grafts. The acellular grafts had a mean distance of 8.5 mm (n=4) and recellularised grafts had a mean distance of 7.1 mm (n =4). Data was analysed using the unpaired Students *t*-test and is presented as the mean ± 95 % C.I ($p<0.01$*)

## 8.4 Discussion

Current research suggests that acellular grafts can increases reinnervation and improves clinical outcome when compared to commercial available NGCs (Whitlock, Tuffaha et al. 2009). Studies have also demonstrated that inclusion of Schwann cells into acellular grafts have shown improved regeneration (Hess, Brenner et al. 2007, Hu, Zhu et al. 2007, Zhang, Luo et al. 2010). A three week *in vivo* study was carried out using acellular and recellularised porcine nerve grafts to repair an 11 mm nerve gap in a rat sciatic injury model. The internal structures of the grafts post implantation were analysed using micro CT. The grafts were also stained with the axonal marker PGP 9.5 to assess the axonal regeneration throughout the nerve grafts.

Post implantation it was noted that the physical appearance of the porcine nerve graft had altered. Visually the grafts did not appear to have a scar tissue formation and no visible inflammation was detected in the surrounding tissues post implantation. It may be hypothesised that grafts had undergone remodelling, appearing smaller and translucent in colour. Similar findings were also reported in a nerve study conducted by Wang et al. (2015), where rat sciatic nerves and rabbit median nerves were decellularised using sodium dodecyl sulphate (SDS) and Triton X-100 and implanted in male Wistar rats (Wang, Itoh et al. 2015). Analysis of the grafts internal structure through micro CT further demonstrated that the acellular graft had undergone remodelling. The internal structure of explanted acellular grafts appeared disordered and inhomogeneous when compared to autografts. To further determine evidence of remodelling histological examination of the grafts could be used to determine the composition of the tissue. The samples could be labelled for the presence of Schwann cells, which are known to help aid nerve regeneration (Hess, Brenner et al. 2007, Hu, Zhu et al. 2007, Zhang, Luo et al. 2010) as well as important ECM components including such as collagen, laminin and fibronectin.

The remodelling process observed is due to the hosts' response to the grafts. Biological scaffolds are capable of provoking either a constructive (so called M2) or pro-inflammatory (M1) cellular response mediated largely by macrophages (Badylak 2014). Constructive remodelling occurs when a biomaterial is gradually replaced by functional tissue whilst a dense scar tissue formation is associated with a pro-inflammatory macrophage and cellular response.

To determine the type and the extent of remodelling within the grafts the levels of the cell-mediated immune response and matrix remodelling components can also be investigated. The tissue can be stained for cells such as neutrophils, lymphocytes ($CD4^+$ T and $CD8^+$ T cells) and macrophages (Hudson, Zawko et al. 2004, Zhang, Luo et al. 2010, Badylak 2014). Furthermore, growth factors such as transforming growth factor-β and matrix metalloproteinases contribute to matrix turnover. These components actively direct cells to increase matrix production, initiate angiogenesis and vasculogenesis, and migrate and proliferate to where they are needed (Hodde and Hiles 2007).

The present data indicated that acellular and recellularised grafts can promote peripheral axonal regeneration. Longitudinal sections of the porcine grafts demonstrated that PGP9.5 positive regenerated axons displayed well-ordered arrangements in the porcine sural grafts, which correlates with previous studies that have studied axonal regeneration in nerve repairs (Wang, Pan et al. 2014, Mobasseri, Faroni et al. 2015).

Quantitative analysis revealed that overall, the autologous graft was significantly better in promoting regeneration over a greater distance with evidence of re-establishment of neural connections from the proximal to the distal end of the nerve. Whilst the acellular grafts did promote axonal regeneration throughout the entire graft in some of the grafts, overall in both the acellular and acellular seeded grafts there were a lower proportion of axons observed in the distal end when compared to the autologous graft. A reason for this may be due to residing chondroitin sulphate proteoglycans (CSPGs) within the acellular grafts. CSPGs can inhibit axonal growth and negate the growth-promoting activities of extracellular matrix components such as laminin (Muir, Engvall et al. 1989, Zuo, Hernandez et al. 1998). Studies suggest that CSPG degrading enzymes such as metalloproteinases or chondroitinase can help restore the growth promoting properties of laminin within a nerve (Zuo, Ferguson et al. 1998, Ferguson and Muir 2000, Krekoski, Neubauer et al. 2001). An *in vivo* study by Krekoski et al.(2001) discovered that acellular nerve grafts treated with chondroitinase improved the ability of axons to navigate across the host–graft interface and significantly increases the number of axons growing into acellular nerve grafts(Krekoski, Neubauer et al. 2001). This enzyme degradation method has also been applied to

Avance® Nerve Graft, the only commercially available acellular graft (Moore, MacEwan et al. 2011).

Several studies have also found the use of predegenerated nerves in rat models have shown superiority over autologous nerve graft treatments and a reduced delay period; the time interval before the axons enter the graft while the rate of regeneration is unaffected (Kerns, Danielsen et al. 1993, Danielsen, Kerns et al. 1994, Danielsen, Kerns et al. 1995, Frerichs, Fansa et al. 2002). A study by Danielsen et al. (1995) also demonstrated that pre-degenerated acellular nerve grafts had a significantly shorter initial delay period (2.7 days) when compared with freshly made acellular nerve grafts (9.5 days).

The mechanism behind this effect is not known. However, it is assumed that during the pre-degeneration period Schwann cells proliferate and the distal nerve stump, which is later to be used as the source for the pre-degenerated nerve graft, is invaded by inflammatory cells (macrophages). During Wallerian degeneration, these cells together with the Schwann cells interact to produce and release a variety of factors which influence regeneration and stimulate axonal growth, including neurotrophic factors such as nerve growth factor (NGF). Furthermore Schwann cells also produce basal lamina components, such as collagen IV and laminin, which has a strong neurite-promoting effect(Davis, Varon et al. 1985). Together, all these products change the composition and structure of the basal lamina and form endoneurial tubes (bands of Büngner). The basal lamina and bands of Büngner then creates a pathway for the growth cone tips of the severed axons (Davis, Varon et al. 1985, Kerns, Danielsen et al. 1993). Therefore, at the time of grafting, many of these changes have already taken place in the pre-degenerated nerve while they are just beginning in the non-degenerated nerve graft.

There was no significant difference between the axonal regeneration observed in acellular or recellularised. Previous studies using similar gap sized models have demonstrated little effect of adding Schwann cells to acellular graft material. A reason for this may be because migrating Schwann cells from the host stumps are able to cross such short distances and provide sufficient assistance to regenerating axons despite the addition of exogenous cells (Frerichs, Fansa et al. 2002, Fox, Schwetye et al. 2005). When Schwann cells migrate over long distances, such as in the case of critical gap models (greater than 15 mm) nerve regeneration fails. This suggests that cell supplementation of acellular grafts may be clinically

beneficial for large gaps, rather than those with adequate host Schwann cell migration (Nadim, Anderson et al. 1990). As a further experiment it would also be of interest to carry out an experiment on autologous rat nerve versus acellular rat nerve as a comparison to determine whether cells play an important role in the nerve regeneration process.

Other reasons for lack of axonal regeneration observed in the porcine grafts may have been due to the processing conditions of the nerves and the methodological assessment of nerve regeneration post implantation. Solutions used in the decellularisation process such as SDS detergent, are known to be cytotoxic (Newby, Barr et al. 2000). If the solutions were not removed efficiently it may have caused cell death to surrounding cells *in vivo* as well as the reseeded cells within the grafts. Labelling the grafts with PGP 9.5 to identify regenerating nerve fibres may not have the greatest of accuracy in demonstrating regenerating nerve fibres. A lack of time frame for loss of PGP 9.5 antigenicity in degenerating axons may arise to false positive PGP 9.5 staining as observed in the distal ends of the nerves. To overcome this a control would be needed to demonstrate that PGP 9.5 labelling is absent if axons are prevented from regenerating. For future work other forms of nerve regeneration assessment such as walking track analysis (Hare, Evans et al. 1992) for longer term *in vivo* studies or the use of thy-1-YFP-H mice to enable visual analysis of axons regenerating through a nerve graft (Feng, Mellor et al. 2000, Harding, Christmas et al. 2014) may also prove beneficial.

For future work other strategies to improve nerve regeneration may also be considered. These include the use of pharmacologic agents, immune system modulators and enhancing factors (Lee and Wolfe 2000). Pharmacologic agents such as gangliosides and forskolin which are neurotrophic and neuritogenic and work on a molecular level to alter nerve regeneration (Horowitz 1989, Klein, Kilmer et al. 1989). Immune system modulators can also be implemented to decrease fibrosis and histiocytic responses to help promote neurite growth (Lee and Wolfe 2000). Additionally, other enhancing factors such as neurotrophins can also be introduced alongside Schwann cells. Neurotrophins such as Nerve Growth Factor are known to promote growth and survival of cells (Schmidt and Leach 2003).

## 8.5 Conclusion

In this present study acellular grafts were shown to promote axon regeneration across a 11 mm nerve gap injury. However, the outcome of the acellular graft was not as good as that of an autologous graft. Previous studies have suggested that the presence of CSPGs, a known inhibitor of axon growth may have impeded the axonal growth. Therefore, enzymatic treatment of the acellular graft with chondroitinase may be beneficial in enhancing axonal growth within the graft. Nonetheless, acellular porcine peripheral nerve grafts with or without seeded Schwann cells hold significant therapeutic potential as a replacement for autologous treatment in peripheral nerve repair.

# Chapter 9 General Discussion

The peripheral nervous system (PNS) is comprised of a vast network of spinal and cranial nerves that are linked to the brain and the spinal cord. The function of the PNS is to integrate various bodily processes and reactions of the organism to its environment (Schmidt and Leach 2003). When damaged the microenvironment surrounding the injury site in the PNS is permissive to axonal regeneration. Over relatively short distances (less than 5 mm), axons can spontaneously regenerate (Rangappa, Romero et al. 2000). Nevertheless if the nerve is transacted and the distance between injury and target is long (greater than 5-10 mm) the clinical, functional recovery is poor (Pfister, Gordon et al. 2011). Several hundred thousand nerve injuries occur worldwide each year, with over 300,000 cases reported annually in Europe (Mohanna, Young et al. 2003). Nevertheless, despite recent advances peripheral nerve injury remains a critical clinical issue with over 50,000 procedures performed annually to repair damaged nerves (Noble, Munro et al. 1998). For longer nerve gaps (greater than 10 mm) the current "gold standard" treatment is autologous grafting; using donor sensory nerve tissue, which is harvested from another site in the body to replace the injured tissue. Limitations using this method include donor site morbidity and chronic pain. Focus has therefore turned to the use of nerve guide conduits (NGCs) and acellular scaffolds as an alternative to treating larger nerve defects. A small number of clinically approved natural and synthetic based NGCs have been used to treat nerve gap injuries, however they are limited to treated gaps of up to 20 mm - 25 mm (Shin, Friedrich et al. 2009). For larger gaps (greater than 20 - 25 mm) autologous nerve grafts are used. Studies comparing autograft to conduit repair of digital nerve injuries concluded that conduits were limited to defects of up to 25 mm. It was noted that the quality of recovery decreased as the gap size increased and that a third of repairs for gaps between 5 and 25 mm had a poor clinical outcome (Weber, Breidenbach et al. 2000).

One of the major reasons for the failure of NGCs to provide sufficient regeneration across larger gaps is that they lack substrate topography, which mimics the natural environment of nerve and functional biological motifs. Studies have shown that axon regeneration is more effective when presented in a surrounding that is similar to the nerves extracellular matrix (ECM) and basal

lamina (Smeal, Rabbitt et al. 2005). It is therefore hypothesised that as a prerequisite for efficient axon extension, next generation NGC's and grafts should incorporate an ECM topography.

The use of allogeneic or xenogeneic nerve tissue may provide an ECM that mimics the native nerve as well as offering the potential for clinically relevant diameter, length and motor versus sensory specificity (Moore, MacEwan et al. 2011). Such grafts contain an endoneurial microstructure, which provides the same level of guidance and regenerative support as nerve autografts. The immunogenic components of a tissue can be removed through a process called decellularisation, producing a non-immunogenic acellular tissue scaffold. Acellular grafts have been shown to retain the 3D structure and ECM components of the native tissue; such a graft may be used clinically without eliciting an adverse immune response. ECM components are generally conserved amongst species and are tolerated well by recipients in the absence of immunogenic cellular components.

The aim of this thesis was to investigate whether a decellularised porcine peripheral nerve would have clinical utility as a nerve graft. Studies have shown porcine nerves to be anatomically similar to human nerves (Zilic, Garner et al. 2015). Sciatic branches (peroneal and tibial) were chosen as the predominant nerves to be used throughout the study due to availability and ease of procurement. Sural nerves were used for the *in vivo* study due to their similar dimensions to the rat sciatic nerve model.

Once decellularised the acellular nerve grafts were studied as an *in vitro* nerve model, as a basis for examining perfused flow within the tissue for introducing Schwann cells. The long-term goal of this work is to translate the *in vitro* nerve model for use in the clinic as a nerve graft to help repair critical nerve gap injuries (greater than 20 mm).

During the course of this study porcine peripheral nerves, located in the lower limb were successfully identified and characterised. The study demonstrated that porcine nerves were comparable to human nerves in terms of anatomical structure and size, and therefore had the potential to be used as grafts for clinical use. Subsequently a decellularisation process was developed, using a combination of chemical and enzymatic treatments, based on the process developed by Wilshaw et al (2012) and modified for porcine peripheral nerve (Zilic, Wilshaw et al. 2016). This process removed all host cells from the porcine peripheral nerves with

minimum effect on the histioarchitecture. Histological characterisation revealed retention of the nerve fascicles, along with its connective tissues. The DNA reduction (by approximately 95 %) was comparable to the two most reported detergent based decellularisation procedures for peripheral nerves, the Sondell method (Sondell, Lundborg et al. 1998) and the Hudson method (Hudson, Liu et al. 2004).

Following decellularisation, the acellular nerves were assessed in terms of their retention of key ECM components, *in vitro* biocompatibility and mechanical integrity. The decellularisation process can alter the ECM composition as well as the components of the nerve. The solutions used in the process such as SDS have been associated with ultrastructure disruption and GAG depletion (Kasimir, Rieder et al. 2003, Gilbert, Sellaro et al. 2006, Ott, Clippinger et al. 2010), whilst peracetic acid treatment has been shown to disrupt the collagen structure (Lomas, Jennings et al. 2004). It is therefore important to retain key ECM components and structure so that the acellular scaffold can provide a suitable microenvironment for cellular growth and nerve regeneration. Characterisation of the nerve ECM and basal lamina demonstrated retention of important structural components such as collagen, laminin and fibronectin, unlike other nerve decellularisation methods which have been known to fracture and damage the basal lamina (Ide, Tohyama et al. 1998, Sondell, Lundborg et al. 1998) and decrease the laminin and fibronectin content (Grauss, Hazekamp et al. 2005).

The presence of an intact basal lamina and ECM components within acellular nerve grafts have been shown to contribute to their enhanced regenerating capacity to support axonal growth (Hudson, Liu et al. 2004, Whitlock, Tuffaha et al. 2009). The importance of an intact basal lamina is further highlighted by the development of Avance ® Nerve Graft. This acellular graft with an intact basal lamina surpasses all the other commercially available NGCs in terms of nerve regeneration (Whitlock, Tuffaha et al. 2009).

*In vitro* cytotoxicity testing demonstrated the biocompatibility of acellular porcine nerves. The biocompatibility of any acellular scaffold is important whether it is to be used as a clinical graft or *in vitro* model. Solutions used in the decellularisation process such as SDS detergent, EDTA, aprotinin and the PAA are known to be cytotoxic (Koulaouzidou, Margelos et al. 1999, Newby, Barr et al. 2000, Sagripanti and Bonifacino 2000). An *in vitro* cytotoxicity test using human

dermal fibroblasts and primary rat Schwann cells found both cell types were able to proliferate up to and in physical contact with the scaffold. Both cell types maintained membrane integrity, a native phenotype and there was no sign of cell lysis, indicating the acellular nerves to be biocompatible.

Biomechanical testing of the acellular nerves (peroneal and tibial) was undertaken as decellularisation solutions applied to biological tissues have previously been shown to affect the mechanical properties of the ECM (Courtman, Pereira et al. 1994, Palsson BO 2004). In terms of clinical applications, any changes in the biomechanical properties of the nerve grafts, can impede the regeneration of the nerve (So and Xu 2015). Unlike other decellularisation methods (Borschel, Kia et al. 2003, Ma, Sun et al. 2011) the process did not decrease the mechanical properties of the acellular nerves. The biomechanical results showed a slight increase in Young's modulus, ultimate tensile strength (UTS) and strain at UTS. These results were found to be similar in other decellularisation studies (Stapleton, Ingram et al. 2008, Williams, Liao et al. 2009, Abdelgaied, Stanley et al. 2015)

For clinical use it is important that nerve grafts maintain their suture-holding ability as well as their ability to maintain a mechanically robust tissue interface with native nerve stump for axonal regeneration. This largely depends on the tensile strength of the tissue. It was therefore concluded that the decellularisation process did not impeded the function of the tissue (Borschel, Kia et al. 2003).

Through mechanical testing it was discovered that the porcine peroneal nerves had a higher UTS value in comparison to the porcine tibial nerves (Zilic, Garner et al. 2015). A previous study by Ugrenović et al. (2014) reported that the peroneal nerve tolerates a greater tensile strength during the leg movement than the tibial nerve, due to the anatomical position (Ugrenović 2014). A study was therefore conducted to evaluate the ultrastructure of porcine peroneal and tibial nerves to investigate whether differences in collagen fibril diameter could explain the observed differences in mechanical properties. The study concluded that the mechanical properties of nerves could not be determined exclusively by their ultrastructure or collagen fibril diameter.

Once successfully decellularised and characterised, acellular nerves were used as an *in vitro* model for the introduction of primary Schwann cells. The study revealed that seeded Schwann cells under static and perfused conditions maintained

their phenotype and viability over a period of time. Furthermore, there are also indications of Schwann cells migrating towards the perineurium and entering the endoneurium where Schwann cells normally reside. The behavior of the cells is dictated largely by the ECM. The ECM provides structural support for cells as well as fundamental cell processes such as cell growth, adhesion, migration, proliferation, differentiation and gene expression (Gao, Wang et al. 2013). It can therefore be assumed that the acellular nerves have retained a suitable ECM for Schwann cells to reside within.

The viability of the cells under static and perfused conditions began to decrease by day 7. This could have been due to a number of factors including seeding density, injection method or lack of a suitable cell viability assay. It was however interesting to note that there was a lower rate of cell death under perfused conditions. A reason for this is that the survival of cells within a scaffold is dependent on the maintenance of nutrient diffusion (Sun, Norton et al. 2005) and under normal physiological conditions cells within the peripheral nerves receive constant nutrients from the surrounding vessels.

The *in vitro* model allowed for a systematic controlled evaluation of the reseeded acellular grafts, and subsequently this led to further investigations using *in vivo* injury models. A three week *in vivo* study was carried out by implanting acellular and reseeded acellular grafts into a rat sciatic injury model to treat an 11 mm nerve gap injury. Throughout the study there was no sign of graft rejection or signs of inflammation when the grafts were harvested. Upon visual inspection post implantation, the grafts appeared to have undergoing degradation, with a substantial loss of the tissue graft. This was also confirmed by Micro CT, which showed the internal structure of the explanted acellular grafts to be disordered and inhomogeneous when compared to an autograft. It has been previously described that ECM derived scaffolds rapidly degrade upon implantation (Badylak 2014). Studies using small intestinal submucosa for tendon and urinary bladder repair have reported that approximately 60% of the mass was degraded and resorbed within 4 weeks of implantation and completely degraded by 3 months (Record, Hillegonds et al. 2001, Gilbert, Stewart-Akers et al. 2007).

It was not fully determined whether the grafts were undertaking a pro-inflammatory or constructive remodelling response. Visually the grafts did not appear to evoke an adverse inflammatory response within the host or surrounding

tissue and there was no appearance of scar tissue which is commonly associated with a pro-inflammatory response. Never the less further investigation needs to be carried out to conclude whether constructive remodelling was taking place. This can include histological analysis of the grafts for lymphocytes, macrophages and matrix metalloproteinases which are known to be present during the remodelling process.

Longitudinal sections of both acellular and recellularised grafts showed PGP9.5 positive regenerated axons. The axons were displayed in well-ordered arrangements and passed through the graft. This correlated with previous studies which investigated axonal regeneration in nerve repairs (Wang, Pan et al. 2014, Mobasseri, Faroni et al. 2015). A plausible reason for the axon regeneration observed in the grafts is the presence of the basal lamina which help guide regenerating axons. The basal lamina consists of continuous laminin tubes along with fibronectin, collagen type IV, heparin sulphate proteoglycans which help promote axonal outgrowth. The basal lamina also presents aligned, linear nano scale features to cells as well as guiding regenerating axons to grow through the basal lamina (Smeal, Rabbitt et al. 2005, Corey, Lin et al. 2007).

When compared to autologous grafts, porcine grafts had a lower density of axons within the distal ends. Quantitative analysis demonstrated that autologous nerves also promoted axon regeneration over a greater distance when compared to the porcine grafts. There was no significant difference between the acellular and recellularised nerve grafts in terms of axonal regeneration. The limited axon regeneration observed in the porcine grafts may have been due to the short period of time, short gap distance, chondroitin sulphate proteoglycans (CSPGs) and methodological issues.

The grafts were implanted for 3 weeks *in vivo.* For a nerve regeneration study this is a relatively short period of time to gain a substantial amount of information on nerve regeneration such as walking track analysis. The *in vivo* study was not long enough to observe whether the grafts would have undergone constructive remodelling and be replaced with a more functional tissue. In addition, the Schwann cells may have also needed more time for growth and differentiation into growth supportive cells to help lead regenerating axons towards the distal nerve stump.

For the *in vivo* study an 11 mm graft was used to bridge the nerve gap injury. Previous studies using similar gap sized models have demonstrated little effect of adding Schwann cells to acellular graft material. This is due to the fact that Schwann cells migrating from the host stumps are able to cross such short distances and provide sufficient regeneration despite the addition of exogenous cells (Frerichs, Fansa et al. 2002, Fox, Schwetye et al. 2005). For future experiments it may be more feasible to increase the gap length to 15 mm, the critical gap length in a rat, where the addition of exogenous Schwann cells may prove more beneficial.

Another reason for the limited regeneration observed in the porcine grafts may be due to chondroitin sulphate proteoglycans (CSPGs) within the porcine grafts. CSPGs can inhibit axonal growth and negate the growth-promoting activities of extracellular matrix components such as laminin (Muir, Engvall et al. 1989, Zuo, Hernandez et al. 1998). Studies suggest that CSPG degrading enzymes such as chondroitinase can help restore the growth promoting properties of laminin within a nerve (Zuo, Ferguson et al. 1998, Ferguson and Muir 2000, Krekoski, Neubauer et al. 2001).

The use of PGP 9.5 antibody to label axons within the grafts may not have been the most efficient method in identifying regenerating fibres. This is because there is no time frame for loss of PGP 9.5 antigenicity in degenerating axons to accurately assess nerve regeneration. For future work if using the same method, a control would be needed to demonstrate that PGP 9.5 is absent if axons are prevented from regenerating. Alternatively other forms of nerve regeneration assessment such as walking track analysis (Hare, Evans et al. 1992), advanced magnetic resonance imaging (MRI) diffusion tensor imaging (DTI) (Hiltunen, Suortti et al. 2005), tractography (Khalil, Budzik et al. 2010) or the use of thy-1-YFP-H mice to enable visual analysis of axons regenerating through a nerve graft (Feng, Mellor et al. 2000, Harding, Christmas et al. 2014) may also prove more efficient.

The *in vivo* study concluded that the acellular and recellularised porcine grafts had the ability to promote axon regeneration across an 11mm nerve gap injury. The grafts, however, were still not equivalent to the autologous graft in terms of axon regeneration. This could be attributed to a number of reasons including time frame, gap size, the presence of CSPGs and methodological assessment. Nonetheless, the acellular graft and recellularised nerve grafts hold

significant therapeutic potential as a replacement for autologous treatment in peripheral nerve repair.

## 9. 1 Future work

The study of creating an acellular nerve graft and reintroducing cells back into the graft has created two possible pathways for the study of peripheral nerve repair. Principally the grafts can be further developed as a three dimensional *in vitro* nerve model to study reseeded grafts for potential use *in vivo*. Alternatively, the acellular nerve grafts can be further optimised and used as potential "off the shelf" nerve graft for clinical applications.

As an *in vitro* nerve model, future challenges include attaining optimal cell attachment, viability, and migration across the graft. To improve cellular adhesion moieties derived from ECM proteins can be used. These are selective in cell binding and can be packed at higher density on the substrate leading to a more specific cell-substrate interaction (Hersel, Dahmen et al. 2003, de Luca, Lacour et al. 2014). Specific amino acids such as RGD (Arg-Gly-Asp) have been shown to facilitate the interaction between ECM proteins and integrins on cell membranes and enhance the adhesion and proliferation of neural cells (de Luca, Stevens et al. 2013).

To promote Schwann cell viability and growth enhancing neurotrophic factors such as neurotrophins can also be introduced alongside Schwann cells. Neurotrophins such as Nerve Growth Factor are known to promote growth and survival of cells (Schmidt and Leach 2003).

Furthermore, for transplant therapies alternative cell types such as adipose derived stem cells (ADSCs) can also be considered. ADSCs are easily harvested and have the ability to differentiate into Schwann-like cells (Kern, Eichler et al. 2006, di Summa, Kalbermatten et al. 2011, Kaewkhaw, Scutt et al. 2011).

Once optimised the reseeded grafts can then be used for *in vivo* studies. Preliminary results have already shown that reseeded grafts are biocompatible with host rat tissue. Nevertheless, there was no substantial difference between the acellular and recellularised nerve grafts in terms of axonal regeneration. For future studies a longer *in vivo* study may prove more beneficial in assessing the porcine

grafts regenerating capacities. This may allow time for neurites to develop and reach the distal portion of the grafts. Immune system modulators can also be implemented to decrease fibrosis and histiocytic responses to help promote neurite growth (Lee and Wolfe 2000). For recellularised porcine grafts it has been suggested that using a larger gap size (greater than 15 mm) may be more beneficial in such a study (Frerichs, Fansa et al. 2002, Fox, Schwetye et al. 2005).

The clinical use of acellular nerves is rather limited, with Avance® being the only commercially available nerve graft available. The Avance® graft which uses human donor nerve tissue has had reported success over the commercially available NGC's (Whitlock, Tuffaha et al. 2009). Nevertheless, the supply of human nerve tissue for decellularisation and use as a graft material is extremely limited in the United Kingdom. Use of xenogeneic tissue has the advantage of unlimited availability in a range of different sizes as observed in chapter three. Therefore, there is an opportunity to create the first commercially available xenogeneic nerve graft.

As a clinical nerve graft future consideration would have to include a terminal sterilisation step for the graft such as gamma irradiation or ethylene oxide. In addition, the graft may also have to undergo enzymatic degradation as chondroitin sulphate proteoglycans are known to inhibit axon regeneration within acellular grafts (Zuo, Ferguson et al. 1998, Ferguson and Muir 2000, Krekoski, Neubauer et al. 2001).

## 9.2 Conclusions

In summary, the present thesis:

1. Optimised a decellularisation method for porcine peripheral nerves which retained the nerves histioarchitecture whilst eliminating over 95 % cellular DNA.

2. Validated through qualitative and quantitative analysis the retention of important extracellular matrix (ECM) proteins such as collagen, glycosaminoglycan's, fibronectin and laminin.

3. Established using an *in vitro* contact cytotoxicity assay and mechanical testing that acellular nerves were biocompatible and that the decellularisation process did not decrease the mechanical properties of the nerves.

4. Verified using histological analysis and transmission electron microscopy (TEM) that porcine tibial nerves were significantly larger than the peroneal nerves and possessed larger collagen fibril diameters within the connective tissues.

5. Developed a three dimensional *in vitro* nerve model and demonstrated that Schwann cells under perfusion maintained their phenotype and had a lower rate of cell death when compared to static conditions.

6. Carried out an *in vivo* nerve regeneration study within a rat sciatic nerve injury model using acellular and recellularised nerve grafts and demonstrated that grafts could potentially support regenerating axons across a 11 mm rat sciatic nerve gap injury

# References


**Abbas, A. K., K. M. Murphy, et al. (1996). "Functional diversity of helper T lymphocytes." Nature 383(6603): 787-793.**

**Abdelgaied, A., M. Stanley, et al. (2015). "Comparison of the biomechanical tensile and compressive properties of decellularised and natural porcine meniscus." J Biomech 48(8): 1389-1396.**

**Aguado, B. A., W. Mulyasasmita, et al. (2011). "Improving viability of stem cells during syringe needle flow through the design of hydrogel cell carriers." Tissue Engineering Part A 18(7-8): 806-815.**

**Ahmed, Z., S. Underwood, et al. (2003). "Nerve guide material made from fibronectin: Assessment of in vitro properties." Tissue Engineering 9(2): 219-231.**

**Allodi, I., M.-S. Guzmán-Lenis, et al. (2011). "In vitro comparison of motor and sensory neuron outgrowth in a 3D collagen matrix." Journal of neuroscience methods 198(1): 53-61.**

**Allodi, I., E. Udina, et al. (2012). "Specificity of peripheral nerve regeneration: Interactions at the axon level." Progress in Neurobiology 98(1): 16-37.**

**Alovskaya, A., T. Alekseeva, et al. (2007). "Fibronectin, collagen, fibrin-components of extracellular matrix for nerve regeneration." Topics in Tissue Engineering 3: 1-26.**

**Amer, M. H., L. J. White, et al. (2015). "The effect of injection using narrow-bore needles on mammalian cells: administration and formulation considerations for cell therapies." Journal of Pharmacy and Pharmacology 67(5): 640-650.**

**Ansselin, A. D., T. Fink, et al. (1997). "Peripheral nerve regeneration through nerve guides seeded with adult Schwann cells." Neuropathology and Applied Neurobiology 23(5): 387-398.**

**Aquino, D., R. Margolis, et al. (1984). "Immunocytochemical localization of a chondroitin sulfate proteoglycan in nervous tissue. I. Adult brain, retina, and peripheral nerve." The Journal of cell biology 99(3): 1117-1129.**

**Arino, H., J. Brandt, et al. (2008). "Implantation of Schwann cells in rat tendon autografts as a model for peripheral nerve repair: long term effects on functional recovery." Scandinavian Journal of Plastic and Reconstructive Surgery and Hand Surgery 42(6): 281-285.**

**Armstrong, S. J., M. Wiberg, et al. (2008). "Laminin activates NF-κB in Schwann cells to enhance neurite outgrowth." Neuroscience letters 439(1): 42-46.**

**Ashley, W. W., Jr., T. Weatherly, et al. (2006). "Collagen nerve guides for surgical repair of brachial plexus birth injury." J Neurosurg 105(6 Suppl): 452-456.**

**Avellino, A. M., D. Hart, et al. (1995). "Differential Macrophage Responses in the Peripheral and Central-Nervous-System during Wallerian Degeneration of Axons." Experimental Neurology 136(2): 183-198.**

**Bader, A., T. Schilling, et al. (1998). "Tissue engineering of heart valves–human endothelial cell seeding of detergent acellularized porcine valves." European journal of cardio-thoracic surgery 14(3): 279-284.**

**Badylak, S. F. (2014). "Decellularized Allogeneic and Xenogeneic Tissue as a Bioscaffold for Regenerative Medicine: Factors that Influence the Host Response." Ann Biomed Eng 42(7): 1517-1527.**

**Badylak, S. F., D. O. Freytes, et al. (2009). "Extracellular matrix as a biological scaffold material: Structure and function." Acta Biomater 5(1): 1-13.**

**Badylak, S. F. and T. W. Gilbert (2008). "Immune response to biologic scaffold materials." Semin Immunol 20(2): 109-116.**

**Badylak, S. F., K. Park, et al. (2001). "Marrow-derived cells populate scaffolds composed of xenogeneic extracellular matrix." Experimental hematology 29(11): 1310-1318.**

**Badylak, S. F., R. Tullius, et al. (1995). "The use of xenogeneic small intestinal submucosa as a biomaterial for Achille's tendon repair in a dog model." Journal of biomedical materials research 29(8): 977-985.**

**Bain, J. R., K. L. Veltri, et al. (2001). "Improved functional recovery of denervated skeletal muscle after temporary sensory nerve innervation." Neuroscience 103(2): 503-510.**

**Baldoni, E., L. Bolognani, et al. (1994). "A rapid procedure for elimination of non-polar lipids hampering the usual polar lipid extraction and TLC separation." European journal of histochemistry: EJH 39(4): 253-257.**

**Bancroft, J. D. and M. Gamble (2008). Theory and practice of histological techniques, Elsevier Health Sciences.**

**Baron-Van Evercooren, A., H. K. Kleinman, et al. (1982). "Fibronectin promotes rat Schwann cell growth and motility." The Journal of cell biology 93(1): 211-216.**

**Barrett, G. L. and P. F. Bartlett (1994). "The p75 nerve growth factor receptor mediates survival or death depending on the stage of sensory neuron development." Proceedings of the National Academy of Sciences 91(14): 6501-6505.**

**Barrs, D. M., C. J. Trahan, et al. (1991). "The porcine model for intratemporal facial nerve trauma studies." Otolaryngol Head Neck Surg 105(6): 845-856.**

**Belkas, J. S., M. S. Shoichet, et al. (2004). "Peripheral nerve regeneration through guidance tubes." Neurological Research 26(2): 151-160.**

**Bell, J. H. and J. W. Haycock (2011). "Next Generation Nerve Guides: Materials, Fabrication, Growth Factors, and Cell Delivery." Tissue Eng Part B Rev.**

**Bernas, T. and J. Dobrucki (2002). "Mitochondrial and nonmitochondrial reduction of MTT: Interaction of MTT with TMRE, JC-1, and NAO mitochondrial fluorescent probes." Cytometry 47(4): 236-242.**

**Bernas, T. and J. W. Dobrucki (2000). "The role of plasma membrane in bioreduction of two tetrazolium salts, MTT, and CTC." Archives of biochemistry and biophysics 380(1): 108-116.**

**Berridge, M. V. and A. S. Tan (1993). "Characterization of the cellular reduction of 3-(4, 5-dimethylthiazol-2-yl)-2, 5-diphenyltetrazolium bromide (MTT): subcellular localization, substrate dependence, and involvement of mitochondrial electron transport in MTT reduction." Archives of biochemistry and biophysics 303(2): 474-482.**

**Booth, C., S. A. Korossis, et al. (2002). "Tissue engineering of cardiac valve prostheses I: development and histological characterization of an acellular porcine scaffold." J Heart Valve Dis 11(4): 457-462.**

**Borschel, G. H., K. F. Kia, et al. (2003). "Mechanical properties of acellular peripheral nerve." Journal of Surgical Research 114(2): 133-139.**

**Bovolenta, P. and I. Fernaud-Espinosa (2000). "Nervous system proteoglycans as modulators of neurite outgrowth." Prog Neurobiol 61(2): 113-132.**

**Brenner, M. J., J. B. Lowe, 3rd, et al. (2005). "Effects of Schwann cells and donor antigen on long-nerve allograft regeneration." Microsurgery 25(1): 61-70.**

**Brigido, S. A. (2006). "The use of an acellular dermal regenerative tissue matrix in the treatment of lower extremity wounds: a prospective 16-week pilot study." International wound journal 3(3): 181-187.**

**Brooks, D. N., R. V. Weber, et al. (2012). "Processed nerve allografts for peripheral nerve reconstruction: A multicenter study of utilization and outcomes in sensory, mixed, and motor nerve reconstructions." Microsurgery 32(1): 1-14.**

**Brown, B., K. Lindberg, et al. (2006). "The basement membrane component of biologic scaffolds derived from extracellular matrix." Tissue engineering 12(3): 519-526.**

**Brown, B. N., J. M. Freund, et al. (2011). "Comparison of three methods for the derivation of a biologic scaffold composed of adipose tissue extracellular matrix." Tissue Engineering Part C: Methods 17(4): 411-421.**

**Brown, S. A., K. Merritt, et al. (2002). "Effects of different disinfection and sterilization methods on tensile strength of materials used for single-use devices." Biomedical instrumentation & technology 36(1): 23-27.**

**Brushart, T. M. (2011). Nerve repair, Oxford University Press.**

**Bunge, M., R. Bunge, et al. (1989). "Role of peripheral nerve extracellular matrix in Schwann cell function and in neurite regeneration." Developmental neuroscience 11(4-5): 348-360.**

**Bunge, M. B., P. M. Wood, et al. (1989). "Perineurium originates from fibroblasts: demonstration in vitro with a retroviral marker." Science 243(4888): 229-231.**

**Bunge, R. P. (1994). "The Role of the Schwann-Cell in Trophic Support and Regeneration." Journal of Neurology 242(1): S19-S21.**

**Burks, S. S., D. J. Levi, et al. (2014). "Challenges in sciatic nerve repair: anatomical considerations." J Neurosurg 121(1): 210-218.**

**Campbell, E. O., R. A. Samlan, et al. (2013). "Developmental changes in the connective tissues of the porcine recurrent laryngeal nerve." Journal of anatomy 222(6): 625-633.**

**Cartmell, J. S. and M. G. Dunn (2000). "Effect of chemical treatments on tendon cellularity and mechanical properties." Journal of biomedical materials research 49(1): 134-140.**

**Cartmell, J. S. and M. G. Dunn (2004). "Development of cell-seeded patellar tendon allografts for anterior cruciate ligament reconstruction." Tissue engineering 10(7-8): 1065-1075.**

**Causey, G. and A. A. Barton (1959). "The cellular content of the endoneurium of peripheral nerve." Brain 82: 594-598.**

**Ceballos, D., X. Navarro, et al. (1999). "Magnetically aligned collagen gel filling a collagen nerve guide improves peripheral nerve regeneration." Experimental Neurology 158(2): 290-300.**

**Chandrasekaran, E. V. and B. K. Bachhawat (1969). "Isolation and characterization of glycosaminoglycans in peripheral nerve and spinal cord of monkey." Journal of Neurochemistry 16(11): 1529-1532.**

**Chafik, D., D. Bear, et al. (2003). "Optimization of Schwann cell adhesion in response to shear stress in an in vitro model for peripheral nerve tissue engineering." Tissue engineering 9(2): 233-241.**

**Chang, C. J., S. H. Hsu, et al. (2005). "Low-intensity-ultrasound-accelerated nerve regeneration using cell-seeded poly(D,L-lactic acid-co-glycolic acid) conduits: An in vivo and in vitro study." Journal of Biomedical Materials Research Part B-Applied Biomaterials 75B(1): 99-107.**

**Chaplin, D. D. (2010). "Overview of the immune response." Journal of Allergy and Clinical Immunology 125(2): S3-S23.**

**Chaudhry, V., J. D. Glass, et al. (1992). "Wallerian Degeneration in Peripheral-Nerve Disease." Neurologic Clinics 10(3): 613-627.**

**Chen, H.-C. and Y.-C. Hu (2006). "Bioreactors for tissue engineering." Biotechnology letters 28(18): 1415-1423.**

**Chen, N. and E. H. Field (1995). "Enhanced type 2 and diminished type 1 cytokines in neonatal tolerance." Transplantation 59(7): 933-941.**

**Chen, Y. S., C. L. Hsieh, et al. (2000). "Peripheral nerve regeneration using silicone rubber chambers filled with collagen, laminin and fibronectin." Biomaterials 21(15): 1541-1547.**

**Cheng, B. and Z. R. Chen (2002). "Fabricating autologous tissue to engineer artificial nerve." Microsurgery 22(4): 133-137.**

**Chentanez, V., P. Cha-oumphol, et al. (2006). "Morphometric data of normal sural nerve in Thai adults." J Med Assoc Thai 89(5): 670-674.**

**Chernousov, M. A., K. Rothblum, et al. (2006). "Glypican-1 and α4 (V) collagen are required for Schwann cell myelination." The Journal of neuroscience 26(2): 508-517.**

**Cole, M. B. (1984). "Alteration of cartilage matrix morphology with histological processing." Journal of microscopy 133(2): 129-140.**

**Colucci, S., G. Giannelli, et al. (1996). "Human osteoclast-like cells selectively recognize laminin isoforms, an event that induces migration and activates Ca2+ mediated signals." Journal of cell science 109(6): 1527-1535.**

**Coons, D. A. and F. A. Barber (2006). "Tendon graft substitutes—rotator cuff patches." Sports medicine and arthroscopy review 14(3): 185-190.**

**Corey, J. M., D. Y. Lin, et al. (2007). "Aligned electrospun nanofibers specify the direction of dorsal root ganglia neurite growth." Journal of Biomedical Materials Research Part A 83A(3): 636-645.**

**Corfas, G., M. O. Velardez, C. P. Ko, N. Ratner and E. Peles (2004). "Mechanisms and roles of axon-Schwann cell interactions." J Neurosci 24(42): 9250-9260.**

**Costa, F. D. A. d., P. M. Dohmen, et al. (2004). "Comparison of cryopreserved homografts and decellularized porcine heterografts implanted in sheep." Artificial organs 28(4): 366-370.**

**Courtman, D. W., C. A. Pereira, et al. (1994). "Development of a pericardial acellular matrix biomaterial: biochemical and mechanical effects of cell extraction." Journal of biomedical materials research 28(6): 655-666.**

**Cox, B. and A. Emili (2006). "Tissue subcellular fractionation and protein extraction for use in mass-spectrometry-based proteomics." Nature protocols 1(4): 1872-1878.**

**Crapo, P. M., T. W. Gilbert, et al. (2011). "An overview of tissue and whole organ decellularization processes." Biomaterials 32(12): 3233-3243.**

**Cullen, D. K., J. A. Wolf, et al. (2011). "Neural tissue engineering and biohybridized microsystems for neurobiological investigation in vitro (Part 1)." Critical Reviews™ in Biomedical Engineering 39(3).**

**Dahl, S. L., J. Koh, et al. (2003). "Decellularized native and engineered arterial scaffolds for transplantation." Cell transplantation 12(6): 659-666.**

**Dahlin, L. B. (2008). "Techniques of peripheral nerve repair." Scand J Surg 97(4): 310-316.**

**Daly, W., L. Yao, et al. (2012). "A biomaterials approach to peripheral nerve regeneration: bridging the peripheral nerve gap and enhancing functional recovery." J R Soc Interface 9(67): 202-221.**

**Danielsen, N., J. M. Kerns, et al. (1995). "Predegeneration enhances regeneration into acellular nerve grafts." Brain research 681(1): 105-108.**

**Daud, M. F., K. C. Pawar, et al. (2012). "An aligned 3D neuronal-glial co-culture model for peripheral nerve studies." Biomaterials 33(25): 5901-5913.**

**Danielsen, N., J. M. Kerns, et al. (1994). "Pre-degenerated nerve grafts enhance regeneration by shortening the initial delay period." Brain research 666(2): 250-254.**

**Davis, G. E., S. Varon, et al. (1985). "Substratum-binding neurite-promoting factors: relationships to laminin." Trends in Neurosciences 8: 528-532.**

**de Luca, A. C., S. P. Lacour, W. Raffoul and P. G. di Summa (2014). "Extracellular matrix components in peripheral nerve repair: how to affect neural cellular response and nerve regeneration?" Neural Regen Res 9(22): 1943-1948.**

**de Luca, A. C., J. S. Stevens, S. L. Schroeder, J. B. Guilbaud, A. Saiani, S. Downes and G. Terenghi (2013). "Immobilization of cell-binding peptides on poly-ε-caprolactone film surface to biomimic the peripheral nervous system." J Biomed Mater Res A 101(2): 491-501.**

**di Summa, P. G., D. F. Kalbermatten, et al. (2011). "Long-Term in Vivo Regeneration of Peripheral Nerves through Bioengineered Nerve Grafts." Neuroscience 181: 278-291.**

**Dodd, J. and T. M. Jessell (1988). "Axon guidance and the patterning of neuronal projections in vertebrates." Science 242(4879): 692-699.**

**Donoghoe, N., G. D. Rosson, et al. (2007). "Reconstruction of the human median nerve in the forearm with the Neurotube." Microsurgery 27(7): 595-600.**

**Donzelli, R., F. Maiuri, et al. (2006). "Role of extracellular matrix components in facial nerve regeneration: an experimental study." Neurological research 28(8): 794-801.**

**Duteille, F., D. Petry, et al. (2001). "A comparison between clinical results and electromyographic analysis after median or ulnar nerve injuries in children's wrists." Ann Plast Surg 46(4): 382-386.**

**Edgar, D., R. Timpl, et al. (1984). "The heparin-binding domain of laminin is responsible for its effects on neurite outgrowth and neuronal survival." EMBO J 3(7): 1463-1468.**

**Edwards, C. A. and W. D. O'Brien, Jr. (1980). "Modified assay for determination of hydroxyproline in a tissue hydrolyzate." Clinica Chimica Acta. 104(2): 161 - 167.**

**Elder, B. D., S. V. Eleswarapu, et al. (2009). "Extraction techniques for the decellularization of tissue engineered articular cartilage constructs." Biomaterials 30(22): 3749-3756.**

**Eng, L. F., R. S. Ghirnikar, et al. (2000). "Glial fibrillary acidic protein: GFAP-thirty-one years (1969–2000)." Neurochemical research 25(9-10): 1439-1451**

**Enver, M. K. and S. M. Hall (1994). "Are Schwann-Cells Essential for Axonal Regeneration into Muscle Autografts." Neuropathology and Applied Neurobiology 20(6): 587-598.**

**Evans, G. R. D. (2001). "Peripheral nerve injury: A review and approach to tissue engineered constructs." Anatomical Record 263(4): 396-404.**

**Evans, G. R. D., K. Brandt, et al. (2002). "Bioactive poly(L-lactic acid) conduits seeded with Schwann cells for peripheral nerve regeneration." Biomaterials 23(3): 841-848.**

**Evans, P. J., S. E. Mackinnon, et al. (1998). "Cold preserved nerve allografts: changes in basement membrane, viability, immunogenicity, and regeneration." Muscle Nerve 21(11): 1507-1522.**

**Fan, L., Z. Yu, et al. (2014). "Schwann-like cells seeded in acellular nerve grafts improve nerve regeneration." BMC musculoskeletal disorders 15(1): 165.**

**Fansa, H. and G. Keilhoff (2004). "Comparison of different biogenic matrices seeded with cultured Schwann cells for bridging peripheral nerve defects." Neurological research 26(2): 167-173.**

**Farndale, R. W., D. J. Buttle, et al. (1986). "Improved quantitation and discrimination of sulphated glycosaminoglycans by use of dimethylmethylene blue." Biochimica et Biophysica Acta. 883(2): 173 - 177.**

**Faweett, J. and R. J. Keynes (1990). "Peripheral nerve regeneration." Annual review of neuroscience 13(1): 43-60.**

**Feneley, M. R., J. W. Fawcett, et al. (1991). "The Role of Schwann-Cells in the Regeneration of Peripheral-Nerve Axons through Muscle Basal Lamina Grafts." Experimental Neurology 114(3): 275-285.**

**Feng, G., R. H. Mellor, M. Bernstein, C. Keller-Peck, Q. T. Nguyen, M. Wallace, J. M. Nerbonne, J. W. Lichtman and J. R. Sanes (2000). "Imaging neuronal subsets in transgenic mice expressing multiple spectral variants of GFP." Neuron 28(1): 41-51.**

**Ferguson, T. A. and D. Muir (2000). "MMP-2 and MMP-9 increase the neurite-promoting potential of schwann cell basal laminae and are upregulated in degenerated nerve." Molecular and Cellular Neuroscience 16(2): 157-167.**

**Ferraz, T., M. Fiuza, et al. (2004). "Comparison of six methods for the extraction of lipids from serum in terms of effectiveness and protein preservation." Journal of biochemical and biophysical methods 58(3): 187-193.**

**Flynn, L. (2010). "The use of decellularized adipose tissue to provide an inductive microenvironment for the adipogenic differentiation of human adipose-derived stem cells." Biomaterials 31(17): 4715-4724.**

**Fox, I. K., K. E. Schwetye, et al. (2005). "Schwann-cell injection of cold-preserved nerve allografts." Microsurgery 25(6): 502-507.**

**Franzen, R., J. Schoenen, et al. (1998). "Effects of macrophage transplantation in the injured adult rat spinal cord: A combined immunocytochemical and biochemical study." Journal of Neuroscience Research 51(3): 316-327.**

**Freed, A. D. and T. C. Doehring (2005). "Elastic model for crimped collagen fibrils." Journal of biomechanical engineering 127(4): 587-593.**

**Frerichs, O., H. Fansa, et al. (2002). "Reconstruction of peripheral nerves using acellular nerve grafts with implanted cultured Schwann cells." Microsurgery 22(7): 311-315.**

**Freyman, T. (2008). Decellularized bone marrow extracellular matrix, Google Patents.**

**Freytes, D. O., S. F. Badylak, et al. (2004). "Biaxial strength of multilaminated extracellular matrix scaffolds." Biomaterials 25(12): 2353-2361.**

**Freytes, D. O., R. M. Stoner, et al. (2008). "Uniaxial and biaxial properties of terminally sterilized porcine urinary bladder matrix scaffolds." Journal of Biomedical Materials Research Part B: Applied Biomaterials 84(2): 408-414.**

**Frykman, G. (1991). "Results of nerve grafting." Operative Nerve Repair and Reconstruction.**

**Gailit, J. and E. Ruoslahti (1988). "Regulation of the fibronectin receptor affinity by divalent cations." Journal of Biological Chemistry 263(26): 12927-12932.**

**Gamba, P., M. Conconi, et al. (2002). "Experimental abdominal wall defect repaired with acellular matrix." Pediatric surgery international 18(5-6): 327-331.**

**Gamboa, O., P. Gutiérrez, et al. (2007). "Absence of relevant effects of 5 mT static magnetic field on morphology, orientation and growth of a rat Schwann cell line in culture."**

**Gao, S., Y. Zheng, et al. (2014). "Combination of Acellular Nerve Graft and Schwann Cells-Like Cells for Rat Sciatic Nerve Regeneration." Neural plasticity 2014.**

**Gao, X., Y. Wang, et al. (2013). "The role of peripheral nerve ECM components in the tissue engineering nerve construction." Rev Neurosci 24(4): 443-453.**

**Gattuso, J. M., M. A. Glasby, et al. (1989). "A comparison of immediate and delayed repair of peripheral nerves using freeze-thawed autologous skeletal muscle grafts--in the rat." Br J Plast Surg 42(3): 306-313.**

**Geuna, S., S. Raimondo, et al. (2015). "In vitro models for peripheral nerve regeneration." European Journal of Neuroscience.**

**Gilbert, T. W., T. L. Sellaro, et al. (2006). "Decellularization of tissues and organs." Biomaterials 27(19): 3675-3683.**

**Gilbert, T. W., A. M. Stewart-Akers, et al. (2007). "Degradation and remodeling of small intestinal submucosa in canine Achilles tendon repair." J Bone Joint Surg Am 89(3): 621-630.**

**Gilbert, T. W., S. Wognum, et al. (2008). "Collagen fiber alignment and biaxial mechanical behavior of porcine urinary bladder derived extracellular matrix." Biomaterials 29(36): 4775-4782.**

**Gingras, M., M. M. Beaulieu, et al. (2008). "In vitro study of axonal migration and myelination of motor neurons in a three-dimensional tissue-engineered model." Glia 56(3): 354-364.**

**Gingras, M., J. Bergeron, et al. (2003). "In vitro development of a tissue-engineered model of peripheral nerve regeneration to study neurite growth." The FASEB journal 17(14): 2124-2126.**

**Gnavi, S., L. Blasio, et al. (2014). "Gelatin-based hydrogel for vascular endothelial growth factor release in peripheral nerve tissue engineering." Journal of tissue engineering and regenerative medicine.**

**Goethals, S., E. Ydens, et al. (2010). "Toll-Like Receptor Expression in the Peripheral Nerve." GLIA 58(14): 1701-1709.**

**Goodwin, C., S. Holt, et al. (1996). "Growth hormone-responsive DT-diaphorase-mediated bioreduction of tetrazolium salts." Biochemical and biophysical research communications 226(3): 935-941.**

**Gouk, S. S., T. M. Lim, et al. (2008). "Alterations of human acellular tissue matrix by gamma irradiation: histology, biomechanical property, stability, in vitro cell repopulation, and remodeling." Journal of Biomedical Materials Research Part B: Applied Biomaterials 84(1): 205-217.**

**Gratzer, P. F., R. D. Harrison, et al. (2006). "Matrix alteration and not residual sodium dodecyl sulfate cytotoxicity affects the cellular repopulation of a decellularized matrix." Tissue engineering 12(10): 2975-2983.**

**Grauss, R. W., M. G. Hazekamp, et al. (2005). "Histological evaluation of decellularised porcine aortic valves: matrix changes due to different decellularisation methods." European journal of cardio-thoracic surgery 27(4): 566-571.**

**Guenard, V., N. Kleitman, et al. (1992). "Syngeneic Schwann-Cells Derived from Adult Nerves Seeded in Semipermeable Guidance Channels Enhance Peripheral-Nerve Regeneration." Journal of Neuroscience 12(9): 3310-3320.**

**Gulati, A. K. (1988). "Evaluation of acellular and cellular nerve grafts in repair of rat peripheral nerve." J Neurosurg 68(1): 117-123.**

**Gulati, A. K. and G. Cole (1994). "Immunogenicity and regenerative potential of acellular nerve allografts to repair peripheral nerve in rats and rabbits." Acta neurochirurgica 126(2-4): 158-164.**

**Gustafson, K. J., Y. Grinberg, et al. (2012). "Human distal sciatic nerve fascicular anatomy: implications for ankle control using nerve-cuff electrodes." J Rehabil Res Dev 49(2): 309-321.**

**Gutmann, E. and F. K. Sanders (1943). "Recovery of fibre numbers and diameters in the regeneration of peripheral nerves." Journal of Physiology-London 101(4): 489-518.**

**Hadlock, T., C. Sundback, et al. (2000). "A polymer foam conduit seeded with Schwann cells promotes guided peripheral nerve regeneration." Tissue engineering 6(2): 119-127.**

**Hadlock, T. A., C. A. Sundback, et al. (2001). "A new artificial nerve graft containing rolled Schwann cell monolayers." Microsurgery 21(3): 96-101.**

**Haftek, J. (1970). "Stretch injury of peripheral nerve acute effects of stretching on rabbit nerve." Journal of Bone & Joint Surgery, British Volume 52(2): 354-365.**

**Hall, S. (1986). "Regeneration in cellular and acellular autografts in the peripheral nervous system." Neuropathology and applied neurobiology 12(1): 27-46.**

**Hall, S. (2005). "The response to injury in the peripheral nervous system." Journal of Bone & Joint Surgery, British Volume 87(10): 1309-1319.**

**Harding, A. J., C. R. Christmas, M. W. Ferguson, A. R. Loescher, P. P. Robinson and F. M. Boissonade (2014). "Mannose-6-phosphate facilitates early peripheral nerve regeneration in thy-1-YFP-H mice." Neuroscience 279: 23-32.**

**Hare, G. M., P. J. Evans, S. E. Mackinnon, T. J. Best, J. R. Bain, J. P. Szalai and D. A. Hunter (1992). "Walking track analysis: a long-term assessment of peripheral nerve recovery." Plast Reconstr Surg 89(2): 251-258.**

**Heath, C. A. and G. E. Rutkowski (1998). "The development of bioartificial nerve grafts for peripheral-nerve regeneration." Trends in Biotechnology 16(4): 163-168.**

**Henry, M. D. and K. P. Campbell (1996). "Dystroglycan: an extracellular matrix receptor linked to the cytoskeleton." Current opinion in cell biology 8(5): 625-631.**

**Hersel, U., C. Dahmen and H. Kessler (2003). "RGD modified polymers: biomaterials for stimulated cell adhesion and beyond." Biomaterials 24(24): 4385-4415.**

**Hess, J. R., M. J. Brenner, et al. (2007). "Use of cold-preserved allografts seeded with autologous Schwann cells in the treatment of a long-gap peripheral nerve injury." Plastic and Reconstructive Surgery 119(1): 246-259.**

**Hilbert, S. L., R. Yanagida, et al. (2004). "Prototype anionic detergent technique used to decellularize allograft valve conduits evaluated in the right ventricular outflow tract in sheep." J Heart Valve Dis 13(5): 831-840.**

**Hiles, R. W. (1972). "Freeze dried irradiated nerve homograft: a preliminary report." The Hand 4(1): 79-84.**

**Hiltunen, J., T. Suortti, S. Arvela, M. Seppä, R. Joensuu and R. Hari (2005). "Diffusion tensor imaging and tractography of distal peripheral nerves at 3 T." Clin Neurophysiol 116(10): 2315-2323.**

**Hodde, J. and M. Hiles (2002). "Virus safety of a porcine-derived medical device: Evaluation of a viral inactivation method." Biotechnology and bioengineering 79(2): 211-216.**

**Hodde, J., A. Janis, et al. (2007). "Effects of sterilization on an extracellular matrix scaffold: part I. Composition and matrix architecture." Journal of Materials Science: Materials in Medicine 18(4): 537-543.**

**Hodde, J., R. Record, et al. (2001). "Vascular endothelial growth factor in porcine-derived extracellular matrix." Endothelium 8(1): 11-24.**

**Hodde, J. P., S. F. Badylak, et al. (1996). "Glycosaminoglycan content of small intestinal submucosa: a bioscaffold for tissue replacement." Tissue engineering 2(3): 209-217.**

**Hodde, J. P., R. D. Record, et al. (2002). "Retention of endothelial cell adherence to porcine-derived extracellular matrix after disinfection and sterilization." Tissue engineering 8(2): 225-234.**

**Horowitz, S. H. (1989). "Therapeutic strategies in promoting peripheral nerve regeneration." Muscle & nerve 12(4): 314-322.**

**Hu, J., Q.-T. Zhu, et al. (2007). "Repair of extended peripheral nerve lesions in rhesus monkeys using acellular allogenic nerve grafts implanted with autologous mesenchymal stem cells." Experimental neurology 204(2): 658-666.**

**Huang, Y. C. and Y. Y. Huang (2006). "Biomaterials and strategies for nerve regeneration." Artif Organs 30(7): 514-522.**

**Hudson, B., S. Reeders, et al. (1993). "Type IV collagen: structure, gene organization, and role in human diseases. Molecular basis of Goodpasture and Alport syndromes and diffuse leiomyomatosis." J Biol Chem 268(35): 26033-26036.**

**Hudson, T. W., S. Y. Liu, et al. (2004). "Engineering an improved acellular nerve graft via optimized chemical processing." Tissue Eng 10(9-10): 1346-1358.**

**Hudson, T. W., S. Zawko, et al. (2004). "Optimized acellular nerve graft is immunologically tolerated and supports regeneration." Tissue Engineering 10(11-12): 1641-1651.**

**Humphries, M. J., S. K. Akiyama, et al. (1988). "Neurite extension of chicken peripheral nervous system neurons on fibronectin: relative importance of specific adhesion sites in the central cell-binding domain and the alternatively spliced type III connecting segment." The Journal of cell biology 106(4): 1289-1297.**

**Ide, C., K. Tohyama, et al. (1983). "Schwann cell basal lamina and nerve regeneration." Brain Research 288(1): 61-75**

**Ide, C., T. Osawa, et al. (1990). "Nerve regeneration through allogeneic nerve grafts, with special reference to the role of the Schwann cell basal lamina." Progress in neurobiology 34(1): 1-38.**

**Ide, C., K. Tohyama, et al. (1998). "Long acellular nerve transplants for allogeneic grafting and the effects of basic fibroblast growth factor on the growth of regenerating axons in dogs: a preliminary report." Exp Neurol 154(1): 99-112.**

**Ignat'eva, N. Y., N. A. Danilov, et al. (2007). "Determination of hydroxyproline in tissues and the evaluation of the collagen content of the tissues." Journal of Analytical Chemistry 62(1): 51 - 57.**

**Inada, Y., H. Hosoi, et al. (2007). "Regeneration of peripheral motor nerve gaps with a polyglycolic acid-collagen tube: technical case report." Neurosurgery 61(5): E1105-1107; discussion E1107.**

**Ingram, J. H., S. Korossis, et al. (2007). "The use of ultrasonication to aid recellularization of acellular natural tissue scaffolds for use in anterior cruciate ligament reconstruction." Tissue engineering 13(7): 1561-1572.**

**Jamur, M. C. and C. Oliver (2010). Cell fixatives for immunostaining. Immunocytochemical Methods and Protocols, Springer: 55-61.**

**Janeway, C. A., P. Travers, et al. (1999). Immunobiology: the immune system in health and disease, Current Biology Publications New York, NY;.**

**Jesuraj, N. J., K. B. Santosa, et al. (2011). "A systematic evaluation of Schwann cell injection into acellular cold-preserved nerve grafts." Journal of Neuroscience Methods 197(2): 209-215.**

**Jia, H., Y. Wang, et al. (2012). "Sciatic nerve repair by acellular nerve xenografts implanted with BMSCs in rats xenograft combined with BMSCs." Synapse 66(3): 256-269.**

**Jiang, X., S. H. Lim, et al. (2010). "Current applications and future perspectives of artificial nerve conduits." Experimental Neurology 223(1): 86-101.**

**Johnson, P. J., P. Newton, et al. (2011). "Nerve Endoneurial Microstructure Facilitates Uniform Distribution of Regenerative Fibers: A Post Hoc Comparison of Midgraft Nerve Fiber Densities." Journal of Reconstructive Microsurgery 27(2): 83-89.**

**Kaewkhaw, R., A. M. Scutt, et al. (2011). "Anatomical site influences the differentiation of adipose-derived stem cells for Schwann-cell phenotype and function." Glia 59(5): 734-749.**

**Kaewkhaw, R., A. M. Scutt, et al. (2012). "Integrated culture and purification of rat Schwann cells from freshly isolated adult tissue." Nat Protoc 7(11): 1996-2004.**

**Kallos, M. S. and L. A. Behie (1999). "Inoculation and growth conditions for high-cell-density expansion of mammalian neural stem cells in suspension bioreactors." Biotechnology and bioengineering 63(4): 473-483.**

**Karabekmez, F. E., A. Duymaz, et al. (2009). "Early clinical outcomes with the use of decellularized nerve allograft for repair of sensory defects within the hand." Hand (N Y) 4(3): 245-249.**

**Kasimir, M., E. Rieder, et al. (2003). "Comparison of different decellularization procedures of porcine heart valves." The International journal of artificial organs 26(5): 421-427.**

**Kehoe, S., X. F. Zhang, et al. (2012). "FDA approved guidance conduits and wraps for peripheral nerve injury: a review of materials and efficacy." Injury 43(5): 553-572.**

**Kerns, J. M., N. Danielsen, et al. (1993). "The influence of predegeneration on regeneration through peripheral nerve grafts in the rat." Experimental neurology 122(1): 28-36.**

**Khalil, C., J. F. Budzik, E. Kermarrec, V. Balbi, V. Le Thuc and A. Cotten (2010). "Tractography of peripheral nerves and skeletal muscles." Eur J Radiol 76(3): 391-397.**

**Kheir, E., T. Stapleton, et al. (2011). "Development and characterization of an acellular porcine cartilage bone matrix for use in tissue engineering." Journal of Biomedical Materials Research Part A 99(2): 283-294.**

**Kim, B. S., J. J. Yoo, et al. (2004). "Peripheral nerve regeneration using acellular nerve grafts." Journal of Biomedical Materials Research Part A 68(2): 201-209.**

**Klebe, R. J. (1974). "Isolation of a collagen-dependent cell attachment factor." Nature 250 (463): 248-51**

**Klein, H. W., S. Kilmer and R. C. Carlsen (1989). "Enhancement of peripheral nerve regeneration by pharmacological activation of the cyclic AMP second messenger system." Microsurgery 10(2): 122-125.**

**Komoriya, A., L. Green, et al. (1991). "The minimal essential sequence for a major cell type-specific adhesion site (CS1) within the alternatively spliced type III**

**connecting segment domain of fibronectin is leucine-aspartic acid-valine." Journal of Biological Chemistry 266(23): 15075-15079.**

**Koopmans, G., B. Hasse, et al. (2009). "The role of collagen in peripheral nerve repair." International review of neurobiology 87: 363-379.**

**Koppes, A. N., A. L. Nordberg, et al. (2013). "Electrical stimulation of Schwann cells promotes sustained increases in neurite outgrowth." Tissue Engineering Part A 20(3-4): 494-506.**

**Korossis, S. A., C. Booth, et al. (2002). "Tissue engineering of cardiac valve prostheses II: biomechanical characterization of decellularized porcine aortic heart valves." J Heart Valve Dis 11(4): 463-471.**

**Korossis, S., F. Bolland, et al. (2005). "Bioreactors in tissue engineering." Topics Tissue Eng 2(8): 1-23.**

**Koshimune, M., K. Takamatsu, et al. (2003). "Creating bioabsorbable Schwann cell coated conduits through tissue engineering." Biomed Mater Eng 13(3): 223-229.**

**Koulaouzidou, E. A., J. Margelos, et al. (1999). "Cytotoxic effects of different concentrations of neutral and alkaline EDTA solutions used as root canal irrigants." Journal of endodontics 25(1): 21-23.**

**Krekoski, C. A., D. Neubauer, et al. (2001). "Axonal regeneration into acellular nerve grafts is enhanced by degradation of chondroitin sulfate proteoglycan." Journal of Neuroscience 21(16): 6206-6213.**

**Krystosek, A. and N. W. Seeds (1981). "Plasminogen activator release at the neuronal growth cone." Science 213(4515): 1532-1534.**

**Kubota, S., K. Tashiro, et al. (1992). "Signaling site of laminin with mitogenic activity." Journal of Biological Chemistry 267(7): 4285-4288.**

**Kwan, M. K., E. J. Wall, et al. (1992). "Strain, stress and stretch of peripheral nerve Rabbit experiments in vitro and in vivo." Acta Orthopaedica 63(3): 267-272.**

**Laura, M., N. D. Leipzig, et al. (2008). "Promoting neuron adhesion and growth." Materials today 11(5): 36-43.**

**Lavdas, A. A., I. Franceschini, et al. (2006). "Schwann cells genetically engineered to express PSA show enhanced migratory potential without impairment of their myelinating ability in vitro." GLIA 53(8): 868-878.**

**Lee, S. K. and S. W. Wolfe (2000). "Peripheral nerve injury and repair." Journal of the American Academy of Orthopaedic Surgeons 8(4): 243-252.**

**Lein, P. J., G. A. Banker, et al. (1992). "Laminin selectively enhances axonal growth and accelerates the development of polarity by hippocampal neurons in culture." Brain Res Dev Brain Res 69(2): 191-197.**

**Li, F., W. Li, et al. (2004). "Low-molecular-weight peptides derived from extracellular matrix as chemoattractants for primary endothelial cells." Endothelium 11(3-4): 199-206.**

**Lin, H. J., T. J. O'Shaughnessy, et al. (2004). "Neural stem cell differentiation in a cell–collagen–bioreactor culture system." Developmental brain research 153(2): 163-173.**

**Lomas, R., L. Jennings, et al. (2004). "Effects of a peracetic acid disinfection protocol on the biocompatibility and biomechanical properties of human patellar tendon allografts." Cell and tissue banking 5(3): 149-160.**

**Lowery, L. A. and D. Van Vactor (2009). "The trip of the tip: understanding the growth cone machinery." Nat Rev Mol Cell Biol 10(5): 332-343.**

**Lumpkins, S. B., N. Pierre, et al. (2008). "A mechanical evaluation of three decellularization methods in the design of a xenogeneic scaffold for tissue engineering the temporomandibular joint disc." Acta biomaterialia 4(4): 808-816.**

**Lundborg, G. (2004). "Commentary: Residual function in peripheral nerve stumps for amputees." Journal of Hand Surgery-American Volume 29A(4): 616-618.**

**Lundborg, G., L. B. Dahlin, et al. (1982). "Nerve regeneration in silicone chambers: influence of gap length and of distal stump components." Experimental neurology 76(2): 361-375.**

**Luo, J., S. A. Korossis, et al. (2014). "Development and Characterization of Acellular Porcine Pulmonary Valve Scaffolds for Tissue Engineering." Tissue Engineering Part A 20(21-22): 2963-2974.**

**Mackinnon, S. E. (2011). "Nerve endoneurial microstructure facilitates uniform distribution of regenerative fibers: a post hoc comparison of midgraft nerve fiber densities." Journal of reconstructive microsurgery 27(2): 83-90.**

**Mackinnon, S. E., V. B. Doolabh, et al. (2001). "Clinical outcome following nerve allograft transplantation." Plast Reconstr Surg 107(6): 1419-1429.**

**MacNeil, S. (2007). "Progress and opportunities for tissue-engineered skin." Nature 445(7130): 874-880.**

**Magnaghi, V., A. Parducz, et al. (2010). "GABA synthesis in Schwann cells is induced by the neuroactive steroid allopregnanolone." Journal of neurochemistry 112(4): 980-990.**

**Maki, C. (2009). "ADAM Student Atlas of Anatomy, 2nd edition." American Journal of Human Biology 21(1): 139-139.**

**Mantovani, A., A. Sica, et al. (2005). "Macrophage polarization comes of age." Immunity 23(4): 344-346.**

**Mantovani, A., A. Sica, et al. (2004). "The chemokine system in diverse forms of macrophage activation and polarization." Trends in immunology 25(12): 677-686.**

**Mantovani, A., S. Sozzani, et al. (2002). "Macrophage polarization: tumor-associated macrophages as a paradigm for polarized M2 mononuclear phagocytes." Trends in immunology 23(11): 549-555.**

**Maravilla, K. R. and B. C. Bowen (1998). "Imaging of the peripheral nervous system: evaluation of peripheral neuropathy and plexopathy." AJNR Am J Neuroradiol 19(6): 1011-1023.**

**Marmor, L. (1964). "The repair of peripheral nerves by irradiated homografts." Clinical orthopaedics and related research 34: 161-169.**

**Martini, R. (1994). "Expression and functional roles of neural cell surface molecules and extracellular matrix components during development and regeneration of peripheral nerves." Journal of neurocytology 23(1): 1-28.**

**Mason, S. and J. B. Phillips (2011). "An ultrastructural and biochemical analysis of collagen in rat peripheral nerves: the relationship between fibril diameter and mechanical properties." J Peripher Nerv Syst 16(3): 261-269.**

**McCrory, P., S. Bell, et al. (2002). "Nerve entrapments of the lower leg, ankle and foot in sport." Sports Medicine 32(6): 371-391.**

**McFetridge, P. S., J. W. Daniel, et al. (2004). "Preparation of porcine carotid arteries for vascular tissue engineering applications." J Biomed Mater Res A 70(2): 224-234.**

**McKeon, R. J., R. C. Schreiber, et al. (1991). "Reduction of neurite outgrowth in a model of glial scarring following CNS injury is correlated with the expression of inhibitory molecules on reactive astrocytes." Journal of Neuroscience 11(11): 3398-3411.**

**Meek, M. F. and J. H. Coert (2002). "Clinical use of nerve conduits in peripheral-nerve repair: Review of the literature." Journal of Reconstructive Microsurgery 18(2): 97-109.**

**Meek, M. F. and J. H. Coert (2008). "US Food and Drug Administration/Conformit Europe-approved absorbable nerve conduits for clinical repair of peripheral and cranial nerves." Annals of Plastic Surgery 60(1): 110-116.**

**Meyer, S. R., B. Chiu, et al. (2006). "Comparison of aortic valve allograft decellularization techniques in the rat." Journal of biomedical materials research Part A 79(2): 254-262.**

**Millesi, H., G. Zoch, et al. (1995). "Mechanical properties of peripheral nerves." Clin Orthop Relat Res(314): 76-83.**

**Mobasseri, A., A. Faroni, et al. (2015). "Polymer scaffolds with preferential parallel grooves enhance nerve regeneration." Tissue Engineering Part A 21(5-6): 1152-1162.**

**Mohanna, P. N., R. C. Young, et al. (2003). "A composite poly-hydroxybutyrate-glial growth factor conduit for long nerve gap repairs." Journal of Anatomy 203(6): 553-565.**

**Monboisse, J. and J. Borel (1992). Oxidative damage to collagen. Free Radicals and Aging, Springer: 323-327.**

**Montoya, C. V. and P. S. McFetridge (2009). "Preparation of ex vivo–based biomaterials using convective flow decellularization." Tissue Engineering Part C: Methods 15(2): 191-200.**

**Moore, A. M., M. MacEwan, et al. (2011). "Acellular Nerve Allografts in Peripheral Nerve Regeneration: A Comparative Study." Muscle & Nerve 44(2): 221-234.**

**Moreau, M. F., Y. Gallois, et al. (2000). "Gamma irradiation of human bone allografts alters medullary lipids and releases toxic compounds for osteoblast-like cells." Biomaterials 21(4): 369-376.**

**Morris, J. H., A. R. Hudson, et al. (1972). "A study of degeneration and regeneration in the divided rat sciatic nerve based on electron microscopy." Zeitschrift für Zellforschung und mikroskopische Anatomie 124(2): 103-130.**

**Mosahebi, A., B. Woodward, et al. (2001). "Retroviral labeling of Schwann cells: In vitro characterization and in vivo transplantation to improve peripheral nerve regeneration." GLIA 34(1): 8-17.**

**Mosser, D. M. (2003). "The many faces of macrophage activation." Journal of leukocyte biology 73(2): 209-212.**

**Muir, D., E. Engvall, et al. (1989). "Schwannoma cell-derived inhibitor of the neurite-promoting activity of laminin." The Journal of cell biology 109(5): 2353-2362.**

**Muir, D. (2010). "The potentiation of peripheral nerve sheaths in regeneration and repair." Experimental Neurology 223(1): 102-111.**

**Murray-Dunning, C., S. L. McArthur, et al. (2011). "Three-dimensional alignment of schwann cells using hydrolysable microfiber scaffolds: strategies for peripheral nerve repair." Methods Mol Biol 695: 155-166.**

**Nadim, W., P. N. Anderson, et al. (1990). "The role of Schwann cells and basal lamina tubes in the regeneration of axons through long lengths of freeze-killed nerve grafts." Neuropathol Appl Neurobiol 16(5): 411-421.**

**Navissano, M., F. Malan, et al. (2005). "Neurotube for facial nerve repair." Microsurgery 25(4): 268-271.**

**Newby, C. S., R. M. Barr, et al. (2000). "Cytokine release and cytotoxicity in human keratinocytes and fibroblasts induced by phenols and sodium dodecyl sulfate." Journal of investigative dermatology 115(2): 292-298.**

**Nguyen, Q. T., J. R. Sanes, et al. (2002). "Pre-existing pathways promote precise projection patterns." Nature Neuroscience 5(9): 861-867.**

**Nilsson, A., L. Dahlin, et al. (2005). "Graft repair of a peripheral nerve without the sacrifice of a healthy donor nerve by the use of acutely dissociated autologous Schwann cells." Scandinavian Journal of Plastic and Reconstructive Surgery and Hand Surgery 39(1): 1-6.**

**Nishiura, Y., J. Brandt, et al. (2004). "Addition of cultured Schwann cells to tendon autografts and freeze-thawed muscle grafts improves peripheral nerve regeneration." Tissue engineering 10(1-2): 157-164.**

**Noback, C. R. (2005). The human nervous system : structure and function. Totowa, N.J., Humana Press.**

**Noble, J., C. A. Munro, et al. (1998). "Analysis of upper and lower extremity peripheral nerve injuries in a population of patients with multiple injuries." J Trauma 45(1): 116-122.**

**Nomizu, M., Y. Kuratomi, et al. (1998). "Cell binding sequences in mouse laminin α1 chain." Journal of Biological Chemistry 273(49): 32491-32499.**

**Obremski, V., M. Johnson, et al. (1993). "Fibroblasts are required for Schwann cell basal lamina deposition and ensheathment of unmyelinated sympathetic neurites in culture." Journal of neurocytology 22(2): 102-117.**

**Osawa, T., K. Tohyama, et al. (1990). "Allogeneic nerve grafts in the rat, with special reference to the role of Schwann cell basal laminae in nerve regeneration." Journal of neurocytology 19(6): 833-849.**

**Ott, H. C., B. Clippinger, et al. (2010). "Regeneration and orthotopic transplantation of a bioartificial lung." Nature medicine 16(8): 927-933.**

**Ott, H. C., T. S. Matthiesen, et al. (2008). "Perfusion-decellularized matrix: using nature's platform to engineer a bioartificial heart." Nature medicine 14(2): 213-221.**

**Palm, S. L. and L. T. Furcht (1983). "Production of laminin and fibronectin by Schwannoma cells: cell-protein interactions in vitro and protein localization in peripheral nerve in vivo." J Cell Biol 96(5): 1218-1226.**

**Palsson BO, B. S. (2004). "Tissue Engineering." 20-33.**

**Partington, L., N. J. Mordan, et al. (2013). "Biochemical changes caused by decellularization may compromise mechanical integrity of tracheal scaffolds." Acta Biomater 9(2): 5251-5261.**

**Petersen, T. H., E. A. Calle, et al. (2010). "Tissue-engineered lungs for in vivo implantation." Science 329(5991): 538-541.**

**Pfister, B. J., T. Gordon, et al. (2011). "Biomedical engineering strategies for peripheral nerve repair: surgical applications, state of the art, and future challenges." Crit Rev Biomed Eng 39(2): 81-124.**

**Phillips, J. B., X. Smit, et al. (2004). "Peripheral nerves in the rat exhibit localized heterogeneity of tensile properties during limb movement." J Physiol 557(Pt 3): 879-887.**

**Piccotti, J. R., S. Y. Chan, et al. (1997). "Are th2 helper t lymphocytes beneficial, deleterious, or irrelevant in promoting allograft survival? 1." Transplantation 63(5): 619-624.**

**Pollard, J. and L. Fitzpatrick (1973). "A comparison of the effects of irradiation and immunosuppressive agents on regeneration through peripheral nerve allografts: an ultrastructural study." Acta neuropathologica 23(2): 166-180.**

**Porzionato, A., M. Sfriso, et al. (2013). "Decellularized omentum as novel biologic scaffold for reconstructive surgery and regenerative medicine." European Journal of Histochemistry 57(1): 4.**

**Prasertsung, I., S. Kanokpanont, et al. (2008). "Development of acellular dermis from porcine skin using periodic pressurized technique." Journal of Biomedical Materials Research Part B: Applied Biomaterials 85(1): 210-219.**

**Pruss, A., M. Kao, et al. (1999). "Virus safety of avital bone tissue transplants: evaluation of sterilization steps of spongiosa cuboids using a peracetic acid–methanol mixture." Biologicals 27(3): 195-201.**

**Purves, D. (2004). Neuroscience. Sunderland, Mass., Sinauer Associates.**

**Qiu, Q. Q., P. Leamy, et al. (2009). "Inactivation of bacterial spores and viruses in biological material using supercritical carbon dioxide with sterilant." Journal of Biomedical Materials Research Part B: Applied Biomaterials 91(2): 572-578.**

**Rampersad, S. N. (2012). "Multiple applications of Alamar Blue as an indicator of metabolic function and cellular health in cell viability bioassays." Sensors 12(9): 12347-12360.**

**Rangappa, N., A. Romero, et al. (2000). "Laminin-coated poly(L-lactide) filaments induce robust neurite growth while providing directional orientation." Journal of Biomedical Materials Research 51(4): 625-634.**

**Ratner, B. D., A. S. Hoffman, et al. (2004). Biomaterials science: an introduction to materials in medicine, Academic press.**

**Recknor, J. and S. Mallapragada (2006). "Nerve regeneration: Tissue engineering strategies." The Biomedical Engineering Handbook: Tissue Engineering and Artificial Organs.**

**Record, R. D., D. Hillegonds, et al. (2001). "In vivo degradation of 14 C-labeled small intestinal submucosa (SIS) when used for urinary bladder repair." Biomaterials 22(19): 2653-2659.**

**Rieder, E., M.-T. Kasimir, et al. (2004). "Decellularization protocols of porcine heart valves differ importantly in efficiency of cell removal and susceptibility of the matrix to recellularization with human vascular cells." The Journal of thoracic and cardiovascular surgery 127(2): 399-405.**

**Riedl, O. and M. Frey (2013). "Anatomy of the sural nerve: cadaver study and literature review." Plastic and Reconstructive Surgery 131(4): 802-810.**

**Rodrigues, M. C., A. A. Rodrigues, Jr., et al. (2012). "Peripheral nerve repair with cultured schwann cells: getting closer to the clinics." ScientificWorldJournal 2012: 413091.**

**Rozzo, C., P. Ratti, et al. (1993). "Modulation of α 1 β 1, α 2 β 1, and α 3 β 1 integrin heterodimers during human neuroblastoma cell differentiation." FEBS letters 332(3): 263-267.**

**Rubartelli, A. and M. T. Lotze (2007). "Inside, outside, upside down: damage-associated molecular-pattern molecules (DAMPs) and redox." Trends in immunology 28(10): 429-436.**

**Rutala, W. A. and D. J. Weber (2004). "Disinfection and sterilization in health care facilities: what clinicians need to know." Clin Infect Dis 39(5): 702-709.**

**Sagripanti, J.-L. and A. Bonifacino (2000). "Cytotoxicity of liquid disinfectants." Surgical infections 1(1): 3-14.**

**Saheb-Al-Zamani, M., Y. Yan, et al. (2013). "Limited regeneration in long acellular nerve allografts is associated with increased Schwann cell senescence." Experimental neurology 247: 165-177.**

**Saladin, K. S. (2011). Human anatomy. New York, McGraw-Hill.**

**Schenke-Layland, K., O. Vasilevski, et al. (2003). "Impact of decellularization of xenogeneic tissue on extracellular matrix integrity for tissue engineering of heart valves." Journal of structural biology 143(3): 201-208.**

**Schmalbruch, H. (1986). "Fiber composition of the rat sciatic nerve." Anat Rec 215(1): 71-81.**

**Schmidt, C. E. and J. B. Leach (2003). "Neural tissue engineering: Strategies for repair and regeneration." Annual Review of Biomedical Engineering 5: 293-347.**

**Schwartz, M. A. (2001). "Integrin signaling revisited." Trends in cell biology 11(12): 466-470.**

**Seckel, B. R. (1990). "Enhancement of peripheral nerve regeneration." Muscle Nerve 13(9): 785-800.**

**Seddon, A. M., P. Curnow, et al. (2004). "Membrane proteins, lipids and detergents: not just a soap opera." Biochimica et Biophysica Acta (BBA)-Biomembranes 1666(1): 105-117.**

**Selinfreund, R. H., S. W. Barger, et al. (1991). "Neurotrophic protein S100 beta stimulates glial cell proliferation." Proceedings of the National Academy of Sciences 88(9): 3554-3558.**

**Seyer, J. M., A. H. Kang, et al. (1977). "The characterization of type I and type III collagens from human peripheral nerve." Biochimica et Biophysica Acta (BBA)-Protein Structure 492(2): 415-425.**

**Shin, R. H., P. F. Friedrich, et al. (2009). "Treatment of a segmental nerve defect in the rat with use of bioabsorbable synthetic nerve conduits: a comparison of commercially available conduits." J Bone Joint Surg Am 91(9): 2194-2204.**

**Smeal, R. M., R. Rabbitt, et al. (2005). "Substrate curvature influences the direction of nerve outgrowth." Annals of Biomedical Engineering 33(3): 376-382.**

**So, K.-F. and X.-M. Xu (2015). Neural Regeneration, Academic Press.**

**Sondell, M., G. Lundborg, et al. (1998). "Regeneration of the rat sciatic nerve into allografts made acellular through chemical extraction." Brain Res 795(1-2): 44-54.**

**Spivey, E. C., Z. Z. Khaing, et al. (2012). "The fundamental role of subcellular topography in peripheral nerve repair therapies." Biomaterials 33(17): 4264-4276.**

**Stang, F., H. Fansa, et al. (2005). "Structural parameters of collagen nerve grafts influence peripheral nerve regeneration." Biomaterials 26(16): 3083-3091.**

**Stapleton, T. W., J. Ingram, et al. (2008). "Development and characterization of an acellular porcine medial meniscus for use in tissue engineering." Tissue Engineering Part A 14(4): 505-518.**

**Stegemann, H. and K. Stalder (1967). "Determination of hydroxyproline." Clin Chim Acta 18(2): 267-273.**

**Stewart, J. D. (2003). "Peripheral nerve fascicles: anatomy and clinical relevance." Muscle Nerve 28(5): 525-541.**

**Stoll, G. and H. W. Müller (1999). "Nerve injury, axonal degeneration and neural regeneration: basic insights." Brain pathology 9(2): 313-325.**

**Stone, K. R., U. M. Abdel-Motal, et al. (2007). "Replacement of human anterior cruciate ligaments with pig ligaments: a model for anti-non-gal antibody response in long-term xenotransplantation." Transplantation 83(2): 211-219.**

**Stone, K. R., G. Ayala, et al. (1998). "Porcine cartilage transplants in the cynomolgus monkey. III. Transplantation of alpha-galactosidase-treated porcine cartilage." Transplantation 65(12): 1577-1583.**

**Stone, K. R., A. W. Walgenbach, et al. (2007). "Anterior cruciate ligament reconstruction with a porcine xenograft: a serologic, histologic, and biomechanical study in primates." Arthroscopy: The Journal of Arthroscopic & Related Surgery 23(4): 411-419. e411.**

**Stout, R. D., C. Jiang, et al. (2005). "Macrophages sequentially change their functional phenotype in response to changes in microenvironmental influences." The Journal of Immunology 175(1): 342-349.**

**Strom, T. B., P. Roy-Chaudhury, et al. (1996). "The Th1/Th2 paradigm and the allograft response." Current opinion in immunology 8(5): 688-693.**

**Subramanian, A., U. M. Krishnan, et al. (2009). "Development of biomaterial scaffold for nerve tissue engineering: Biomaterial mediated neural regeneration." J Biomed Sci 16: 108.**

**Sun, T., D. Norton, et al. (2008). "Development of a bioreactor for evaluating novel nerve conduits." Biotechnology and Bioengineering 99(5): 1250-1260.**

**Sun, W. Q. and P. Leung (2008). "Calorimetric study of extracellular tissue matrix degradation and instability after gamma irradiation." Acta biomaterialia 4(4): 817-826.**

**Sunderland, S. (1945). "The Adipose Tissue of Peripheral Nerves." Brain 68(2): 118-122.**

**Sunderland, S. (1965). "The connective tissues of peripheral nerves." Brain 88(4): 841-854.**

**Sunderland, S. (1968). Nerves and nerve injuries. Edinburgh, E. & S. Livingstone.**

**Sunderland, S. (1990). "The Anatomy and Physiology of Nerve Injury." Muscle & Nerve 13(9): 771-784.**

**Sunderland, S. and K. C. Bradley (1961). "Stress-Strain Phenomena in Human Peripheral Nerve Trunks." Brain 84(1): 102-&.**

**Sunderland, S. and L. J. Ray (1948). "The intraneural topography of the sciatic nerve and its popliteal divisions in man." Brain 71(Pt. 3): 242-273.**

**Taras, J. S. and S. M. Jacoby (2008). "Repair of lacerated peripheral nerves with nerve conduits." Tech Hand Up Extrem Surg 12(2): 100-106.**

**Tassler, P. L., A. L. Dellon, et al. (1994). "Identification of Elastic Fibers in the Peripheral-Nerve." Journal of Hand Surgery-British and European Volume 19B(1): 48-54.**

**Terenghi, G. (1999). "Peripheral nerve regeneration and neurotrophic factors." Journal of Anatomy 194: 1-14.**

**Thomas, P. K. and D. G. Jones (1967). "Cellular Response to Nerve Injury .2. Regeneration of Perineurium after Nerve Section." Journal of Anatomy 101: 45-&.**

**Timpl, R. (1996). "Macromolecular organization of basement membranes." Current opinion in cell biology 8(5): 618-624.**

**Topp, K. S. and B. S. Boyd (2006). "Structure and biomechanics of peripheral nerves: nerve responses to physical stresses and implications for physical therapist practice." Physical Therapy 86(1): 92-109.**

**Tulla, M., M. Huhtala, et al. (2007). "Analysis of an ascidian integrin provides new insight into early evolution of collagen recognition." Febs Letters 581(13): 2434-2440.**

**Udina, E., F. J. Rodriguez, et al. (2004). "FK506 enhances regeneration of Axons across long peripheral nerve gaps repaired with collagen guides seeded with allogeneic Schwann cells." GLIA 47(2): 120-129.**

**Ueno, T., L. C. Pickett, et al. (2004). "Clinical application of porcine small intestinal submucosa in the management of infected or potentially contaminated abdominal defects." Journal of gastrointestinal surgery 8(1): 109-112.**

**Ugrenović, S. (2014). "Morphological and morphometric analysis of fascicular structure of tibial and common peroneal nerves." Facta universitatis series 16: 18-22.**

**Ugrenovic, S. Z., I. D. Jovanovic, et al. (2013). "Similarities and Dissimilarities of the Blood Supplies of the Human Sciatic, Tibial, and Common Peroneal Nerves." Clinical Anatomy 26(7): 875-882.**

**Ushiki, T. and C. Ide (1990). "Three-dimensional organization of the collagen fibrils in the rat sciatic nerve as revealed by transmission- and scanning electron microscopy." Cell Tissue Res 260(1): 175-184.**

**Uygun, B. E., A. Soto-Gutierrez, et al. (2010). "Organ reengineering through development of a transplantable recellularized liver graft using decellularized liver matrix." Nature medicine 16(7): 814-820.**

**Voet, D., J. G. Voet, et al. (1999). Fundamentals of biochemistry, Wiley New York.**

**Voytik-Harbin, S. L., A. O. Brightman, et al. (1997). "Identification of extractable growth factors from small intestinal submucosa." Journal of cellular biochemistry 67(4): 478-491.**

**Vrbova, G., N. Mehra, et al. (2009). "Chemical communication between regenerating motor axons and Schwann cells in the growth pathway." European Journal of Neuroscience 30(3): 366-375.**

**Wakimura, Y., W. Wang, et al. (2015). "An Experimental Study to Bridge a Nerve Gap with a Decellularized Allogeneic Nerve." Plastic and reconstructive surgery 136(3): 319e-327e.**

**Waldram, M. (2003). "Peripheral nerve injuries." SAGE.**

**Wallquist, W., M. Patarroyo, et al. (2002). "Laminin chains in rat and human peripheral nerve: distribution and regulation during development and after axonal injury." Journal of Comparative Neurology 454(3): 284-293.**

**Walsh, S., J. Biernaskie, et al. (2009). "Supplementation of acellular nerve grafts with skin derived precursor cells promotes peripheral nerve regeneration." Neuroscience 164(3): 1097-1107.**

**Walsh, S. and R. Midha (2009). "Practical considerations concerning the use of stem cells for peripheral nerve repair." Neurosurgical focus 26(2).**

**Wang, K. K., I. R. Nemeth, et al. (1998). "Hyaluronic acid enhances peripheral nerve regeneration in vivo." Microsurgery 18(4): 270-275.**

**Wang, Q., C. Zhang, et al. (2014). "The preparation and comparison of decellularized nerve scaffold of tissue engineering." Journal of Biomedical Materials Research Part A.**

**Wang, W., S. Itoh, et al. (2015). "Comparative study of the efficacy of decellularization treatment of allogenic and xenogeneic nerves as nerve conduits." Journal of Biomedical Materials Research Part A.**

**Wang, X., M. Pan, et al. (2014). "A novel artificial nerve graft for repairing long-distance sciatic nerve defects: a self-assembling peptide nanofiber scaffold-containing poly (lactic-co-glycolic acid) conduit." Neural regeneration research 9(24): 2132.**

**Weber, R. A., W. C. Breidenbach, et al. (2000). "A randomized prospective study of polyglycolic acid conduits for digital nerve reconstruction in humans." Plast Reconstr Surg 106(5): 1036-1045; discussion 1046-1038.**

**Weinstein, D. E. (1999). "The role of Schwann cells in neural regeneration." Neuroscientist 5(4): 208-216.**

**White, E. S. and A. F. Muro (2011). "Fibronectin splice variants: understanding their multiple roles in health and disease using engineered mouse models." IUBMB life 63(7): 538-546.**

**Whitlock, E. L., S. H. Tuffaha, et al. (2009). "Processed Allografts and Type I Collagen Conduits for Repair of Peripheral Nerve Gaps." Muscle & Nerve 39(6): 787-799.**

**Wilcox, H., S. Korossis, et al. (2005). "Biocompatibility and recellularization potential of an acellular porcine heart valve matrix." The Journal of heart valve disease 14(2): 228-236; discussion 236-227.**

**Williams, C., J. Liao, et al. (2009). "Altered structural and mechanical properties in decellularized rabbit carotid arteries." Acta Biomaterialia 5(4): 993-1005.**

**Williams PL, W. R., Dyson M, Bannister LH (eds) (1995). "Gray's Anatomy." British Journal of Surgery 76(12).**

**Wilshaw, S.-P., J. N. Kearney, et al. (2006). "Production of an acellular amniotic membrane matrix for use in tissue engineering." Tissue engineering 12(8): 2117-2129.**

**Wilshaw, S. P., P. Rooney, et al. (2012). "Development and characterization of acellular allogeneic arterial matrices." Tissue Eng Part A 18(5-6): 471-483.**

**Witzel, C., C. Rohde, et al. (2005). "Pathway sampling by regenerating peripheral axons." Journal of Comparative Neurology 485(3): 183-190.**

**Woods, T. and P. F. Gratzer (2005). "Effectiveness of three extraction techniques in the development of a decellularized bone–anterior cruciate ligament–bone graft." Biomaterials 26(35): 7339-7349.**

**Xu, C. C., R. W. Chan, et al. (2007). "A biodegradable, acellular xenogeneic scaffold for regeneration of the vocal fold lamina propria." Tissue engineering 13(3): 551-566.**

**Xu, H., B. Xu, et al. (2014). "Comparison of decellularization protocols for preparing a decellularized porcine annulus fibrosus scaffold." PLoS One 9(1): 86-723.**

**Yang, C., T. M. John, et al. (2007). Decellularized omentum matrix and uses thereof, Google Patents.**

**Yu, H., J. Peng, et al. (2009). "Improvement of peripheral nerve regeneration in acellular nerve grafts with local release of nerve growth factor." Microsurgery 29(4): 330-336.**

**Zalewski, A. A. and A. K. Gulati (1982). "Evaluation of histocompatibility as a factor in the repair of nerve with a frozen nerve allograft." Journal of neurosurgery 56(4): 550-554.**

**Zhang, F., B. Blain, et al. (2002). "Autogenous venous graft with one-stage prepared Schwann cells as a conduit for repair of long segmental nerve defects." Journal of Reconstructive Microsurgery 18(4): 295-300.**

**Zhang, M., D. Methot, et al. (2001). "Cardiomyocyte grafting for cardiac repair: graft cell death and anti-death strategies." Journal of molecular and cellular cardiology 33(5): 907-921.**

**Zhang, Y., H. Luo, et al. (2010). "A nerve graft constructed with xenogeneic acellular nerve matrix and autologous adipose-derived mesenchymal stem cells." Biomaterials 31(20): 5312-5324.**

**Zilic, L., P. E. Garner, et al. (2015). "An anatomical study of porcine peripheral nerve and its potential use in nerve tissue engineering." Journal of anatomy 227(3): 302-314.**

**Zilic, L., S.-P. Wilshaw, et al. (2016). "Decellularisation and histological characterisation of porcine peripheral nerves." Biotechnology and Bioengineering.**

**Zuo, J., T. A. Ferguson, et al. (1998). "Neuronal matrix metalloproteinase-2 degrades and inactivates a neurite-inhibiting chondroitin sulfate proteoglycan." The Journal of neuroscience 18(14): 5203-5211.**

**Zuo, J., Y. J. Hernandez, et al. (1998). "Chondroitin sulfate proteoglycan with neurite-inhibiting activity is up-regulated following peripheral nerve injury." J Neurobiol 34(1): 41-54.**